DISSOCIATION DYNAMICS OF DIATOMIC MOLECULES IN INTENSE FIELDS

by

MAIA MAGRAKVELIDZE

B.S., Ivane Javakhishvili Tbilisi State University, Georgia, 2003

M.S., Ivane Javakhishvili Tbilisi State University, Georgia, 2005

M.S., Kansas State University, Manhattan, Kansas, 2009

AN ABSTRACT OF A DISSERTATION

submitted in partial fulfillment of the requirements for the degree

DOCTOR OF PHILOSOPHY

Department of Physics
College of Arts and Sciences

KANSAS STATE UNIVERSITY
Manhattan, Kansas

2013

Abstract

We study the dynamics of diatomic molecules (dimers) in intense IR and XUV laser fields theoretically and compare the results with measured data in collaboration with different experimental groups worldwide. The first three chapters of the thesis cover the introduction and the background on solving time-independent and time-dependent Schrödinger equation. The numerical results in this thesis are presented in four chapters, three of which are focused on diatomic molecules in IR fields. The last one concentrates on diatomic molecules in XUV pulses.

The study of nuclear dynamics of H_2 or D_2 molecules in IR pulses is given in Chapter 4. First, we investigate the optimal laser parameters for observing field-induced bond softening and bond hardening in D_2^{+}. Next, the nuclear dynamics of H_2^{+} molecular ions in intense laser fields are investigated by analyzing their fragment kinetic-energy release (KER) spectra as a function of the pump-probe delay τ. Lastly, the electron localization is studied for long circularly polarized laser pulses.

Chapter 5 covers the dissociation dynamics of O_2^{+} in an IR laser field. The fragment KER spectra are analyzed as a function of the pump-probe delay τ. Within the Born-Oppenheimer approximation, we calculate *ab-initio* adiabatic potential-energy curves and their electric dipole couplings, using the quantum chemistry code GAMESS.

In Chapter 6, the dissociation dynamics of the noble gas dimer ions He_2^{+}, Ne_2^{+}, Ar_2^{+}, Kr_2^{+}, and Xe_2^{+} is investigated in ultrashort pump and probe laser pulses of different wavelengths. We observe a striking ‘‘delay gap’’ in the pump-probe-delay-dependent KER spectrum only if the probe-pulse wavelength exceeds the pump-pulse wavelength. Comparing pump-probe-pulse-delay dependent KER spectra for different noble gas dimer cations, we quantitatively discuss quantum-mechanical versus classical aspects of the nuclear vibrational motion as a function of the nuclear mass.

Chapter 7 focuses on diatomic molecules in XUV laser pulses. We trace the femtosecond nuclear-wave-packet dynamics in ionic states of oxygen and nitrogen diatomic molecules by comparing measured kinetic-energy-release spectra with classical and quantum-mechanical simulations. Experiments were done at the free-electron laser in Hamburg (FLASH) using 38-eV XUV-pump–XUV-probe.

The summary and outlook of the work is discussed in Chapter 8.

DISSOCIATION DYNAMICS OF DIATOMIC MOLECULES IN INTENSE FIELDS

by

MAIA MAGRAKVELIDZE

B.S., Ivane Javakhishvili Tbilisi State University, Georgia, 2003

M.S., Ivane Javakhishvili Tbilisi State University, Georgia, 2005

M.S., Kansas State University, Manhattan, Kansas, 2009

A DISSERTATION

submitted in partial fulfillment of the requirements for the degree

DOCTOR OF PHILOSOPHY

Department of Physics
College of Arts and Sciences

KANSAS STATE UNIVERSITY
Manhattan, Kansas

2013

Approved by:

Major Professor
Uwe Thumm

Copyright

Abstract

We study the dynamics of diatomic molecules (dimers) in intense IR and XUV laser fields theoretically and compare the results with measured data in collaboration with different experimental groups worldwide. The first three chapters of the thesis cover the introduction and the background on solving the time-independent and time-dependent Schrödinger equations. The numerical results in this thesis are presented in four chapters, three of which are focused on diatomic molecules in IR fields. The last one concentrates on diatomic molecules in XUV pulses.

The study of nuclear dynamics of H_2 or D_2 molecules in IR pulses is given in Chapter 4. First, we investigate the optimal laser parameters for observing field-induced bond softening and bond hardening in D_2^{+}. Next, the nuclear dynamics of H_2^{+} molecular ions in intense laser fields are investigated by analyzing their fragment kinetic-energy release (KER) spectra as a function of the pump-probe delay τ. Lastly, the electron localization is studied for long circularly polarized laser pulses.

Chapter 5 covers the dissociation dynamics of O_2^{+} in an IR laser field. The fragment KER spectra are analyzed as a function of the pump-probe delay τ. Within the Born-Oppenheimer approximation, we calculate *ab-initio* adiabatic potential-energy curves and their electric dipole couplings, using the quantum chemistry code GAMESS.

In Chapter 6, the dissociation dynamics of the noble gas dimer ions He_2^{+}, Ne_2^{+}, Ar_2^{+}, Kr_2^{+}, and Xe_2^{+} is investigated in ultrashort pump and probe laser pulses of different wavelengths. We observe a striking ‘‘delay gap’’ in the pump-probe-delay-dependent KER spectrum only if the probe-pulse wavelength exceeds the pump-pulse wavelength. Comparing pump-probe-pulse-delay dependent KER spectra for different noble gas dimer cations, we quantitatively discuss quantum-mechanical versus classical aspects of the nuclear vibrational motion as a function of the nuclear mass.

Chapter 7 focuses on diatomic molecules in XUV laser pulses. We trace the femtosecond nuclear-wave-packet dynamics in ionic states of oxygen and nitrogen diatomic molecules by comparing measured kinetic-energy-release spectra with classical and quantum-mechanical simulations. Experiments were done at the free-electron laser in Hamburg (FLASH) using 38-eV XUV-pump–XUV-probe.

The summary and outlook of the work is discussed in Chapter 8.

Table of Contents

List of Figures

List of Tables

Acknowledgements

First of all I want to express my deepest gratitude to Dr. Uwe Thumm for giving me the chance to pursue my Ph.D. at Kansas State University, for his guidance and outstanding support during all stages of this work, and for being so understanding and giving me all the confidence I needed.

I wish to thank all my teachers past and present for all that they have taught me; I could not have done it without you. Thanks to Dr. Brett DePaola, Dr. Igor Litvinyuk and Dr. Lew Cocke for introducing me to experimental AMO physics. Thanks to Professor Christine Aikens of the KSU Chemistry department for helping me to understand how the GAMESS software package works. Thanks to the head of the KSU Physics department Dr. Amit Chakrabarti for allowing me to teach engineering physics studio in the spring 2013 semester and Dr. Bruce Law for guiding me in the teaching process. I would like to acknowledge people with whom I have worked in collaboration: Drs. Jian, Wu, Reinhard Dörner, Oliver Herrwerth, Matthias Kling, Sankar De, C. Lew Cocke and many others.

I am thankful to the Physics Department support staff Scott Chainey, Bob Krause, Peggy Matthews, Deanna Selby, Peter Nelson, Barbara Steward, Jane Peterson, Terry Turner, Larry McFeeters, Kim Coy, and Lindsay Thompson for being so supportive and helpful.

Thanks to Dr. Kevin Carnes and my committee members: Dr. Larry Weaver, Dr. Kristan Corwin, Dr. Paul Smith, and Dr. Medhat Morcos for reading and editing my thesis and for interesting comments and questions.

Thanks to my colleagues Feng He and Chang-hua Zhang and group members Qing Liao, Aihua Liu, and Jianxiong Li for being there for me. Thanks to all my friends at Kansas State University and Tbilisi State University; I could not have done it without your love and support.

Finally, I heartily thank my mom მზია, my sister დალი and my niece თათული for all the encouragement and emotional support on every step of my life, ძალიან მიყვარხართ.

Dedication

To my mom, my sister, my niece, and the memory of my dad.

ვუძღვნი ჩემს უსაყვარლეს ადამიანებს, დედას, და, თათულიკოს და მამას.

Preface

"The eternal mystery of the world is its comprehensibility".

Albert Einstein 1936.

Chapter 1 - INTRODUCTION

The investigation of the interaction of atoms and molecules with intense laser fields is one of the most interesting areas of the current research in atomic and molecular physics. The general motivation for studying molecules in laser fields lies in the possibility of gaining fundamental understanding of the dynamics and the intermediate processes involved in various physical, chemical and biological reactions.

The time scales of the atomic and molecular motion are orders of magnitude less than those in our life. The typical scales of length are less than a nanometer for small molecules, and the scales of time vary from attoseconds for the electronic dynamics, to femtoseconds for molecular vibration, to picoseconds for molecular rotation. To trace all the processes that take place during these interactions short laser pulses are used. To access the sub-femtosecond time scale, pump-probe techniques are being further developed to track electrons on their natural attosecond time scale [Alnaser-05, Bocharova-11, Calvert-10, Corkum-07, De-11, Ergler-06-2, Geißler-12, Johnsson-07, Légaré-05, Magrakvelidze-12-1, Magrakvelidze-12-2, Ullrich-12, Wu-13-2].

The control, time-resolved observation, and analysis of the nuclear dynamics in small diatomic molecules such as H_2^+ and D_2^+ [Kremer-09, Ray-09, Sansone-10, Singh-10, Ergler-06-2, Feuerstein-07, Bocharova-08, Winter-09] and, more recently, in heavier diatomic molecules with several binding electrons [De-10, De-11, Bocharova-11, Geißler-12] have been made possible by significant advances in femtosecond laser technology [Brixner-05, Dantus-04, Feuerstein-07, Hertel-06, Kling-06, Posthumus-04, Zewail-00]. “Pump-probe” experiments, which use short and intense time-delayed laser pulses, are performed in many laboratories [Alnaser-05, Baker-06, Corkum-07, Ergler-06-2, Johnsson-07, Légaré-05, Miller-88, Niikura -03, Sansone-06]. In these experiments a short pump pulse (with pulse lengths of only a few fs corresponding to bandwidths that are larger than the vibrational level spacing) electronically excites or ionizes the neutral target molecule and also coherently excites a superposition of stationary vibrational states of the molecular ion, resulting in a moving nuclear wave packet. With the help of a second delayed probe pulse the probability density of the wave packet can be imaged. The probe pulse rapidly ionizes the molecular ion leading to its fragmentation by Coulomb explosion (CE) [Chelkowski-02, Chelkowski-07, Feuerstein-03]. The fragments of the reaction are detected and kinetic-energy release (KER) spectra are measured [Alnaser-05, Ergler-

06-2, Martín-07, Niederhausen-07, Rudenko-06]. From the KER spectra, the dynamics of the nuclear wave packet can be reconstructed. The pump-probe technique is by now routinely applied in many fields of physics, chemistry and biochemistry [Zewail-88, Crespo-Hernández-05, Ergler-06-2].

The current work focuses on the dissociation dynamics of the diatomic molecules in infra-red (IR) or extreme ultraviolet (XUV) fields. We mainly calculate evolution of the wave packet in time for the dissociation process of the diatomic molecules in laser fields. Some background on molecular orbital theory and the theoretical tools used in the calculations are covered in Chapters 2 and 3. In particular, Chapter 2 reviews approximation methods for solving the time-independent Schrödinger equation and also some details on computing potential curves and dipole coupling elements using the quantum chemistry code GAMESS. Those calculations from GAMESS are used in the calculations of the KER spectra. Chapter 3 describes methods for solving the time-dependent Schrödinger equation (TDSE) based on discretizing operators and a finite-differencing scheme for the time propagation.

In the first chapter of the main part of this work (Chapter 4), the simplest molecule H_2^+ (D_2^+) in an IR field is discussed. At the beginning of the chapter, time-resolved studies of vibrational motion for the small molecules (H_2 and D_2) in laser fields are covered. The vibrational dynamics of wave packet motion of H_2 and D_2 molecules have been studied by analyzing the KER of the molecular ion fragments produced by a pump and second delayed probe laser pulse [Posthumus-04, Bocharova-11, Ergler-06-1, Alnaser-05, De-10, De-11]. The last part of Chapter 4 discusses the localization of electrons for symmetric laser pulses, which is in contrast to the general belief that electron localization cannot be measured in symmetric laser pulses. There are several techniques for studying electron localization in diatomic molecules that includes CEP locked [Kling-06, Kremer-09, Znakovskaya-12] or two color asymmetric pump-probe pulses [Ray-09, Wu-13-1, He-08-1, He-08-2, Sansone-10, Singh-10]. “Electron localization” with a single symmetric circularly polarized pulse is discussed in Section 4.4.

Interaction of laser fields with heavier molecules such as O_2 and noble gas dimers are described in Chapters 5 and 6 respectively. Compared to the H_2^+ molecule the dissociative dynamics for the heavier molecules is more complicated due to more adiabatic states involved. In chapter 5 we present a method that we developed for identifying the relevant electronic states involved in the dissociation dynamics with one color IR pump and probe pulses using the O_2

molecule as an example. Chapter 6 focuses on dissociation dynamics of noble gases with different pump and probe field wavelengths by analyzing the KER spectra as a function of the pump-probe delay. Using the pump and probe pulses with different wavelengths allows us to observe additional features of the KER spectra such as striking "delay gap".

The interaction of a XUV pulse with O_2 and N_2 molecules is described in Chapter 7, where in the calculations, we try to identify the electronic states of the molecular ions that are populated by ionizing the neutral molecule. We model the femtosecond nuclear wave packet dynamics in the ionic states of oxygen and nitrogen molecules for one of the first experimentally measured KER spectra for the XUV-pump and XUV-probe pulses. In contrast to intense NIR pulses, the interaction of XUV pulses with atomic and molecular targets is characterized by large Keldysh parameters, corresponding to ionization by the absorption of no more than a few energetic photons. In addition, with regard to identifying reaction pathways, the absorption of a known small number of energetic photons tends to induce electronic transitions to a more narrowly defined part of the target electronic spectrum. In addition, since these XUV and X-ray sources are tunable, transitions into specific spectral regions can be selected. In dissociative reactions, the KER can thus be resolved with regard to the number of absorbed photons and the pump-pulse-generated intermediate charge states of the molecular ion. Finally, conclusions and final remarks are presented in Chapter 8. We use atomic units (a.u.) throughout this work unless indicated otherwise (Appendix F).

Chapter 2 - INTRODUCTION TO MOLECULAR ORBITAL THEORY

In this chapter approximation methods for solving the time-independent Schrödinger equation are summarized.

For simple systems such as the harmonic oscillator, a particle in a box, or the hydrogen atom, the time-independent Schrödinger equation can be solved exactly. For more complex systems (for example molecules), however approximations need to be made to solve it numerically.

There are several steps involved in solving the time-independent Schrödinger equation for molecules: first, the Born-Oppenheimer (BO) approximation, leading to the idea of a potential energy surface. Next, the expansion of the many-electron wavefunction in terms of the so-called Slater determinants; and finally, representation of the Slater determinants in terms of molecular orbitals (MO), which are linear combinations of atomic-like-orbital functions - the basis set.

To describe molecules in an intense laser field accurately, one needs to consider both the electronic and also the nuclear degrees of freedom. The typical Hamiltonian for the molecule is written as the sum of the nuclear (T_N) and electronic (T_e) kinetic and potential (V_{NN} nuclear-nuclear, V_{eN} nuclear-electron and V_{ee} electron-electron interactions) energies:

$$H = T_N + T_e + V_{NN} + V_{eN} + V_{ee}$$
$$= -\frac{1}{2}\sum_k \frac{1}{m_l}\nabla_k^2 - \frac{1}{2}\sum_i \nabla_i^2 + \sum_k \sum_{k>l} \frac{Z_k Z_l e^2}{r_{kl}} - \sum_k \sum_i \frac{Z_k e^2}{r_{ik}} + \sum_j \sum_{i>j} \frac{e^2}{r_{ij}} \qquad (2.\ 1)$$

where labels k and l correspond to the nuclei and i and j to the electrons, m_l is nuclear mass, $Z_k e$ and $Z_l e$ nuclear charges, r_{kl} are internuclear distances, r_{ij} are distances between two electrons, and r_{ik} are the distances from nuclei to electrons .

2.1 Born-Oppenheimer approximation

"The underlying physical laws necessary for the mathematical theory of a large part of physics and the whole of chemistry are thus completely known, and the difficulty is only that the exact application of these laws leads to equations much too complex to be soluble".

P.A. Dirac 1929.

The wave-function of the many-electron molecular system is a function of electron and nuclear coordinates: $\psi(R,r)$, where R represents the nuclear coordinates, and r the electron

coordinates), and the motions of the nuclei and electrons are coupled. The BO approximation is based on the fact that the nuclei are almost 2000 times heavier than electrons and move much more slowly, so that to the electrons they appear "fixed". In the BO approximation, to a high degree of accuracy, we can separate electron and nuclear motion

$$\psi(R,r) = \psi_{el}(r;R)\psi_N(R) \tag{2.2}$$

where the electronic wavefunction depends on the nuclear coordinates only parametrically. We start with the Schrödinger equation

$$H\psi(R,r) = E\psi(R,r) \ . \tag{2.3}$$

In the BO approximation [Cramer-04], the T_N term is taken as independent of electrons in the Hamiltonian and the V_{eN} term becomes constant for a fixed R. Note that even with the separated wavefunction equation (2.3) cannot be solved exactly (except for simplest molecule H_2^+) and further approximations has to be made.

A. Electronic Schrödinger equation

Under the BO approximation we can solve the electronic part of the Schrödinger equation separately:

$$H_{el}\psi_{el}(r;R) = E_{el}\psi_{el}(r;R) \tag{2.3a}$$

with the electronic Hamiltonian

$$H_{el}(R) = T_e + V_{eN} + V_{ee} = -\frac{1}{2}\sum_i \nabla_i^2 - \sum_\alpha \sum_i \frac{Z_\alpha e^2}{r_{i\alpha}} + \sum_j \sum_{i>j} \frac{e^2}{r_{ij}} \tag{2.3b}$$

that depends on R only parametrically. The electronic energy E_{el} is not a constant but depends on the nuclear geometry (internuclear distance for diatomic molecules). The solution of the electronic part of the Schrödinger equation (2.3) for different geometry (internuclear distance) leads to the potential energy surfaces

$$V(R) = E_{el} + V_{NN} \tag{2.3c}$$

where V_{NN} is given in equation (2.1).

B. Nuclear Schrödinger equation

Once we have the potential energy surface, we can solve the nuclear Schrödinger equation that describes the nuclei in the average field generated by the fast moving electrons:

$$H_N\psi_N(R) = E_N\psi_N(R) \tag{2.3b}$$

where $H_N = T_R + V(R) + V_{eN}$ is the total energy of the molecule in BO. Note that each electronic state corresponds to a different potential energy surface.

2.2. Hartree-Fock method and SCF procedure

While in BO approximation the Hamiltonian is separated in electronic and nuclear parts, it is still not possible to solve the electronic part (equation (2.3a)) exactly for complicated molecules. Thus, it is necessary to make more approximations. One of the popular approaches is the Hartree–Fock self consistent field method (HF-SCF) [Hartree-28, Atkins-05]. This method gives an approximate solution of the electronic Schrödinger equation (2.3a) using the Hamiltonian H_{el} as obtained from the Born–Oppenheimer approximation.

Till now we have assumed that we could solve the electronic Schrödinger equation. But the last term V_{ee} in the Hamiltonian (2.1), which depends on electron-electron separation, is problematic in the calculations. As a first step we are going to ignore this term and solve the Schrödinger equation for *n* electrons

$$H^0\psi^0 = E^0\psi^0 \quad ; \quad H^0 = \sum_{i=1}^{n} h_i \tag{2.4}$$

where

$$h_i = -\frac{1}{2}\nabla_i^2 - \sum_k \frac{Z_k}{r_{ik}} \tag{2.4a}$$

is the so-called *core Hamiltonian* for electron *i* in the field of a nucleus of charge Z_k [Szabo-82, Atkins-05]. The *n* electron equation (2.4) can be separated into *n* one-electron equations with ψ^0 as a product (*Hartree product*) of the one-electron $\psi_\alpha^0(i)$ wavefunctions (orbitals):

$$h_i\psi_\alpha^0(i) = E_\alpha^0\psi_\alpha^0(i); \quad \psi^0 = \psi_\alpha^0\psi_\beta^0 \ldots \psi_\omega^0 \tag{2.5}$$

with $E_\alpha{}^0$ the energy of an electron in the α-th orbital. Note that simplified notation $\psi_\alpha^0(i)$ is introduced for the orbital $\psi_\alpha^0(r_i)$ occupied by electron *i* with coordinate r_i. Applying the Pauli principle, the product wavefunction ψ^0 is symmetrized or antisymmetrized, depending on the symmetry of the total spin wavefunction leading to the Slater determinants in place of ψ^0. Introducing spin-orbitals as a product of the spin wavefunctions and the orbital wavefunctions, the wavefunctions ψ^0 can be written in terms of the Slater determinant as:

$$\psi^0(r,R) = (n!)^{-0.5}\begin{bmatrix} \phi_1(1) & \phi_2(1) & \cdots & \phi_n(1) \\ \phi_1(2) & \phi_2(2) & & \phi_n(2) \\ \vdots & & \ddots & \vdots \\ \phi_1(n) & \phi_2(n) & \cdots & \phi_n(n) \end{bmatrix} \tag{2.6}$$

where $\phi_\alpha(i)$ are orthonormal spin-orbitals of electron *i* with the indices corresponding to the spin states as well as spatial states. The single particle $\phi_\alpha(i)$ wavefunctions are determined by minimizing the *Rayleigh* ratio:

$$E = \frac{\langle \psi_{el}(\vec{r};R)|H_{el}|\psi_{el}(\vec{r};R)\rangle}{\langle \psi_{el}(\vec{r};R)|\psi_{el}(\vec{r};R)\rangle}. \tag{2.6a}$$

Execution of this procedure leads to the equations for each spin-orbitals $\phi_\alpha(i)$.

Up to this point, the electron-electron repulsion has been neglected. In the *Hartree-Fock method* the electron-electron repulsion is included in an averaged way, meaning that each electron is moving in the average field of the other electrons and the nuclei. The HF equation for a spin-orbital $\phi_\alpha(1)$ occupied by electron 1 is

$$f_1\phi_\alpha(1) = \varepsilon_\alpha\phi_\alpha(1) \tag{2.7}$$

with spin-orbital energy ε_α and HF operator f_1 instead of the Hamiltonian:

$$f_1 = h_1 + \sum_\mu\{J_\mu(1) - K_\mu(1)\} \tag{2.8}$$

where the sum is over all spin-orbitals $\alpha, \beta, \ldots, \omega$, h_1 is core Hamiltonian of electron 1, and the *Coulomb operator* $J_\mu(1)$ and *exchange operator* $K_\mu(1)$ are defined as

$$J_\mu(1)\phi_\alpha(1) = \int \phi_\mu^*(2)\frac{1}{r_{12}}\phi_\mu(2)dr_2\phi_\alpha(1) \tag{2.9}$$

$$K_\mu(1)\phi_\alpha(1) = \int \phi_\mu^*(2)\frac{1}{r_{12}}\phi_\alpha(2)dr_2\phi_\mu(1) \tag{2.10}$$

Note that if the Hartree-Fock equation is written for spatial orbitals a factor of 2 emerges in front of the Coulomb operator; each spatial orbital is doubly occupied [Atkins-05]. The Coulomb operator reflects the electron-electron Coulombic repulsion, and the exchange operator takes into account the electron exchange energy including spin correlation effects.

For each spin-orbital the HF equation (2.7) need to be solved, but for that one needs to know the Coulomb and exchange operators that depend on spin-orbitals of n-1 other electrons. Thus the solution of (2.7) needs to be known up front. This dilemma is solved with *self-consistent field* (SCF) method [Cramer-04]. The SCF procedure is as follows:

1. Construct trial spin-orbitals.
2. Construct HF operator.
3. Solve the Hartree-Fock equations; obtain a new set of spin-orbitals.
4. Construct the new HF operator with the new spin orbitals and again solve the HF equations.

5. Check convergence (usually the energies of HF wavefunctions are compared and if the difference is less than, say, 10^{-6} a.u. the result is considered to be converged).

Roothaan suggested using an expansion of the spin-orbitals (more correctly spatial part of the orbitals) in terms of known basis set functions (for example Gaussian basis sets (see Section 2.3 for the basis sets)), which leads to the HF-SCF method for molecules [Roothaan-51].

The HF equation for spatial orbital $\psi_\alpha(1)$ with electron 1 can be written as

$$f_1\psi_\alpha(1) = \varepsilon_\alpha\psi_\alpha(1) \tag{2.11}$$

with HF operator for spatial orbitals $f_1 = h_1 + \sum_\mu\{2J_\mu(1) - K_\mu(1)\}$ [Atkins-05]; where the $J_\mu$and K_μ operators are defined for spatial orbitals. Each spatial orbital can be expanded in terms of n basis Roothaan basis functions φ_j

$$\psi_i = \sum_{j=1}^{n} a_{ij}\varphi_j \tag{2.12}$$

with unknown a_{ij} coefficients. For molecules the orbitals are called molecular orbitals (MOs).

Substituting (2.12) in (2.11), multiplying both sides of the equation by $\varphi_i^*(1)$, and integrating over the electronic coordinates r_1 leads to

$$\sum_{j=1}^{n} a_{\alpha j}\int \varphi_i^*(1)f_1\varphi_j(1)dr_1 = \varepsilon_\alpha\sum_{j=1}^{n} a_{\alpha j}\int \varphi_i^*(1)\varphi_j(1)dr_1 \tag{2.13}$$

Introducing the overlap matrix S and Fock matrix F

$$S_{ij} = \int \varphi_i^*(1)\varphi_j(1)dr_1 \tag{2.14}$$

$$F_{ij} = \int \varphi_i^*(1)f_1\varphi_j(1)dr_1 \tag{2.15}$$

equation (2.13) becomes

$$\sum_{j=1}^{n} F_{ij}a_{\alpha j} = \varepsilon_\alpha\sum_{j=1}^{n} S_{ij}a_{\alpha j}\ ; \quad or \quad \boldsymbol{Fa} = \boldsymbol{Sa\varepsilon} \tag{2.16}$$

where $\boldsymbol{\varepsilon}$ is an *n* x *n* diagonal matrix with elements ε_α and $\boldsymbol{a}$ is an *n* x *n* matrix with elements of a_{ij}. Equation (2.16) is called the *Roothaan equation*. In order to determine MOs the Roothaan equation needs to be solved. To obtain nontrivial solutions of the Roothaan equations the following secular equation need to be solved with the SCF method (**F** and **S** depend on the MO):

$$|\boldsymbol{F} - \varepsilon_\alpha\boldsymbol{S}| = 0 \tag{2.17}$$

Let us write F_{ij} explicitly:

$$F_{ij} = h_{ij} + \sum_{\mu,k,l} P_{kl}[(ij|kl) - \tfrac{1}{2}(il|kj)] \tag{2.18}$$

where the *density matrix* elements are defined as $P_{kl} = 2\sum_\mu a_{k\mu}^* a_{l\mu}$ and the *one-electron integrals* h_{ij} and *two-electron integrals* $(ij|kl)$ are defined as:

$$h_{ij} = \int \varphi_i^*(1)h_1\varphi_j(1)dr_1 \tag{2.18a}$$

$$(ij|kl) = a^*_{k\mu} a_{l\mu} \int \varphi^*_i(1)\varphi_j(1)\varphi^*_k(2)\frac{1}{r_{12}}\varphi^*_k(2)\varphi_l(2)dr_1 dr_2 \qquad (2.18b)$$

The schematic of the SCF procedure is given in Fig. 2.1. First, the trial set of Roothaan basis functions and initial orbitals with initial $a_{i\alpha}$ coefficients need to be chosen to construct ψ_i (2.12) and, using equations (2.14) and (2.15), to calculate the overlap and Fock matrices. Then, the Slater determinant (2.17) is solved for the energies ε_α and coefficients $a_{i\alpha}$. Using this new set of coefficients, the process is started again and continued until the convergence criteria are reached (usually energies are compared at every step and the result is considered converged if the difference is less than 10^{-6}). During this iteration process, one-electron integrals are calculated once, but two-electron integral indices run over the total number of basis functions and in principle need to be calculated n^4 times. Thus, the choice of basis set functions is very important, meaning that one cannot use an excessively large set in the calculations.

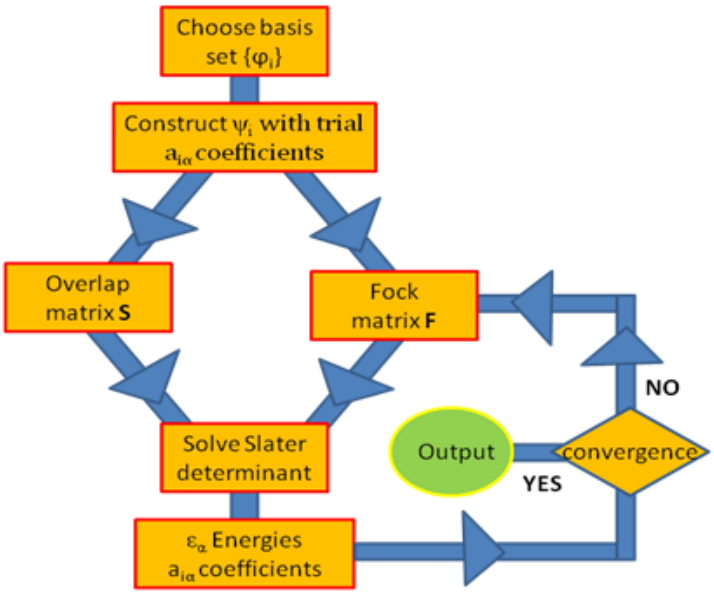

Figure 2.1 ***The schematic of the SCF procedure.***

To summarize, the Hartree-Fock method is variational and uses a variational wavefunction in the form of the single Slater determinant. Slater determinant, on the other hand, is built from the complete set of spin-orbitals. By variation of the set of coefficients in the Slater determinant in addition to the simultaneous variation of MO coefficients in the basis set expansion, the total electronic wavefunction is obtained with the lowest possible energy for a given set of orbitals.

2.3. Basis sets

From HF theory, the energy (HF limit) that can be reached in the limit of infinite basis set is well defined. As already mentioned, one cannot use infinite basis sets in the calculation, thus optimizing the mathematical functions (basis sets) that allow reaching the HF limit is very important. Using finite basis sets generates basis-set *truncation errors*. Choosing the finite basis set that minimizes this error is important.

The basis set is the set of mathematical functions from which the wavefunction (spatial orbital) is constructed. While choosing the basis sets one needs to keep in mind that the number of two-electron integrals increases as n^4, n being the number of basis functions; truncation error needs to be minimal; and, finally, the basis functions need to be physical, meaning that these functions need to have larger amplitudes where electron probability density is high. In general, many different kinds of basis sets could be used. Two common choices are described below.

2.3.1 Slater type orbitals

Mathematically, Slater type orbitals (STOs) that neglect radial nodes are neglected [Slater-30] written as

$$\phi_{nlm}(r,\theta,\phi;\xi) = Nr^{n^*-1}e^{-\xi r}Y_l^m(\theta,\phi) \tag{2.19}$$

where $Y_l^m(\theta,\phi)$ are spherical harmonics depending on angular momentum quantum numbers l and m, ξ can be chosen from the Slater rules [Slater-30] and is related to the effective charge as $\xi=Z_{eff}/n^*$, n^* is the effective principal quantum number and is related to the true principal quantum number as follows: $n\rightarrow n^*$: 1→1, 2→2, 3→3, 4→3.7, 5→4, 6→4.2…, and the normalization constant is given as $N = \frac{(2\xi)^{n^*+0.5}}{[(2n^*)!]^{0.5}}$. The effective charge is defined as $Z_{eff} = Z - \sigma$, where Z is the atomic number and σ is the shielding or screening constant. The screening constant can be evaluated using Slater rules [Slater-30]:

For each group of electrons (for a given principal quantum number grouped as (1*s*)(2*s*,2*p*)(3*s*,3*p*) (3*d*) (4*s*,4*p*) (4*d*) (4*f*) (5*s*,5*p*) ... the shielding constant is a sum of the following contributions:

(i) All the other electrons in the same group as the electron of interest shield an amount of $\sigma = 0.35$ except for the 1s group where the contribution amounts to 0.30.

(ii) For the (s, p) type of group, the shield amount is 0.85 from each (n-1) and 1.00 from (n-2) and lower shell electrons.

(iii) For group types (d) and (f) the shield amount is 1.00 from all the electrons below the one of interest.

For example, consider nitrogen with electronic configuration ($1s^2$) ($2s^2$, $2p^3$). The screening constant and effective nuclear charge for each electron can be calculated using Slater rules:

2p electron: $\sigma = (4\times0.35) + (2\times0.85) = 3.10$ $Z_{eff} = Z - \sigma = 7 - 3.10 = 3.90$

2s electron: $\sigma = (4\times0.35) + (2\times0.85) = 3.10$ $Z_{eff} = Z - \sigma = 7 - 3.10 = 3.90$

1s electron: $\sigma = (1\times0.30) = 0.30$ $Z_{eff} = Z - \sigma = 7 - 0.30 = 6.70$

The farthest electron from the core "sees" the least positive charge of the nucleus. The calculated screening constants and effective charges are summarized in Clementi *et al*. [Clementi-63].

At larger distances from the nucleus, STO basis sets very closely approximate hydrogen-like atomic orbitals. However, for different systems such as molecules with more than two atoms, the STOs are not practical.

2.3.2 Gaussian type orbitals

Gaussian type orbitals (GTOs), proposed by S. F. Boys [Boys-50] make *ab-initio* calculations computationally more effective compared with STOs.

A GTO in Cartesian coordinates is written as

$$\phi_{ijk}(x, y, z; \alpha) = N x^i y^j z^k e^{-\alpha(x^2+y^2+z^2)} \tag{2.20}$$

where *i*, *j* and *k* are positive integers, α is the positive exponent controlling the width of the GTO, and the normalization constant is $N = \left(\frac{2\alpha}{\pi}\right)^{3/4} \left[\frac{(8\alpha)^{i+j+k} i!j!k!}{(2i)!(2j)!(2k)!}\right]^{1/2}$. The orbitals are called *s*- type orbitals if $i = j = k = 0$, *p*-type if $i = j = k = 1$, and *d*-type when $i = j = k = 2$.

The "Gaussian product theorem" puts GTO at an advantage compared with STO in terms of computational speed. According to the theorem, the product of two GTOs centered on two different centers is equivalent to the Gaussian function centered on a point along the axis connecting them. Thus, for example, four-center integrals are reduced to two-center integrals, and eventually one-center integrals. However, GTOs have its disadvantages also. For instance, a

single GTO basis function has significant errors when compared to a single STO, especially near the nucleus.

2.3.3 Contracted Gaussian functions

Using GTOs (for atoms and molecules) two-electron integrals are calculated very effectively (compared with STO), but are not optimal basis sets and have different functional behavior (especially near and far from nucleus) from the behavior of molecular orbitals. Thus, a better basis set is preferable. Hehre, Stewart, and Pople had the idea to linearly combine GTOs to approximate STOs to produce the so-called contracted Gaussian functions [Pople-69].

A number of GTOs- called *primitives*- are linearly combined, each with different α values, and normalized to give a "contracted" Gaussian function,

$$G_c = \sum_{i=1}^{M} c_i G_p \tag{2.21}$$

where G_p is a primitive Gaussian, M the number of Gaussians, and the c_i are contraction coefficients **[**Pople-69]. The contraction coefficients are optimized to mimic STOs. The term used for the "contracted" Gaussian functions is STO-MG (Single-ζ [Cramer-04]) where M is the number of primitive GTOs used. For example, for STO-3G three primitive GTOs are used per AO or MO.

2.4. Configuration interaction

Until now, the electron correlation term has been treated in an averaged way, such that each electron is moving in an averaged field of nuclei and other (n-1) electrons, leading to the Hartree-Fock SCF procedure. Improving inclusion of electron correlation is an ongoing task in electronic structure calculations. The first choice is to construct a wavefunction using not one but many Slater determinants or so called "configuration state functions" (CSF). The exact electronic wavefunction can be written as:

$$\psi_{el} = \sum_i \ A_i \varphi_i \tag{2.22}$$

where the sum is over finite number (in all applications) of determinants φ_i (over all configurations of the orbitals) and A_i are expansion coefficients. This *ab-initio* method, in which the total electronic wavefunction is expressed as a linear combination of the Slater determinants, is known as "configuration interaction" (CI). It includes electron correlation neglected in the HF

method. Ideally one would need to use an infinite number of Slater determinants and also an infinite number of basis sets to obtain an exact solution of the time independent Schrödinger equation as shown schematically in Fig. 2.2, but this is computationally impossible and the infinite sum in (2.22) is truncated at some point. Existing *ab-initio* methods (for example the MCSCF-method) provide a systematic approach to the solution of the time-independent Schrödinger equation (Fig.2.2) (Chapter 2.5).

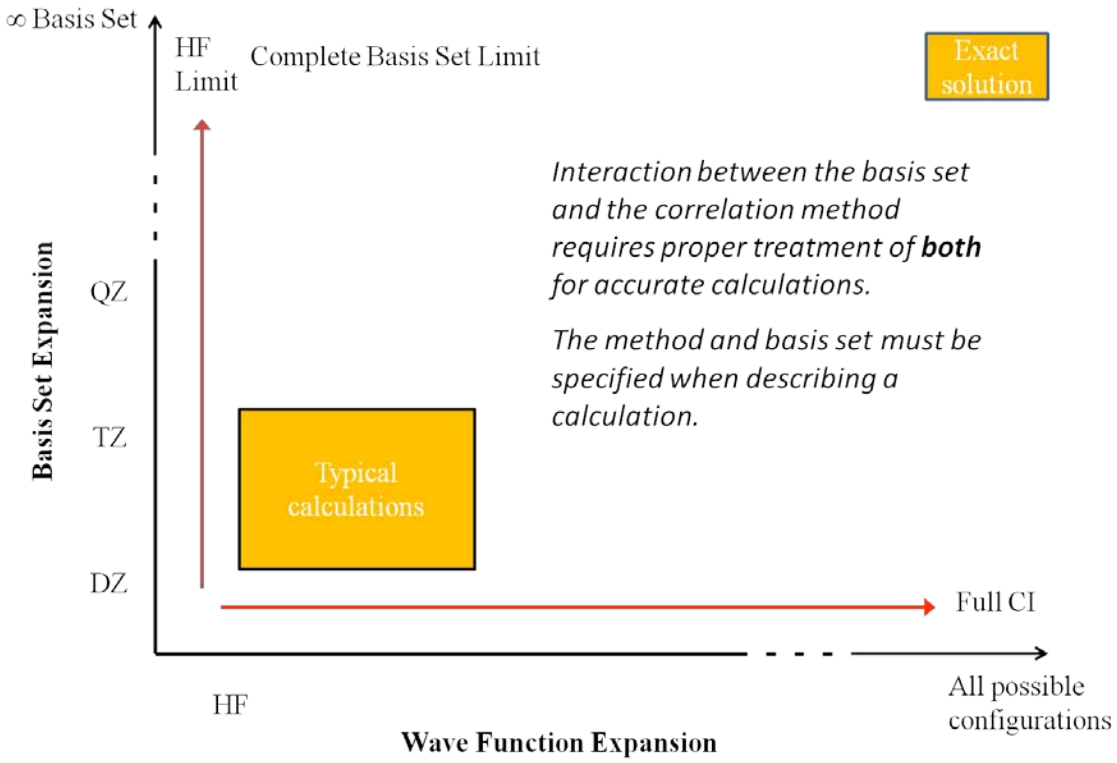

Figure 2.2. ***Schematic of a systematic approach to the exact solution of the time-independent Schrödinger Equation.***

2.5. Multiconfiguration self-consistent field (MCSCF) method

In MCSCF calculations a (finite) linear combination of CSFs (or configurations of Slater determinants) is used to approximate the exact electronic wavefunction of a system, in contrast

to the HF method, where only one determinant is used. The Slater determinants (configurations) correspond to the possible electron occupation of different molecular orbitals (MOs).

$$\psi_{el} = \sum_i^N A_i \varphi_i \tag{2.23}$$

Such a wavefunction is called 'multiconfiguration self-consistent-field' (MCSCF) wavefunction, in which the basis functions are optimized for a *combination* of configurations. By a variation of the set of expansion coefficients (A_i) in the CSFs or determinants, in addition to the MO coefficients (a_{ij}), the total electronic wavefunction is obtained with the lowest possible energy [Hinze-67].

In MCSCF calculations, the specification of how many MOs are occupied is crucial. One needs to specify the so-called "active" space. MCSCF active space choices are often abbreviated as '(*m*,*n*)' where *m* is the number of electrons and *n* is the number of orbitals (see chapter 5 for the calculations of potential curves of the oxygen molecular ion, and Appendix E for an input-output example).

Chapter 3 - THEORY AND NUMERICAL METHODS

"It is the theory that decides what can be observed".
Albert Einstein 1921.

In this chapter the theory and the numerical methods used in our calculations are summarized.

3.1 Time-dependent Schrödinger equation

In 1926 the basic equation of quantum mechanics was introduced by Erwin Schrödinger (1887-1961). The solution of the equation is the wavefunction, which is used to describe, for example, atoms or molecules in intense laser fields, collisions, or interactions with metal surfaces.

For describing molecular dynamics in intense laser fields, one needs to solve the time dependent Schrödinger equation (TDSE). The single-particle three-dimensional TDSE has the form:

$$i\frac{\partial}{\partial t}\Psi(\vec{r},t) = \hat{H}\Psi(\vec{r},t) \tag{3.1}$$

where atomic units have been used with e = ħ = m_e = 1 (Appendix F), and typically the Hamiltonian is given as:

$$\hat{H} = \hat{T} + \hat{V} = -\frac{\nabla^2}{2} + \hat{V}(\vec{r},t) \tag{3.2}$$

where $\hat{T}$ is kinetic energy and $\hat{V}$ is potential energy operator of the system. If the Hamiltonian is time independent (3.1) can be integrated to obtain:

$$\Psi(\vec{r},t) = \exp\left(-i\hat{H}t\right)\Psi(\vec{r},0) \ . \tag{3.3}$$

Introducing small time intervals Δt such that $t = N\Delta t$ and the full time dependence of the wave packet is obtained by iteratively propagating each of the N time step:

$$\Psi(\vec{r},t+\Delta t) = \exp\left(-i\hat{H}\Delta t\right)\Psi(\vec{r},t) + \mathcal{O}(\Delta t^2) \tag{3.4}$$

3.1.1. Crank-Nicholson split operator method (C-N method)

The *Crank-Nicolson* (CN) method is a finite difference method which is used to solve differential equations such as the TDSE. It is unconditionally stable [Press-92].

For a particle in an external field $V(r,t)$, the Hamiltonian is given as equation (3.2). Since the kinetic T and potential V energy operators do not commute, the sum in the exponent in equation

(3.4) cannot be written as a product of the exponential functions containing only *V* and only *T* operators. Therefore the *Baker–Campbell–Hausdorff* formula [Reinsch-00, Bialynicki-69, Niederhausen-07] is applied which gives:

$$\exp\left(-\left(\hat{T}+\hat{V}\right)\Delta t\right)=\exp\left(-\hat{V}\Delta t/2\right)\exp\left(-i\hat{T}\Delta t\right)\exp\left(-\hat{V}\Delta t/2\right)+\mathcal{O}(\Delta t^3).$$

This expression is called the *split-operator* method and is accurate up to errors of the order Δt^3. Using *Cayley's* form for expressing the exponent in (3.3a) for a time step Δt

$$\exp\left(-i\hat{H}\Delta t\right)=\frac{1-\frac{1}{2}i\hat{H}\Delta t}{1+\frac{1}{2}i\hat{H}\Delta t} \tag{3.5}$$

one can obtain:

$$\Psi(t+\Delta t)\left(1+\frac{1}{2}i\hat{H}\Delta t\right)=\Psi(t)(1-\frac{1}{2}i\hat{H}\Delta t)\,. \tag{3.6}$$

Let us assume that the time independent Hamiltonian has the form:

$$\hat{H}=A\frac{\partial^2}{\partial x^2}+B\frac{\partial}{\partial x}+CV(x) \tag{3.7}$$

where A, B and C are constants, *V* potential energy. Using so called three-point formulas for the differentials

$$\frac{\partial}{\partial x^2}\Psi_n=\frac{\Psi_{n+1}-2\Psi_n+\Psi_{n-1}}{\Delta x^2}\quad\text{and}\quad\frac{\partial}{\partial x}\Psi_n=\frac{\Psi_{n+1}-\Psi_{n-1}}{2\Delta x} \tag{3.8}$$

(where n stands for the grid point number in the *x* direction) one obtains by combining (3.7) and (3.5)

$$\begin{aligned}\Psi_n(t+\Delta t)+i\frac{\Delta t}{2}\Bigg(A_n\frac{\Psi_{n+1}(t+\Delta t)-2\Psi_n(t+\Delta t)+\Psi_{n-1}(t+\Delta t)}{\Delta x^2}\\+B_n\frac{\Psi_{n+1}(t+\Delta t)-\Psi_{n-1}(t+\Delta t)}{2\Delta x}+V_n\Psi_n(t+\Delta t)\Bigg)=\\=\Psi_n(t)-i\frac{\Delta t}{2}\left(A_n\frac{\Psi_{n+1}(t)-2\Psi_n(t)+\Psi_{n-1}(t)}{\Delta x^2}+B_n\frac{\Psi_{n+1}(t)-\Psi_{n-1}(t)}{2\Delta x}+V_n\Psi_n(t)\right)\end{aligned} \tag{3.9}$$

which is a tridiagonal matrix equation:

$$\begin{bmatrix} X_1^2 & X_1^3 & 0 & & & 0 & 0 & 0 \\ X_2^1 & X_2^2 & X_2^3 & \cdots & & 0 & 0 & 0 \\ 0 & X_3^1 & X_3^2 & & & 0 & 0 & 0 \\ & \vdots & & \ddots & & \vdots & & \\ 0 & 0 & 0 & \cdots & X_{N-1}^1 & X_{N-1}^2 & X_{N-1}^3 & \\ 0 & 0 & 0 & & 0 & X_N^1 & X_N^2 & \end{bmatrix} \begin{pmatrix} \Psi_1(t+\Delta t) \\ \Psi_2(t+\Delta t) \\ \Psi_3(t+\Delta t) \\ \vdots \\ \Psi_{N-1}(t+\Delta t) \\ \Psi_N(t+\Delta t) \end{pmatrix} =$$

$$= \begin{bmatrix} Y_1^2 & Y_1^3 & 0 & & & 0 & 0 & 0 \\ Y_2^1 & Y_2^2 & Y_2^3 & \cdots & & 0 & 0 & 0 \\ 0 & Y_3^1 & Y_3^2 & & & 0 & 0 & 0 \\ & \vdots & & \ddots & & \vdots & & \\ 0 & 0 & 0 & \cdots & Y_{N-1}^1 & Y_{N-1}^2 & Y_{N-1}^3 & \\ 0 & 0 & 0 & & 0 & Y_N^1 & Y_N^2 & \end{bmatrix} \begin{pmatrix} \Psi_1(t) \\ \Psi_2(t) \\ \Psi_3(t) \\ \vdots \\ \Psi_{N-1}(t) \\ \Psi_N(t) \end{pmatrix} \tag{3.10}$$

N is the total number of grid points in the *x* direction and the matrix elements are:

$$\begin{aligned} X_n^1 &= i\frac{\Delta t}{2(\Delta x)^2}A_n - i\frac{\Delta t}{4\Delta x}B_n \\ X_n^2 &= 1 - i\frac{\Delta t}{(\Delta x)^2}A_n + i\frac{\Delta t}{2}V_n \\ X_n^3 &= i\frac{\Delta t}{2(\Delta x)^2}A_n + i\frac{\Delta t}{4\Delta x}B_n \\ Y_n^1 &= -i\frac{\Delta t}{2(\Delta x)^2}A_n + i\frac{\Delta t}{4\Delta x}B_n \\ Y_n^2 &= 1 + i\frac{\Delta t}{(\Delta x)^2}A_n - i\frac{\Delta t}{2}V_n \\ Y_n^3 &= -i\frac{\Delta t}{2(\Delta x)^2}A_n - i\frac{\Delta t}{4\Delta x}B_n \end{aligned} \tag{3.11}$$

This system of equations is solved using the TRIDIAG routine (adjusted to double precision) from Numerical Recipes [Press-92] (see also [Niederhausen-07]).

3.1.2 FFT method

There is another method to do time evolution of the wave packet instead of the CN method. This method involves transforming the Schrödinger equation into momentum space where the momentum operator and kinetic energy operator are multiplicative operators.

$T + V(x,t) = p^2/2m + V(x,t)$. Using (3.4) and the split-operator method results in:

$$\Psi(x, t+\Delta t) = \exp\left(-i\frac{V}{2}\Delta t\right)\exp\left(-i\frac{p^2}{2m}\Delta t\right)\exp\left(-i\frac{V}{2}\Delta t\right)\Psi(x,t) \tag{3.12}$$

The procedure of time evolution of the wave packet is as follows: the first step is to multiply the wave packet by the exponent containing the potential energy; the second step is to

Fourier transform the product and multiply that by the exponent containing the momentum operator; the last step to inverse Fourier transform the product and multiply that by the third exponent containing the potential energy.

3.2 Imaginary time propagation

Imaginary time propagation is a reliable method for obtaining the ground state of the system. The wavefunction in (3.1) can be expanded as a superposition of eigenstates φ_v:

$$\Psi(\vec{\mathbf{r}}, t) = \sum_v a_v \varphi_v(\vec{r}) e^{-iE_v t} \tag{3.13}$$

By substituting $t \rightarrow -i\tau$, the time evolution equation (3.3) leads to an exponential decay of the wavefunction

$$\Psi(\vec{r}, \tau) = \exp\left(-\hat{H}\tau\right) \Psi(\vec{r}, 0) = \sum_v a_v \varphi_v(\vec{r}) e^{-E_v \tau} \tag{3.14}$$

When propagated in imaginary time the eigenfunctions decay exponentially with a rate given by their energies. The ground state decays slowest. Thus, starting with a randomly chosen wavefunction Ψ, in the limit of large τ, the wavefunction will be proportional to the ground state

$$\lim_{\tau \to \infty} \Psi(\vec{r}, \tau) = a_0 \varphi_0 e^{-iE_0 \tau} \tag{3.15}$$

After choosing an initial trial wavefunction the imaginary time propagation is carried out using the CN propagation method until the ground state wavefunction is obtained to predetermined accuracy.

3.3 Absorbers

In the simulation it is impossible to make an infinite numerical grid. It always has limits that could cause reflection of the wave packet. There are several methods for avoiding this reflection including complex rotation [Ho-83], splitting the wavefunction at the boundaries [Chelkowski-96], and a negative imaginary potential [Hussain-00, Poirier-03, Muga-04]. The last method- negative imaginary potential - is the one used in our calculations.

A negative imaginary potential $-iW(r)$ is added to the Hamiltonian

$$H_{tot} = H + H_a = H - iW(r) \tag{3.16}$$

where H is the original Hamiltonian (see equation (3.2) for example) and H_a is the negative imaginary potential, called “absorbers” [Niederhausen-07].

3.4 Coupled channel propagation

The Crank-Nicolson scheme described above can be applied to systems including propagation of the coupled wave packets on two or more potential curves. This application for the motion of the nuclear wave packet on two BO potential curves – coupled with dipole coupling matrix elements – is given in Chapters 4, 5 and 6.

In general there can be any number of coupled channels, but the case of three coupled wavefunctions is discussed below. The TDSE for the nuclear part of the wavefunction in the case of the three states can be written as:

$$-i\frac{d}{dt}\begin{pmatrix}\Psi_1(R)\\ \Psi_2(R)\\ \Psi_3(R)\end{pmatrix} = (\hat{H}+\hat{H}_c)\begin{pmatrix}\Psi_1(R)\\ \Psi_2(R)\\ \Psi_3(R)\end{pmatrix} \tag{3.17}$$

where the Hamiltonian $\hat{H} = \hat{T} + \hat{V}$ corresponds to the wave packet propagation discussed in previous sections (Chapter 2.1) and $\hat{H}_c$ accounts for the coupling of wave packets propagating on given states. Note that notation is changed, we dropped subscript *N* for nuclei ($\psi_N\,(R)$) and now Ψ_i(R) (i =1,2,3) refers to a nuclear wavefunction in each state (in this case three). Note that the phases between the wave functions in (3.17) do not matter because we are considering the phase of the electronic wavefunction.

The Hamiltonian of the uncoupled system is given by a tridiagonal matrix. The total Hamiltonian of the coupled system is therefore given by a block matrix, where the diagonal blocks are tridiagonal and the off-diagonal blocks, which introduce the coupling, are diagonal

$$\hat{H}_{tot} = \hat{H} + \hat{H}_c = \begin{pmatrix}\boxed{\backslash\backslash\backslash} & \boxed{\backslash} & \boxed{\backslash}\\ \boxed{\backslash} & \boxed{\backslash\backslash\backslash} & \boxed{\backslash}\\ \boxed{\backslash} & \boxed{\backslash} & \boxed{\backslash\backslash\backslash}\end{pmatrix} =$$

$$= \begin{pmatrix}\boxed{\backslash\backslash\backslash} & \boxed{} & \boxed{}\\ \boxed{} & \boxed{\backslash\backslash\backslash} & \boxed{}\\ \boxed{} & \boxed{} & \boxed{\backslash\backslash\backslash}\end{pmatrix} + \begin{pmatrix}\boxed{} & \boxed{\backslash} & \boxed{\backslash}\\ \boxed{\backslash} & \boxed{} & \boxed{\backslash}\\ \boxed{\backslash} & \boxed{\backslash} & \boxed{}\end{pmatrix} \tag{3.18}$$

Note that if $\hat{H}_c = 0$ wave packets propagate on each state separately (no coupling). The wave packet time evolution is achieved by the split-operator scheme at each time step:

$$\exp(-iH_{tot}\Delta t) = \exp\left(-iH_c\frac{\Delta t}{2}\right)\exp(-iH\Delta t)\exp\left(-iH_c\frac{\Delta t}{2}\right) + \mathcal{O}(\Delta t^3) \tag{3.19}$$

The coupling part of the Hamiltonian can be written as a sum of three separate matrices

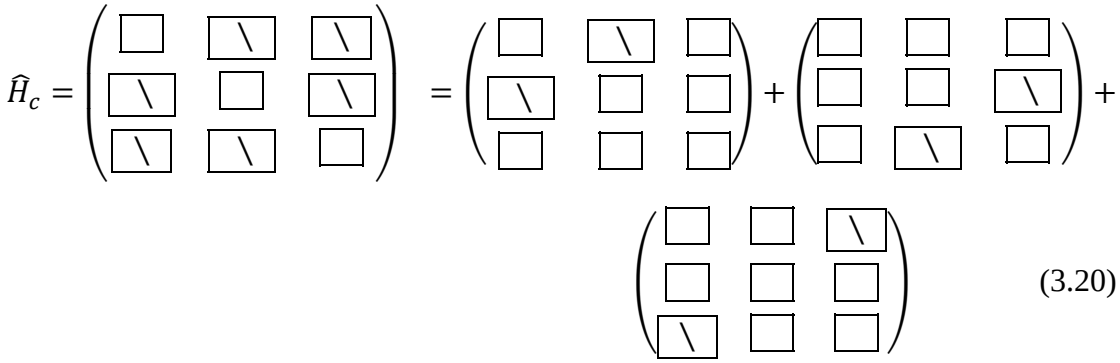

(3.20)

Again using the split-operator technique (3.19), the coupling will reduce to 2x2 couplings $\hat{H}_c^{ij}$ acting only on the two sattes *i* and *j* with $i \neq j$. It can be shown that

$$\exp\left(-i\hat{H}_c^{ij}\frac{\Delta t}{2}\right) = \begin{pmatrix}1 & 0\\ 0 & 1\end{pmatrix} cos\left(D\frac{\Delta t}{2}\right) - i\begin{pmatrix}0 & 1\\ 1 & 0\end{pmatrix} sin\left(D\frac{\Delta t}{2}\right) \qquad (3.21)$$

where $D=d_{ij}E$ is the off-diagonal coupling matrix element corresponding to the coupled states *i* and *j* multiplied by an electric field strength [Niederhausen-07].

Thus the coupling of the wavefunction for the three states can be represented as a successive application of two-channel couplings involving the split-operator scheme, leading to simple rotations of the wavefunction between the two sates. The case of a coupled state calculation for two states of D_2^+ is discussed next (see Chapter 4 for the numerical results using this model).

3.4.1 Two - state model for the nuclear wave packet dynamics in molecular ions

We model the nuclear dynamics in the pump-probe sequence (Fig. 4.1), where pump pulse is ionizing the neutral diatomic molecules and delayed (delay is designated as τ in further discussions) probe pulse can either dissociate (Chapters 4-6) or Coulomb explode the molecular ion (Chapter 7). In our model we assume that the neutral diatomic molecules are singly ionized by an intense short laser field. The quantum state of the resulting molecular ion can be approximated as

$$\Phi(\vec{r}, R; t) = \frac{1}{\sqrt{2}}\left[\Psi_1(R,t)\psi_{el_1}(\vec{r}, R, t) + \Psi_2(R,t)\psi_{el_2}(\vec{r}, R, t)\right] \qquad (3.22)$$

where Ψ_1 and Ψ_2 are nuclear wave-functions, ψ_{el_1} and ψ_{el_2} are the electronic states of the molecular ion in the BO approximation (for example $1s\sigma_g$ and $2p\sigma_u$ states for H_2^+), and $\vec{r}$ is the electron position vector. The bound and dissociating nuclear motions of the molecular ion can be described in this two-electronic-state model by projecting out the electronic states. The Ψ_1 and Ψ_2 nuclear wave-function components can be obtained from a set of coupled equations,

$$i\frac{\partial}{\partial t}\begin{pmatrix}\Psi_1(R,t)\\ \Psi_2(R,t)\end{pmatrix} = \begin{pmatrix} T_R + V_1(R) & d_{12}(R)E(t-\tau)\\ d_{12}(R)E(t-\tau) & T_R + V_2(R)\end{pmatrix} \times \begin{pmatrix}\Psi_1(R,t)\\ \Psi_2(R,t)\end{pmatrix} \qquad (3.23)$$

where μ is the reduced mass of the nuclei, $T_R = -\frac{1}{2\mu}\frac{\partial}{\partial R^2}$, and $V_1(R)$ and $V_2(R)$ are the BO potential curves of the molecular ion. The dipole coupling between the two electronic states in the laser field is defined as $d_{12} = \langle\psi_{el_1}|\vec{r}|\psi_{el_2}\rangle$ [Kulander-96]. The laser field E is linearly polarized along the internuclear axis. Note that the maximal propagation times in our numerical applications are significantly smaller than the rotational periods of the diatomic molecules, therefore, we can neglect the rotation of the molecules.

We assume that the initial state of the molecular ion is bound and solve Eq. (3.23) numerically using the Crank-Nicholson method [Feuerstein-03-1, Press-92, Thumm-08] assuming that

$$\Psi_1(R,0) = \sum_\mu a_\mu \Psi_\mu(R), \qquad \Psi_2(R,0) = 0 \quad , \qquad (3.24)$$

where $\{a_\mu\}$ are the set of amplitudes (in general complex) in the basis of the stationary vibrational eigenstates $\{\Psi_\mu\}$ of the diatomic molecular ion electronic ground-state potential $V_1(R)$. The ionization process is often modeled with Franck-Condon (FC) factors $\{|a_\mu|^2\}$ in the sudden approximation [Bransden-03, Thumm-08, Magrakvelidze-09] and all phases are randomly set to zero in order to obtain the set of real amplitudes $\{a_\mu\}$ for the bound initial wave packet (please see Chapter 6 for the alternative ADK ionization model). Using imaginary time propagation the trial function (for example Gaussian) on the ground-state BO potential curve of the molecule is propagated, and the ground state wavefunction Ψ_0 of the neutral parent molecule is calculated. Subsequent projection on the vibrational states of the molecular ion $\{a_\mu = \langle\Psi_\mu|\Psi_0\rangle\}$ generates the real function $\Psi_1(R,0)$. Without an external laser field, the two states in Eq. (3.23) are decoupled, and the nuclear wavefunction evolves as a bound nuclear wave packet on the V_1 potential curve, undergoing characteristic cycles of dephasing and revival [Feuerstein-03-1, Thumm-08].

3.4.2. Quantum beat spectra (R-dependent power spectra)

Quantum beat (QB) spectra (known also as power spectra [Thumm-08]) are very useful to identify the given potential curve characteristics that are obtained by Fourier transforming the probability density as a function of internuclear distance and propagation time (see Eq. 3.25 below). The oscillation (beating) occurs because the bound nuclear vibrational wavefunctions on a given potential curve undergo dephasing, oscillating at different frequencies. Each of the QB frequencies can be linked to the contributing vibrational energy levels of the vibrational wave packet and, most importantly, the derivative of the molecular potential energy curve can be mapped from the power spectra. The details on how we numerically obtain power spectra are discussed below.

In the two-state model (discussed in 3.4.1), the amplitudes $\{a_\mu\}$ in Eq. (3.24) remain time independent during the field-free propagation from $t = 0$ to the probe time delay τ (Fig. 4.1). The nuclear probability density as a function of time at τ is written as

$$\rho(R,\tau) = \int dr|\Phi(\vec{r},R;\tau)|^2 = \left|\Psi_g(R,\tau)\right|^2 + |\Psi_u(R,\tau)|^2$$
$$= \sum_\mu \left|a_\mu\right|^2 \left|\Psi_\mu(R)\right|^2 + \sum_{\mu\neq\nu} a_\mu^* a_\nu e^{-i(E_\nu - E_\mu)\tau}\Psi_\mu^*(R)\Psi_\nu(R) \qquad (3.25)$$

It is very important to note that the diagonal term (first term in the second line) is time independent and gives an incoherent background to the wavefunction probability density. We subtract this diagonal contribution from the probability density spectra thereby getting rid of static terms in the incoherent sum included in Eq. (3.25). We Fourier transform the remaining coherent (time dependent) terms over the finite sampling time T and take the square of the result, obtaining the power spectrum

$$P(R,\omega;T) = \left|\sum_{\mu,\nu=0}^{N} a_\mu^* a_\nu \Psi_\mu^*(R)\Psi_\nu(R)\delta_T(\Delta\omega_{\mu,\nu} - \omega)\right|^2 \qquad (3.26)$$

where the "broadened delta function" is defined as

$$\delta_T(\Omega) \equiv \frac{1}{2\pi}\int_0^T dt e^{i\Omega t} = \frac{1}{\pi} e^{i\Omega T/2}\frac{\sin(\Omega T/2)}{\Omega} \qquad (2.27)$$

and centered at the QB energies $\Delta\omega_{\mu,\nu}=\omega_\nu-\omega_\mu$. It is broadened due to the Fourier transformation over a *finite* time interval. In the limit of large sampling times, it becomes identical with the usual delta "function", and the power spectrum $P(R, \omega, T)$ reproduces the QB spectrum at

infinite resolution. Further details on the properties and interpretation of $P(R, \omega; T)$ can be found in [Thumm-08].

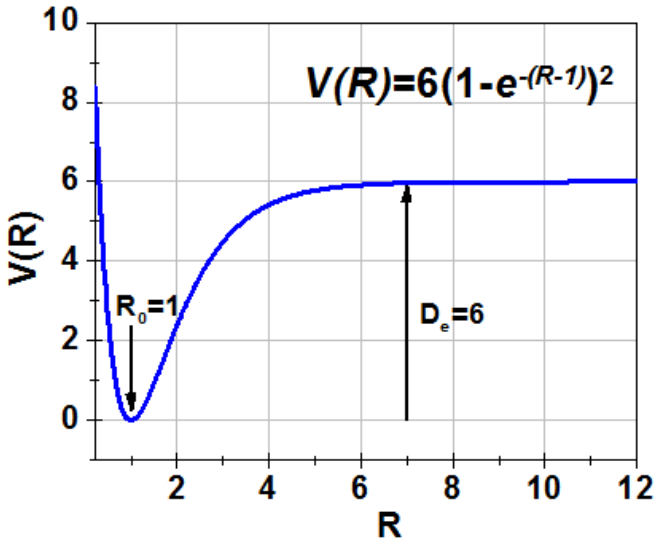

Figure 3.1 ***Morse potential for D_e=6, α=1 and R_0=1.***

3.5 Morse oscillator

The potentials for diatomic molecules are often parameterized using the Morse potential [Morse-29]:

$$V(R) = D_e(1 - \mathrm{e}^{-\alpha(R-R_0)})^2 \tag{3.28}$$

where D_e is the depth of the potential well (often called the dissociation energy), α accounts for the measure of the curvature at the bottom of the well, R is the internuclear distance, and R_0 is the equilibrium bond distance. Figure 3.1 shows the Morse potential (3.28) for parameters D_e=6, α=1 and R_0=1. Actually, Morse proposed a potential in the form [Morse-29]

$$V(R) = D_e\mathrm{e}^{-2\alpha(R-R_0)} - 2D_e\mathrm{e}^{-\alpha(R-R_0)}\,, \tag{3.28a}$$

but since the zero of the potential is relative one can subtract D_e from (3.28a) and obtain (3.28). With the Morse potential, an exact solution of the TDSE can be obtained [Morse-29]. Stationary states on a Morse potential have eigenvalues:

$$E(v) = \omega_0\left(v + \tfrac{1}{2}\right) - \omega_0\chi_0\left(v + \tfrac{1}{2}\right)^2 + \cdots \tag{3.29}$$

where $\omega_0 = \alpha\sqrt{2D_e/\mu}$ is the vibrational constant with the reduced mass μ of the diatomic molecule, and $\chi_0\omega_0 \approx \omega_0^2/(4D_e) = \alpha^2/(2\mu)$ is the anharmonicity constant.

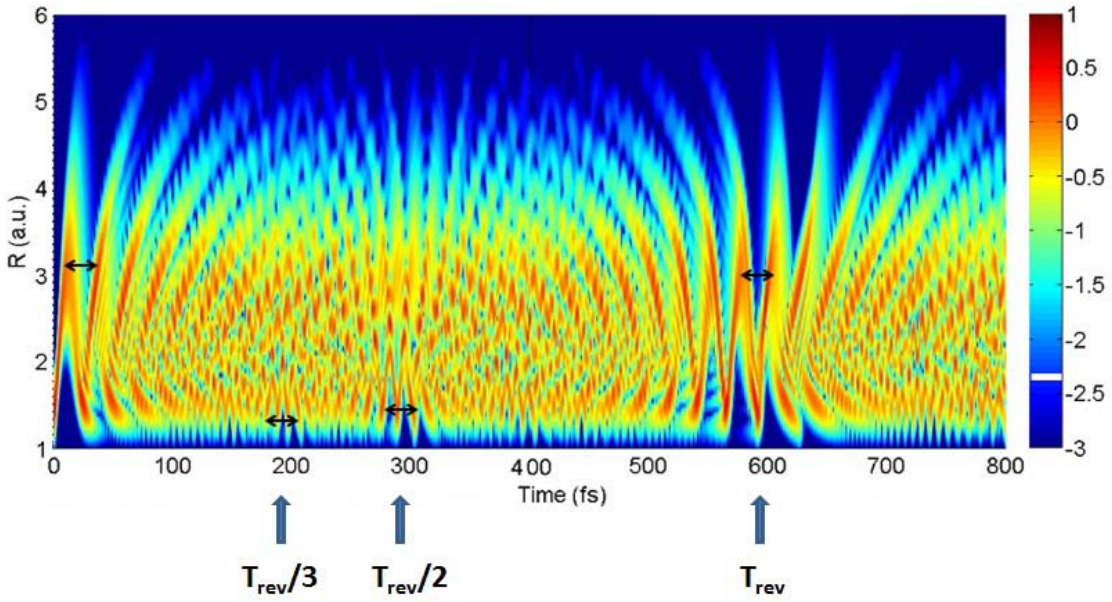

Figure 3.2 ***Probability density as a function of internuclear distance R and propagation time for D_2. Black arrows indicate the oscillation period at the beginning of the propagation. Full and partial revival times are indicated with blue arrows.***

3.6 Quantum revivals

The anharmonicity of the potential results in a quick dephasing of the wave packet, but only certain, possibly long propagation time, the relative phases of the nuclei vibrational wave packet can become similar or identical to the relative phases of the initial wave packet, leading to wavefunction revivals [Robinett-04]. In Fig. 3.2, the dephasing of the wave packet on the ground state of D_2^+, partial (wave packet oscillates at integer fractions of the original oscillation period), and full revivals (wave packet oscillates at the initial oscillation period) are shown [Robinett-04].

For one dimensional systems, the wave packet can be written as a superposition of φ_ν eigenfunctions

$$\Psi(x,t) = \sum_{\nu=0}^{\infty} a_\nu \varphi_\nu(x) e^{-iE_\nu t}, \tag{3.30}$$

where a_v are expansion coefficients (FC amplitudes) and E_v are energy eigenvalues, given by Eq.(3.29) for the Morse potential. At the revival, the condition $\Psi(x, T_{rev}) = \Psi(x, 0)$ needs to be satisfied (up to an overall arbitrary phase factor), which requires

$$E_v T_{rev} = \left\{\omega_0 \left(v + \frac{1}{2}\right) - \omega_0 \chi_0 \left(v + \frac{1}{2}\right)^2\right\} T_{rev} = 2\pi N_v \tag{3.31}$$

where N_v are integers. Equation (3.31) for the next vibrational state can be written as:

$$E_{v+1} T_{rev} = \left\{\omega_0 \left(v + \frac{3}{2}\right) - \omega_0 \chi_0 \left(v + \frac{3}{2}\right)^2\right\} T_{rev} = 2\pi N_{v+1} \tag{3.32}$$

Subtracting (3.31) from (3.32) will lead to:

$$\{\omega_0 - 2\omega_0 \chi_0 v - 2\omega_0 \chi_0\} T_{rev} = 2\pi M_v \tag{3.33}$$

where M_v are also integers. Repeating the same subtraction procedure on Eq.3.33 gives revival time for the Morse potential:

$$T_{rev} = \pi / \omega_0 \chi_0 \tag{3.34}$$

According to equation (3.34) the half, third, quarter and so on fractional revivals are defined as $T_{rev}/2$, $T_{rev}/3$ $T_{rev}/4$..., and wave packet oscillates with corresponding fractional periods (Fig.3.2). Note that if one follows the definition of T_{rev} by [Robinett-04], the result is twice the T_{rev} defined by Eq. (3.34). One can fit any given binding potential curve with a Morse potential to get the Morse parameters and, using Eq. (3.34), calculate the revival time on this potential curve, so that the oscillation period at $T_{rev}/2$ ($T_{rev}/3$) is two (three) times the oscillation period at T_{rev} (see Fig. 3.2).

3.7 KER spectra calculations (FT method)

In order to simulate KER spectra, we numerically propagate the coupled equations (3.23) for a sufficiently long time *T*, including field-free propagation of the nuclear wave packets after the action of the probe pulse. This allows us to separate the bound and dissociating parts of the nuclear motion by introducing the internuclear distance R_1 as an effective range for the bound nuclear motion. The probability current associated with the dissociation of the molecular ion has relevant contributions for $R > R_1$, whereas the bound motion remains restricted to distances $R < R_1$. Fourier transformation of the dissociating parts of the nuclear wave packets over the interval $[R_1, R_{max}]$ yields the momentum representations of the dissociating wave packets in the adiabatic channel *i* [De-11, Magrakvelidze-12-1]

$$\tilde{\Psi}_i^{diss}(P, T) = \int_{R_1}^{R_{max}} dR\, \Psi_i^{diss}(R, T)\, e^{-iPR} \tag{3.35}$$

where R_{max} is related to the size of the numerical grid. By incoherently adding the corresponding momentum distributions, we obtain the pump-probe-delay (τ) - dependent distribution of fragment KERs

$$C^{diss}(E,\tau) \propto \sum_i \rho_i^{incoh}(P,\tau) \tag{3.36}$$

where $E = P^2 / 2M$ is the kinetic energy per fragment. Subtracting the large incoherent static contribution

$$C_{incoh}^{diss}(E) = \frac{1}{T}\int_0^T d\tau C^{diss}(E,\tau) \tag{3.36a}$$

from C_{diss} we obtain the power spectrum as a function of the QB frequency $f = \omega/2\pi$

$$P^{diss}(E,f) = \left|\int_0^T d\tau C_{coh}^{diss}(E,\tau)e^{-i2\pi f\tau}\right|^2 \tag{3.36b}$$

Results using the FT method are given in Chapters 4, 5, and 6 for D_2, and O_2 molecules, and noble gas dimers, respectively.

3.8 Virtual detector

Virtual detector (VD) is a method for extracting momentum distributions without propagating the wave packet over a large numerical grid [Feuerstein-03-1, Magrakvelidze12-1]. The momentum distribution is obtained for each time step at the fixed location and width of the VD. The wavefunction can be written as

$$\Psi(\vec{r},t) = A(\vec{r},t)\exp\left(i\varphi(\vec{r},t)\right) \tag{3.37}$$

where $\varphi(\boldsymbol{r},t)$ and $A(\boldsymbol{r},t)$ are the time-dependent phase and amplitude, respectively. The momentum information at a given detector position $\vec{r}_d$ can be extracted from the phase $\varphi(\boldsymbol{r},t)$. To reveal this information, we consider the current density $\vec{j}$ at $\vec{r}_d$ of the outgoing particles with mass μ,

$$\vec{j}(r_d,t) = \frac{\rho(\vec{r}_d,t)}{\mu}\vec{\nabla}\varphi(\vec{r}_d,t) \quad \text{with} \quad \rho(\vec{r}_d,t) = \left|\vec{A}(\vec{r}_d,t)\right|^2 \tag{3.38}$$

The momentum can be obtained from the gradient of the phase $\varphi(\vec{r}_d,t)$ at each time and at a fixed position $\vec{r}_d$ where the virtual detector is located.

$$k(\vec{r}_d,t) = \mu v = \nabla\varphi(\vec{r}_d,t). \tag{3.39}$$

Then, by applying a 'binning' or 'histogramming' procedure, the momentum distribution dN/dk can be derived.

For simplicity, consider the one-dimensional case, where the VD is located at x_d. The probability for finding the number ΔN of events that have momenta k within a small momentum interval Δk around the momentum value k_j is then given by

$$\Delta N(k_j) = \Delta k \int_0^\infty dt\, j(x_d, t) \begin{cases} 1 & for\ \ k \in [k_j - \Delta k/2,\ k_j + \Delta k/2] \\ 0 & else \end{cases} \qquad (3.40)$$

See [Feuerstein-03-1] for more details.

3.9 Dipole selection rules

When the system is introduced into an electromagnetic field, the probability of finding it in a different state is non-zero. To obtain the so-called dipole selection rules, one needs to calculate the matrix elements of the electric dipole moment: $D_{ij} = \int \psi_i^* d\psi_j dr$, where $d = e_k r_k$ with e_k being the charges of N particles at coordinates r_k and ψ_i and ψ_j are the wavefunctions of the states involved in the transition.

The quantum numbers used below are defined as:

L – electron orbital angular momentum;

Λ – projection of L on the rotation axis;

S – spin;

Σ – projection of the spin (not to confuse with the same notation for Λ=0) ;

J – electron total angular momentum ($\vec{J} = \vec{L} + \vec{S}$);

Ω – projection of J (Ω = Λ+Σ).

Selection rules for the homonuclear diatomic molecules in the same charge states are as follows. We need to distinguish the cases when light is polarized along the molecular axis and when it is polarized perpendicular to the molecular axis. In the first case the value of the projection Λ of the angular momentum on the internuclear axis needs to be same for both states. In addition, for states with defined parity, g (gerade symmetry) states are connected with u (ungerade symmetry) states and for the Σ - Σ (Λ = 0 - Λ = 0) transition, only + ↔ + and – ↔ – transitions are allowed (for diatomic molecules the system has additional symmetry- mirror reflection through an internuclear axis leading to + or -). For the perpendicular polarizations the last rule holds, but only transitions between states with ΔΛ= ±1 are allowed.

Thus, summarizing the selection rules we have:

$$\Delta\Lambda = \begin{cases} 0 & \text{for parallel transitions} \\ \pm 1 & \text{for perpendicular transitions} \end{cases}$$

$$+\leftrightarrow +\,;\,-\leftrightarrow -;\ \text{and}+\nleftrightarrow -\text{in}\ \Sigma-\Sigma\ \text{transitions;}$$

$$g \leftrightarrow u;\ u \nleftrightarrow u\ \text{and}\ g \nleftrightarrow g\ \text{for homonuclear molecules.}$$

In addition, for light molecules $\Delta\Sigma = 0$ since there is no spin in the dipole moment operators. For heavier molecules, where Ω, the total electronic angular momentum about the internuclear axis, is a good quantum number, dipole-allowed transitions require $\Delta\Omega = 0,\pm1$ $\Omega=|\Sigma+\Lambda|$. Note that the selection rules above are different for the photoionization of the homonuclear molecule in different charge states due to different symmetry of the states [Zare-98, Xie-90].

Chapter 4 - HYDROGEN MOLECULES IN IR LASER FIELDS

The focus of this chapter is the H_2 (D_2) molecule in IR fields.

4.1 Introduction

H_2 (D_2) molecules have been heavily studied both experimentally and theoretically [Posthumus-04, Giusti-Suzor-95, Calvert-10]. When H_2(D_2) molecules are subjected to a strong laser field different processes can happen, such as: dissociation via one- or two- photons also known as *bond softening (BS)* [Bucksbaum-90, Posthumus-04] and *above threshold dissociation* [Zavriyev-90, Giusti-Suzor-90, Posthumus-04], *bond hardening* (BH) [Posthumus-04, Châteauneuf-98, Frasinski-99, Bandrauk-81, Walker-93, Bucksbaum-90], *charge resonance enhanced ionization* (CREI) [Zuo-95, Seideman-95, Codling-93, Cornaggia-91, Dietrich-92, Strickland-92, Williams-00] *high order harmonic generation* [Liang-94, Baker-06, Budil-93, Mercer-96, Hay-02], and CE occurring after removal of a second electron from the molecule [Ergler-06-2, Alnaser-05, Bandrauk-99, Ellert-98, Légaré-06, Chelkowski-07, Feuerstein-03]. The theoretical study of the dependence of BS and BH on laser parameters is presented in Section 4.2.

The vibrational dynamics of wave packet motion of H_2 and D_2 molecules have been studied by analyzing the KER of the molecular ion fragments produced by a pump and second delayed probe laser pulse [Posthumus-04, Bocharova-11, Ergler-06-1, Alnaser-05, De-10, De-11]. Section 4.3 focuses on the process of weakening the bond by a strong field, which induces the dissociation (also known as photo-dissociation) of D_2^+ molecules, by comparing the measured and calculated KER spectra.

There are several techniques for studying electron localization in diatomic molecules that include CEP locked or two-color asymmetric pump-probe pulses. “Electron localization” with a single symmetric circularly polarized pulse is discussed in Section 4.4.

4.2 Dependence of bond softening and bond hardening on laser intensity, wavelength, and pulse duration for D_2^+

By solving the TDSE, the time evolution of the wave packet can be calculated theoretically. We calculate the time evolution of an initial nuclear vibrational wave packet in D_2^+ generated by the rapid ionization of D_2 in an ultrashort pump-laser pulse based on a quantum-mechanical model. The QB frequency and internuclear distance-dependent power spectra are obtained by Fourier transformation of the nuclear probability density with respect to the time delay between the spike of the pump pulse and the high-intensity spike of an intense probe-laser pulse. The probe pulse causes immediate Coulomb explosion, which allows imaging of the wave packet. The QB frequency spectra serve as a tool for visualizing and analyzing the nuclear dynamics in D_2^+ in an intermittent external laser field (See Chapter. 3, Thumm-08, and Niederhausen-07 for more details). In this work, we model the external laser pulse with a pedestal (with about 5% of the peak intensity of the main pulse) to obtain more realistic pulses (Fig. 4.1). Variation in the intensity, wavelength, and duration of this probe-pulse pedestal allows us to identify the optimal laser parameters for the observation of field-induced BS and BH in D_2^+.

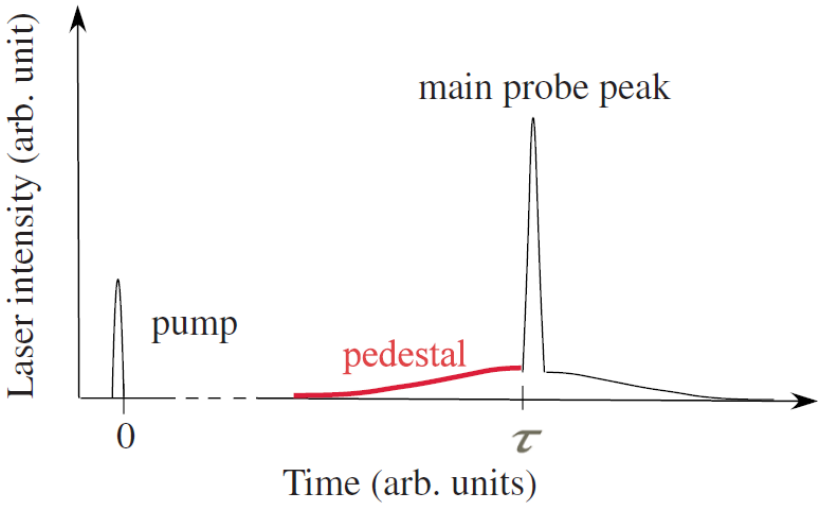

Figure 4.1 ***Schematics for the pump-probe pulse sequence. The main pulses (spikes) are shown in black and the pedestal (Gaussian-shape) of the pulse in red. In our simulations we assume that CE is instantaneous (ionization happens in the main peak of the probe pulse).***

In Floquet theory, the interactions of the continuum wave (CW) laser field with the molecule are described using adiabatic laser-dressed potential curves [Giusti-Suzor-92, Sändig-00, Williams-00], which are also referred to as "Floquet adiabatic molecular potential curves" or simply "Floquet curves." The field-dressed curves (Floquet curves) correspond to the field-free adiabatic molecular potential curves that are shifted in energy by one or several photons due to the interaction with the laser field. The shift in energy depends on the net number of photons the molecule absorbs from the field. We used short laser pulses in our simulation for which the CW Floquet picture may not be applicable without restrictions. The Floquet picture is a very good reference for the description of laser-molecule interactions with laser pulses of finite duration.

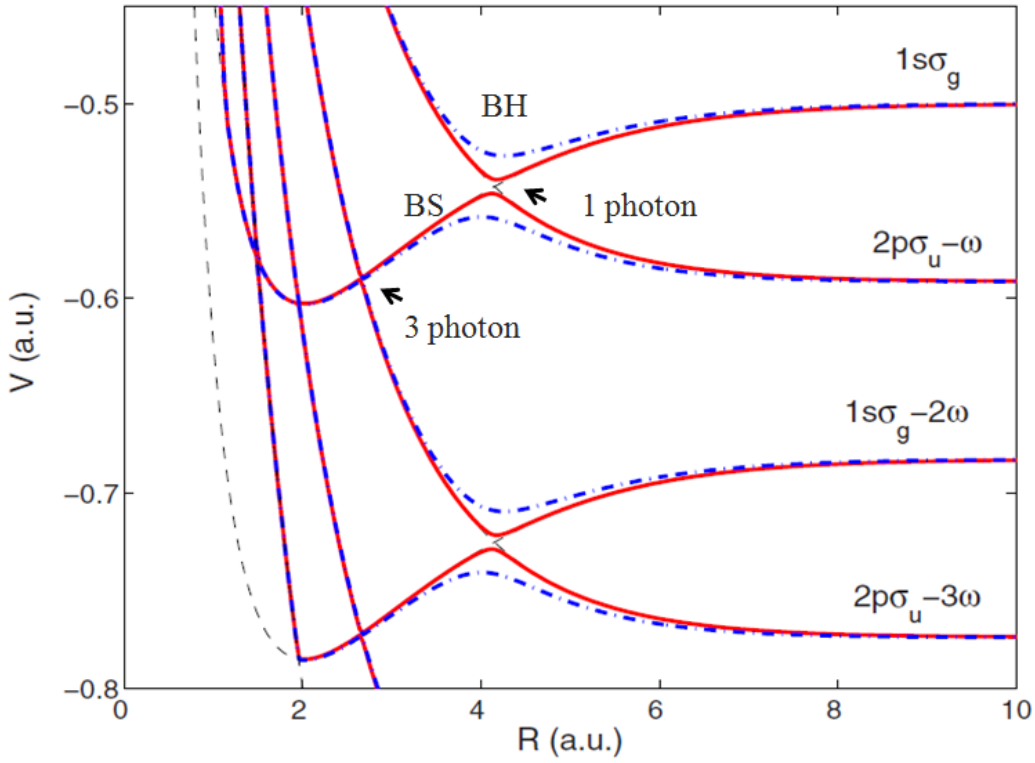

Figure 4.2. ***Laser-dressed adiabatic molecular potential curves for D_2^+ and a 500 nm CW laser field with an intensity of 5×10^{11} (solid red lines) and 10^{13} W/cm^2 (dashed-dotted blue lines). Thin black dashed lines show field-free BO potential curves.***

As an example, Fig. 4.2 shows the field-dressed adiabatic potential curves for D_2^+ in a 500 nm CW laser field for two different intensities, 5×10^{11} (solid red lines) and 10^{13} W/cm^2 (dashed -dotted blue lines) [Bates-53]. The curves are labeled as $1s\sigma_g - 2n\omega$ and $2p\sigma_u - (2n-1)\omega$,

corresponding to the field-free potential curves and the net number of photons $2n$ and $(2n\text{-}1)$, respectively, that are released to the photon field. The dipole-allowed coupling between field-free potential curves of gerade and ungerade symmetries [Bransden-03], due to the absorption or release of an odd number of photons, leads to characteristic "avoided" crossings between Floquet curves. The avoided crossings near internuclear distances of R=4 and R=3 correspond to the one and three photon exchange between the molecular ion and the CW laser field, respectively. The gap between the adiabatic Floquet curves increases with increasing laser intensity. Near avoided crossings the BH well, which is also referred to as "vibrational trapping" or "dynamical dissociation quenching" [Châteauneuf-98], can be formed and the depth and shape of it is laser intensity dependent. At higher intensities it becomes shallower and wider, and, at sufficiently high intensities, loses the ability to bind BH states. The other interesting feature of field-dressed adiabatic curves is BS - dissociation of the molecule due either to classically allowed over-the-barrier escape or by tunneling [Bucksbaum-90, Posthumus-04]. The less energetic Floquet potential curve below the gap forms a barrier that may enable BS dissociation.

In sections 4.2.1- 4.2.3, the bound and dissociating nuclear motion of D_2^+ in a laser pulse are discussed by examining how power spectra are affected by the laser pedestal parameters intensity, frequency, and duration. Even though all simulations were carried out for laser pulses with a finite pulse length (including the pedestal), it is shown that the terminology developed based on the Floquet picture is appropriate. For example, even though stable BH states can only exist in CW laser fields, evidence for transient BH states in laser *pulses* over a large range of pulse lengths is found.

4.2.1 Intensity dependence

The R-dependent power spectra $P(R,\omega;T)$ for D_2^+ propagating through 200 nm 20 fs (FWHM) Gaussian pedestal laser pulses are shown in Fig. 4.3 for different peak intensities (upper panels) and the corresponding Floquet field-dressed potential curves, which are displayed in red in the lower panels. The three different pedestal intensities are 10^{13} (left), 5×10^{13} (middle), and 10^{14} W/cm^2 (right column). Note that the thin black lines in the lower panels correspond to the field-free adiabatic molecular potential curves. As for all other numerical results shown below, the molecular ion is assumed to be produced by the rapid ionization of D_2 and is characterized by a FC distribution of stationary vibrational states, as described in Chapter 3.4.1.

The nodal structure of the spectra is due to the beating of two adjacent stationary vibrational states $|\chi_\mu\rangle$ and $|\chi_\nu\rangle$ with frequency $f = \Delta\omega_{\mu,\nu}/2\pi$ [Thumm-08]. The thin black vertical lines link the minima of the 1-ω BH wells in the power spectra (upper row of graphs in Fig. 4.3) to BH wells in the Floquet potential curves (lower row). For the given intensities, the power spectra show a significant amount of nuclear probability density that is intermittently trapped in the 1-ω BH well.

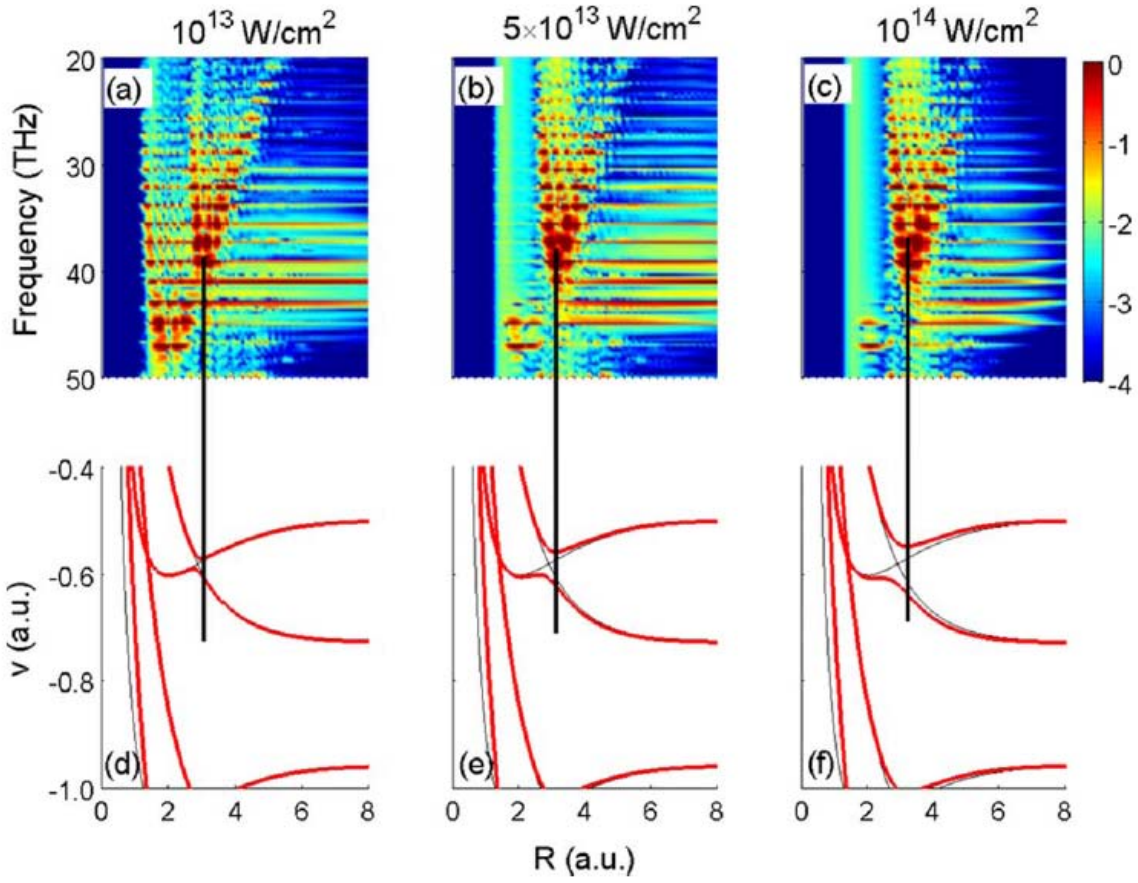

Figure 4.3 ***R-dependent power spectra for a logarithmic color scale (a)-(c) and field-dressed potential curves (res lines) (d)-(f) of D_2^+ for different pedestal intensities. Graphs are plotted for 200 nm pedestal laser pulses with intensities of 0.1×10^{14} W/cm^2 [(a) and (d)], 0.5×10^{14} W/cm^2 [(b) and (e)], and 1×10^{14} W/cm^2 [(c) and (f)].***

As the intensity increases the nuclear probability density in the 1-ω BH well increases due to the increase of probability that is associated with the bound motion of the molecular ions in field-dressed $1s\sigma_g$ potential curve. The calculations for intensity-dependent power spectra

confirm the intuitive expectations. First, the dissociation due to classical over-the-barrier motion of the two nuclei or by tunneling across the 1-ω BS barrier increases with increasing peak intensity. Second, BS progresses from depleting the highest vibrational state components of the nuclear wave packet with vibrational quantum numbers $\nu \geq 4$ (left column in Fig. 4.3) to the lowest vibrational components of the initial FC distribution (right column).

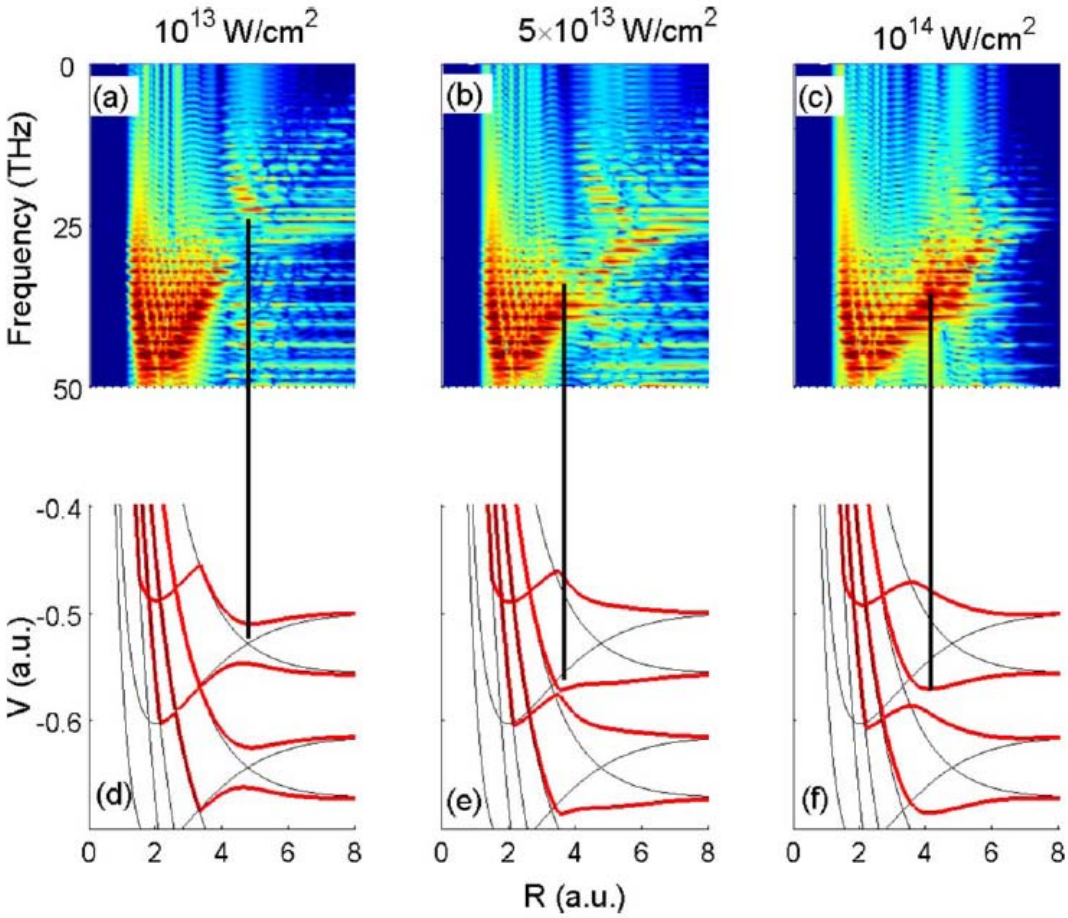

Figure 4.4 ***Same as Fig. 4.3, but for 800 nm pedestal laser pulses.***

4.2.2 Wavelength dependence

The same power spectra as in Fig. 4.3, but calculated for 800 nm in Fig. 4.4, indicate that the nuclear motion in D_2^+ sensitively depends on the carrier wavelength. This dependence can be understood within the Floquet picture. As the photon energy decreases, the spacing in energy between Floquet potential curves decreases. This decrease increases the significance of couplings between more than two curves, which, in turn, may result in the overlap of (1-ω with 3-ω) BH

wells, reducing the BH effectiveness of the resulting, flatter, well. At 800 nm and 10^{13} W/cm^2 peak intensity (left column in Fig. 4.4), the power spectrum shows only weak evidence for the temporary trapping of nuclear probability density in the 1-ω BH well that is centered near R=5. The molecular ion remains most likely bound in the electronic ground state. At the higher intensities (middle and right columns), dissociation via BS becomes increasingly important but cannot be as clearly assigned to the 1-ω BS barrier as for the case of 200 nm wavelength.

For the 800 nm and 5×10^{13} W/cm^2 case shown in the middle column of Fig. 4.4, the corresponding 1-ω BH well has disappeared in the Floquet potential curve in graph (e) and most of the BH happens on the 3-ω BH well centered at smaller distances near R=3.5 in the power spectrum. The same can be seen for the 10^{14} W/cm^2 intensity (right column). Note that despite the absence of the BH well on graph (e), graph (b) also shows weak evidence for BH states in the 1-ω well near R=5 due to temporary vibrational trapping during the increasing laser intensity of the pedestal.

Figure 4.5 summarizes a more systematic study of the wavelength dependence of BS and BH at a fixed intensity of 10^{13} W/cm^2. For the different pulse wavelengths, the positions of one (or three) photon crossing(s) are different (thin black lines in the lower panels). For this reason we expect laser wavelength to affect BS and BH. In Figs. 4.5 (a)–(e), the power spectra show that dissociation by BS decreases with increasing wavelength, while the 1-ω BH well moves to larger internuclear distances. A very prominent BH well is visible for 200 nm wavelength in Figs. 4.5(a) and (f). For this wavelength, all vibrational eigenstates in the initial FC distribution above ν=2 are being depleted by BS, while the deep BH well traps even the highest initially occupied vibrational states. In Figs. 4.5(b) and 4.5(g) for 500 nm, the 1- ω BH well is visible but compared to the 200 nm case it has less probability density, while the nuclear motion in the electronic ground state remains bound. This trend continues for 800, 1024, and 1600 nm (the three right columns in Fig. 4.5) to the point that BH in the 1-ω well disappears at 1600 nm. The same conclusion can be drawn from the comparison of Figs. 4.3(c) and 4.4(c) above. As the wavelength increases, BS through and over the 3-ω well becomes energetically possible for an increasing number of stationary vibrational states of the nuclear wave packet. However, as the simulated power spectra show, the peak intensity of 10^{13} W/cm^2 is too low for three-photon processes to become relevant. Therefore, 3-ω BS and BH are not clearly noticeable in Fig. 4.5. In

the left four columns of Fig. 4.5, the positions of the 1-ω BH well agree in the power spectra and Floquet potential curves.

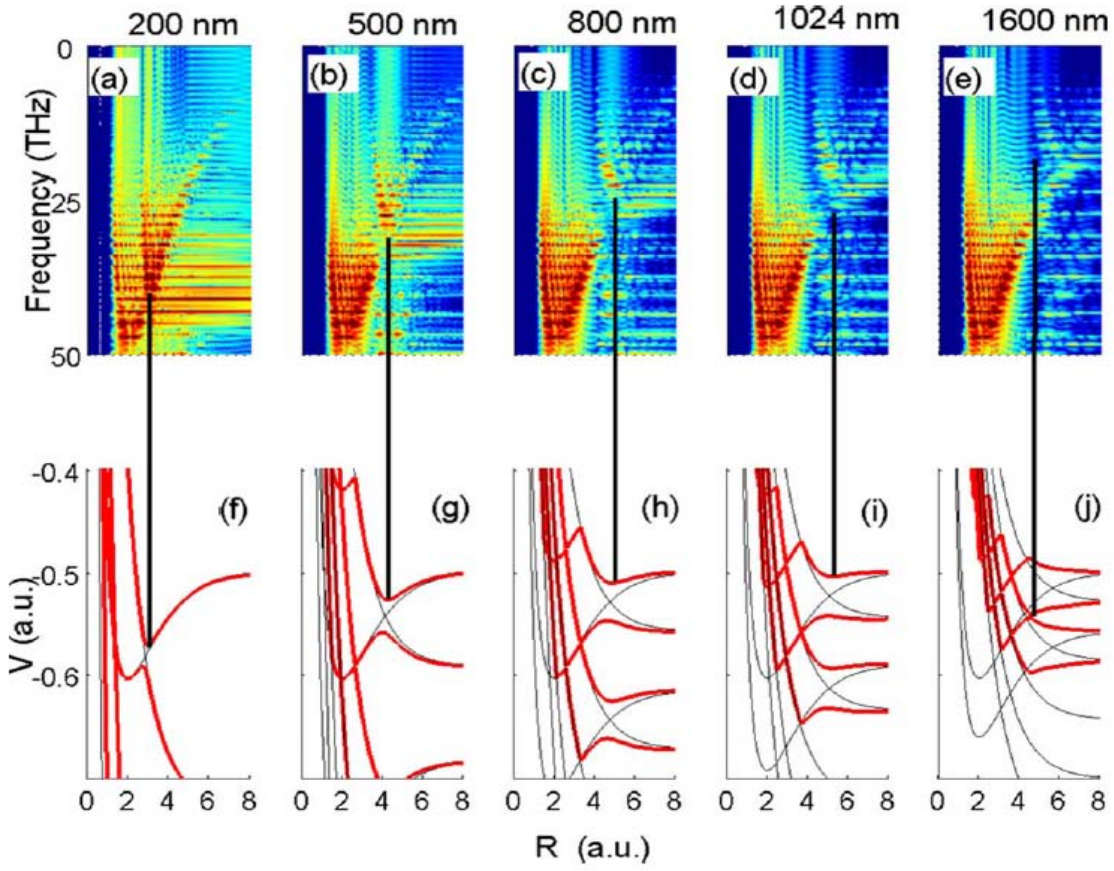

Figure 4.5 ***The power spectra (a)-(e) for the different laser wavelengths of 200 nm [(a) and (f)], 500 nm [(b) and (g)], 800 nm [(c) and (h)], 1024 nm [(d) and (i)], and 1600 nm [(e) and (j)]. (Same logarithmic color scale as in Fig. 4.3) at fixed 10^{13} W/cm^2 peak intensity pedestal laser pulses. Graphs (f)-(j) are field-dressed potential curves (red lines) for corresponding intensities. Field-free potentials are plotted as thin black lines.***

At 1600 nm, however, according to the Floquet picture the 1-ω BH has disappeared and BH is expected to happen near the 3-ω crossing point (Fig. 4.5(j)). This prediction of the CW Floquet picture is not fully confirmed in the power spectrum in Fig. 4.5(e) that shows very weak evidence of 1-ω BH states centered near R=7 and no apparent traces of 3-ω BS or BH. This mismatch can be related to the fact that the Floquet picture assumes infinite pulse lengths, while at 1600 nm the power spectrum simulates the propagation of the nuclear wave packet across a pedestal pulse with a length of L=20 fs (FWHM), corresponding to the illumination of the wave packet by the pedestal laser pulse over just two optical cycles and with a rapidly changing

envelope. Thus we interpret this discrepancy as due to both the onset of the breakdown of the Floquet picture for short pulses, and more importantly, an *effective* laser intensity in the power spectra that is much smaller than the peak intensity for which the Floquet curves were calculated.

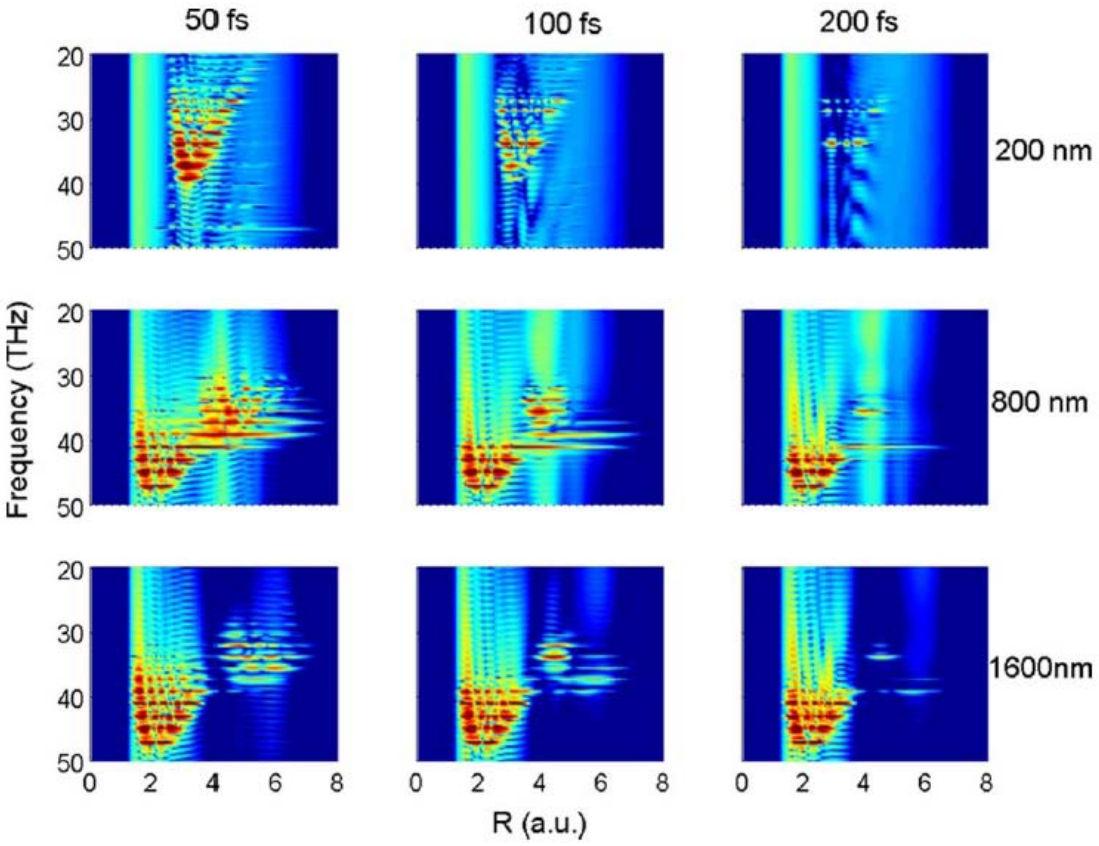

Figure 4.6 ***Power spectra as a function of QB frequency and internuclear distance in log scale. (Same color scale as in Fig. 4.4) for fixed peak intensity of 10^{14} W/cm^2. The power spectra are plotted for different (200, 800, 1600 nm) wavelengths and pedestal lengths (FWHM 50, 100, and 200 fs).***

4.2.3 Pulse-length dependence

Figure 4.6 summarizes the pulse length dependence of power spectra for different wavelengths, where the panels are ordered with pedestal wavelengths increasing from 200 (top) to 1600 nm (bottom). From left to right the pedestal length increases from 50 to 200 fs. For each wavelength, the BH probability decreases with increasing pulse length. Intuitively one would expect that for longer pedestals BH would be more pronounced due to longer trapping times, but our simulations show the opposite. We relate this to the dominant influence of the pulse energy - longer pedestals transfer more energy to the molecule. This favors both dissociation by BS

directly from the electronic ground state (leaving less probability to be potentially trapped in a BH well) and the decay of BH states by nonadiabatic couplings to dissociative potential curves that are neglected in the BO approximation [Bransden-03]. For the lower wavelengths, the same pedestal pulse envelope includes more optical cycles. Thus, the power spectrum in Fig. 4.6 with the shortest wavelength and longest pulse duration is the most agreeable to an interpretation within the Floquet picture. However, as shown in the top right corner of Fig 4.6, this trend is somewhat difficult to follow over a large range of pulse lengths, since, for high pulse durations (high pulse energies) BS can dominate to the point that all bound states become depleted. For the 200 nm case, BS depletes the ground state of the molecular ion leaving almost no population for the longest pulse length (200 fs). In contrast, for the higher wavelength cases (800 and 1600nm), the electronic ground state remains populated at all displayed pulse lengths but, as expected, gets increasingly depleted with increasing pulse length by BS over and through the 1-ω BS barrier. Thus, comparing all the calculated power spectra in Fig 4.6 suggests that BH is most pronounced at the shortest wavelengths and for the shortest pedestals. Adding Fig. 4.3 to the comparison, we can in addition conclude that BH at short wavelengths is robust over a large range in peak intensities.

4.2.4 Conclusion

To summarize, by simulating the *R*-dependent QB power spectra we investigated the nuclear dynamics of the D_2^+ molecules in a short laser field for different peak intensities, wavelengths, and pedestal lengths. We focused on dissociation by BS and BH while analyzing the power spectra in terms of field-dressed Floquet potential curves. We confirmed that the Floquet picture is appropriate for characterizing the main features of the nuclear dynamics in few-cycle laser pulses despite its inherent CW assumption, except for the longest wavelengths used in our simulations (1600 nm). Our simulations suggest that pulses with a wavelength between 200 to 300 nm, a peak intensity of about 10^{14} W/cm^2, and a duration of less than 50 fs (FWHM) are well suited for the observation of transient vibrational trapping of the molecular motion in the 1-ω BH well. At wavelengths of 1600 nm, we found that dissociation proceeds via both 1-ω and 3-ω BS. For the same wavelength, our simulations indicate transient trapping in the 3-ω BH well. To the best of our knowledge, our theoretical findings can be tested experimentally considering existing technology [Alnaser05].

4.3 Dissociation dynamics of D_2^+ in strong laser fields

In this sub-chapter, starting with the simple diatomic molecule D_2, we investigate dissociation dynamics of diatomic molecules in intense laser fields, test the FT method described in Chapter 3, and compare the calculations with the measured data [Rudenko-07]. In the case of D_2, electronic states potentially involved in the dynamics are not so hard to identify, since there are two main states of D_2^+, bound $1s\sigma_g$ (the only bound state of D_2^+), and repulsive $2p\sigma_u$. These states are widely available from the literature, but we have done *ab inito* calculations using GAMESS code.

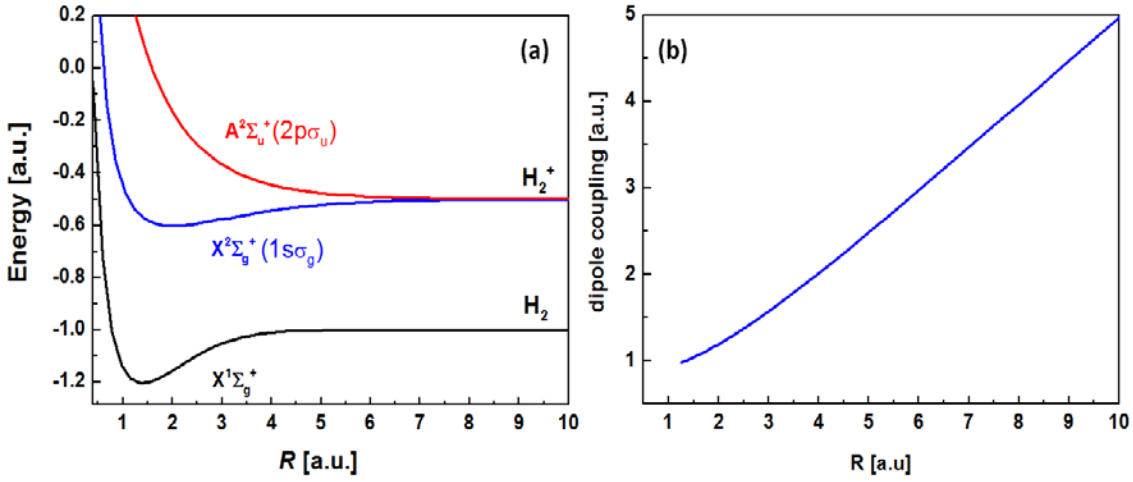

Figure 4.7 ***(a) Potential curves of H_2 and H_2^+ calculated using MCSCF/cc-pVTZ method with GAMESS. (b) Dipole couplings. For R>4 the dipole couplings are approaching R/2 limit.***

4.3.1 Potential curve calculations

Potential curves and dipole couplings were calculated with the MCSCF/cc-pVTZ method (Details of the method used in the calculations can be found in Chapter 3 and Appendix E). We optimized the molecular geometry of neutral (equilibrium internuclear distance 1.35) and singly charged (equilibrium internuclear distance 2) deuterium molecules using restricted open-shell SCF wavefunctions. Calculations were done for different fixed internuclear separations with steps of 0.05Å. The ground state of H_2 (D_2) has the configuration $(1\sigma_g)^2$. In the calculations, both of the molecular orbitals $1\sigma_g$ and $1\sigma_u$ were allowed to vary. The electronic state $1s\sigma_g$ ($X^2\Sigma_g^+$) has the configuration $(1\sigma_g)^1(1\sigma_u)^0$ and the state $2p\sigma_u$ ($A^2\Sigma_u^+$) has the configuration $(1\sigma_g)^0(1\sigma_u)^1$.

The calculated D_2 and D_2^+ curves and dipole couplings are shown in Fig. 4.7. The calculated curves are in excellent agreement with the "known" results based on the solution of time independent Schrödinger equation discussed in Chapter 2 [Thumm-08]. The minimum of the ground state of H_2 (H_2^+) is at around 1.35 (2.0), and the dipole couplings approach the $R/2$ limit at large R.

4.3.2 Experiment and theoretical model

The experiment was done using cold target recoil ion momentum spectroscopy (COLTRIMS, also known as a reaction microscopy) with a pump-probe scheme to map the H_2^+ nuclear wave packets by three-dimensional CE imaging in intense laser pulses [Rudenko-07]. The laser parameters were 800 nm wavelength, ~ 10fs FWHM pulse width, and 3×10^{14} W/cm^2 intensity. In the pump-probe process a pump pulse singly ionized the molecule, and a probe pulse could photo-dissociate the molecular ion, or ionize it further and Coulomb-explode.

In this particular study we were interested in the photo-dissociation process. The measured proton energy as a function of pump-probe delay was compared to the measured spectra (see the next section). In our theoretical model we solve the two-state TDSE as described in Chapter 3, and using the FT method we plot proton energy as a function of delay. We used 10 fs FWHM pulses with an intensity of 3×10^{14} W/cm^2.

4.3.3 Results

The measured energy spectrum for the photo-dissociation process is compared with the calculations in Fig. 4.8. The revival time of ~580 fs is reproduced in the calculations, with the wave packet oscillation period ~20 fs (in the $1s\sigma_g$ state). Even a fractional revival is visible at around 290 fs.

The dissociative line coming down from energies around 4 eV and merging with the dissociative energy limit below 1 eV is not relevant. This path comes from so-called "delayed dissociation" [Rudenko-07], that is, dissociative ionization first by the pump and then ionization of the bound part of the wave packet by the probe (not included in the simulation).

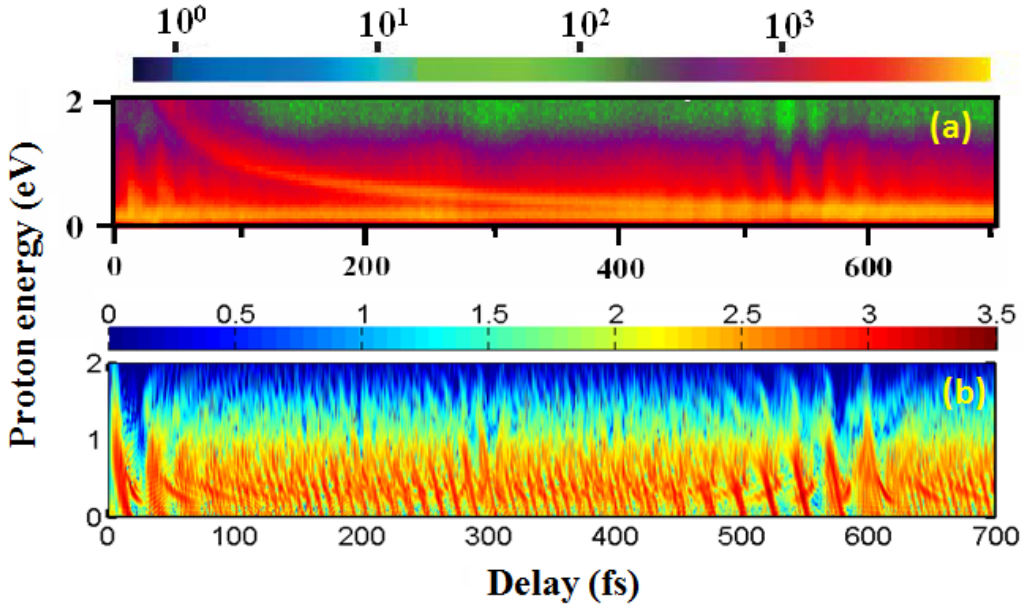

Figure 4.8 ***(a) Measured [Rudenko-07] and (b) calculated proton energy for the process of dissociation of $D_2^+ \rightarrow D^+ + D$ (logarithmic color scale). The pulse parameters are 10 fs width and 3x10^{14} W/cm^2 intensity.***

4.3.4 Conclusions

The main features of the measured energy spectra, such as the oscillation period and revivals, are reproduced in the calculation. Our FT method works for small diatomic molecules. The next step is to try heavier molecules (Chapters 5 and 6).

4.4 Electron localization

In this sub-chapter the localization of the electron in an IR field is discussed [Wu-13-3].

In the previous experiments the asymmetry of the pulses was achieved either by CEP stabilizing a few-cycle pulse [Kling-06, Kremer-09, Znakovskaya-12, Kling-13] or by composing a pulse of two different carrier frequencies [Ray-09, Wu-13-1]. The asymmetric fields drive and eventually localize the bound electron at one of the dissociating nuclei [He-08-1, He-12]. Alternatively, an attosecond pulse [He-08-2, Sansone-10, Singh-10] has been used to first launch a H_2^+ vibrational wave packet by single-photon ionization of H_2. Next, a phase-locked near-infrared laser pulse drives the remaining electron back and forth between the nuclei until its final localization at one of them, governed by the relative time delay between the excitation and the driving pulses.

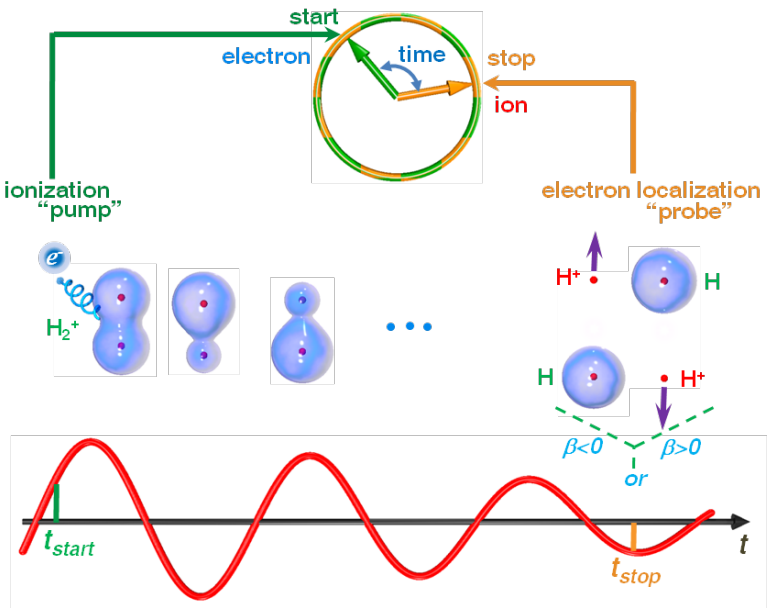

Figure 4.9 ***Schematic of an ultrafast stopwatch. The times t_{start} and t_{stop} indicate the start and stop times of the stopwatch that are retrieved by coincident detection of the emitted electron and ion from a breaking chemical bond of H_2^+. Electrons are indicated as blue "bubbles" and nuclei are shown as red dots. In the bottom panel, the laser field that drives an electron up and down during the breaking of the chemical bond is shown as a red curve with start and stop times indicated by lines. (Figure by Jian Wu with POV-Ray for Windows).***

This section of the chapter focuses on answering a question - *do symmetric long laser pulses preserve symmetry in breaking chemical bonds?* To answer the question, experiments were done in Frankfurt, Germany using a two-particle-coincidence technique achieving attosecond time resolution in a long circularly polarized multicycle femtosecond laser pulse. This allowed the time resolution of the laser-driven ionization and fragmentation of H_2 by relating the instant of ionization of H_2 to the ejected electron direction and by subsequently breaking the H_2^+ bond in the same pulse. This approach provides an ultrafast stopwatch using the jointly measured directions of two emitted particles as hands (Fig. 4.9). In its basic implementation used here, the technique is extremely robust and easy to use as it is independent of the carrier-envelope phase [Kling-06, Kremer-09, Znakovskaya-12] and pulse length and does not require attosecond pulses [Hentschel-01, Sansone-06, Goulielmakis-04, Drescher-02, Cavalieri-07, Gräfe-08]. It is scalable to more than two particles as each electron carries its individual time stamp [Pfeiffer-11] and can be encoded by using different polarizations. This technique allows the measurement of time

intervals based on the momentum differences which can be detected with extremely high precision, even for long pulses, thereby providing a powerful tool for ultrafast science.

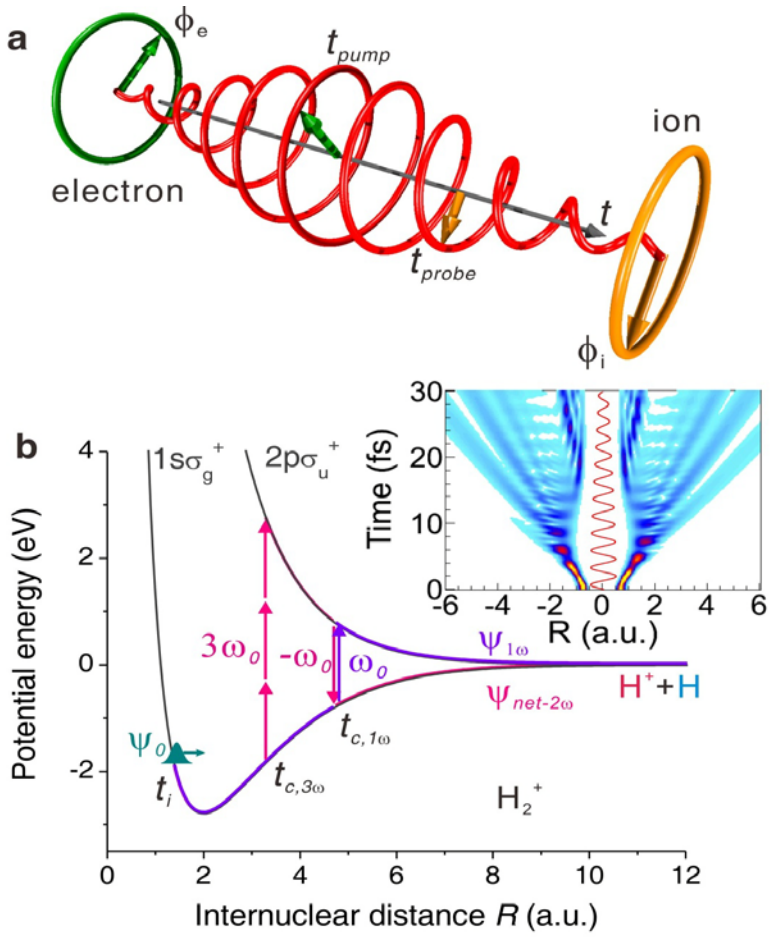

Figure 4.10 ***(a) Schematics of coincidence detection of the electron and ion for a circularly polarized laser field (red spiral). At time t_{pump} the electron is emitted due to the pump pulse and detected at one of the detectors (green circle) with angle ϕ_e, and the ions are detected coincidently with angle ϕ_i on the other detector (orange circle) at probe time t_{probe}. (b) Dissociation dynamics of the singly ionized H_2^+. The inset shows the calculated forced left-and-right motion of the nuclear wave packet by the laser field (red curve) which finally localizes at one of the nuclei during the dissociation of H_2^+ with increased internuclear distance. (Figures by Jian Wu).***

4.4.1 Experiment

In the experiment the particles emitted from the same molecule are detected in coincidence (Fig. 4.9). As displayed in Fig. 4.10(a), we use the rotating electric field vector of a

circularly polarized long laser pulse as ultrafast clockwork and the coincidence detection of the two particles which are both driven by this clockwork as two hands marking the start and stop of the clock. We then read the time elapsed between start and stop as the angle between the detected particle momenta. This coincident angular streaking technique is used to probe the attosecond dynamics of an electron in a breaking chemical bond of H_2^+ as shown in Fig. 4.9. By realizing both the pump and probe step in a single near-infrared multicycle circularly polarized pulse (Fig. 4.10(a)), we clearly observe the asymmetric release of the proton by simultaneously tracking the electron localization as a function of the moment of ionization and the proton kinetic energy.

Figure 4.10a illustrates the coincidence detection measurement: at time t_{pump} the nuclear vibrational wave packet is launched by the first part of the laser pulse (acting as the pump) releasing one electron from the neutral molecule at the same time. After the ionization the remaining electron is driven by the second part of the same laser pulse (acting like a probe) until its final localization at time t_{probe}. A vibrational nuclear wave packet is created by the pump on the $1s\sigma_g^+$ potential curve of H_2^+ at time t_i as marked in Fig. 4.10(b). The wave packet is coupled to the repulsive $2p\sigma_u^+$ state at a later time t_c and eventually dissociates into H^++H. Due to the coherent superposition of $1s\sigma_g^+$ and $2p\sigma_u^+$ contributions, the nuclear probability density is then localized (asymmetrically) at the nuclei. The electron localization dynamics is governed by the laser phases at the instants of field ionization (t_i) and at the couplings ($t_{c,3\omega}$ and $t_{c,1\omega}$). The angle of the final momentum of the released electron ϕ_e provides the laser phase at the ionization instant t_i [Eckle-08-1, Eckle-08-2, Pfeiffer-12, Holmegarrd-10, Wu-12]. In a long pulse and without coincidence detection, the information on the instantaneous field direction is physically meaningless. For an analog clock this would correspond to having one hand of the clock, but lacking an oriented clock face. In our case the orientation of the clock face is given by the dissociation direction ϕ_i of the proton measured in coincidence, which is determined by the laser phases at the field-coupling instants $t_{c,3\omega}$ and $t_{c,1\omega}$. The angle difference between the electron and proton momentum vectors (or the electron angle in the molecular frame), $\phi_e^{mol} = \phi_e - \phi_i$, is equivalent to the time delay in a traditional pump-probe scheme.

A COLTRIMS [Ullrich-03] reaction microscope was used to measure in coincidence the directions and energies of the ion and electron produced by 35 fs (~13.3 cycle at 790-nm) circularly polarized laser pulses. The experiments were performed with femtosecond laser pulses (35 fs, 790 nm, 8 kHz) produced from a multipass amplifier Ti:sapphire laser system (KMLabs

Dragon). The laser pulses were sent into a standard COLTRIMS setup [Ullrich-03] and focused by a concave reflection mirror with a focal length of 7.5 cm onto a supersonic gas jet. The jet was a mixture of H_2 and D_2 with a ratio of 1:1, so that both targets could be probed under identical conditions. The ions and electrons created by the laser were accelerated by a static electric field (~14.7 V/cm) and detected by two time and position sensitive micro channel plate detectors[28] at opposite sides of the spectrometer. A weak homogeneous magnetic field (~9.2 Gauss) was used to enable the detection of the electrons within a 4π solid angle. The three-dimensional momentum vectors of the correlated ions and electrons were retrieved from the measured time-of-flight and position information during the offline analysis. The polarization of the laser pulse was changed from linear to circular by using a quarter waveplate with its fast-axis orientated at 45° with respect to the input linear polarization. The handedness of the circular polarization could be switched from anticlockwise to clockwise by rotating the fast-axis of the quarter waveplate by 90°.

4.4.2 Methods

In this subsection two different models - semiclasical and quantum mechanical - are discussed for a quantitative insight into the observed localization mechanism. Note that dissociation is considered along the direction of the molecular axis, and only the component of the laser field along this axis is used in our simulations.

4.4.2.1 Semiclassical model

In a semi-classical approach, we model the classical motion of the nuclei on the potential curves of H_2^+ keeping track of the quantum phases. As illustrated in Fig. 4.10(b), we start the nuclear motion on the $1s\sigma_g^+$ potential surface at time t_i and consider dissociation along two possible pathways: the 1ω (violet curve) or the net-2ω pathway (pink curve).

We propagate the nuclear wave packet as a classical particle with reduced mass on the potential curves of H_2^+. Its motion follows Newton's laws and is driven by the force $F=-\partial U/\partial R$ [Bocharova-11]. As illustrated in Fig. 4.10(b), the classical nuclear motion in the molecular ion is initiated at the equilibrium distance of the neutral molecule (R_0~1.4 a.u.) at time t_i with an initial energy of $E_0=U_{g0}+E_{k0}$ given by the sum of the potential and kinetic energy. An initial kinetic energy (stemming from the finite width of the original wave packet in momentum space)

is given to the particle so that it can reach the one-photon or three-photon energy gap and thus can be laser coupled to the repulsive state. As illustrated in Fig. 4.10(b), the two possible dissociation pathways are: the 1ω pathway (violet curve; propagation on the $1s\sigma_g^+$, followed by coupling to the $2p\sigma_u^+$ curve at time $t_{c,1\omega}$ by absorption of one laser photon, followed by dissociation along the $2p\sigma_u$ curve) or the net-2ω pathway (pink curve; propagation on the $1s\sigma_g^+$, followed by coupling to the $2p\sigma_u^+$ curve at time $t_{c,3\omega}$ by absorption of three photons, followed by propagation on the $2p\sigma_u^+$ curve and coupling back to the$1s\sigma_g^+$ curve by emitting one photon at time $t_{c,1\omega}$, followed by dissociation along the $1s\sigma_g^+$ curve). For the 1ω and net-2ω dissociation pathways, the accumulated phase of the wave packet during the dissociation from R_0 to R_f ($R_f >$ 100 a.u.) can be approximated as

$$\varphi_{1\omega} = (E_{0,1\omega} + \omega_0)\big(t_{c,1\omega} - t_i\big) + \varphi_{gu} + \big(E_{0,1\omega} + \omega_0\big)\big(t_f - t_{c,1\omega}\big) - \int_{R_0}^{R_f} p_{1\omega}(R)dR \quad (4.1)$$

$$\varphi_{net-2\omega} = (E_{0,net-2\omega} + 3\omega_0)\big(t_{c,3\omega} - t_i\big) + \varphi_{gu} + \big(E_{0,net-2\omega} + 3\omega_0\big)\big(t_{c,1\omega} - t_{c,3\omega}\big) - \omega_0\big(t_{c,1\omega} - t_i\big) - \varphi_{gu} + \big(E_{0,net-2\omega} + 2\omega_0\big)\big(t_f - t_{c,1\omega}\big) - \int_{R_0}^{R_f} p_{net-2\omega}(R)dR \quad (4.2)$$

where φ_{gu}=π is the phase change due to coupling of the gerade state to the ungerade state and $p_{...}(R)$ is the momentum of the wave packet. The probabilities for electron localization on the left or right nucleus are

$$P_l = |\psi_l|^2 = \frac{1}{2}|\psi_{1\omega} + \psi_{net-2\omega}|^2 \quad (4.3)$$

$$P_r = |\psi_r|^2 = \frac{1}{2}|\psi_{1\omega} - \psi_{net-2\omega}|^2. \quad (4.4)$$

By assuming$|\psi_{1\omega}| = |\psi_{net-2\omega}|$, the asymmetry parameter within this semiclassical model is

$$\beta_c = \frac{P_l - P_r}{P_l + P_r} = \cos(\varphi_{1\omega} - \varphi_{net-2\omega}) = \cos(\Delta\varphi) \quad . \quad (4.5)$$

Therefore, the asymmetrical electron localization due to interference between dissociating wave packets on the 1ω and net-2ω pathways is governed by the phase difference between them.

4.4.2.2 Quantum model

In our second two-state quantum mechanical model, we numerically solved the one-dimensional TDSE for the vibrational nuclear wave packet [Thumm-08]. The quantum dynamics of the nuclear wave packet is modeled by solving the TDSE in the subspace of the gerade ($1s\sigma_g^+$) and ungerade ($2p\sigma_u^+$) electronic states of H_2^+ [Thumm-08]. Since mainly the laser polarization component parallel to the molecular axis influences the electron localization dynamics [Kling-

06, Kremer-09, Znakovskaya-12, Ray-09, He-08-1, He-08-2, Sansone-10, Singh-10], a simplified one-dimensional model is sufficient to reproduce the observed asymmetry in our experiment. The initial vibrational nuclear wave packet in H_2^+ is modeled based on molecular Ammosov-Delone-Krainov (ADK) rates for the depletion of the neutral hydrogen molecules as described in references [Niederhausen-08, Brichta-06]. In brief, the molecular ADK rate, which depends on the internuclear distance and instantaneous laser intensity, is integrated over time, divided by two, and exponentiated in order to provide the *R*-dependent neutral-molecule-depletion factor *d*. The initial wave packet in H_2^+ is then obtained by multiplying the vibrational (and electronic) ground state wavefunction of the neutral molecule by (1-*d*) followed by normalization of this product. The launch time defines the detected electron angle ϕ_e and corresponds to the instantaneous ionization by the attosecond pulse in the two-color pump-probe experiment [He-08-2, Sansone-10, Singh-10]. After the wave packet is launched, the remainder of the laser pulse is used to drive its motion. We assume the ionization occurs mainly in the seven most intense laser cycles around the pulse peak. The wave packets launched during different laser cycles for the same laser phase (modulo 2π) are coherently added at the end of the propagation from the gerade ($\psi_{net\text{-}2\omega}$) or ungerade ($\psi_{1\omega}$) potential curves, respectively. The probability for finding the electron localized on the left or right nucleus is calculated similar to the semiclassical model. Here, in order to determine the kinetic energy spectrum of the ion, we Fourier transform the dissociating parts of the nuclear wave packets to obtain the momentum representations $P_{\omega,l}$ and $P_{\omega,r}$ and calculate the asymmetry parameter as

$$\beta_q = \frac{P_{\omega,l} - P_{\omega,r}}{P_{\omega,l} + P_{\omega,r}}. \tag{4.6}$$

The peak laser intensity in the simulation, adjusted to obtain the best agreement of the kinetic energy spectra, is $I_0 = 7.0 \times 10^{13}$ W/cm^2. It is lower than to the peak intensity in the experiment for the linear component along the molecular axis, which is 1.2×10^{14} W/cm^2. (We divided the peak intensity for the circularly polarized pulse by 2 to take into account the circular polarization). By using a lower peak intensity in the quantum simulation, we effectively average over the laser intensity profile in the experiment (focal-volume effect).

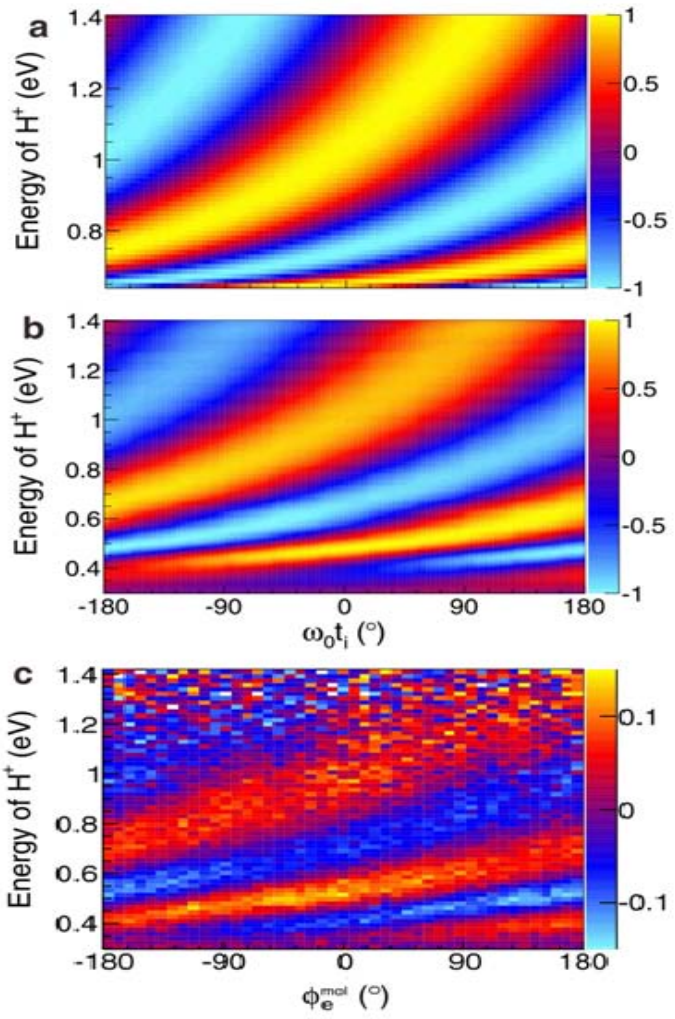

Figure 4.11 ***Localization of the electron in the dissociation process of singly ionized H_2. (a) Semi-classically calculated asymmetry parameter β_c as a function of the laser phase $\omega_0 t_i$ and H^+ kinetic energy. (b) Quantum-mechanically calculated asymmetry parameter β_q. (c) Measured electron localization β_m in dissociative single ionization of H_2 as a function of the emission angle ϕ_e^{mol} of the correlated electron in the molecular frame and the H^+ kinetic energy.***

4.4.3 Results

Figure 4.11a displays the semiclassically calculated asymmetry parameter β_c as a function of the laser phase at ionization instant t_i and the final kinetic energy E_k, in good agreement with our measured asymmetry β_m for $E_k > 0.6$ eV. The final kinetic energy from the 1ω and net-2ω pathways are $E_{k,1\omega} = E_{0,1\omega} + \omega_0$ and $E_{k,net\text{-}2\omega} = E_{0,net\text{-}2\omega} + 2\omega_0$, respectively.

Interference between the dissociating wave packets requires equal final kinetic energy, i.e., $E_{k,1\omega} = E_{k,net\text{-}2\omega}$.

This requirement and the applied initial kinetic energy give the lower limit of the final KER in the classical calculation. To compare with the emission angles of the electron for circular polarization, the absolute phase of the laser is shifted by 90° in the simulation. This accounts for the 90° rotation of the electron angle due to the angular streaking. Figure 4.11b depicts the results from the quantum calculation, which agrees well with the experiments (Fig. 4.11(c)) for the whole observed kinetic energy range. This confirms that our measured asymmetry is indeed predominantly due to the interference between the 1ω and net-2ω dissociating wave packets.

4.4.4 Summary

Our findings are in contrast to the general belief that electron localization cannot be measured in symmetric laser fields, such as our multicycle laser pulse composed of a single carrier frequency. Our data show that electron localization is not something which has to be artificially enforced by optical means as done so far [He-08-1, He-08-2, Kling-06, Kremer-09, Ray-09, Sansone-10, Singh-10, Znakovskaya-12], but that it occurs naturally, even in pulses which are perfectly symmetric. This ubiquitous localization is, however, hidden to all techniques which detect only one particle, thus integrating over all time delays. Our coincidence technique in contrast looks into the electron dynamics with attosecond resolution and shows the underlying dynamics in a very transparent and general way.

The technique to measure time spans by coincidence detection using the rotating electric field vector of circular or elliptical laser light as a clock is highly versatile. The key advantage as compared to techniques detecting only one particle from a sequence of events is that the time resolution is not limited by the width of the pulse as demonstrated in the present work. Coincidence techniques allow the measurement of time intervals based on the differences in momenta (in either magnitude or direction) which can be detected with extremely high precision, even for long pulses, thereby providing a powerful tool for ultrafast science.

Chapter 5 - OXYGEN MOLECULES IN IR LASER FIELDS

In this chapter the dissociation dynamics of O_2^+ molecular ions in IR fields is summarized.

5.1 Introduction

Significant advances in femtosecond laser technology have made it possible to control and analyze the nuclear dynamics in small diatomic molecules [Zewail-88, Niikura-06, Posthumus-04]. In particular, the nuclear dynamics in H_2 and D_2 molecular ions have been studied by analyzing the measured (or calculated) KER spectra of the fragments produced by ultra-short IR pulses with a carrier wavelength of 800 nm and pulse lengths between 7 fs and 20 fs [Bocharova-11, De-11]. In comparison with heavier molecules, the vibrational nuclear motion in H_2^+ (and its isotopes) is simple as it primarily involves the two lowest adiabatic potential curves of the molecular ion. For H_2^+, the dissociative wave packet emerges mainly on the repulsive $|2p\sigma_u>$ state, while a bound oscillating part of the wave packet may remain in the electronic ground state $|1s\sigma_g>$ (see Chapter. 4). The extension of these investigations to heavier molecules is not straightforward, and the interpretation of experimental data is intricate due to the large number of molecular potential curves involved. By analyzing KER spectra from dissociated oxygen ions as a function of the time delay, we found that several intermediate electronic states of the molecular ion usually contribute to the same KER [Bocharova-11, De-10, De-11]. In references [Bocharova-11] and [De-11], we studied the dynamics of N_2, O_2, and CO molecules in intense laser pulses using the CE imaging technique. In comparison with classical and quantum mechanical simulations, we identified transiently populated intermediate states for molecular ions in different charge states and associated dissociation pathways. The occurrence of vibrational revivals in measured KER spectra was scrutinized in reference [De-10] and allowed the identification of relevant molecular potential curves.

In this chapter we present a method for identifying the relevant electronic states involved in the dynamics of the O_2 molecule. First we employ the General Atomic and Molecular Electronic Structure System (GAMESS) quantum chemistry code [Gordon-05] to calculate potential curves and dipole coupling strengths between adiabatic potential curves using the multi-configuration (MC) self-consistent field (SCF) method with a correlation consistent (cc) polarized triple-ξ (pVTZ) basis set (MCSCF/cc-pVTZ) [Schmidt-98, Cramer-04]. Next, in Sec 5.3, we numerically solve the TDSE for the evolution of a given initial vibrational wave packet in the molecular ion on a given BO potential curve. In our quantum mechanical calculations, we

neglect molecular rotation and model the initial state of the molecular ion by assuming instantaneous ionization of the neutral parent molecule in the pump pulse based on the Franck-Condon approximation [Bransden-03]. Our calculations provide KER spectra as a function of the pump-probe delay that reveal the vibrational period and revival times of binding molecular potential curves. The vibrational period and revival times in a *given* electronic state serve as a first criterion for selecting relevant potential curves. This selection process starts by comparing simulated KER spectra that were obtained in separate calculations under the assumption that the nuclear motion in the molecular ion proceeds on a single electronic potential curve with measured KER spectra [De-11]. This comparison involves the scrutiny of simulated and measured KER spectra as a function of time and frequency. For this purpose we derive internuclear-distance (R)-dependent power spectra [Thumm-08, Magrakvelidze-09, Winter-10, Feuerstein-07, Niederhausen-08] by Fourier transformation of the calculated time-dependent nuclear probability density. The power spectra allow us to identify vibrational QB frequencies associated with the bound motion of the vibrationally excited molecular ion. This enables us to further scrutinize the relevance of any given binding electronic state of the molecular ion by comparing revival times [Robinett-04], oscillation periods, and QB frequencies with measured values.

After comparing separate calculations performed for individual BO molecular potential curves with measured KER spectra, we select a small set (in this work two) of curves that agree best with the measured data. In a final separate calculation, we then investigate the dissociative dynamics of the molecule, including dipole couplings between the selected electronic states of the molecular ion in the electric field of the probe-laser pulse (Sec.5.3.2). As an example we present numerical results for the dissociation of O_2^+ molecules. In Sec. 5.3.3 we compare two alternative methods for deriving KER spectra in nuclear wave-function-propagation calculations. The effect of an added long-probe pedestal is investigated in Sec. 5.3.4. Section 5.4 compares measured KER spectra for O_2^+ ions [De-11] with simulated spectra for dipole-coupled potential curves [Magrakvelidze-12-1]. A brief summary and our conclusions follow in Sec. 5.5.

5.2 Potential curve and dipole coupling calculations

For our calculations we used the MCSCF method (See Chapter 2), where a linear combination of configuration state functions (CSF), i.e. Slater determinants of MOs, are

employed to approximate the exact electronic wavefunction of a system. This is an improvement over the HF method where only one determinant is used. By variation of the set of coefficients in the MCSCF expansion in addition to the simultaneous variation of MO coefficients in the basis set expansion, the total electronic wavefunction for a given BO channel is obtained with the lowest possible energy for a given set of occupied and active orbitals [Hartree-28, Roothaan-51] (See Appendix E for input and output examples).

5.2.1 Gaussian basis set

In our calculations we choose AOs that are modeled as Gaussian functions centered at each nucleus of the diatomic molecule (or molecular ion). These AO orbitals are linearly combined to form MOs with a set of expansion coefficients $\{a_i\}$. The MOs are multiplied with electron spin orbitals and combined to make Slater determinants in order to satisfy the Pauli Exclusion Principle. The CSF wavefunctions are equivalent to these Slater determinants and are linearly combined to create the MC wavefunction with coefficients $\{A_k\}$. The expansion coefficients $\{a_i\}$ and $\{A_k\}$ are determined simultaneously based on a variational principle [Bransden-03].

For the accuracy of the calculated potential curves, it is very important to choose appropriate basis functions. The basis set is the set of (mathematical) functions (for example Gaussians) from which the wavefunction is constructed. Since HF and MCSCF methods are variational, larger basis sets tend to produce more accurate results. The basis set with two Gaussians on each AO is called a double-ξ basis. The higher the number of Gaussians used for each AO the more complete the basis is (multiple-ξ basis set). We used the Dunning-type correlation-consistent polarized valence triple-ξ basis set (cc-pVTZ) [Dunning-89]. The "Dunning-type basis set" is an example of a multiple-ξ basis set. The "correlation-consistent" part of the name indicates that the basis set was optimized for calculations including electron correlation through excited CSFs.

5.2.2 Configuration state function

We calculated potential curves and dipole-coupling strengths between adiabatic potential curves using the MCSCF/cc-pVTZ method. The MCSCF wavefunctions were optimized with the $[(1\sigma_g)^2(1\sigma_u)^2(2\sigma_g)^2(2\sigma_u)^2]$ "frozen core", meaning that the occupations of those MOs were not

allowed to vary. The calculations were done for fixed internuclear separations R with steps of 0.02 Å. Dipole-coupling matrix elements for different Rs were calculated including configuration interaction within the graphical unitary group approach (GUGA) [Gould-90].

The ground state of the oxygen molecule has the configuration $[(1\sigma_g)^2(1\sigma_u)^2(2\sigma_g)^2(2\sigma_u)^2](3\sigma_g)^2(1\pi_u)^4(1\pi_g)^2$. A large number of final molecular ion states with different multiplicities and symmetries can be generated after valence photoionization. Those states are given in Table 5.1. The table shows the main configurations that contribute more than 70% to the norm of the MCSCF wavefunction. GAMESS outputs only designate electronic configurations. To link the calculated potential curves and dipole-coupling matrix elements to a given MCSCF state, we used Table 5-1.

Table 5.1. ***The electronic configurations of the calculated states of O_2^+.***

State	Main electronic configuration							
	$1\sigma_g$	$1\sigma_u$	$2\sigma_g$	$2\sigma_u$	$3\sigma_g$	$1\pi_u$	$1\pi_g$	$3\sigma_u$
$X^2\Pi_g$	2	2	2	2	2	4	1	0
$a^4\Pi_u$	2	2	2	2	2	3	2	0
$A^2\Pi_u$	2	2	2	2	2	3	2	0
$^4\Sigma_g^+$	2	2	2	2	2	3	1	1
$f^4\Pi_g$	2	2	2	2	2	2	3	0

The MCSCF process minimizes energy using the variational principle. "Root switching" can be a problem if two states are close in energy and MO and CSF coefficients are only optimized for one MCSCF state. To avoid this problem, we carried out state-averaged MCSCF calculations [Diffenderfert-82], where MO orbitals are optimized not for any one state energy E_j (which is usually the ground state), but for the average of two or more states $\bar{E} = \sum_j^N w_j E_j$, where N is the number of states (in our case 14) included in the average, and the coefficients w_j are positive constants with normalization $\sum_j w_j = 1$. The MCSCF wavefunctions are optimized to minimize the energies E_j. The number of MOs used in the variation space was 60; the number of the Cartesian Gaussian basis functions (atomic orbitals) used was 70. In MCSCF calculations, the specification of how many MO are occupied is crucial. One needs to specify the so-called "active" space. We use the notation- "(m, n)" where m is the number of active electrons and n is the number of orbitals (Chapter 2). As an active space we used MCSCF (7, 6) for O_2^+. The six orbitals are the σ, π, σ*, and π* orbitals of O_2.

5.2.3 Geometry optimization

When performing computations it is important to understand the geometry of the molecule, since many of the physical and chemical properties of the molecule depend on it. We optimized the molecular geometry of neutral (equilibrium internuclear distance 1.152Å) and singly-charged (equilibrium internuclear distance 1.087Å) oxygen molecules using restricted open-shell SCF wavefunctions, where the occupation of closed shells by the electrons are assumed to be fixed, with the wavefunctions represented as a single Slater determinant. "Restricted" indicates that the spin-up and spin-down orbital coefficients in the expansion and energies are the same. The symmetry used was D_{4h} for the linear molecule with inversion center [Cotton-90], since the full $D_{\infty h}$ point group is not supported in GAMESS.

5.2.4 Results

Four of the calculated electronic states for the O_2^+ molecular ion are shown in Fig. 5.1. For selected states ($a^4\Pi_u$ and $f\,^4\Pi_g$ states), we compared data from the literature [Marian-82] with our MCSCF/cc-pVTZ results and found good agreement for both adiabatic potential curves and electric dipole transition matrix elements D_{ij} between two adiabatic electronic states that correspond to potential curves $V_i(R)$ and $V_j(R)$, where indices i and j label electronic states. As an example, our calculated potential curves for the $a^4\Pi_u$ and $f\,^4\Pi_g$ states of O_2^+ and their dipole-coupling matrix elements are compared to results in [Marian-82] in Figs. 5.2 (a) and (b) respectively. In Marian *et al*. [Marian-82], a multi-reference double-excitation configuration interaction (MRD-CI) treatment [Buenker-83] and a double-ξ basis set were used in the calculation (MRD-CI/DZP). MRD-CI includes electron correlation from excited determinants in addition to correlation within the active space. To make sure that our MCSCF/cc-pVTZ method was sufficient compared to calculations that better represent electron correlation, we performed full second-order CI calculations (FSOCI) for the $a^4\Pi_u$ state at four different internuclear distances. FSOCI calculations are similar to MRD-CI but include single and double excitations, while MRD-CI includes only double excitations. Blue dots in Fig. 5.2 (a) indicate results from FSOCI/cc-pVTZ calculations which are in good agreement (within 0.7%) with our MCSCF calculations (red line in Fig. 5.2 (a)). The computational time for FSOCI calculations is 3 orders of magnitude larger than for MCSCF calculations. Since the calculated values from both

methods are similar, we used the numerically less expensive method (MC-SCF) for obtaining electronic states and dipole-coupling matrix elements. Using a larger cc-pVTZ basis set than the basis used in [Marian-82], we can be confident that our calculated results are at least as accurate with regard to the complete basis set limit.

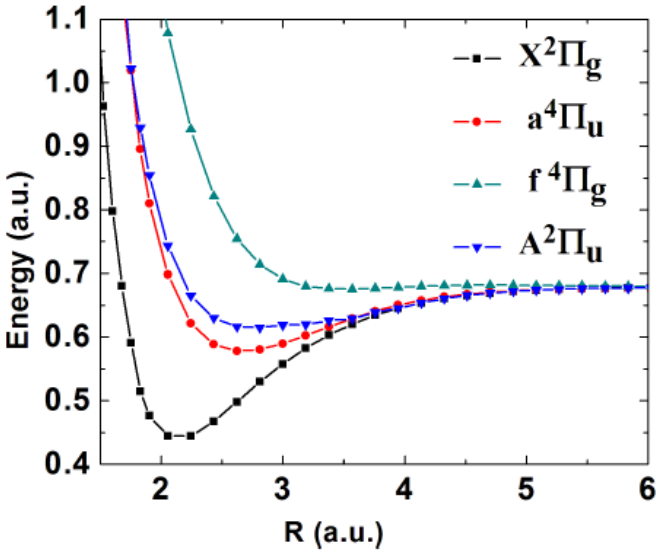

Figure 5.1 ***Calculated potential energies for the O_2^+ molecule using the MCSCF/cc-pVTZ method. The zero of the energy axis is taken as the v = 0 level of the $X^3\Sigma_g^-$ ground state of O_2.***

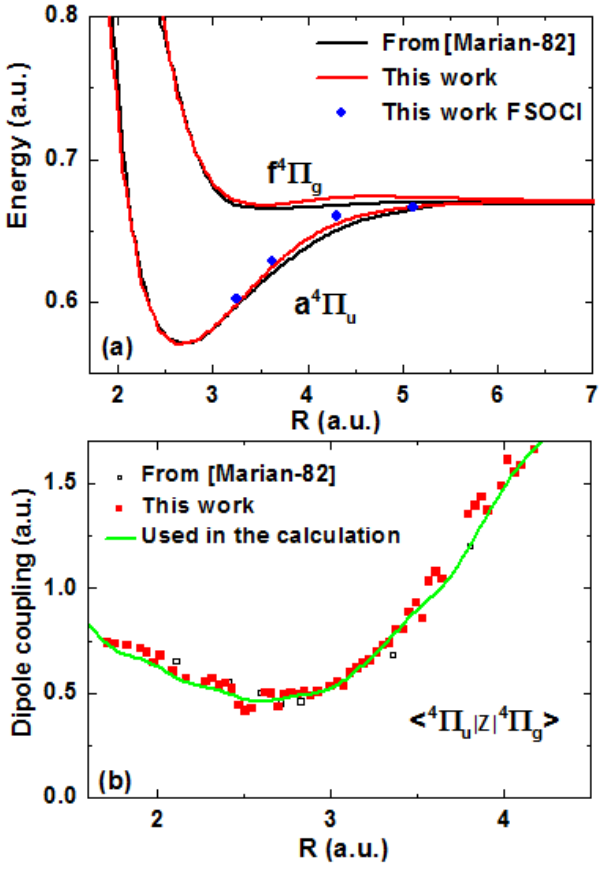

Figure 5.2 ***(a) Calculated potential energies and (b) dipole coupling elements from [Marian-82] using the MRD-CI/DZD method in comparison with our MCSCF/cc-pVTZ application. Blue dots in (a) correspond to the FSOCI -cc-pVTZ method.***

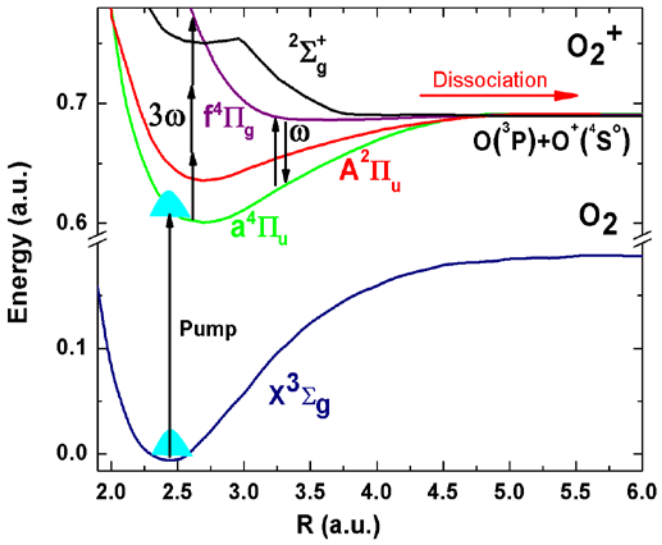

Figure 5.3 ***Schematics for the mapping of the nuclear dynamics in oxygen molecular ions. The pump-laser pulse launches a nuclear wave packet onto the O_2^+ potential curves ($a^4\Pi_u$ and $f\,^4\Pi_g$) by ionizing O_2. After a variable time delay, an intense short probe pulse can cause the dissociation of the molecular ion through one or net two photon processes.***

5.3 Nuclear dynamics

5.3.1 Free nuclear motion in a single electronic state (single-cation-curve calculations)

The dynamics of the nuclear vibrational wave packet can be reconstructed from the KER spectra obtained for a sequence of pump-probe delays τ. This is shown schematically in Fig. 5.3 for the $a^4\Pi_u$ and $f\,^4\Pi_g$ states where a pump pulse singly ionizes an oxygen molecule. In general, the pump pulse can ionize oxygen molecules to any state of O_2^+, for example the $X^2\Pi_u$ and $b^4\Sigma_g^-$ states, but as our calculations show, several characteristic parameters, such as the oscillation period, revival time, and QB frequency for the $a^4\Pi_u$ state match the experimental data best. The probe pulse is assumed to be linearly polarized along the molecular axis throughout this work. The excited oxygen molecule can dissociate through a one-photon or net two-photon process. In order to reveal relevant intermediate electronic states of the molecular ion, we compared the oscillation period and revival times of the bound motion of the wave packet in a given electronic state with *measured* values. We also checked whether transitions between these states are dipole allowed and calculated the strength of their dipole coupling in the electric field.

To identify which of the states are main contributors to the dynamics, we allow the wave packet to freely propagate separately on individual adiabatic potential curves $V_i(R)$ of the

molecular ion. We assume the propagation times to be short enough to neglect the rotation of the molecule and solve the 1-D TDSE

$$i\,\frac{d}{dt}\,\Psi_i = [T_R + V_i(R)\,]\,\Psi_i \qquad (5.1)$$

where $T_R = -(M^{-1})\partial^2/\partial R^2$ is the kinetic energy operator of the nucleus with mass M, V_i are the electronic states.

Starting with a neutral O_2 molecule in the ground state, we model the creation of the O_2^+ vibrational wave packet by the pump pulse in the FC approximation [Bransden-03, Thumm-08, Magrakvelidze-09]. We solve (5.1) for the initial wave packet

$$\Psi_i(R, t=0) = \sum_\nu a_{i,\nu}\,\varphi_{i,\nu}(\mathrm{R}) \qquad (5.2)$$

that is expressed in terms of the FC amplitudes $a_{i\nu}$. The index ν corresponds to vibrational states $\varphi_{i,\upsilon}$ in the i'th bonding adiabatic electronic state of the molecular ion with vibrational energy $\omega_{i,\upsilon}$. We usually assume real amplitudes $\{a_{i\nu}\}$.

After calculating the spectrum $\{\omega_{i,\upsilon}\}$ by either diagonalization of the single-curve Hamiltonian $T_R + V_i(R)$ or by numerical wave-packet propagation of (5.1) subject to the initial condition (5.2), we obtain the field-free evolution of (5.2)

$$\Psi_i(R, t) = \sum_\nu a_{i,\nu}\,\varphi_{i,\nu}(\mathrm{R})\mathrm{e}^{-i\omega_{i,\nu}t}. \qquad (5.3)$$

Repeating single-curve calculations for several potential energy curves (we use one bound potential curve at a time), we aim at identifying relevant electronic states by comparing characteristics of the bound wave packet motion in $V_i(R)$, such as vibrational periods T_i and full and partial revival times $T_{rev,i}$ [Robinett-04], with pump-probe-delay-dependent measured KER data [Bocharova-11, De-10, De-11, Zohrabi-11, Magrakvelidze-12-2,12-1].

We obtain additional information for selecting electronic states that participate in the bound and dissociative nuclear motion of the molecular ion by comparing probability densities obtained from single-curve calculations with measured KER spectra as a function of the pump-probe delay and QB frequency [Thumm-08, Magrakvelidze-09, Winter-10, Feuerstein-07, Niederhausen-08]. The comparison of probability density as a function of propagation time and QB frequency with measured KER spectra gives information about oscillation period and revival times of the bound motion of the wave packet in a given electronic state. By splitting the nuclear probability density

$$\rho_i(R,t) = |\Psi_i(\mathrm{R,t})|^2 = \rho_i^{incoh}(R) + \sum_{\mu\neq\nu} a_{i,\mu}^* \, a_{i,\nu} e^{-i\omega_{i;\nu,\mu}t} \varphi_{i,\mu}^* \varphi_{i,\nu} \qquad (5.4)$$

after getting rid of the incoherent part in equation (5.4) as discussed in Chapter 3, and Fourier transformation the coherent contribution over the finite sampling time T, we obtain power spectrum

$$W_i(R,\omega) = |\widetilde{\rho}_i(R,\omega;T)|^2 \quad , \qquad (5.5)$$

The frequency resolution in ω_i increases with T. Typically, sampling times of the order of a few picoseconds are required to clearly resolve vibrational QB frequencies in the power spectrum of heavy diatomic molecular ions. Examples for single-curve calculations are shown in Fig. 5.4 (a) and (b) for the $A^2\Pi_u$ and in Fig. 5.4 (c) and (d) for the $a^4\Pi_u$ states of O_2^+. Comparison of the simulated vibrational periods, revival times, and QB frequencies for a number of electronic states with measured KER spectra reveals the $a^4\Pi_u$ state as the best match to the experimental oscillation period and the beat frequencies. Table 5.2 shows a comparison of the calculated and measured parameters (oscillation period, revival time, and QB frequencies) for each potential curve we tried in our calculations. The best match to the measured ones is obtained for the state $a^4\Pi_u$.

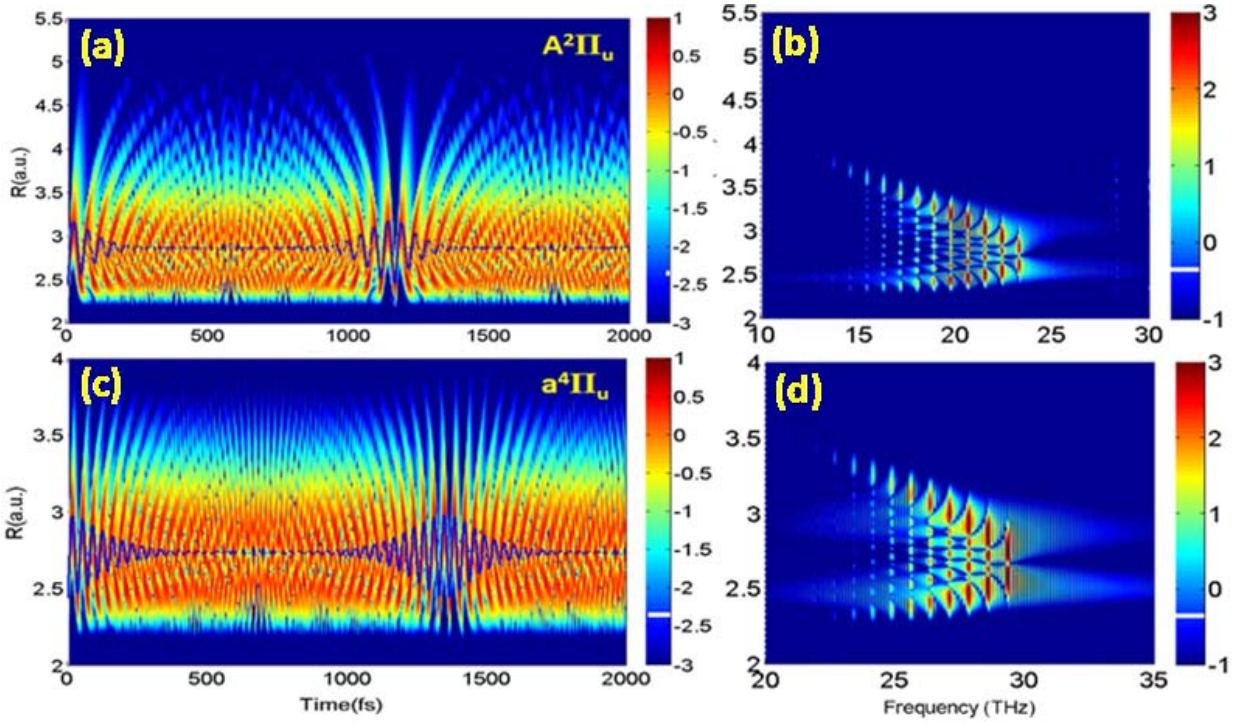

Figure 5.4 ***Single-curve calculations for the A $^2\Pi_u$ (a,b) and a $^4\Pi_u$ (c,d) states of O_2^+. Nuclear probability densities (a,c) and corresponding power spectra (b,d).***

Table 5.2 ***Comparison of calculated and measured revival times and QB frequencies for electronic states of O_2^+.***

	Calculation			Experimental values		
State	Oscillation period (fs)	Revivals (fs)	(THz) QB frequency (v=1 → *v*=2)	Oscillation period (fs)	First full Revivals (fs)	(THz) QB frequency (v=1 → *v*=2)
$X^2\Pi_g$	17	670	58	34	~1200	30
$a^4\Pi_u$	33	1400	30			
$A^2\Pi_u$	36	1200	25			
$b^4\Sigma_g^-$	29	900	35			

5.3.2 Nuclear dynamics on dipole-coupled electronic states

After conducting single curve calculations for several potential curves of O_2^+ and identifying the states by their oscillation periods, revival times and QB frequencies matching the measured values ($a^4\Pi_u$ and $A^2\Pi_u$), we have carried out a full solution of the TDSE (Eq.9, see below) by including the combination of states $a^4\Pi_u$ / $f\,^4\Pi_g$, $a^4\Pi_u$ / $^4\Sigma_g^+$, and $A^2\Pi_u$ / $^2\Sigma_g^+$ in our two-state calculations in order to understand the dissociation channels (the best match to the measured KER corresponds to the $a^4\Pi_u$ / $f\,^4\Pi_g$ process).

Modeling the coherent motion of nuclear vibrational wave packets on several FC-populated adiabatic potential curves of the diatomic molecular ion, we allow for dipole couplings of (coherently launched) nuclear wave packets $\Psi_i(R,t)$ in the electric field of the probe laser pulse by numerically propagating the coupled TDSE with initial condition (5.2) [Thumm-08, Magrakvelidze-09, Winter-10, Feuerstein-07, Niederhausen-08].

$$i\frac{d}{dt}\begin{pmatrix}\Psi_1\\ \Psi_2\end{pmatrix} = \begin{pmatrix}T_R + V_1 & D_{12}\\ D_{21} & T_R + V_2\end{pmatrix}\begin{pmatrix}\Psi_1\\ \Psi_2\end{pmatrix} \quad . \tag{5.6}$$

Fourier transformation of the total nuclear probability density

$$\rho(R,t) = \sum_i \rho_i(R,t) \qquad i = 1,2 \tag{5.7}$$

as discussed in Chapter 3.4 for the sampling time T leads to a power spectrum

$$W(R,\omega) = |\tilde{\rho}(R,\omega;T)|^2. \tag{5.8}$$

In order to simulate KER spectra, we numerically propagate the coupled equations (5.6) for a sufficiently long time t_{max}, including field-free propagation of the nuclear wave packets for

typically ~800 fs after the action of the probe pulse (t_{probe}=10 fs). This allows us to separate the bound and dissociating parts of the nuclear motion in terms of the internuclear distance R, such that the probability current associated with the dissociation of the molecular ion has no relevant contributions for $R > R_1$, whereas bound motion remains restricted to distances $R < R_1$ (see Fig. 5.5). Fourier transformation of the dissociating parts of the nuclear wave packets over the interval $[R_1, R_{max}]$ (typically R_1=4 and R_{max}=330 in our calculations) then yields the momentum representation of the dissociating wave packets

$$\tilde{\Psi}_i^{diss}(P, t_{max}) = \int_{R_1}^{R_{max}} dR \Psi_i^{diss}(R, t_{max}) e^{-iPR} \quad , \tag{5.9}$$

and the momentum representation of the total wave packet (after Fourier transforming the total wave packet $\Psi_i(R,t)$):

$$\tilde{\Psi}_i(P, t_{max}) = \int_{0}^{R_{max}} dR \Psi_i(R, t_{max}) e^{-iPR} \quad , \tag{5.10}$$

where R_{max} (typically about 330 for converged results) is related to the size of the numerical grid. By incoherently adding the corresponding momentum distributions, we obtain the pump-probe-delay (τ) - dependent distribution of fragment KERs as discussed in Chapter 3.7.

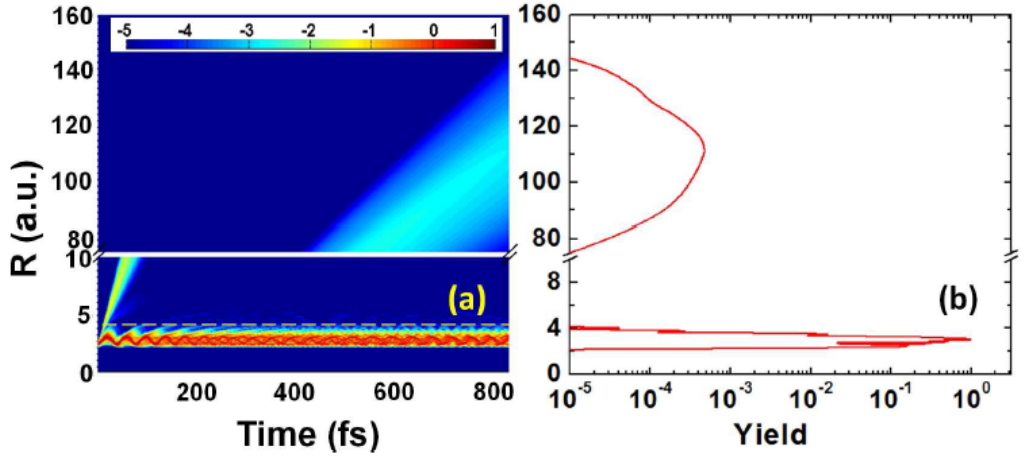

Figure 5.5 ***(a) Probability density ρ(R; t) (Eq.5.4) for O_2^+ at fixed pump-probe delay τ = 10 fs for the $a^4\Pi_u$ - $f\,^4\Pi_g$ two-state calculation. The yellow dashed line corresponds to R_1 = 4. The vibrational wave packet is considered purely dissociative and is propagated for 800 fs after the probe pulse. (b) Probability density as a function of internuclear distance R at t = 800 fs (logarithmic scale).***

Figure 5.5 shows the probability density (see equation (5.4)) as a function of propagation time and the internuclear distance at fixed pump-probe delay (τ = 10 fs) for a calculation with two coupled states, $a^4\Pi_u$ and $f\,^4\Pi_g$. In this calculation we assumed that initially only the $a^4\Pi_u$

state is populated, through a Franck-Condon transition from the ground state of O_2. However, we found that the KER spectra do not change if initially both $a^4\Pi_u$ and $f\ ^4\Pi_g$ states are equally populated. The delayed probe-pulse dipole couples the initial wave packet motion with the $f\ ^4\Pi_g$ state. As mentioned above, for the KER spectra calculations we took only the dissociative part of the wave packet into account. The horizontal yellow dashed line indicates the internuclear separation R_1=4, beyond which the wave packet is considered as purely dissociative. Figure 5.5 (b) shows the probability density on a logarithmic scale as a function of the internuclear distance 800 fs after the pump pulse.

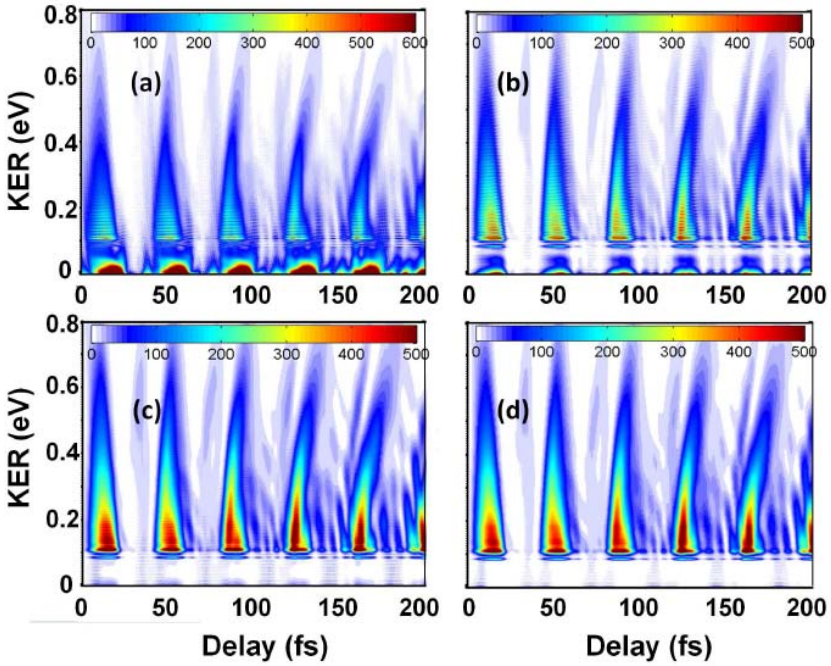

Figure 5.6 ***Calculated KER spectra for the dipole- coupled states $a^4\Pi_u$ and $f\ ^4\Pi_g$ as a function of pump-probe delay for (a) R_1=3, (b) 4, (c) 4.5, and (d) 5 for a 10 fs, 3×10^{14} W/cm^2 probe laser pulse.***

We investigated the effect of the parameter R_1 on the KER spectra. The calculated KER, obtained using the FT method, as a function of pump-probe delay is given in Fig. 5.6 for 10 fs, 3×10^{14} W/cm^2 probe pulses, and for R_1=3 (Fig. 5.6 (a)), R_1=4 (Fig. 5.6 (b)), R_1=4.5 (Fig. 5.6 (c)), and R_1=5 (Fig. 5.6 (d)). From Fig. 5.5 (b) one can see that for all values R_1>4.5 the KER spectra should give the same result. Indeed, the KER spectra shown in Fig. 5.6 (c) (R_1=4.5) and (d) (R_1=5) are almost the same. We found that simulations with R_1 = 4 yield the best agreement with measured KER spectra (in Sec.5.4 below).

5.3.3 Comparison with the "virtual detector method" for simulating KER spectra

In addition to the FT calculations, we also applied an alternative methods, the so-called "virtual detector" (VD) method, described in Chapter 3.8, for obtaining KER spectra [Feuerstein-03]. This method allows the computation of fragment-momentum distributions without propagating the wave packet over a large numerical grid. In these VD calculations only, we used a grid length of R_{max} = 40 with spacing ΔR = 0.01 (Fig. 5.7). The VD covers the R interval $[R^{VD}_{min}, R^{VD}_{max}]$ = [6.5, 16.5]. The calculation was carried out for a total propagation time of 800 fs with time steps of Δt = 1. Applying the VD method, we calculated the momentum expectation value of the fragments, $p(t_i)$, at each time step t_i. We then combined fragment momenta that fall into small momentum bins in a histogram. From this histogram we obtained the KER spectrum (see [Feuerstein-03] for more details). The KER spectrum obtained with the VD method in Fig. 5.8 is almost identical with our results obtained using the FT method for R_1=4.5 (Fig. 5.6 (c))).

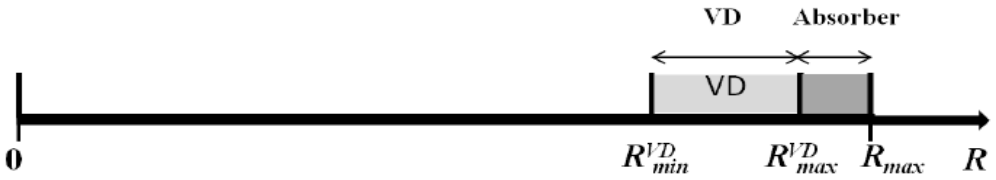

Figure 5.7 ***Partitioning of the numerical grid into a propagation, virtual detector (VD), and absorption interval. The VD covers the interval*** $[R^{VD}_{min}, R^{VD}_{max}]$.

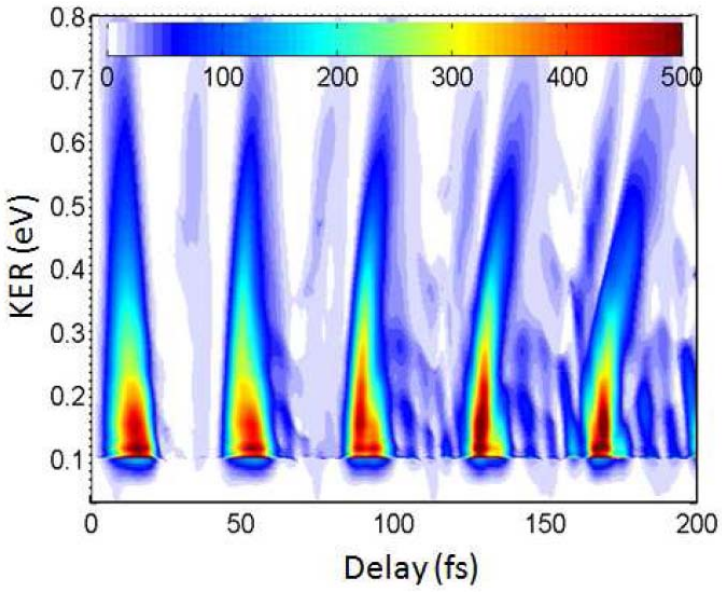

Figure 5.8 ***KER for dipole-coupled*** $a^4\Pi_u$ ***and*** $f^4\Pi_g$ ***states as a function of the pump-probe delay for calculations using the VD method [Marian-82] and a 10 fs,*** 3×10^{14} ***W/cm*** ^{2} ***probe laser pulse.***

5.3.4 Influence of a probe-pulse pedestal

Figure 5.9 shows calculated KER spectra for the same laser parameters as in Fig. 5.8 using the FT method, with the exception that R_1=4 and a long Gaussian pedestal [Thumm-08, Magrakvelidze-09, Winter-10], with a length of 100 fs and intensity 5×10^{11} W/cm^2, is added to the main pulse (see Chapter 4. - Fig. 4.1). Due to the long pedestal a prominent energy-dependent structure appears in the KER spectra. The reason why the energy-dependent structure is present only if a long pedestal is included can be explained based on the relation $\delta E \delta t \geq h$. If only short pulses are present, the resolution in energy is such that one cannot observe the energy-dependent structure. On the other hand, if only the pedestal of the probe pulse is present, the oscillatory motion cannot be resolved [De-11]. For example, in order to resolve energies up to 0.1 eV, corresponding to the vibrational energy spacing in $a^4\Pi_u$, one needs to use pulses that are longer than 45 fs. The time-dependent structure is due to the periodic motion of the coherent vibrational wave packet on the given O_2^+ state (the oscillation period for the $a^4\Pi_u$ state is 33 fs, Table 5.1). A fragment-kinetic-energy dependent structure in the KER spectra was predicted as due to photoionization of vibrational states [De-11, Zohrabi-11].

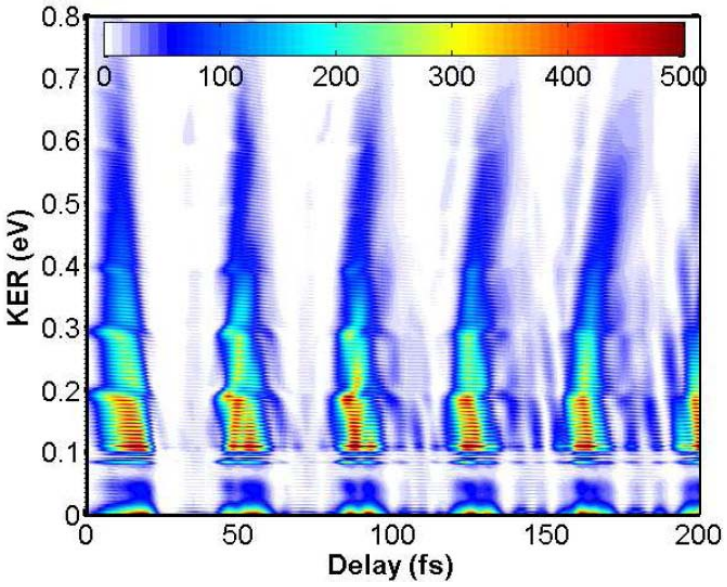

Figure 5.9 ***KER as a function of pump-probe delay for the calculations using the FT method described in Sec. 5.3.2. for R_1 = 4. The probe pulse includes the Gaussian pedestal. The parameters used for the main pulse were 10 fs, with intensity 3×10^{14} W/cm^2 and for the pedestal 100 fs with the intensity 5×10^{11} W/cm^2 (propagated for 800 fs after the end of FWHM of the probe).***

5.4 Comparison with the experiment

The calculated KER as a function of the delay and the corresponding power spectrum (5.16) as a function of the QB frequency f for the $a^4\Pi_u$ - $f\,^4\Pi_g$ two state calculation are shown in Fig. 5.10 (a) and (b) for a 10 fs probe pulse with a peak intensity of 3×10^{14} W/cm^2 and a 100 fs

5×10^{11} W/cm^2 Gaussian probe-pulse pedestal. Figures 5.10 (c) and (d) show the measured KER and power spectrum for a pump-probe intensity of 3×10^{14} W/cm^2 and pulse duration of 10 fs. The measurements were done using velocity map imaging (VMI) spectrometer. The sampling time in the experimental spectrum in Fig. 5.10 (d) is T = 2000 fs with the revival time 1200 fs (not shown) [De-11]. Comparison with the experimental results in Fig. 5.10 (c) and (d) shows that several features of the experimental data are reproduced.

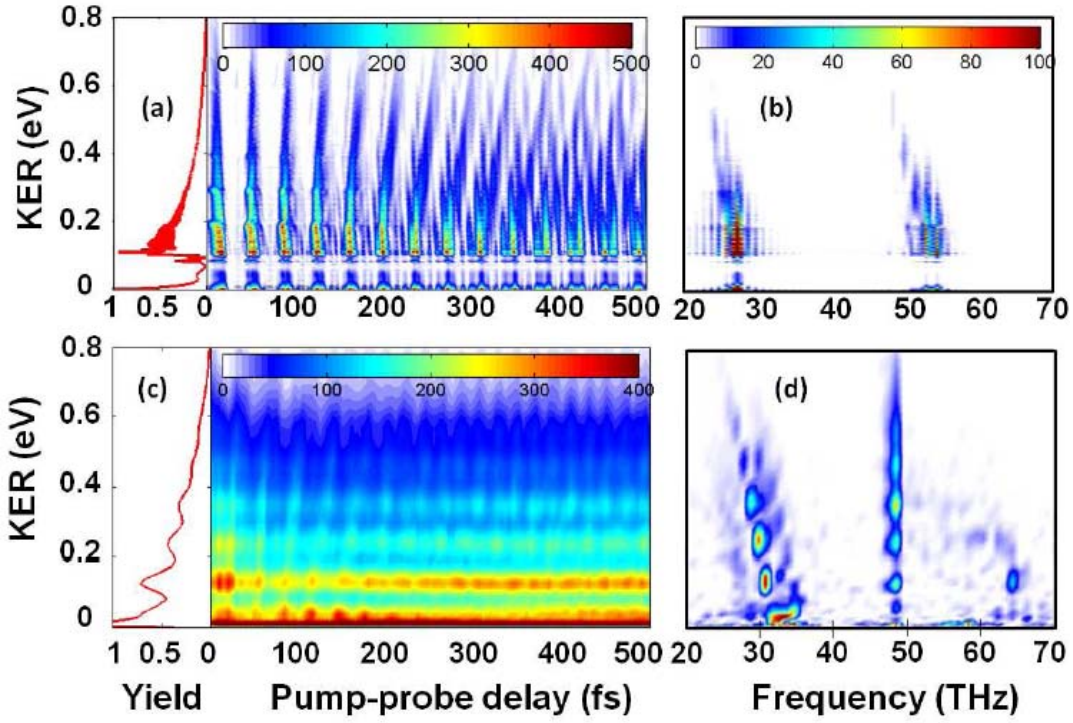

Figure 5.10 ***Calculated (a,b) and measured (c,d) [De-11] KER spectra for O_2^+ as a function of pump-probe delay (a,c) and frequency f (b,d). Calculated KER spectra include dipole-coupling of the $a^4\Pi_u$ and f $^4\Pi_g$ states by the 10 fs probe laser pulse with 3×10^{14} W/cm^2 peak intensity and a 100 fs 5×10^{11} W/cm^2 Gaussian pedestal. The power spectra (b,d) are obtained for a sampling time of 2 ps.***

The oscillatory structure, with a period near 33 fs, is similar to the experimental period near 34 fs. The progressive tilt in the KER with increasing delay complies with a slightly larger return time of the more energetic spectral components of the vibrational wave packet and was noticed earlier in the fragmentation of D_2^+ [Ergler-06-2, Feuerstein-07, Niederhausen-08, Feuerstein-03-1] and O_2^+ [De-11]: a nuclear wave packet with dominant spectral contribution from low-lying vibrational states oscillates faster than a vibrationally warmer wave packet

(corresponding to higher KER), causing the KER structure to tilt toward larger delays. The difference in the classical oscillation periods [Feuerstein-07, Niederhausen-08] that correspond to wave packet components centered around on v=11 and 13 vibrational states amounts to ~2.5 fs. This is consistent with the oscillation period difference between the peaks on energy cuts at 0.13 eV and 0.32 eV in the calculated KER spectra. However, the same difference in oscillation periods is obtained from the measured data for 0.14 eV and 0.25 eV.

For better comparison with the measured KER we focal-volume-averaged our calculations for the intensity range 10^{13} - 4×10^{14} W/cm^2 with steps of 10^{13} W/cm^2, keeping the ratio between the peak intensities of the main pulse and the pedestal constant, according to

$$\overline{C^{diss}}(E,\tau) = \frac{1}{N}\sum_{n=1}^{N} C^{diss}(I_n; E, \tau) \qquad (5.11)$$

where C_{diss} is given by (3.36 in Chapter 3.7) (Fig. 5.11) and $I_n = (n+1)\times10^{13}$ W/cm^2, with n=1, ..., N=13. The volume averaging effect on the energy-dependent structure is small.

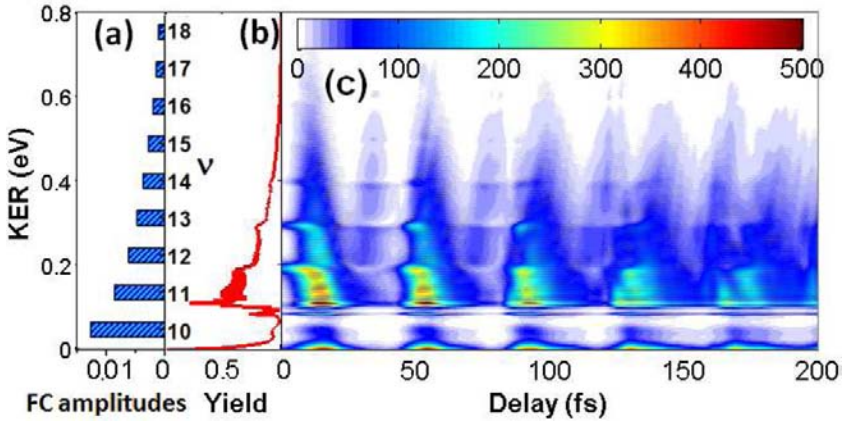

Figure 5.11 ***(a) Franck-Condon amplitudes $\{|a_v|^2\}$ for the vertical ionization from the ground state of O_2 to the $a^4\Pi_u$state of O_2^+. (b) Delay-integrated focal-volume averaged KER as a function of the pump-probe delay, with main pulse length 10 fs, Gaussian pedestal length 100 fs, and for R_1=4. The focal-volume average is performed for peak intensities of the probe pulse between 10^{13} W/cm^2 and 4×10^{14} W/cm^2, with a fixed ratio of the peak intensities of the main pulse and pedestal of 0.01. (c) Delay-dependent focal-volume-averaged KER spectrum.***

As in Figs. 5.9 and 5.10 (a), the energy-dependent structure, with a spacing of approximately 0.1 eV, is still seen in the focal volume averaged result (Fig. 5.11 (b)), where the separation between the peaks corresponds to the kinetic energies from the vibrational states in the $a^4\Pi_u$ electronic state: v = 10 (0.03 eV), v = 11 (0.13 eV), v =12 (0.23 eV), v = 13 (0.32 eV), and v = 14 (0.41

eV). The expected KERs in the brackets are calculated as the dissociation energy limit of the $a^4\Pi_u$ state subtracted from the sum of the given vibrational level and photon energy. The vibrational state ν=10 of the $a^4\Pi_u$ state is energetically just above the dissociation limit of the $f\,^4\Pi_g$ -ω field-dressed Floquet potential energy curve. Fig. 5.11 (a) shows the Franck-Condon amplitudes $\{|a_v|^2\}$ for vertical ionization. The population decreases as the vibrational quantum number increases. Thus, we conclude that the origin of the energy structure likely arises from the vibrational states as predicted in [De-11, Zohrabi-11].

5.5 Summary

To summarize, we developed a method for identifying the adiabatic potential curves involved in the dissociation dynamics that contains three steps. First, we calculate adiabatic potential curves and electric-dipole-coupling matrix elements using the quantum chemistry code GAMESS. Next, we calculate nuclear probability-density spectra as a function of time and QB frequency for one molecular potential curve at a time and compare calculated revival times and QB frequencies with experimental data. After identifying relevant electronic states, we include laser-induced dipole-coupling in improved wave packet propagation calculations and again compare the resulting KER spectra with experimental data. We applied this scheme to O_2 molecules. After separately employing different combinations of electronic states of O_2^+ in our calculations, we concluded that the $a^4\Pi_u$ and $f^4\Pi_g$ states are key players in the dissociation dynamics, as the calculated and measured KER are similar with matching oscillation periods (see Table 5.2) and revival times (not shown in Fig. 5.10). Calculating KER spectra in nuclear wave packet propagation calculations based on the Fourier -transformation method discussed in Sec. 5.3.2 and the virtual detector method in Sec. 5.3.3, we obtained almost identical results. KER calculations including long probe-pulse pedestals were found to add an energy-dependent structure that is reminiscent of but does not clearly reproduce the energy dependence in measured KER spectra. The interpretation of this observed energy dependence remains a challenge for future investigations.

Chapter 6 - NOBLE GAS DIMERS IN TWO-COLOR IR LASER FIELDS

The focus of this chapter is the study of the dissociation process of noble gas dimer ions by analyzing the KER spectra as a function of the pump-probe delay.

6.1 Introduction

Control and imaging of the nuclear wave packet dynamics of diatomic molecules in real time have been made possible by advances in laser technology [Ullrich-12, Calvert-10]. In particular, pump-probe-spectroscopic imaging is being employed to trace the nuclear motion in both, the smallest diatomic molecules, H_2 and D_2 [Ergler-05, Alnaser-05, Feuerstein-07, Ergler-06-2, Winter-09, Calvert-10], and heavier diatomic molecules, such as O_2, N_2, and CO [De-11, Magrakvelidze-12-1, Bocharova-11], most recently including XUV-pump-XUV-probe experiments at free-electron laser facilities [Jiang-10, Magrakvelidze-12-2]. In these experiments the pump pulse ionizes the neutral molecule and a delayed probe pulse dissociates the molecular ion, revealing the nuclear dynamics in the bound and dissociating molecular ions through pump-probe-delay dependent KER spectra.

The noble gas dimers are more weakly bound and have much larger vibrational periods than the diatomic molecules mentioned above. Binding energies of the neutral dimers are in the 1-25 meV range, orders of magnitude less than the binding energy of the dimer ions. Their vibrational periods are of the order of hundreds of femtoseconds, an order of magnitude larger than those of H_2, O_2, N_2 and CO. Another characteristic feature of all noble gases is that the equilibrium distance of the neutral dimer is larger than for the dimer ion, so that the dimer ions contract after photoionization of the neutral parent dimers, before the molecular-ion nuclear wave packet reflects at the inner turning point of its adiabatic molecular state (Figs. 6.1- 6.3).

All these features, especially their comparatively slow nuclear motion, make noble gas dimers very attractive targets for the detailed investigation of their bound and dissociative nuclear dynamics in pump-probe experiments. For example the properties of the noble gas dimers are very important in the modeling of the larger clusters [Poisson-07]. Due to their weak binding, noble gases are metastable and can be made by cooling [Vassen-12].

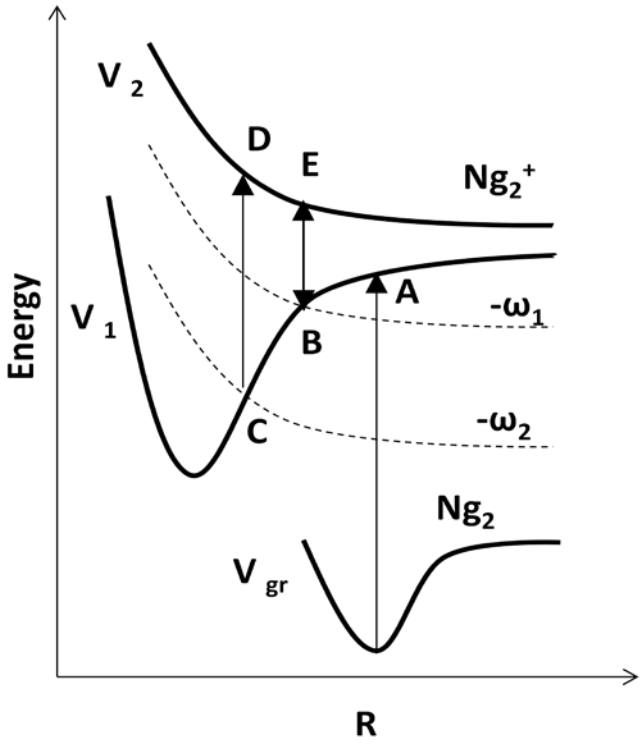

Figure 6.1 ***Schematics of nuclear wave packet motion on generic Ng_2 and Ng_2^+ states. Pont A indicates the center of the Franck-Condon region. Points B-E and C-D correspond to the one photon transitions due to the laser pulses (ω_1 = 1400 or 700 nm and ω_2 = 800 or 500 nm in our calculations) .***

The focus of this chapter is the study of the dissociation process by analyzing the KER spectra as a function of the pump-probe delay for noble gas dimers Ng_2 (**Ng = He, Ne, Ar, Kr, Xe**) and to see whether the "delay gap" observed in measured and calculated KER spectra for the Ar_2 dimer ion [Wu-13-2] can also be observed for other noble gas dimers and explained within the same two-color "pump-dump" mechanism. The chapter is organized as follows. Section 6.2 explains the theoretical model. Our numerical results are presented and discussed in Sect. 6.3. In particular, Section 6.3.1 discusses theoretical and experimental results for Ar_2^+ dimers; Section 6.3.2 covers numerical results for the rest of the noble gas dimers [Magrakvelidze-13]. Section 6.3.2.1 discusses results for the single-cation-curve calculations. Classical vs. quantum aspects of the dissociation process are discussed in Section 6.3.2.2, and KER spectra resulting from the dipole-coupled calculations for the states with and without spin-orbit couplings are shown and discussed in Section 6.3.2.3, followed by a brief summary in Sect. 6.4.

6.2 Theoretical model

Figure 6.1 shows the pump-probe process schematically. The pump pulse singly ionizes a Ng_2 dimer. The nuclear motion in Ng_2^+ can be traced from the KER spectra as a function of the delay between the pump and probe pulses. The delayed probe pulse (with a different wavelength) dissociates the ionized dimer ($Ng_2^+ \rightarrow Ng + Ng^+$). Several dissociation paths are possible depending on the central wavelength of the laser pulse. After the ionization, the wave packet starts moving inward from point A of the Ng_2^+ state ($^2\Sigma_u^+$ or $I(1/2)_u$) to the one-photon crossing points B (ω_1) and C (ω_2), where it may undergo a laser-induced transition to higher states of Ng_2^+ ($^2\Sigma_g^+$ or $II(1/2)_g$), leading to the two different energy bands in the KER spectra depending on the paths ABE or ACD.

As described in Chapter 5, we perform two kinds of calculations. The first are single-cation-curve calculations, in order to identify the wave packet's oscillating motion on $^2\Sigma_u^+$ or $I(1/2)_u$ bound states of Ng_2^+. We plot the nuclear wave packet probability density as a function of propagation time and internuclear distance R, obtaining the wave packet revival times and oscillation periods in a given adiabatic molecular state [Magrakvelidze-12-1]. The calculations were done with time steps of $\Delta t = 1$, a grid spacing of $\Delta R = 0.01$, and with a numerical grid length of 100 (excluding the absorber length of 10). The second type of calculations includes plotting the KER spectra for the dipole-coupled states. The calculations were done with a numerical grid length of 330 (including the absorber with a length of 20), with the same grid spacing and with the same time steps as in the single-cation-curve calculation.

The potential energy curves used in our calculations are shown in Fig. 6.2 without spin-orbit (SO) couplings and in Fig. 6.3 including SO couplings [Havermier-10, Gdanitz-00, Gadea-96, Wüest-03, Cohen-74, Ansari-08, Ha-03, Stevens-77, Slavıček-03, Kalus-03, Paidarová-01, Wadt-80, NIST] The dipole-coupling elements between $I(1/2)_u$ –$II(1/2)_g$ and $^2\Sigma_u^+$ and $^2\Sigma_g^+$ states were taken from [Gadea-96, Ha-03, Paidarová-01, Wadt-80]. Out of all noble gas dimers, He_2 is the weakest bound, with an energy around 1 meV, and the only one not having SO coupled states (The splitting for He_2^+ vanishes because it has only s-electrons [Bransden-03]). For all dimers the equilibrium distance for the neutral is larger than the one for the ionic state.

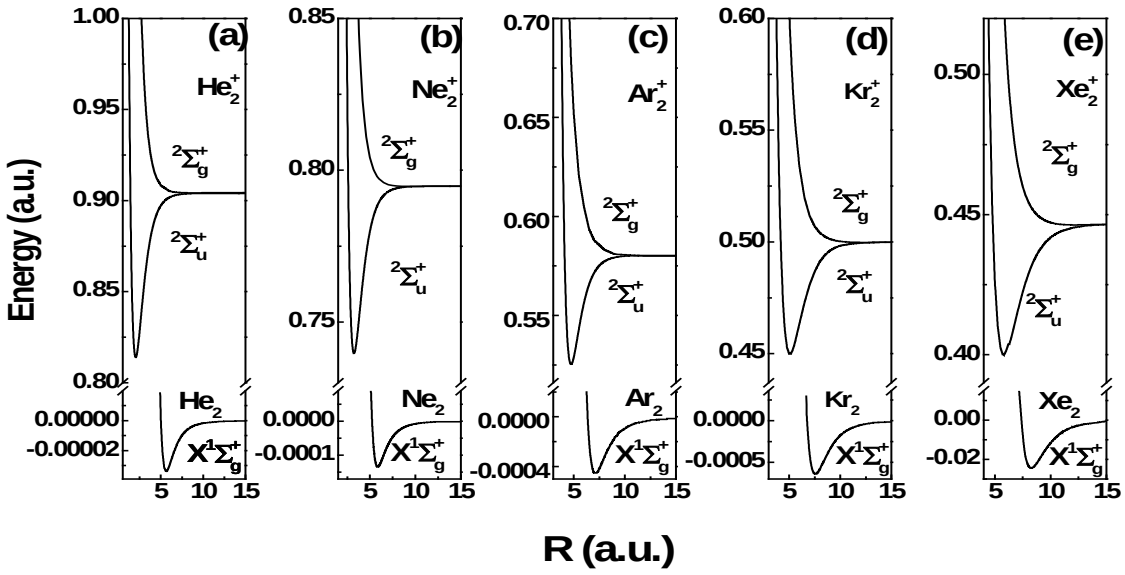

Figure 6.2 ***Potential energy curves of Ng_2 and Ng_2^+ dimers, calculated without including spin-orbit coupling. (a) Ground state of He_2 (according to* [Havermier-10, Gdanitz-00]*), and the two lowest states of He_2^+ (from* [Gadea-96]*). (b) Ground state of Ne_2 (from* [Wüest-03]*), and the two lowest states of Ne_2^+ (from* [Cohen-74, Ha-03]*). (c) Ground state of Ar_2 (from* [Ansari-08]*), and the two lowest states of Ar_2^+ (from* [Ansari-08, Ha-03, Stevens-77]*). (d) Ground state of Kr_2 (from* [Slavıček-03]*), and the two lowest states of Kr_2^+ (from* [Kalus-03]*). (e) Ground state of Xe_2 (from* [Slavıček-03]*), and the two lowest states of Xe_2^+ (from* [Paidarová-01]*).***

6.2.1 Free nuclear motion in a single electronic state

The free nuclear motion in a single electronic state has already been discussed in Chapter. 5, but we briefly repeat the main points and state the grid parameters here as well. We allow the wave packet to freely propagate separately on individual adiabatic potential curves $V_i(R)$ of the dimer ion. We neglect the rotation of the dimer and solve the TDSE

$$i\,\frac{d}{dt}\,\Psi_i = [T_R + V_i(R)\,]\,\Psi_i \qquad (6.1)$$

where $T_R = -(1/M)\partial^2/\partial R^2$ is the kinetic energy operator of the nucleus with mass M, and V_i designates an adiabatic molecular potential curve of a noble gas dimer ion.

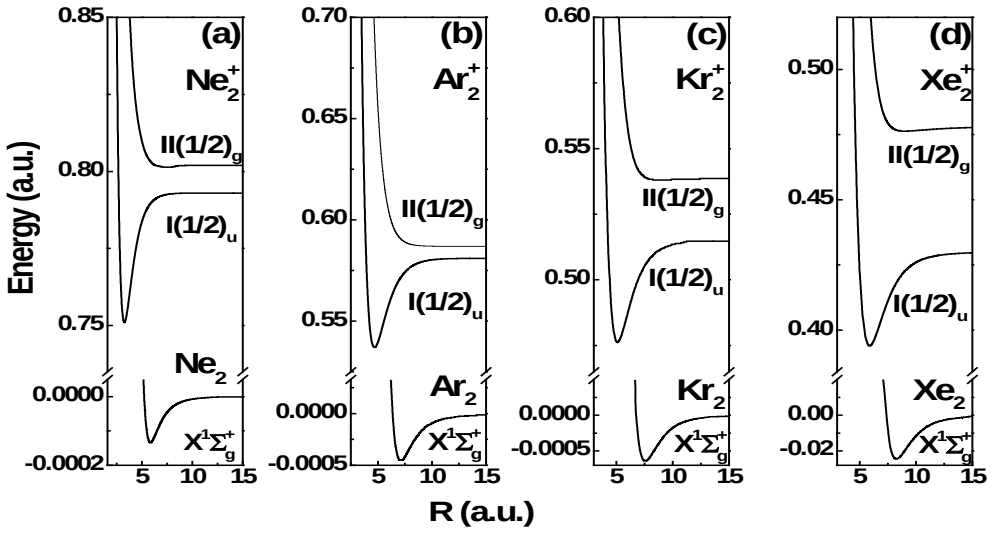

Figure 6.3 ***Potential energy curves of Ng_2 and Ng_2^+ dimers, calculated including spin-orbit coupling. (a) Ground state of Ne_2 (from* [Wüest-03]*), and the two lowest states of Ne_2^+ (from* [Cohen-74]*). (b) Ground state of Ar_2 (from* [Ansari-08]*), and the two lowest states of Ar_2^+ (from* [Ha-03]*). (c) Ground state of Kr_2 (from* [Slavíček-03]*), and the two lowest states of Kr_2^+ (from* [Kalus-03]*). (d) Ground state of Xe_2 (from* [Slavíček-03]*), and the two lowest states of Xe_2^+ (from* [Paidarová-01]*).***

Starting with the neutral dimer Ng_2 in the ground state we model the creation of the Ng_2^+ vibrational wave packet by the pump pulse in the FC approximation [Bransden-03, Thumm-08, Magrakvelidze-09]. For modeling a more "realistic" ionization process, ADK transition rates [Niederhausen-08, Brichta-06] could be used that give very similar results, so the results we show for single-cation-curve calculations are for FC approximation. We solve (6.1) for the initial wave packet

$$\Psi_1(R, t = 0) = \sum_\nu a_{1,\nu}\, \varphi_{1,\nu}(R) \tag{6.2}$$

that can be viewed as a coherent superposition of vibrational states $\varphi_{1,\nu}$ in $V_1(R)$ with amplitudes $a_{1,\nu} = \langle \varphi_{1,\nu} | \Psi_{\mathrm{gr}}(R, t = 0) \rangle$, where $\Psi_{\mathrm{gr}}(R, t = 0)$ is the ground state of the neutral dimer. The index ν corresponds to vibrational states $\varphi_{1,\upsilon}$ in the V_1 vibrational state of the molecular ion with vibrational energy $\omega_{1,\upsilon}$. By numerical wave packet propagation (Chapter 3) [Thumm-08, Magrakvelidze-09] of (6.1) with the initial condition (6.2), we obtain the field-free evolution of Ψ_1

$$\Psi_1(R, t) = \sum_\nu a_{1,\nu}\, \varphi_{1,\nu}(R) e^{-i\omega_{1,\nu} t}. \tag{6.3}$$

Examining the nuclear probability density

$$\rho_1(R,t) = |\Psi_1(R,t)|^2 \tag{6.4}$$

as a function of the propagation time t in $V_1(R)$ allows us to identify oscillation periods and revival times [Bocharova-11, Robinett-04].

6.2.2 Dipole-coupled calculation

Ionization and dissociation by pump and probe pulse

Nuclear dynamics on dipole-coupled electronic states are discussed in Chapter 3.4 and Chapter 5.3.2, but modeling the ionization in the pump pulse in FC approximation. Here we present the dipole-coupled calculations for the ionization by pump and probe pulses using ADK rates. Starting with neutral Ng_2 dimers, the parts of the wave packet from the ground potential of Ng_2 V_{gr} are moved onto the Ng_2^+ bound potential curves V_1 ($^2\Sigma_u^+$ or $I(1/2)_u$) during the pump and probe pulses using ADK transition rates Γ_{ADK} [Niederhausen-08, Brichta-06]. In general, wave packets can be launched onto both bound and repulsive states of Ng_2^+ (V_1 ($^2\Sigma_u^+$ or $I(1/2)_u$), and V_2 ($^2\Sigma_g^+$ or $II(1/2)_g$)), respectively. The part that is launched onto the excited state does not change the main features of the KER spectra. Therefore, we assume that initially only the bound state is populated. The pump pulse and delayed probe pulse can dissociate the Ng_2^+ ion. The TDSE for this process can be written as:

$$i\frac{d}{dt}\begin{pmatrix}\Psi_{gr}\\ \Psi_1\\ \Psi_2\end{pmatrix} = \begin{pmatrix}V_{gr}-i\Gamma_{ADK} & 0 & 0\\ 0 & T_R+V_1+i\Gamma_{ADK} & D_{21}\\ 0 & D_{12} & T_R+V_2\end{pmatrix}\begin{pmatrix}\Psi_{gr}\\ \Psi_1\\ \Psi_2\end{pmatrix} \tag{6.5}$$

where T_R= - (1/M) $\partial^2/\partial R^2$ is the kinetic energy of the nuclei, Ψ_{gr} is the ground-state vibrational wavefunction obtained by imaginary time propagation in the ground state V_{gr} of Ng_2, and $D_{ij} = E(t)d_{ij}$, with $d_{ij} = \langle\Psi_i|R|\Psi_j\rangle$, are transition dipole matrix elements between the two cation adiabatic electronic states. The combined external electric field $E(t)$ of the pump and probe pulses is

$$E(t,\tau) = E_{01}\cos[\omega_1(t)]exp\left[-2ln2\left(\frac{t}{T_1}\right)^2\right] + E_{02}\cos[\omega_2(t-\tau)]exp\left[-2ln2\left(\frac{t-\tau}{T_2}\right)^2\right] \tag{6.6}$$

The pump (probe) pulse is assumed to have a Gaussian envelope with electric field amplitude E_{01} (E_{02}), frequency ω_1 (ω_2), and pulse length (full width – half intensity maximum) T_1 (T_2).

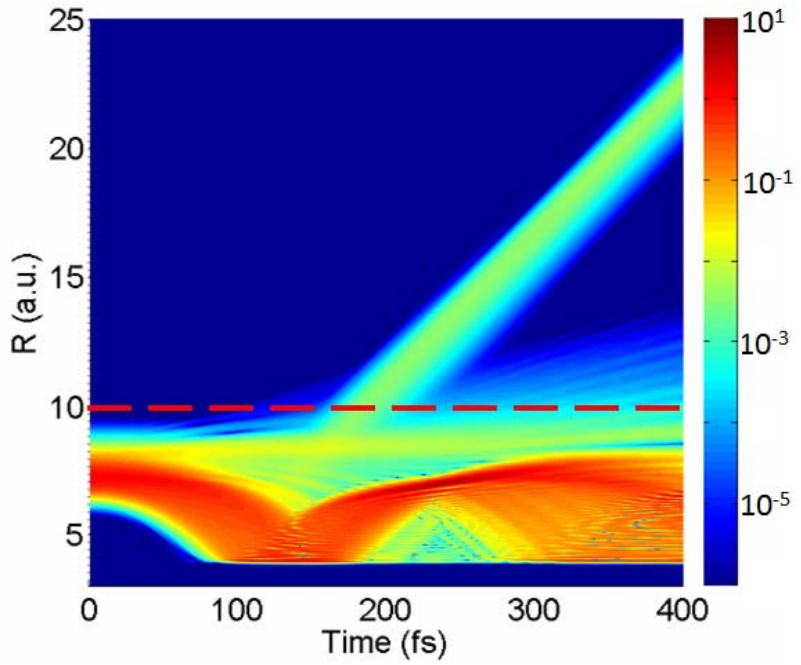

Figure 6.4 ***Probability density of the nuclear wave packet moving on the $^2\Sigma_u^+$ state of Ar_2^+ for a pump-probe (800 -1400 nm) delay of 150 fs and laser intensity 10^{14} W/cm^2. The dashed red line corresponds to the R_1=10 cut. The 500 fs propagation time begins after the end of the FWHM of the probe pulse.***

After the probe pulse has passed, the wave packet is allowed to freely propagate for a sufficiently long time (~500 fs). This allows the nuclear wave packet to completely enter the region $R > R_1$ (R_1=10), and the bound part of the wave packet becomes separable from its dissociating part (Fig. 6.4) [He-10]. In order to determine the KER spectrum of the molecular ion, we Fourier transform the dissociating parts of the nuclear wave packet over the interval [R_1,R_{max}] to obtain the momentum representation,

$$\tilde{\Psi}_i^{diss}(P,t) = \int_{R_1}^{R_{max}} dR \Psi_i^{diss}(R,t) e^{-iPR}, \tag{6.7}$$

where R_{max} is the maximum size of the numerical grid (310 in our calculations excluding the absorber), and R_1 is 10. The distribution of the Ng^+ fragment energies as a function of the delay can then be written as (Chapter 3.7)

$$C^{diss}(E,\tau) \propto \sum_i \left|\tilde{\Psi}_i^{diss}(P,t)\right|^2 \tag{6.8}$$

where $E = P^2/2M$ is the energy, and P is the momentum of the Ng^+ fragment. The total KER is twice E.

6.3 Results and discussions

6.3.1 Measured and calculated results for Ar_2^+ dimers

6.3.1.1 Experiment

The experiment was done at the Institute of Nuclear Physics (IKF) in the Goethe University in Frankfurt, Germany. In the experiment a *Ti*:sapphire laser system was used to generate 780 nm pulses that were split into a pump and probe pulse, then one pulse was sent to an optical parametric amplifier to vary its wavelength (1400 nm). The time delay between the pump and probe pulse was controlled using a motorized translation stage with a step size of 10 fs. Neutral Ar_2 was generated from a collimated supersonic gas jet and ionized by linearly polarized laser pulses at various wavelengths. The COLTRIMS apparatus was used to detect charged fragments [Ullrich-03]. The 3D momenta and KER as a function of pump-probe delay of the Ar^+ ions from ionization and dissociation events were reconstructed from the detected times of flight and positions of the charged particles.

6.3.1.2 Results

Before conducting a TDSE calculation including dipole couplings, we first try to identify electronic states that contribute to the dissociation dynamics by examining the dynamics of a nuclear wave packet separately on individual adiabatic potential curves of the molecular ion, in our case $^2\Sigma_u$ or $I(1/2)_u$. Looking at the oscillation period and revival times [Bocharova-11, Robinett-04] for each state and comparing those values to the measured ones, we choose the state contributing to the dynamics.

As an example, the probability density (6.4) of the freely propagated wavefunction on the $I(1/2)_u$ potential curve is given in Fig. 6.5. As one can see the revival time for the wavefunction is around 7.4 ps and the wavefunction oscillation period for this state is around 250fs, matching the oscillations observed in the experiment. Thus, the $I(1/2)_u$ electronic state plays a major role in the dissociation dynamics. The $^2\Sigma_u$ state has an oscillation period around 230 fs, close to the experimental value, but the expected KER for this state does not match the measured KER (Table 6.1). Table 6.1 shows all the combinations and expected KERs for the Ar_2^+ states with and without SO coupling. The combination of the $I(1/2)_u$ state coupled with the $II(1/2)_g$ state gives an expected KER closest to the experimental values.

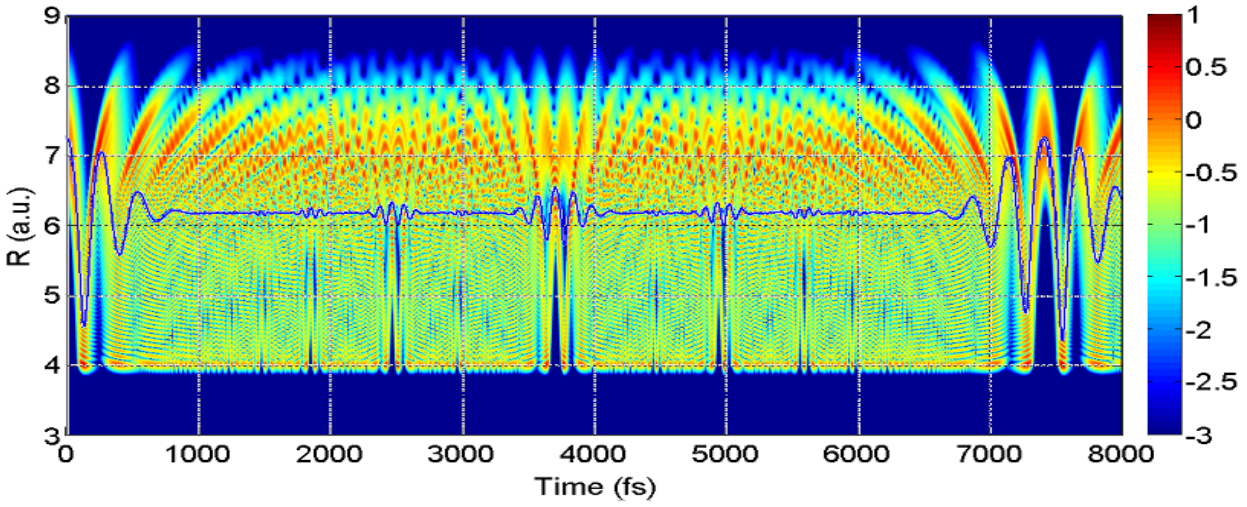

Figure 6.5 ***Probability density of a freely propagated wavefunction on an Ar_2^+ potential curve ($I(1/2)_u$). The solid blue line corresponds to the expectation value of the internuclear distance <R>.***

Table 6.1 ***Expected KERs for electronic states of Ar_2^+ with and without SO coupling.***

Electronic state	Expected KER (1400nm) eV	Expected KER (800nm) eV	Measured KER (1400nm) eV	Measured KER (800nm) eV
$^2\Sigma_u / ^2\Sigma_g^+$	0.75	1.41	0.5	1.2
$^2\Sigma_u / ^2\Pi_g^+$	0.70	1.40		
$I(1/2)_u$ / $I(1/2)_g$	0.71	2.24		
$I(1/2)_u$ / $I(3/2)_g$	0.72	2.26		
$I(1/2)_u$ / $II(1/2)_g$	0.53	1.22		

We have done calculations including the following states. Without SO coupling $^2\Sigma_u$ / $^2\Sigma_g^+$, $^2\Sigma_u$ / $^2\Pi_g^+$, and with SO coupling $I(1/2)_u$ / $II(1/2)_g$, $I(1/2)_u$/ $I(3/2)_g$, *and* $I(1/2)_u$/ $I(1/2)_g$. The states leading to the best agreement with experimental KER spectra are: $I(1/2)_u$ and $II(1/2)_g$.

Figure 6.6(b) shows our calculated time-delay-dependent KER spectrum focal-volume averaged over intensities between 10^{12} and 10^{14} W/cm^2. The numerical simulation reproduces several features of the experimental data in Fig. 6.6(a), such as the strong enhancement of the dissociation yield near zero time delay and (for both positive and negative delays) and the periodic stripes that map the oscillation of the vibrational wave packet on the $I(1/2)_u$ potential

curve. Most importantly, the frustrated dissociation effect, i.e., the "delay gap" in the band of KERs near 1.18 eV for positive delays, is reproduced in the calculation. Numerical tests show that this gap also occurs at different combinations of wavelengths (we tried the pump/probe wavelengths 600-1200 nm, 790-1000 nm, and 790-1800 nm), as long as the wavelengths of the pump and probe pulse remain sufficiently different for the resulting two bands of KER to be distinguishable in the KER spectrum. Two pulses of different wavelength can thus be used as a gate, either allowing or terminating the previously initiated dissociation along a specific adiabatic molecular potential curve.

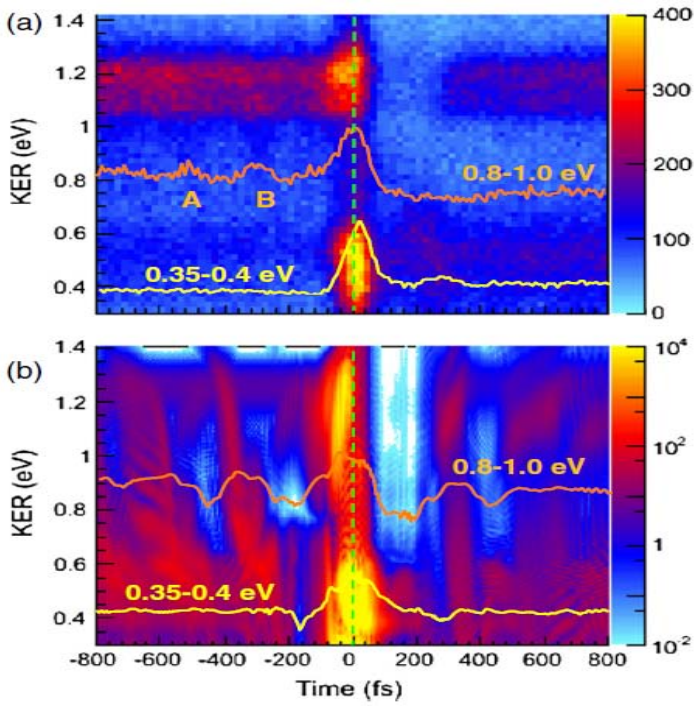

Figure 6.6 ***(a) Measured KER spectrum for Ar^+ as a function of the pump-probe time delay for 60 fs laser pulses with a peak intensity of 10^{14} W/cm^2. The orange and yellow curves are partial fragment yields obtained by integrating the spectrum in (a) over the KER ranges from 0.8 to 1.0 eV and 0.35 to 0.4 eV, respectively. (b) Corresponding calculated KER spectrum.***

6.3.2 Calculated results for Ng_2^+ dimers

6.3.2.1 Single-cation-curve calculations

First, the numerical results for single-cation-curve calculations are discussed for the nuclear motion in Ng_2^+ dimers on $I(1/2)_u$ potential curves [De-10, De-11, Magrakvelidze-12-1, Thumm-08]. Figure 6.7 shows the probability density (6.4) of the freely propagated vibrational

wave packets in the $I(1/2)_u$ states of Ne_2^+, Ar_2^+, Kr_2^+, and Xe_2^+. Our single-cation-curve calculations for the $^2\Sigma_u^+$ states yield similar probability densities with slightly different oscillation periods and full revival times (not shown). The full revival times and wave packet oscillation periods for the wave packet motion in the $^2\Sigma_u^+$ and $I(1/2)_u$ states, excluding and including SO coupling, respectively, are summarized in Table 6.2. This table also lists the number of bound vibrational states in both electronic cation states. The oscillation period and revival time for the Ar_2^+ $I(1/2)_u$ state are close to those observed [Wu-13-2].

Some periodic oscillatory structure is present for the He_2^+ dimer in the single-cation-curve calculations, and the revival time is of the order of 525 fs, but the structure does not allow the extraction of a vibrational oscillation period due to the very delocalized vibrational ground state of He_2 (Fig. 6.7(a)). The width of this state is 15 a.u. Table 6.3 summarizes some of the characteristic parameters of the noble gas dimers and their cations, such as the SO splitting, reduced mass, ionization and dissociation energies, ground-state equilibrium distances, and the width of the ground state probability densities as obtained from our calculations.

Table 6.2 ***Revival times and wave packet oscillation period for $I(1/2)_u$ and $^2\Sigma_u^+$ states of Ng_2^+ dimers, and variance $(\Delta R)^2$ calculated at the oscillation period T_{osc}.***

Dimer	$^2\Sigma_u^+$			$I(1/2)_u$			Variance $(\Delta R)^2$ (a.u.) calculated at T_{osc}
	Number of bound vibrational states	Oscillation period (fs)	Revival times (ps)	Number of bound vibrational states	Oscillation period (fs)	Revival times (ps)	
He_2^+	23	-	0.5	-	-	-	>12
Ne_2^+	41	250	2.8	32	230	2.2	0.85
Ar_2^+	69	290	7.9	63	250	7.5	0.15
Kr_2^+	111	490	22	91	460	19.0	0.09
Xe_2^+	149	550	39	131	510	38.2	0.03

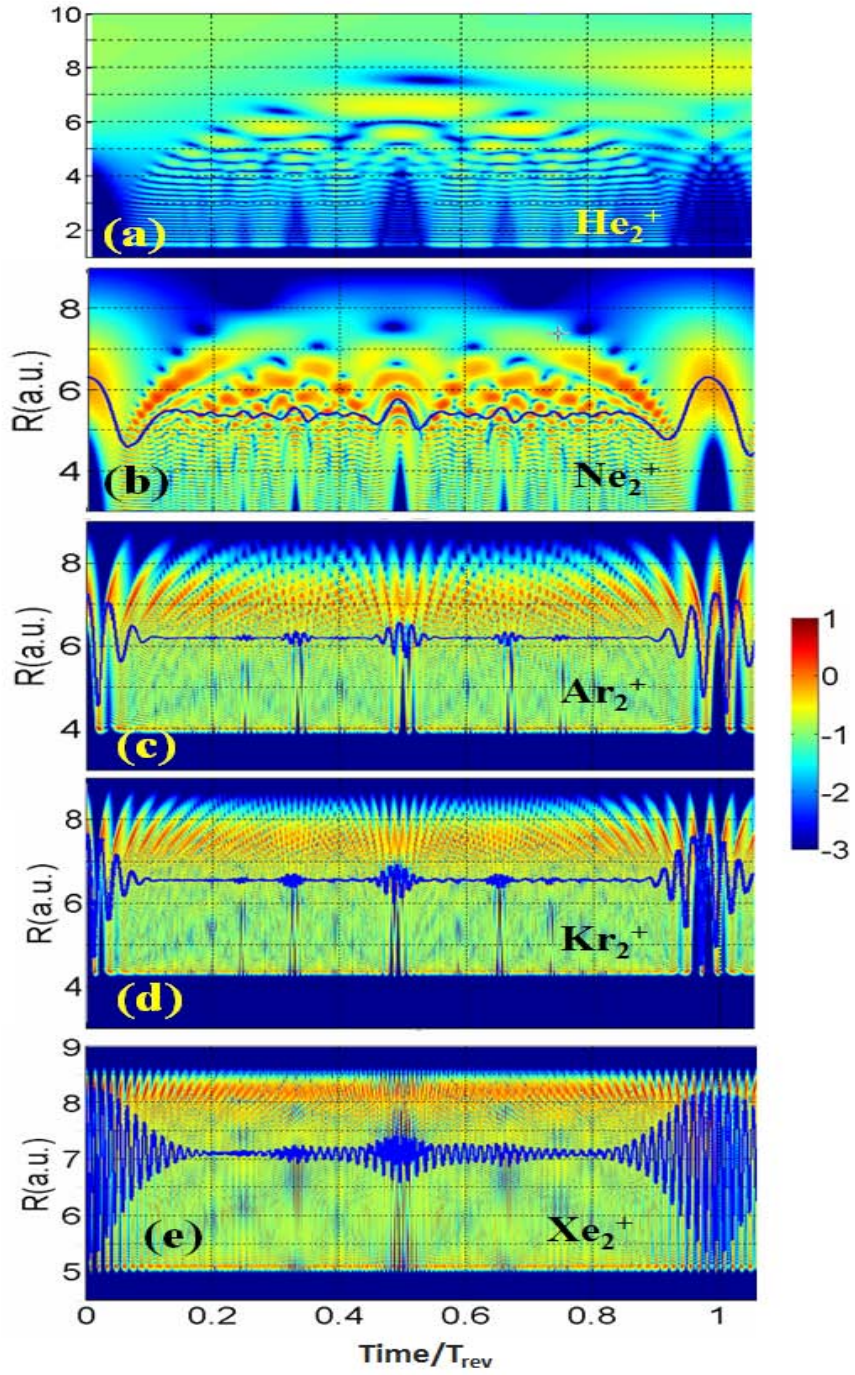

Figure 6.7 ***Probability density of the nuclear wave packet as a function of the internuclear distance R and scaled propagation time for*** $I(1/2)_u$ ***states of*** He_2^+ ***(a),*** Ne_2^+ ***(b),*** Ar_2^+ ***(c),*** Kr_2^+ ***(d) and*** Xe_2^+ ***(e) dimers. The superimposed blue curve shows the expectation value <R>.***

Table 6.3 ***Selected properties of noble gas dimers (Ng_2) and their cations (Ng_2^+). Column 2 – reduced mass, 3 – equilibrium distance $R_0(Ng_2)$ of the ground state of neutral dimer, 4 – equilibrium distance of the dimer cation $R_0(Ng_2^+)$ without SO coupling, 5 – dissociation energy of the neutral dimer ground state $D_e(Ng_2)$, 6 – dimer cation dissociation energy in the ground state $D_e(Ng_2^+)$ without spin-orbit coupling, 7 – dissociation energy in the ground state $D_e(Ng_2^+)$ with spin-orbit coupling. 8 – ionization energy I_p of Ng_2, 9 – spin-orbit splitting of Ng_2^+ (eV), 10 – the full width at half maximum of the ground state dimer nuclear probability density.***

1	2	3	4	5	6	7	8	9	10
Dimer	**Reduced mass of Ng_2 (a.u.)**	**$R_0(Ng_2)$ (a.u.)**	**$R_0(Ng_2^+)$ (a.u.)**	**$D_e(Ng_2)$ (meV)**	**$D_e(Ng_2^+)$ $^2\Sigma_u^+$ (eV)**	**$D_e(Ng_2^+)$ $I(1/2)_u$ (eV) [10]**	**I_p (eV) of Ng_2 [7]**	**SO splitting of Ng_2^+ (eV)**	**Width of Ng_2 vibrational ground state (a.u.)**
He_2	3651.91	5.61[4]	2.4 [8]	0.94 [4]	2.5[8]	-	24.6	-	15
Ne_2	18411.65	5.8[5]	3.3[1]	3.6[5]	1.2[9]	1.17	21.76	0.096[1]	1.6
Ar_2	36447.90	7.1 [2]	4.6[1,2]	12.3[2]	1.24[10]	1.19	14.51	0.18[1,2]	1.0
Kr_2	76456.01	7.6 [6]	5.0[1]	17.3[6]	1.23[10]	1.05	12.87	0.67[1]	0.7
Xe_2	119789.70	8.3 [6]	5.9[3]	24.4[6]	1.08[10]	0.79	11.24	1.31[3]	0.3

[1] Ha-03, [2] Ansari-08, [3] Paidarová-01, [4] Gdanitz-00, [5] Wüest-03, [6] Slavíček-03, [7] NIST, [8] Gadea-96, [9] Cohen-74, [10] Wadt-80

6.3.2.2 Classical and quantum mechanical approach to dissociation dynamics

With increasing mass of the dimer the number of oscillations during which the vibrational motion in the dimer cation dephases increases (Fig. 6.7(b-e)). For the Xe_2^+ dimer the nuclear wave packet dephases much slower compared to Ne_2^+. The number of vibrational oscillations the wave packet completes before dephasing is 1 for Ne_2^+, ~3 for Ar_2^+, ~ 5 for Kr_2^+, and ~14 for Xe_2^+, indicating that heavier dimers more closely resemble classical particles, in compliance with the correspondence principle. In addition, the vibrational ground states of heavier dimers are more localized. For example, the ground-state probability density has a width of 0.5 a.u. for Xe_2 and ~15 a.u. for He_2.

To expand more on the "classical" character of heavier dimers, briefly mentioned in section 6.3.2.1, the classical approach to dissociation dynamics is discussed based on the variances ΔR^2 and ΔP^2. Figure 6.8 summarizes the calculated variances $\Delta R^2 = \langle R^2 \rangle - \langle R \rangle^2$, $\Delta P^2 = \langle P^2 \rangle - \langle P \rangle^2$, and $\Delta R \Delta P$ for wave packet motion in $I(1/2)_u$ state of Ng_2^+ ions as a function of time, scaled with the revival times of corresponding molecular ion. As shown in Fig. 6.8 and in the last colomn of Table 6.2, the calculated ΔR^2 variance is more than one order of magnitude less for Xe_2^+ compared to Ne_2^+ after one vibrational oscillation period T_{osc} in $I(1/2)_u$, pointing to less spread of the wave packet as the mass of the dimer increases. The variance oscillation is

consistent with the wave packet oscillation in $I(1/2)_u$ states and the $(\Delta R)^2$ variances have clear minima at the revival times (corresponding to $t / T_{rev} = 1$ on the graph). As the mass of the dimer icreases, the minima become more distinctive. The same is true for the momentum variance $(\Delta P)^2$; the spread has noticable structure at the revival times. The last column in Fig. 6.8 the plots calculated uncertainty product $\Delta R \Delta P$.

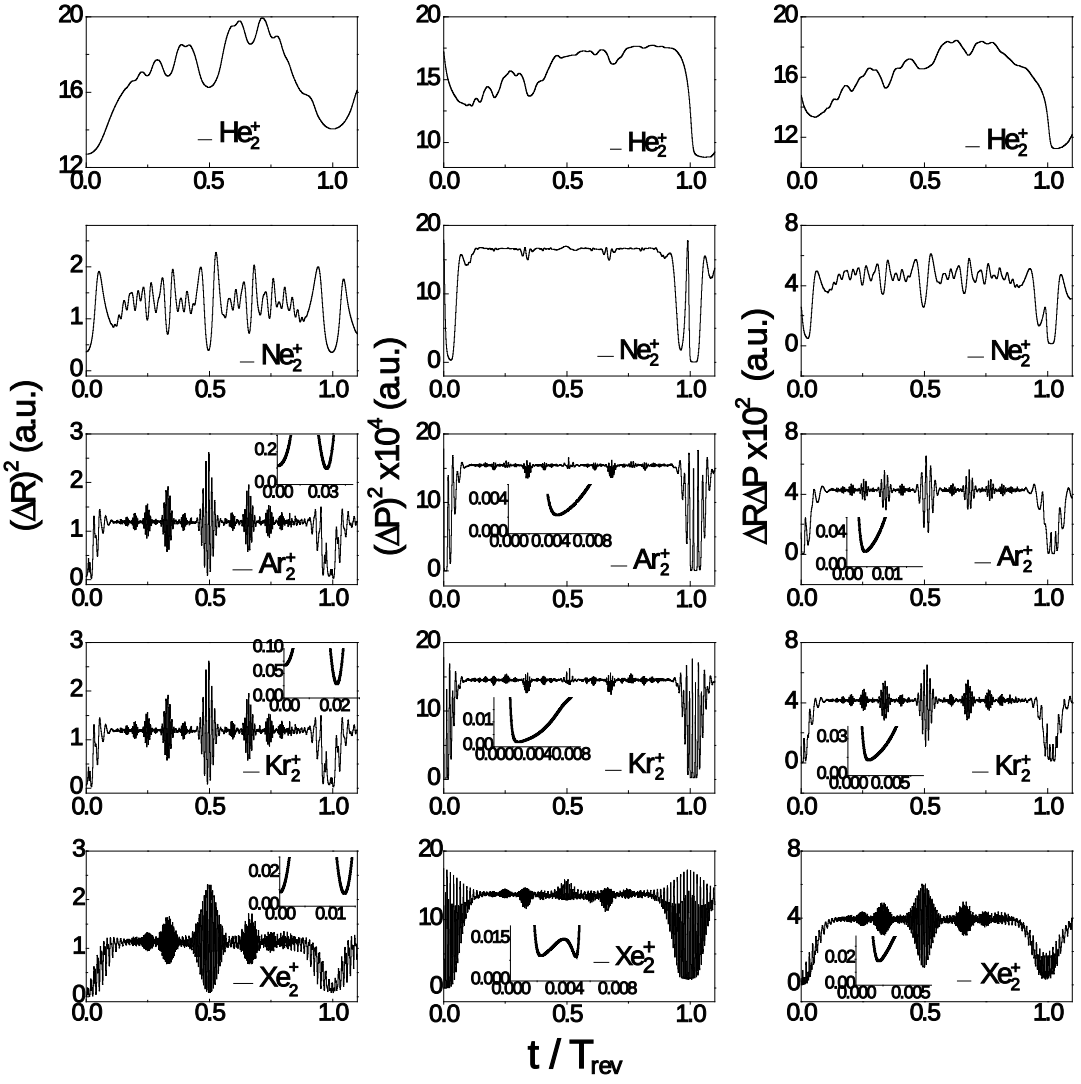

Figure 6.8 ***Position variance $(\Delta R)^2$, momentum variance $(\Delta P)^2$, and uncertainty product $\Delta R \Delta P$ as a function of time scaled with respective revival times for Ne_2^+, Ar_2^+, Kr_2^+, and Xe_2^+ noble gas dimers in the $I(1/2)_u$ state. Due to the absence of a clear wavefunction revival in our He_2^+ propagation calculation ($^2\Sigma_u^+$ state), we scale the time in the first row by the approximate revival time 525 fs.***

Table 6.4 ***Expected KERs for calculations based on adiabatic molecular potential curves that include or do not include SO coupling. In calculations without SO coupling we include the dipole-coupled $^2\Sigma_u$ and $^2\Pi_g^+$ states of the dimer cation; for calculations with SO coupling the $I(1/2)_u$ and $II(1/2)_g$ states.***

Dimer	KERs (800nm) no SO	KERs (1400nm) no SO	KERs (800nm) with SO	KERs (1400nm) with SO
He_2^+	1.6 eV	0.8 eV	1.6 eV	0.8 eV
Ne_2^+	1.45 eV	0.75 eV	1.3 eV	0.6 eV
Ar_2^+	1.35 eV	0.6 eV	1.18 eV	0.45 eV
Kr_2^+	1.3 eV	0.54 eV	0.25 eV	0.008 eV
Xe_2^+	1.2 eV	0.5 eV	0.1 eV	-
			KERs (500nm) with SO	**KERs (700nm) with SO**
Kr_2^+	-	-	1.0 eV	0.4 eV
Xe_2^+	-	-	0.9 eV	0.25 eV

6.3.2.3 Discussion of the dipole-coupled calculations

The distinctive "delay gap" is observed in KER spectra for Ar_2^+, measured for 800 and 1400 nm pump probe pulses with pulse length 80 fs and an intensity of 10^{14} W/cm^2 [Wu-13-2]. Calculations using the same pulse parameters and the $I(1/2)_u$ and $II(1/2)_g$ states of Ar_2^+ reproduce the gap [Wu-13-2]. It is interesting to see whether the gap is present for other noble gas dimers and whether it has the same explanation. In this subsection the calculations for Ng_2^+ are presented including states without and with SO couplings.

KER spectra as a function of internuclear distance and pump-probe delay for calculations that include dipole coupling for the states Ng_2^+ ($^2\Sigma_u^+$ and $^2\Sigma_g^+$) are given in Fig. 6.9. The parameters for the pump (probe) pulse used were 800 (1400) nm wavelength, 80 fs pulse length and a peak intensity of 10^{14} W/cm^2, as in the experiment from Ref. [Wu-13-2]. The oscillating structures visible for the energy bands on both the negative and positive delay sides correspond to the wave packet oscillations in the $^2\Sigma_u^+$ states of Ng_2^+: ~230 fs for Ne_2^+, ~250 fs for Ar_2^+, ~460 fs for Kr_2^+, and ~550 fs for Xe_2^+. Two separate energy bands are present corresponding to dissociation through different avoided one-photon crossings (800 or 1400nm). The "delay gap" discussed in [Wu-13-2] is observed only for positive delays. The width of the "gap" is on the order of 150-200 fs. Expected KERs are summarized in Table 6.4.

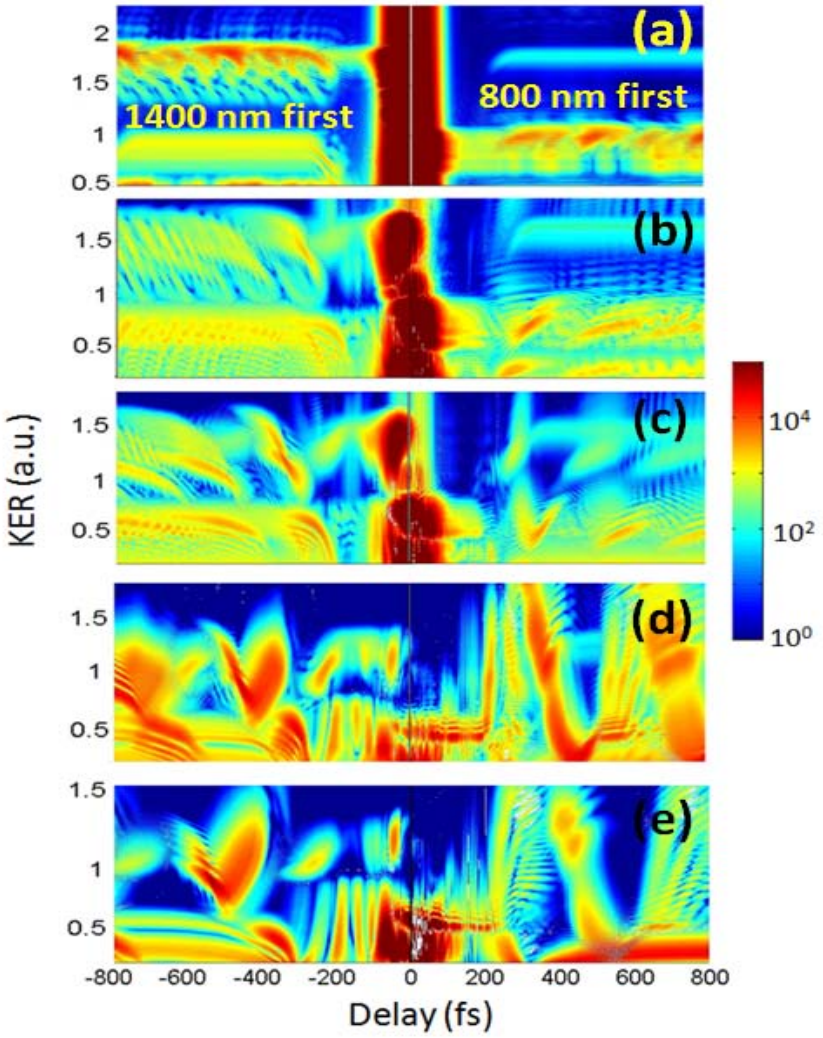

Figure 6.9 ***KER spectra as a function of pump-probe delay for He_2^+, Ne_2^+, Ar_2^+, Kr_2^+, and Xe_2^+ states with no spin-orbit coupling, and 800 -1400 nm pump-probe pulses with 80 fs length and 10^{14} W/cm^2 intensity.***

For positive (negative) delays, the 1400 (800) nm probe pulse comes after the 800 (1400) nm pump. Starting from the negative delays, we try to explain the main features of the KER spectra. The 1400 nm pump couples part of the wave packet from the $^2\Sigma_u^+$ (or $I(1/2)_u$) state into the $^2\Sigma_g^+$ (or $II(1/2)_g$) state (B to E in Fig. 6.1), which dissociates giving the lower energy band in the KER spectra (0.1-0.9 eV range). The rest of the wave packet continues moving inward on the $^2\Sigma_u^+$ (or $I(1/2)_u$) state to the point where the 800 nm probe couples it onto the $^2\Sigma_g^+$ (or $II(1/2)_g$) state (C to D in Fig. 6.1), resulting in the higher energy band in the KER spectra (0.9-1.9 eV range). In the case of positive delays, the pump-probe sequence is reversed. The 1400 nm probe couples part of

the wave packet into the excited Ng_2^+ ($^2\Sigma_g^+$ or $II(1/2)_g$) state, leading to the lower energy bands in the KER spectra (B to E in Fig. 6.1), and the rest of the wave packet is coupled from the lower Ng_2^+($^2\Sigma_u^+$ or $I(1/2)_u$) to the higher Ng_2^+($^2\Sigma_g^+$ or $II(1/2)_g$) state by the 800 nm pump pulse (C to D in Fig. 6.1). This would result in dissociation into the higher energy band. However, the 1400 nm probe pulse couples the wave packet back to the $^2\Sigma_u^+$ (or $I(1/2)_u$) state (E to B in Fig. 6.1), leading to the "delay gap" in the KER spectra. Note that if the 1400 nm probe pulse comes after the dissociative wavefunction passes the 1400 nm crossing, the "gap" is no longer present (more details can be found in [Wu-13-2]). For Xe_2^+, the time from A to C on $^2\Sigma_u^+$ is larger than the pulse length (80 fs), so we do not see the upper band on the positive delay side in Fig. 6.9e (Table 6.5).

Table 6.5. ***Results of the classically calculated propagation times from point A to B and from B to C in Fig. 6.1 along the diabatic potential curves of noble gas dimer cations in $^2\Sigma_u^+$ and $I(1/2)_u$ electronic states for the wavelength combinations 800+1400 and 500+700 nm.***

Dimer	$^2\Sigma_u^+$ 800+1400		$I(1/2)_u$ 800+1400		$I(1/2)_u$ 500+700	
	t_{AB} (fs)	t_{BC} (fs)	t_{AB} (fs)	t_{BC} (fs)	t_{AB} (fs)	t_{BC} (fs)
Ne_2^+	22	9	21	12	-	-
Ar_2^+	30	15	38	20	-	-
Kr_2^+	36	29	0	46	51	28
Xe_2^+	45	42	0	-	50	53

Figure 6.10 summarizes the dipole-coupled calculations for the states including SO coupling, $I(1/2)_u$ and $II(1/2)_g$. We used the same pulse parameters as in the calculations shown in Fig. 6.9. The "delay gap" we are looking for is also present in these calculations for the dimers He_2^+-Ar_2^+. The KER spectra for Kr_2^+ and Xe_2^+ calculated for the 800-1400 nm wavelength combination (Fig. 6.10(d,e)) have only one energy band below 0.2 eV, because the one photon crossing that corresponds to 1400 nm does not exist for Xe_2^+ due to SO coupling of the ungerade and gerade states. The resulting KER (from the one-photon crossing corresponding to 1400 nm) for Kr_2^+ is close to zero (Table 6.4). The KER spectra in Fig. 6.9 show lower energies compared to the spectra in Fig. 6.10. The reason for this lowering of KER bands is the change of the shape of the potential energy curves: the width and depth of the $I(1/2)_u$ and the slope of $II(1/2)_g$ states are different from the $^2\Sigma_u^+$ and $^2\Sigma_g^+$ states due to SO coupling.

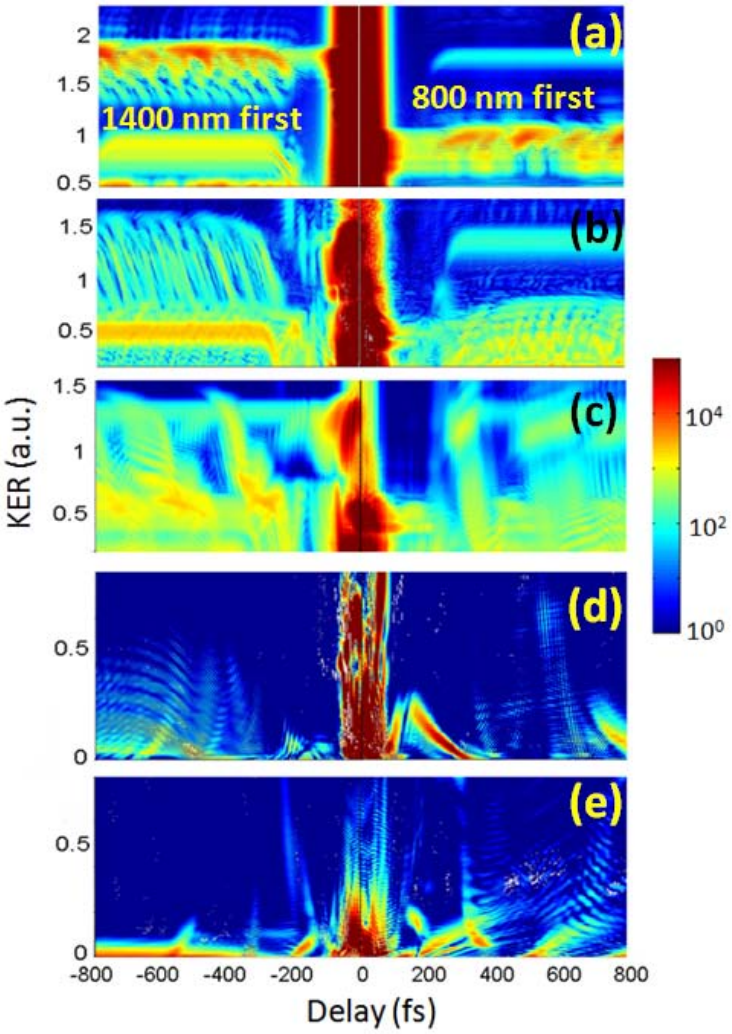

Figure 6.10 ***(a) Same as Fig. 6.8(a). (b)-(e) KER spectra for states including SO coupling of Ne_2^+-Xe_2 calculated with 800 - 1400 nm pump-probe wavelengths.***

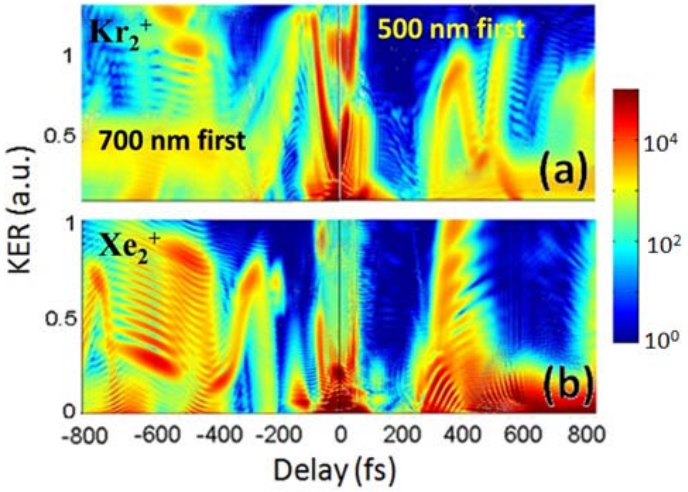

Figure 6.11 ***KER spectra as a function of pump-probe delay for Kr_2^+ and Xe_2^+ states with spin-orbit coupling, and 500-700nm pump-probe pulses with 80 fs length and 10^{14} W/cm^2 intensity.***

For the Kr_2^+ and Xe_2^+ we have used different pump-probe wavelength combination, 500-700 nm, and plot KER spectra as shown in Fig. 6.11. The reason why we have to use different wavelength combination is that the one photon crossing for 1400 nm wavelength is not present due to the large gap of SO coupled states of Xe_2^+; the resulting KER from the one photon crossing is close to zero for Kr_2^+ as mentioned above. The "delay gap" for the given wavelengths is present, but the double-band energy structure is not clearly visible for the same reason as for the calculations including non-SO-coupled states (the time the wave packet takes from A to C in Fig 6.1 is longer than the pulse length for Xe_2^+, Table 6.5). In principle one can find wavelength and pulse length combinations such that the KER spectra would have two energy bands for Xe_2^+.

6.4 Summary

We have investigated the dissociation dynamics in noble gas dimers in two-color IR pump and probe fields. The "delay gap" on the positive side of the KER spectra, observed in the Ar_2^+ dimer, is also present for He_2^+ , Ne_2^+ , Kr_2^+ and Xe_2^+ dimers. This striking feature can be explained by a simple model where the wave packet is coupled by two-color laser pulses on the $I(1/2)_u$ (or $^2\Sigma_u^+$) and $II(1/2)_g$ (or $^2\Sigma_g^+$) states of Ng_2^+. Comparing pump-probe-pulse delay-dependent kinetic-energy-release spectra for different noble gas dimer cations, we quantitatively discussed quantum-mechanical versus classical aspects of the nuclear vibrational motion as a function of the nuclear mass. In addition, based on the study of the variances, as the mass of the system increases, the more it resembles a classical particle as the wave packet spreads less for the heavier dimers. Also, we found that as the mass of the dimer increases, the fine structure effects become more noticable in the KER spectra.

Chapter 7 - OXYGEN AND NITROGEN MOLECULES IN XUV FIELDS

7.1 Introduction

Investigating nuclear wave-packet dynamics of diatomic and more complex molecules in various charge states with time-resolved experiments gives detailed insight into reaction pathways as a function of the excitation conditions and offers the possibility to test calculated potential energy surfaces for these species [Bocharova-11, De-11, Feuerstein-07, Thumm-08].

Ultrafast nuclear wave-packet dynamics in various charge states of diatomic molecules, up to now, were almost entirely examined with time-resolved pump-probe spectroscopy using intense few-cycle near-infrared (NIR) laser pulses [Bocharova-11, De-11, De-10, Ergler-05]. However, these high-peak-intensity pulses tend to induce strong couplings between dipole-allowed adiabatic molecular states. Accordingly, NIR pump – NIR probe spectroscopy very sensitively probes the nuclear dynamics near curve crossings that result from such couplings. Importantly, the localization of NIR-induced couplings at avoided crossings means that NIR pump – NIR probe experiments examine the nuclear dynamics of field-dressed, rather than external-field-free adiabatic molecular potential curves. Moreover, the presence of intense NIR pulses, in general, perturbs the target of interest significantly, such that those pulses also alter the outcome of chemical reactions. For this reason, strictly speaking, NIR pulses are not suitable for detecting and exploring nuclear motion on unperturbed potential curves. On the other hand, intense, ultra-short extreme ultraviolet (XUV) radiation would be much better suited for the task as detailed below. Recent progress in the development of tunable intense XUV laser sources led to the realization of isolated XUV pulses with pulse durations below 100 attoseconds [Goulielmakis-08]. XUV and X-ray laser pulses are produced by either employing high-harmonic generation [L'Huillier-83, Krausz-09] or free-electron lasers [Hoener-10]. In contrast to intense NIR pulses, their interaction with atomic and molecular targets is characterized by large Keldysh parameters, corresponding to ionization by the absorption of no more than a few energetic photons. In addition, with regard to identifying reaction pathways, the absorption of a known small number of energetic photons (rather than a large, not-well determined number of less energetic photons provided by a NIR pulse of comparable spectral width) tends to induce

electronic transitions to a more narrowly defined part of the target electronic spectrum. Furthermore, since these XUV and X-ray sources are tunable, transitions into specific spectral regions can be selected. In dissociative reactions, the KER can thus be resolved with regard to the number of absorbed photons and the pump-pulse-generated intermediate charge states of the molecular ion. This is done for a comparatively narrow spectral range of intermediate adiabatic states which are populated by short-wavelength pump and probe pulses, facilitating the assignment of possible dissociation (reaction) pathways. Time resolutions on the order of a few femtoseconds can be realized, which is short enough to trace even the fastest motion of nuclei in molecules. Attempts to achieve even higher resolution in time, in order to simultaneously follow the electronic motion during chemical reactions or to zoom into fast rearrangement processes, would decrease the spectral resolution.

Recently, the nuclear wave-packet dynamics in diatomic molecular ions have been investigated in several XUV pump - NIR probe experiments [Cao-10, Cao-11, Gagnon-07, Kelkensberg-09, Sandhu-08, Sansone-10]. In those experiments the pump pulse is perturbative but the NIR-probe pulse efficiently couples potential energy curves of the molecular ion, making these studies sensitive mainly to confined regions of internuclear distances where the coupling is strong. This limitation is removed in XUV pump – XUV probe spectroscopy pioneered in [Rudenko-10], where the first XUV pulse ionizes the neutral molecule and initializes a nuclear wave-packet in the ionic species of interest on potential energy curves that lie within a specific spectral range of the molecular ion. The second XUV pulse probes the dynamics by a subsequent ionization step, removing one or several electrons. In contrast to NIR probe pulses, for sufficiently high XUV photon energy, the final charge state of the molecular ion will be reached for any given pump-probe delay. Hence, the wave-packet motion can be observed along the entire reaction coordinate. In addition, this scheme often leads to multiple ionization and, as a result, to fragmentation by CE. Measurement of the resulting KER and momentum distributions as a function of the pump-probe delay then enables the imaging of the wave-packet dynamics (if the reflection principles can be applied and the fragmentation potential energy surfaces are known) in the same way as for NIR pump – NIR probe CE experiments (see, e.g., [De-10]), but without the limitations described above. Following this approach, XUV pump – XUV probe experiments have recently been conducted to trace the nuclear wave-packet motion in the D_2

cation [Jiang-10-1] and to measure the isomerization dynamics in the acetylene cation [Jiang-10-2].

In this chapter, we report on XUV pump – XUV probe studies performed at FLASH with the goal of elucidating the nuclear wave-packet dynamics following the XUV ionization of O_2 and N_2 at a central photon energy of 38 eV. By comparing our experimental results with classical and quantum-mechanical calculations, based on available potential energy curves for various charge states of these molecules, we describe a method for identifying the dominant dissociation pathways.

7.2 Experimental method

A reaction microscope (also known as COLTRIMS) [Ullrich-03] was used to record the three-dimensional momentum vectors of fragment ions at beam line BL3 of FLASH. The temporal overlap between the two XUV pulses was determined by detecting the delay-dependent dissociation of the coincident $O^+ + O^{2+}$ ($N^+ + N^{2+}$) fragments, where a maximum in the dissociation yield at zero delay-time was observed [Jiang-09]. With a focus diameter of ~20 μm and pulse energies of a few μJ at an estimated average pulse duration of ~80 fs [Jiang-10], the experiment reached peak intensities of the order of 10^{13} W/cm^2 at a photon energy of 38±0.5 eV. Ionic fragments were projected by means of an electric field (40 V/cm) onto a time- and position-sensitive micro-channel plate detector (diameter 120 mm, position resolution 0.1 mm, multi-hit delay-line read-out) and recorded as a function of the pump-probe time delay. From the measured time-of-flight (TOF) and position of each individual fragment, the initial three-dimensional momentum vector was reconstructed. The resolution in the KER is better than 50 meV for all fragment energies detected. For more details see [Rudenko-10, Jiang-10-2, Magrakvelidze-12-2].

7.3 Theoretical methods

We use two separate numerical methods for identifying dissociation pathways in terms of adiabatic electronic states involved in the molecular fragmentation dynamics. In the first "classical" model we calculate the KER, $K(\tau)$, as a function of the pump-probe delay, τ, [Bocharova-11] by solving Newton's equations for nuclear motion on adiabatic molecular potential curves in order to understand the main features in the measured spectra. In the second,

more accurate quantum-mechanical model, we solve the TDSE for the motion of the nuclear wave-packet on selected molecular potential curves. This allows us to simulate KER spectra for given dissociation paths, i.e., for a given sequence of adiabatic molecular states that are successively populated by ionization of the neutral molecule with the pump and, subsequently, of the molecular ion with the probe XUV pulse. Finally, by comparing the simulated and measured KER spectra, we attempt to assess the importance of specific dissociation pathways considered in our quantum calculations.

7.3.1 "Classical" simulations

In this model the XUV pump pulse is assumed to instantaneously ionize the neutral molecule by removing one or more electrons at time zero. In response, the nuclei are assumed to start moving as classical point particles on a selected intermediate (bonding) adiabatic molecular potential curve of the molecular ion in a specific charge state and at an internuclear distance, R that is equal to the equilibrium distance in the neutral molecule before ionization. This modeling of the pump process corresponds to the FC approximation in quantum mechanical calculations (Chapter 3). The subsequent nuclear motion is described by solving Newton's equations of motion for the selected adiabatic potential curve of the molecular ion.

Similarly, the delayed XUV probe pulse is assumed to instantaneously (multiply) ionize the molecular ion at the pump-probe-delay time τ. The nuclei start their classical motion after the probe pulse with the relative velocity they had just before the action of the probe pulse. Their classical motion after the probe pulse is assumed to be dissociative and to proceed on a repulsive Coulomb potential curve α/R, with $\alpha=qp$, where q and p are the charges of the two fragments. The KER for a given delay is thus obtained by adding the kinetic energy of the relative motion of the nuclei at time τ to the Coulomb repulsion energy $\alpha/R(\tau)$ (see **[**Bocharova-11, De-11**]** for details). This calculation is repeated for several intermediate adiabatic electronic states.

7.3.2 Quantum mechanical simulations

As for our classical model, we describe the action of both XUV pump and XUV probe pulses as a sudden removal of one or more electrons. Prior to the pump pulse, for times $t<0$, we assume the neutral molecule to be in its electronic and vibrational ground state. The instantaneous ionization of the neutral molecule by the pump pulse is modeled to result in a

vertical (FC) transition to a preselected bonding adiabatic potential curve, $E_i(R)$, of the molecular ion in a given charge state, on which a nuclear vibrational wave packet, $\Psi(R,t)$, starts to evolve. This wave packet can be thought of as a coherent superposition of vibrational eigenstates φ_v ,

$$\Psi(R,t) = \sum_v a_v \, exp(-i\omega_v t)\, \varphi_v(R),$$

with energies ω_υ on the selected potential curve $E_i(R)$. In the absence of external fields, $\Psi(R,t)$ propagates freely on $E_i(R)$, starting at time t=0 in the vibrational ground state of the *neutral* parent molecule. We obtain $\Psi(R,t)$ by propagating the TDSE for 300 fs with time steps of Δt = 1 a.u. on a numerical grid that covers the interval $0 \le R \le 100$ a.u. with equidistant grid spacing $\Delta R = 0.02$ a.u. [Feuerstein-03-1].

The free propagation of $\Psi(R,t)$ on $E_i(R)$ is interrupted by the probe pulse at the delay time τ. This action further ionizes the molecular ion and is assumed to instantaneously project the nuclear wavefunction onto a dissociative final adiabatic molecular potential curve, $E_f(R)$. We thus obtain the KER distribution

$$Y(K,\tau) = |\Psi(R(K),\tau)|^2 \left|\frac{dE_f(R)}{dR}\right|^{-1} \tag{7.1}$$

by mapping the nuclear probability density $|\Psi(R,\tau)|^2$ at a given delay onto $E_f(R)$. For dissociation along a pure Coulomb potential curve, $E_f(R) = \alpha/R$, (7.1) simplifies to

$$Y(K,\tau) = |\Psi(R(K),\tau)|^2 \frac{R^2}{\alpha} \tag{7.2}$$

Note that K in (7.1) and (7.2) is the sum of the kinetic energies released by the two nuclei. Note also that these transformations neglect the kinetic energy, $E_{kin} = \langle \Psi(R,t)|\hat{K}|\,\Psi(R,t)\rangle$, of the nuclei at the ionization time $t = \tau$ [Feuerstein-03-1], where $\hat{K}$ is the operator for the relative kinetic energy of the nuclei. We include E_{kin} in our quantum mechanical simulation by shifting the argument in the right-hand sides of (7.1) and (7.2) according to

$$Y(K_{tot},\tau) = |\Psi(R(K_{tot} - E_{kin}),\tau)|^2 \left|\frac{dE_f(R)}{dR}\right|^{-1}, \tag{7.3}$$

where K_{tot}=K+ E_{kin} and the R-derivative is taken without including E_{kin}, *i.e., at* $R(K_{tot} - E_{kin})$. In our numerical calculations below, we find small contributions of E_{kin} that do not exceed 0.5 eV for the oxygen and 0.3 eV for the nitrogen targets. The inclusion of E_{kin} does not noticeably affect the comparison with measured KER spectra discussed in the following sections.

7.4 Results and discussion

7.4.1 Oxygen

The relevant lowest potential curves for O_2, O_2^+ and O_2^{2+} molecules, adapted from [Lundqvist-96-1, Marian-82, Steinfeld-05], are given in Fig. 7.1. States with *gerade* symmetry are plotted in Fig.7.1(a) as dashed lines (including the ground states of the O_2 and O_2^+ molecules) and *ungerade* states are given as solid lines. Similarly, states with *gerade* (dashed lines) and *ungerade* (solid lines) symmetry are shown in Fig.7.1(b) for O_2^{2+}. The pure $1/R$ Coulomb potential, shifted to match the dissociation limit at 39.0 eV, is shown as a dotted line in Fig. 7.1(b).

Figure 7.2 shows the measured KER vs. pump-probe delay for the $O_2 \rightarrow O^+ + O^+$ (a), $O_2 \rightarrow O^{2+} + O^+$ (b), and $O_2 \rightarrow O^{2+} + O^{2+}$ (c) dissociation channels (on the right) alongside the delay integrated KER spectra (on the left). The breakup channels can be reached by various pathways. An analysis of the intensity-dependent yield (as done in ref. [Jiang-10] for N_2^{q+}) indicates that the $O_2 \rightarrow O^+ + O^+$ channel involves two photons, the $O_2 \rightarrow O^{2+} + O^+$ channel three photons, and the $O_2 \rightarrow O^{2+} + O^{2+}$ channel between 4 and 6 photons. Note that energy conservation alone merely requires the absorption of one (two) photon(s) to generate singly-(doubly-) charged molecular ions. At the intensities used in the current study, the $O_2 \rightarrow O^+ + O^+$ channel can be populated both directly and sequentially, where the latter involves intermediate O_2^+ states. The distinct peaks in Fig. 7.2(a), labeled a-d, can be assigned to the direct population of the O_2^{2+} $W^3\Delta_u$, $B^3\Sigma_u^-$, $1^1\Delta_u$, and $B^3\Pi_g$ states [Lundqvist-96-1, Voss-04].

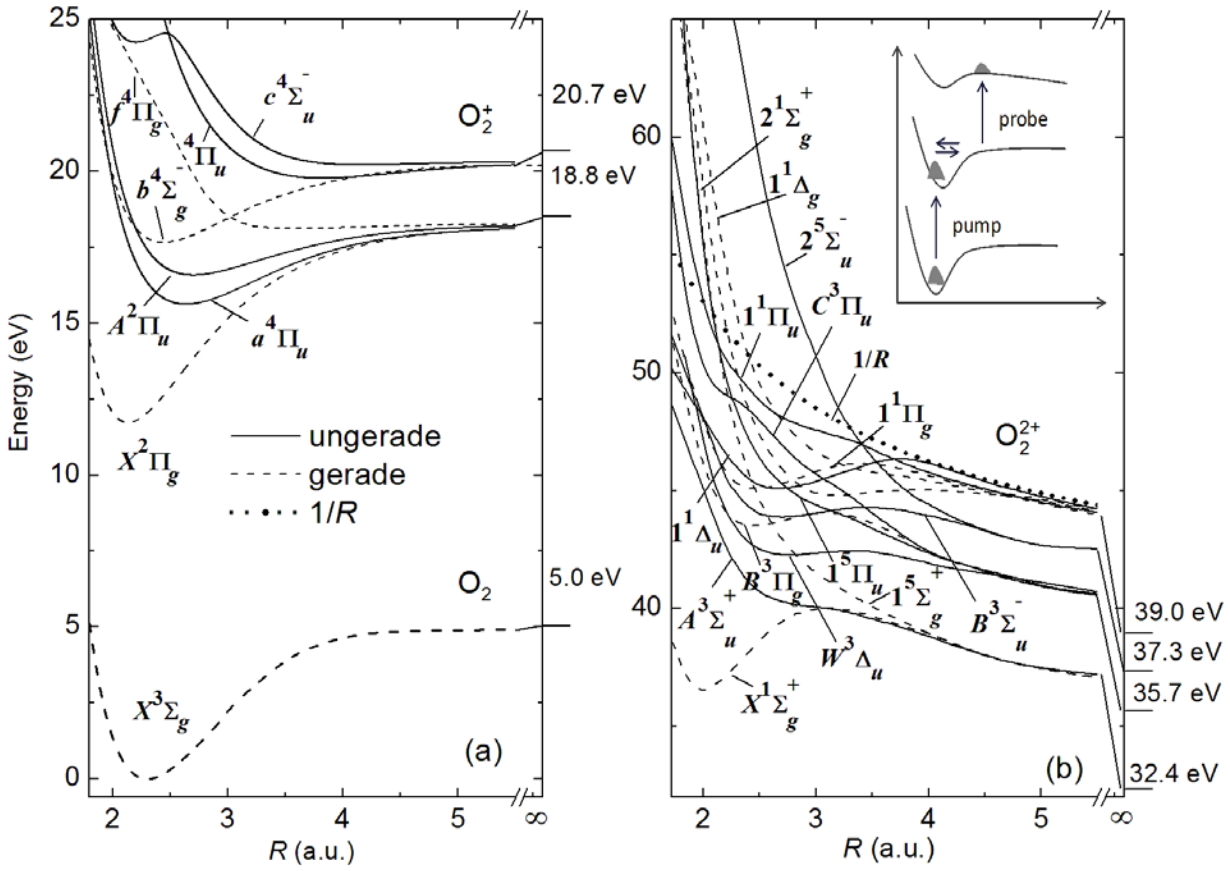

Figure 7.1. ***Adiabatic electronic states for (a) neutral O_2 and the O_2^+ and (b) O_2^{++} molecular ions adapted from [Lundqvist-96-1, Marian-82, Steinfeld-05]. Gerade states are indicated as dashed lines and ungerade states as solid lines. The repulsive 1/R Coulomb potential, shifted to match the 39.0 eV dissociation limit, is shown as a dotted line. Dissociation limits are indicated to the right of the potential curves.***

In Fig. 7.2 we compare the experimental data to the classically calculated KER lines for the intermediate electronic states $f\,^4\Pi_g$, $c^4\Sigma_u^-$, $^4\Pi_u$, and $a^4\Pi_u$ of the O_2^+ molecule and $A^3\Sigma_u^+$ and $1^1\Delta_u$ of the O_2^{2+} molecule (the latter being relevant for the sequential population of triply and quadruply charged O_2). Note that the angular distributions of the fragment emission can in principle help to narrow down the choices for intermediate states. For the measurement on O_2, however, the limited signal-to-noise ratio did not permit the exclusion of any intermediate states based on the fragment angular distributions. For our calculations in Fig. 7.2, we assumed dissociation along the α/R Coulomb potentials with potential strengths $\alpha = qp$ in the break-up channels $O_2 \rightarrow O^{q+} + O^{p+}$. The KER lines are strikingly different for dissociation paths that involve dissociative and bound intermediate states. While dissociative intermediate states ($f\,^4\Pi_g$,

$c^4\Sigma_u^-$, $^4\Pi_u$, $A^3\Sigma_u^+$) yield KER lines which decrease monotonously as functions of the pump-probe delay, the bound and predissociating intermediate states, $a^4\Pi_u$ and $1^1\Delta_u$, yield KER lines that oscillate with periods of 34 and 41 fs, respectively. For the bound and predissociating intermediate states, the calculated asymptotic energies are in good agreement with the measured spectra, except for the $O_2 \rightarrow O^{2+} + O^{2+}$ dissociation channel. Performing separate classical calculations using all bound states in Fig.7.1 as intermediate states, we found that none could reproduce the dissociative energy limit measured for the $O_2 \rightarrow O^{2+} + O^{2+}$ channel.

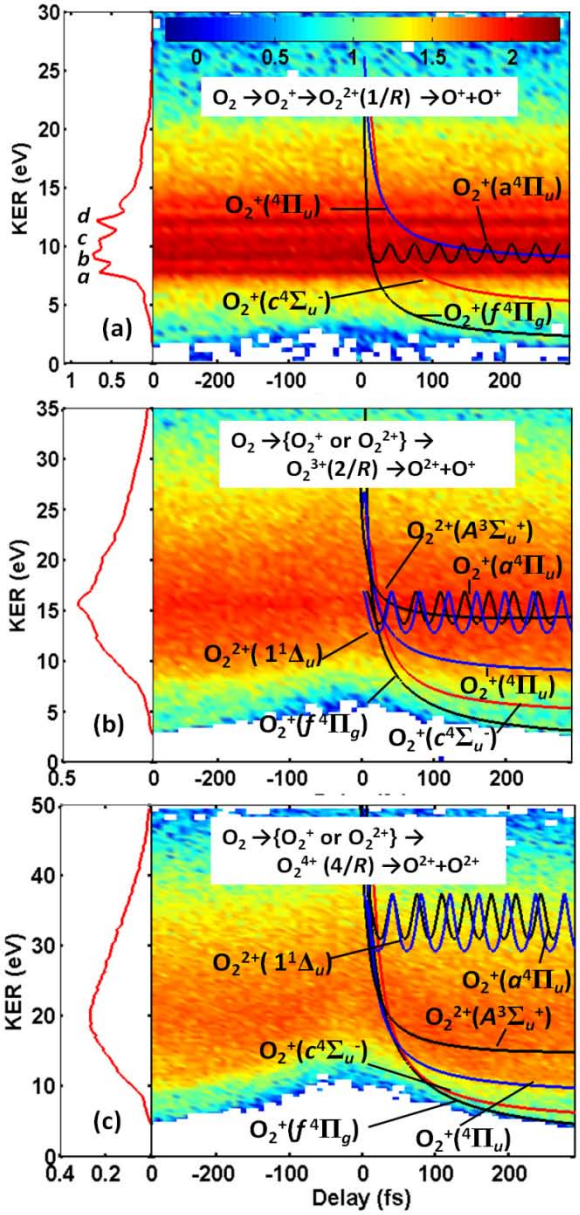

Figure 7.2 ***Measured KER spectra as a function of the pump-probe delay, τ, (same logarithmic color/gray scale for the fragment yield in all plots) compared with the classically calculated KER curves, for different break-up channels: (a) O^++O^+, (b) O^{2+}+O^+, and (c) O^{2+}+O^{2+}. The delay-integrated KER spectra are shown on the left. The classical calculations were done using the dissociative $f\ ^4\Pi_g$, $c^4\Sigma_u^-$, and $^4\Pi_u$ and bound $a^4\Pi_u$ states of O_2^+ and dissociative $A^3\Sigma_u^+$ and the bound $1^1\Delta_u$ states of O_2^{2+}.***

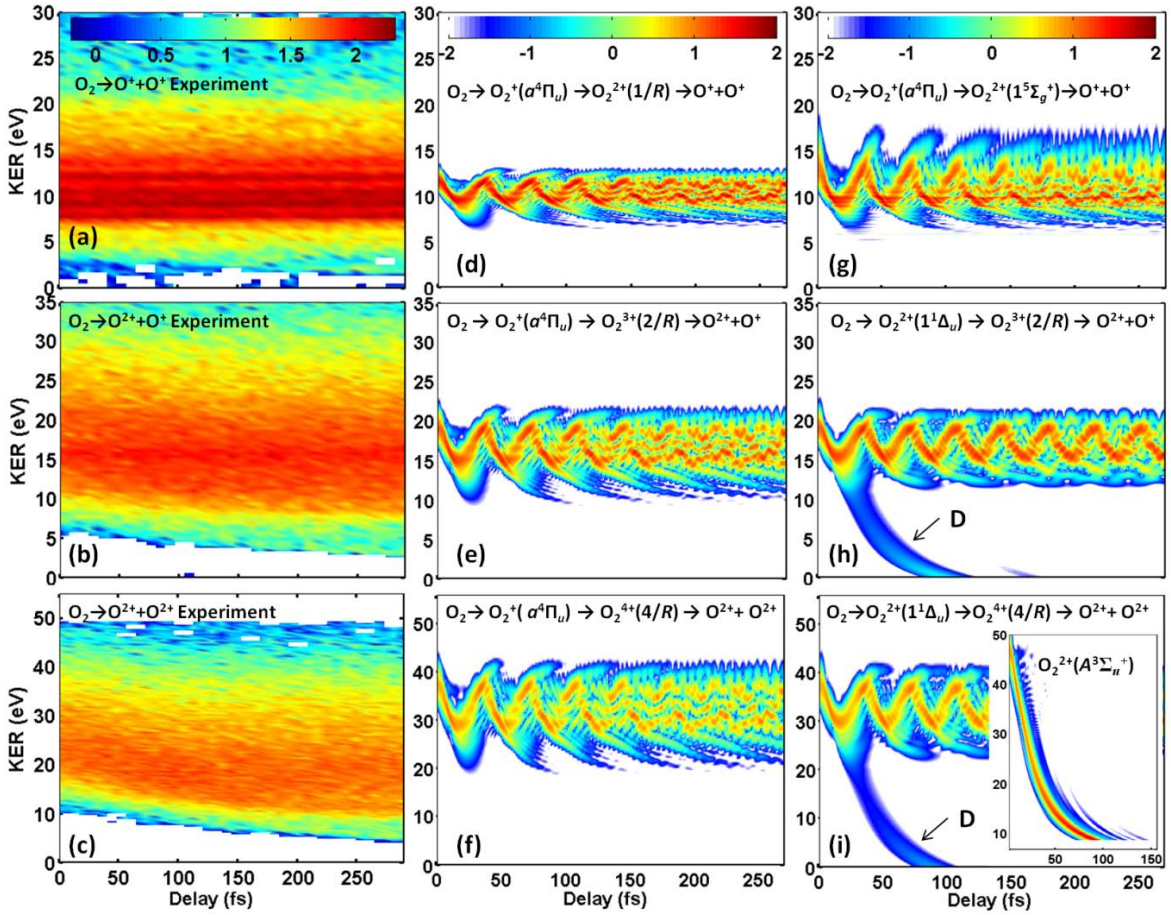

Figure 7.3 ***(a) Measured KER spectra as a function of pump-probe delay, τ, for the $O_2 \rightarrow O^+ + O^+$ break-up channel and (d, g) corresponding quantum mechanical calculations. (b) Measured KER spectra for the $O_2 \rightarrow O^{2+} + O^+$ channel and (e, h) corresponding quantum mechanical calculations. (c) Measured KER spectra for the $O_2 \rightarrow O^{2+} + O^{2+}$ break-up channel and (f, i) corresponding quantum mechanical calculations (same logarithmic color/gray scales for the fragment yield within each column). The dissociation bands are marked as D (see text). The measured KER spectra are taken from Fig. 7.2 for positive delays and shown on a slightly different color/grey scale, as indicated. The inset in panel (i) shows the calculated KER for the dissociative intermediate state $O_2^{2+}(A^3\Sigma_u^+)$.***

Next, we carried out quantum mechanical calculations, including those intermediate states which best reproduced the measured KER limits in our classical calculations in Fig. 7.2(a,b), with the exception of the $O_2 \rightarrow O^{2+} + O^{2+}$ channel. Since, for this particular channel, dissociation through bound intermediate states does not reproduce the measured data, we also performed a separate calculation including the dissociative $A^3\Sigma_u^+$ state of O_2^{2+}, which yields the best agreement with the measured KER spectrum in Fig. 7.2(c). Figure 7.3 shows a comparison

between the measured KER values for positive delays (left column) and the results from our quantum mechanical calculations (middle and right column) for the dissociation channels: $O_2 \rightarrow O^+ + O^+$ (top), $O_2 \rightarrow O^{2+} + O^+$ (middle), and $O_2 \rightarrow O^{2+} + O^{2+}$ (bottom row). In the calculations for the O^++O^+ dissociation channel, the XUV pump pulse singly ionizes O_2 and the XUV probe pulse removes a second electron, moving the nuclear wave-packet onto O_2^{2+} states and causing dissociation. Explicitly, the wave-packet is launched from the O_2 ground state via a FC transition onto the bound potential curve of the O_2^+ ($a^4\Pi_u$) state.

We also calculated KER spectra for dissociation along the $2^1\Sigma_g^+$, $1^1\Delta_g$, $1^1\Pi_g$, and $B^3\Pi_g$ repulsive states of O_2^{2+} (not shown) and obtained KER spectra that agree equally well with the experimental results in Fig. 7.3(a,b,c). Figure 7.3(d) shows the result for the intermediate bound O_2^+ ($a^4\Pi_u$) state that is Coulomb imaged onto a final $1/R$ state, while the same intermediate state imaged onto the $1^5\Sigma_g^+$ state of O_2^{2+} is considered in Fig. 7.3(g). For both cases, the positions of the energy bands in the KER are in agreement with the measurement. This indicates that populating the O_2^+ ($a^4\Pi_u$) intermediate state is consistent with the measured dissociation dynamics in the $O^+ + O^+$ break-up channel. We found equally good agreement with the experimental data, with a slightly larger oscillation period, by replacing the O_2^+ ($a^4\Pi_u$) intermediate state with the O_2^+ ($A^2\Pi_u$) state (not shown). Similarly, by substituting the O_2^+ ($a^4\Pi_u$) intermediate state with either the O_2^+ ($X^2\Pi_g$) or O_2^+ ($b^4\Sigma_g^-$) state, we obtained spectra (not shown) with a smaller oscillation period than the calculated spectra in Fig. 7.3(d,g) that, however, agree equally well with the experimental data in Fig. 7.3(a). The unambiguous identification of one (or several) intermediate states would require experiments with shorter XUV pulses that are able to resolve the vibrational motion in the molecular ions. The larger spread in KER for dissociation on the O_2^{2+} ($1^5\Sigma_g^+$) potential curve (Fig. 7.3(g)) relative to the CE in Fig. 7.3(d) is consistent with the steeper decrease with R of the $1^5\Sigma_g^+$ curve compared with the $1/R$ Coulomb curve (cf., Fig. 7.1(b)) in the FC region near the equilibrium position of the O_2^+ ($a^4\Pi_u$) curve.

For the dissociation channels $O_2 \rightarrow O^{2+} + O^+$ and $O_2 \rightarrow O^{2+} + O^{2+}$, the KER spectra are calculated assuming probe-pulse-induced CE along the *2/R* and *4/R* curves (Fig. 7.3(e,h,f,i)), respectively, and compared with the experimental data for positive delays (Fig. 7.3(b,c)). In particular, Fig. 7.3(e) shows the quantum mechanically calculated KER for CE out of an intermediate bonding state of the *singly-charged* O_2^+ ion along the dissociation path $O_2 \rightarrow O_2^+(a^4\Pi_u) \rightarrow O_2^{3+}(2/R) \rightarrow O^{2+} + O^+$, while in Fig. 7.3(h) dissociation is modeled for an

intermediate adiabatic state of the *doubly-charged* O_2^{2+} ion, specifically, $O_2 \rightarrow O_2^{2+}(1^1\Delta_u) \rightarrow O_2^{3+}(2/R) \rightarrow O^{2+} + O^+$. For both dissociation paths, the position of the energy band in the calculated KER agrees with the experimental data. However, the dissociative branch for delays below 120 fs (labeled with "D" in Fig. 7.3(h,i)) is not seen in the experimental data. This track of decreasing KER corresponds to dissociation of the most energetic vibrational components of the initial wave packet after approximately half a vibrational period (T_{vib} = 41 fs) on the $O_2^{2+}(1^1\Delta_u)$ potential curve (cf. Fig. 7.1(b)). In our FC model for the pump process, a significant fraction of unbound nuclear states of the $O_2^{2+}(1^1\Delta_u)$ potential are populated, since the equilibrium distance of the O_2 ground state lies well within the repulsive part above the shallow well of the $O_2^{2+}(1^1\Delta_u)$ potential curve (cf. Fig. 7.1(b)).

For CE by the probe pulse leading to $O^{2+} + O^{2+}$ fragmentation (Fig. 7.3(f,i)), our quantum mechanical calculations overestimate the measured KER, indicating that fragmentation along a pure Coulomb potential is inappropriate in this case. As for the $O^{2+} + O^+$ break-up in Fig. 7.3 (h), our calculated spectrum in Fig. 7.3(i) shows the dissociative branch ("D") emerging from the intermediate $O_2^{2+}(1^1\Delta_u)$, which is not seen in the experimental data. The wave-packet oscillations in our quantum mechanical calculations in Fig. 7.3 are not resolved in the experimental data. The periods of these oscillations in the calculated KER are consistent with the oscillation periods we obtain directly from the intermediate-state potential energy curves. By fitting these potential curves to Morse potentials [Brandsen-03], we obtain periods of ~37 and ~40 fs, respectively, for the intermediate bound states $O_2^+(a^4\Pi_u)$ and $O_2^{2+}(1^1\Delta_u)$, in good agreement with the oscillations in Fig. 7.3(d-i). We are confident that CE (along the 4/*R* potential curve) is a realistic assumption and performed simulations with the $2^1\Sigma_g^+$, $1^1\Delta_g$, $1^1\Pi_g$, and $B^3\Pi_g$ repulsive intermediate states of O_2^{2+} (not shown) replacing the $O_2^+(a^4\Pi_u)$ and $O_2^{2+}(1^1\Delta_u)$ states in Fig. 7.3 (f,i). However, these simulations did not improve the agreement with the measured spectrum in Fig. 7.3(c). Simulations for the dissociative $O_2^{2+}(A^3\Sigma_u^+)$ state, which gives the closest match to the measured KER in the classical calculations (Fig. 7.2(c)) are shown in the inset in Fig. 7.3(i). The calculated KER for this intermediate state follows the classically calculated KER line. For the $O^{2+} + O^{2+}$ break-up, our simulations fail to reproduce the measured overall slow decrease in KER for increasing pump-probe delay.

In view of the limited resolution of the measured spectra, our classical and quantum simulations are in good agreement with the experimental data for the $O_2 \rightarrow O^+ + O^+$ and

$O_2 \rightarrow O^+ + O^{2+}$ breakup channels. In contrast, for the $O_2 \rightarrow O^{2+} + O^{2+}$ channel our simulations, both classical and quantum, predict larger KERs than the experiment, not only for the intermediate states employed to calculate the results shown in Figs. 7.2 (c) and 7.3 (f,i), but also for all other intermediate states of O^+ and O^{2+} (not shown) for which we found adiabatic potential curves in the literature (cf. [Lundqvist-96-1, Marian-82, Steinfeld-05]). The lack of agreement for this particular dissociation channel might in part be related to pump-pulse-induced dipole couplings between adiabatic intermediate states of O^+ and O^{2+}. The latter effect has been addressed by Quaglia *et al.* [Quaglia-02] in the IR-laser induced dissociation of O^{4+}. Their measured KERs for IR-laser peak intensities between $6x10^{14}$ and 6×10^{15} W/cm^2 are between 4 and 21 eV smaller than predicted by CE at the ground-state equilibrium distance of neutral O_2. The decrease of the KER due to deviations from pure Coulomb dissociation in their IR experiments is thus comparable to the mismatch we find between our measured and simulated results for the $O^{2+} + O^{2+}$ channel. It is left to future investigations to address both effects, i) and ii), based on new *ab-initio* calculations of O^+, O^{2+}, and O^{4+} adiabatic potential curves, allowing for dipole couplings of selected electronic states in the electric fields of the XUV pump and probe pulses [Magrakvelidze-12-2]. Future investigations should also scrutinize to what degree the simultaneous (coherent versus incoherent) population of vibrational wave packets in two (or more) electronic states by the pump pulse changes the KER.

7.4.2 Nitrogen

Adiabatic electronic potential curves for N_2, N_2^+, and N_2^{2+}, adapted from [Aoto-06, Lundqvist-96-2], are shown in Fig. 7.4. States with *gerade* symmetry are plotted as dashed lines (including the ground states of the N_2 and N_2^+ molecules in Fig. 7.4(a)) and those with *ungerade* symmetry as solid lines. Similarly, states with *gerade* (dashed lines) and *ungerade* (solid lines) symmetry are shown in Fig. 7.4(b) for N_2^{2+}. The pure $1/R$ Coulomb curve, shifted to match the dissociation limit at 38.9 eV, is given as a dotted line in Fig. 7.4(b).

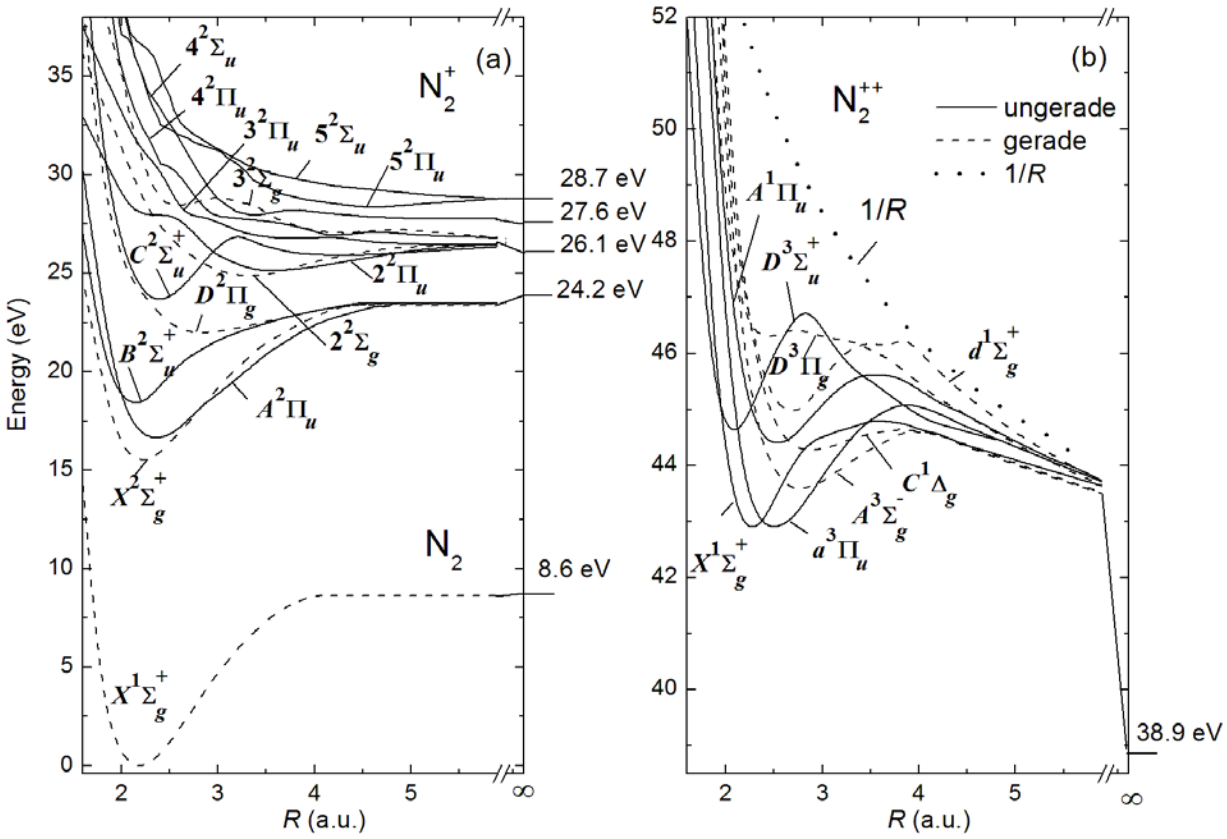

Figure 7.4 ***Adiabatic electronic states for (a) neutral N_2 and the N_2^+ and (b) N_2^{++} molecular ions adapted from [Aoto-06, Marian-82, Lundqvist-96-2]. Gerade states are indicated as dashed lines and ungerade states as solid lines. The repulsive 1/R Coulomb potential, shifted to match the 38.9 eV dissociation limit, is shown as a dotted line. Dissociation limits are indicated to the right of the potential curves.***

As in section 7.4.1, we assume in our classical simulations that the pump pulse populates a *selected* intermediate state of the molecular ion in a *given* charge state, out of which the probe pulse induces fragmentation. Figure 7.5 shows the measured KER vs. pump-probe delay for the dissociation channels $N^+ + N^+$, $N^{2+} + N^+$, and $N^{2+} + N^{2+}$ alongside the delay-integrated KER spectra.

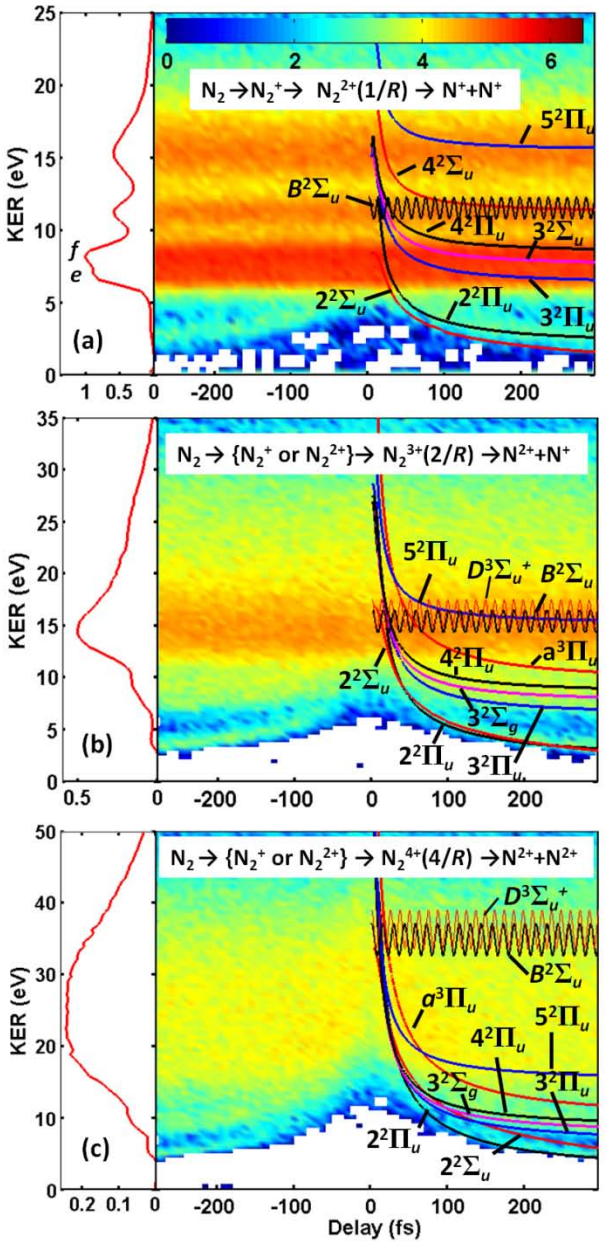

Figure 7.5 ***Measured KER spectra as a function of pump-probe delay, τ, (same logarithmic color/gray scale for the fragment yield in all plots) compared with the classically calculated KER curves, K(τ), for different break-up channels (a) N^++N^+, (b) N^{2+}+N^+, and (c) N^{2+}+N^{2+}. The delay-integrated KER spectra are shown on the left. The classical calculations were done for the dissociative $2^2\Sigma_u$, $2^2\Pi_u$, $3^2\Pi_u$, $3^2\Sigma_g$, $4^2\Pi_u$, $4^2\Sigma_u$, and $5^2\Pi_u$ and the bound $B^2\Sigma_u^+$ states of N_2^+ and the dissociative $a^3\Pi_u$ and bound $D^3\Sigma_u^+$ states of N_2^{2+}.***

Preliminary data for angular distributions measured for the N^+ fragment emission from the dissociation of N_2^{2+} into $N^+ + N^+$ indicate predominantly parallel transitions in the energy windows 0-5 eV and 10-13 eV and perpendicular transitions for 5-10 eV and 13-20 eV. The asymptotic energies and dissociation bands appear to be in agreement with the measured spectra. Similar to the O_2 molecule, the calculations including bound states $B^2\Sigma_u^+$ of N_2^+ and $D^3\Sigma_u^+$ of N_2^{2+} show oscillations related to the periodic wave packet motion. Their oscillation period is about 16 fs. All of the bound states we considered in our calculations for the $N^+ + N^+$ dissociation

channels (Fig. 7.4(a)) reproduced KERs of approximately 10 eV. The peaks labeled e and f in Fig. 7.5(a) are in agreement with a direct population of the N_2^{2+} $A^1\Pi_u$ and $d^1\Sigma_g^+$ states [Voss-04, Lundqvist-96-2].

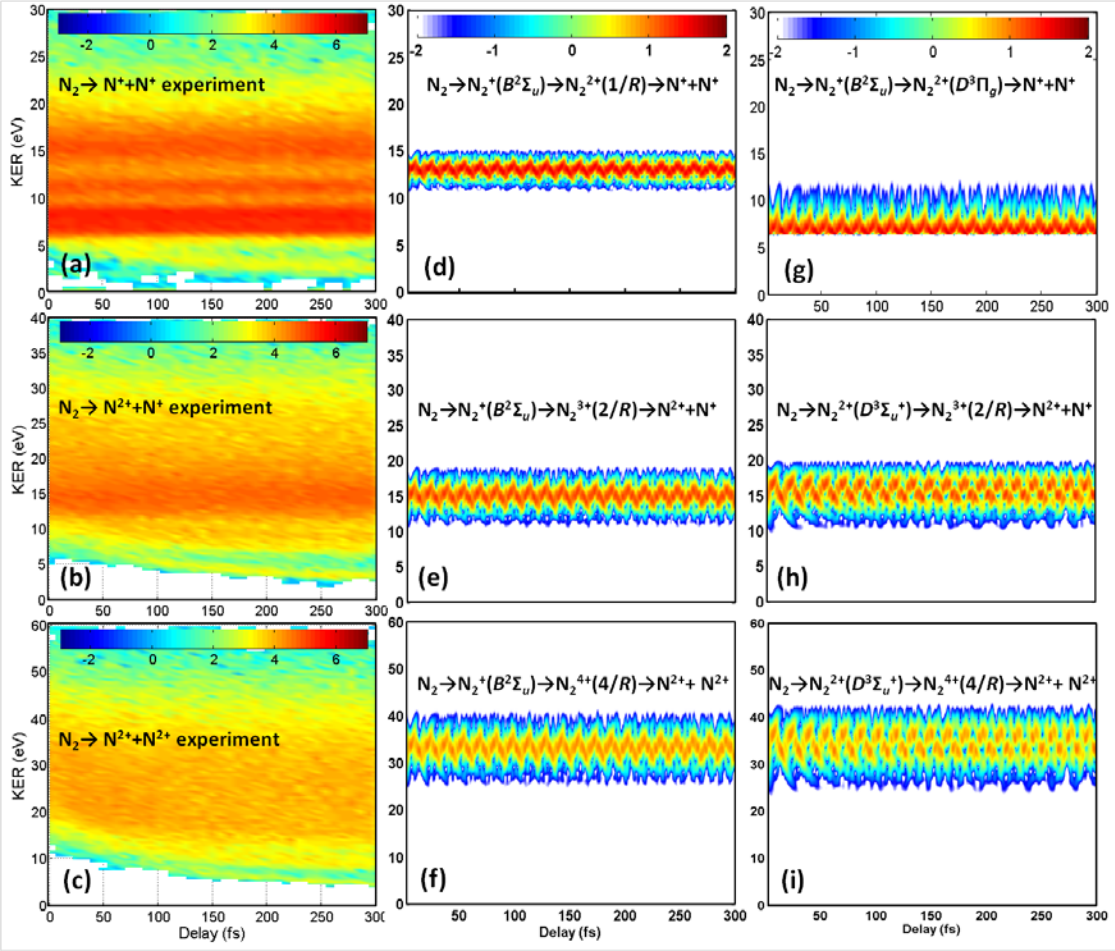

Figure 7.6 ***(a) Measured KER spectra as a function of pump-probe delay, τ, for the $N_2 \rightarrow N^+ + N^+$ break-up channel and (d, g) corresponding quantum mechanical calculations. (b) Measured KER spectra for the $N_2 \rightarrow N^{2+} + N^+$ channel and (e, h) corresponding quantum mechanical calculations. (c) Measured KER spectra for the $N_2 \rightarrow N^{2+} + N^{2+}$ break-up channel and (f, i) corresponding quantum mechanical calculations (same logarithmic color/gray scales for the fragment yield within each column). The measured KER spectra are taken from Fig. 7.5 for positive delays and shown on a different color/grey scale, as indicated.***

Figure 7.6 (a-c) shows the measured KER spectra for positive delays compared to the results from quantum mechanical calculations (described above) for the dissociation channels $N_2 \rightarrow N^+ + N^+$ (top), $N_2 \rightarrow N^{2+} + N^+$ (middle), and $N_2 \rightarrow N^{2+} + N^{2+}$ (bottom row). Calculations for the $N^+ + N^+$ break-up channel (Fig. 7.6(d,g)) were carried out as for the O_2 molecule in section A.

Starting from the ground state of N_2, a nuclear wave-packet is launched on the N_2^+ ($B^2\Sigma_u^+$) potential curve via a FC transition, and dissociation by the probe pulse is modeled as either CE (Fig. 7.6(d)) or dissociation in the N_2^{2+} ($D^3\Pi_g$) electronic state (Fig. 7.6(g)). For separate calculations with CE-imaged intermediate states $X^2\Sigma_g^+$, $A^2\Pi_u$, or $C^2\Sigma_u^+$ of N_2^+, we obtained KER spectra (not shown) at the same level of (dis)agreement with the experimental data in Fig. 7.6(a) as our calculated spectra shown in Fig. 7.6(d). Similarly, if these intermediate states are mapped onto the N_2^{2+} ($D^3\Pi_g$) potential curve, we found similar KER spectra (not shown) that agree equally well with the experimental data in Fig. 7.6(a) as our calculated spectra in Fig. 7.6(g). The KER band for $1/R$ CE (Fig. 7.6(d)) tends to exceed the measured KER, while the calculation is in better agreement with the measurement for dissociation along the N_2^{2+} ($D^3\Pi_g$) potential curve (Fig. 7.6(g)). More specifically, the calculated KER for CE in Fig. 7.6(d) is ~ 6 eV larger than for dissociation on the non-Coulombic repulsive N_2^{2+} ($D^3\Pi_g$) state in Fig. 7.6(g). This is consistent with the potential energy diagrams in Fig. 7.4, where, in the FC region of the N_2^+ ($B^2\Sigma_u^+$) state (roughly between 2 and 2.5 a.u.), the shifted $1/R$ curve is energetically ~ 5 eV higher than the $D^3\Pi_g$ state. Note that this discrepancy does not emerge for the O_2 molecule, where the $1/R$ curve happens to be energetically comparable to the O_2^{2+} ($1^5\Sigma_g^+$) state (cf. Fig. 7.1(b)) in the FC region of the O_2^+($a^4\Pi_u$) state.

For $N_2 \rightarrow N^{2+} + N^+$ and $N_2 \rightarrow N^{2+} + N^{2+}$ dissociation the calculated KER plots are shown for CE along $2/R$ and $4/R$ repulsive curves in Fig. 7.6(e,h) and Fig. 7.6(f,i), respectively, and are compared with the experimental spectra for positive pump-probe delays in Fig. 7.6(b,c). For these dissociation processes, the calculated KERs are generally in good agreement with the experimental data. This is in contrast to the O_2 results for the highest-charged dissociation channel, $O_2 \rightarrow O^{2+} + O^{2+}$, where the calculated KER spectra do not reproduce the measured data. Nevertheless, our simulated KERs for $N_2 \rightarrow N^{2+} + N^{2+}$ dissociation are clearly larger than the center of energy of the measured KERs (Figs. 7.6(c,f,i)). Even though less pronounced than for the case of $O_2 \rightarrow O^{2+} + O^{2+}$ dissociation, this might in part be due to dissociation along non-Coulombic potential curves of N^{4+} [Quaglia-02]. As for the case of O_2, we leave it to future investigations to address simulations non-Coulomb and dipole-coupling effects, and effects that are due to the initial creation by the pump pulse of nuclear vibrational wave packets on more than one adiabatic potential curve. These simulations will likely need to include new independent

ab-initio calculations of N^+, N^{2+}, and N^{4+} potential curves [Magrakvelidze-12-1], some of which (in particular for N^{4+}) are not available in the literature.

In our search for relevant intermediate N_2^+ electronic states, we included all potential curves that are reproduced in Fig. 7.4(a) [Steinfeld-05, Aoto-06, Lundqvist-96-2]. These electronic states include most of the states identified in the analysis of the N_2^+ vibrational structure with He II radiation in the spectral range between 23 and 35 eV by Baltzer *et al.* [Baltzer-92]. With regard to the few electronic states of N_2^+ discussed by Baltzer *et al.* but not considered by us, corresponding potential curves are not available to us. We nevertheless are confident that none of these states would noticeably further improve the agreement we find between our simulated and measured spectra. In the same way as for the dissociation of the O_2 molecule, our quantum mechanical calculations for the dissociation of N_2 in Fig. 7.6 predict wave-packet oscillations that are not resolved in the experimental data. By fitting the potential curves for the intermediate states N_2^+ ($B^2\Sigma_u^+$) and N_2^{2+} ($D^3\Sigma_u^+$) to Morse potentials [Brandsen-03], we obtain periods of ~16 and ~15 fs, respectively, in good agreement with the oscillations in Fig. 7.6(d-i).

7.5 Summary and outlook

The main features of the measured KER spectra are reproduced by classical calculations, implying that following the classical nuclear dynamics on quantum mechanical adiabatic potential curves is a valid scheme for approximating the dissociation dynamics of homonuclear diatomic molecules (with limited accuracy). In comparison with measured KER spectra, we theoretically investigated the dissociation of oxygen molecules via XUV-pumped transitions to specific intermediate states of O_2^+ or O_2^{2+}. These intermediate states are assumed to fragment upon irradiation with the XUV probe pulse. The same was found for the dissociation of nitrogen molecules.

Different dissociation paths were investigated in the quantum mechanical model by calculating KER spectra separately for different (intermediate and dissociating) adiabatic electronic states of $O_2^{+,2+}$ and $N_2^{+,2+}$ molecular ions. These simulated KER spectra are (for most cases) compatible with the experimental data. For $N^+ + N^+$ dissociative ionization of N_2, our quantum mechanical calculation predicts different KERs for $1/R$ CE and dissociation along the N_2^{2+} ($D^3\Pi_g$) anti-bonding state. In contrast, for $O^+ + O^+$ dissociation of O_2, we find that CE and

dissociation along the $O_2^{2+}(1^5\Sigma_g^+)$ state yield comparable KERs. Interestingly, for the $N_2 \rightarrow N^{2+} + N^{2+}$ dissociation channel, CE produces KER spectra that agree with the measured data, while this is not the case for the $O_2 \rightarrow O^{2+} + O^{2+}$ dissociation channel (Fig. 7.3(f,i)). Overall, taking the limited resolution of the measured spectra into account, our classical and quantum simulations are in reasonable agreement with the experiments, with the exception of the $O_2 \rightarrow O^{2+} + O^{2+}$ channel. We hope this lack of agreement will be resolved in the future employing quantum mechanical simulations. These simulations should explore additional simulation paths by including more than one (dipole-coupled) intermediate state [Magrakvelidze-12-1] and should be based on experimental XUV pump – XUV probe data with improved statistics and time resolution, taken for a large range of pump-probe delays, that will allow the application of additional criteria for the selection of dissociation pathways, such as nuclear oscillation periods and revival times.

The XUV pulse lengths used in the measured spectra are slightly longer than the nuclear vibrational periods for O_2 and N_2 molecular ions and thus prohibited the explicit identification of intermediate states and dissociation paths. Future XUV-pump – XUV-probe experiments with shorter pulses and higher temporal resolution may allow for better identification of relevant intermediate states, based not only on the measured time-averaged KER but also on the time-resolved nuclear motion within a vibrational period and on QB structures in transiently populated electronic states [De-11, Feuerstein-07, Thumm-08, Magrakvelidze-12-1]. This may eventually enable the *complete* identification of dissociation pathways in the XUV-triggered dissociation of small molecules. Moreover, initial encouraging attempts at FLASH have been undertaken to coincidently detect the emitted photoelectron(s) [Kurka-09]. If successful, this will allow for the unambiguous energetic identification of the intermediate state involved within the achieved energy resolution.

In general, XUV pump pulses coherently populate more than one electronic state such that the vibrational wavefunction consists of a superposition of vibrational eigenstates in several electronic states. It is left to future calculations to address the sensitivity of KER spectra to the coupling of adiabatic electronic states in the electric fields of the pump and probe pulses. Higher selectivity in the XUV population of electronic states can be achieved by analyzing the data as a function of the alignment of the molecules. The current data contain the full information on the molecular alignment, but due to limited statistics have not been analyzed to reveal this alignment

dependence. Future experiments with better statistics may be able to examine dissociation pathways for selected molecular alignment angles. An approach to increasing the statistics even further without increasing the data acquisition times would be to employ non-adiabatic alignment [LéPine-07] and orientation in intense laser fields [De-09, Sayler-07] in conjunction with XUV pump – XUV probe experiments.

Chapter 8 - SUMMARY

To summarize, we covered basic concepts and molecular orbital theory in chapter 2, including approximations used to solve the TDSE. The theoretical models and the calculation techniques for solving the TDSE are discussed in chapter 3.

In chapter 4, we investigated the nuclear dynamics in H_2^+ (D_2^+) in intense laser fields. In particular, the dynamics of the D_2^+ molecule for different peak intensities, wavelengths, and pedestal lengths of the laser pulses, based on simulated *R*-dependent QB power spectra was studied in chapter 4.1. [Magrakvelidze-09]. By analyzing these spectra in terms of field-dressed Floquet potential curves we focused on dissociation by BS and transient binding of the nuclear motion by BH. We confirmed that, despite the incoherent CW assumption, the Floquet picture is suitable for characterizing the main features of nuclear dynamics, such as BS and BH in few-cycle laser pulses, except for the longest wavelength we used in simulations (1600 nm). From the simulations, we concluded that a peak intensity of about 10^{14} W/cm^2, pulses with a wavelength between 200 to 300 nm, and a duration of less than 50 fs (FWHM) are most suitable for observing the vibrational trapping of the molecular motion in the 1- ω BH well. At wavelengths of 1600 nm, dissociation can proceed via both 1-ω and 3-ω BS, and our simulations indicate transient trapping in the 3-ω BH well at the same wavelength. Existing technologies [Hertel-06, Feuerstein-07] can be used to test our findings experimentally. Next, in section 4.2 the dissociation dynamics of H_2^+ molecule were investigated using the FT method discussed in Chapter 3 and compared with the measured data. The excellent match with the measurements led us to believe that the FT method works for small diatomic molecules (Chapter 3.4). The last part of the chapter (Chapter 4.4.) discussed the localization of the electron in the H_2^+ molecular ion using elliptically polarized long IR fields and coincidence techniques. The methods used so far for investigating the localization involve either two color [Ray-09, Wu-13-1] or carrier-envelope-phase-stabilized short IR pulses [Kling-06, Kremer-09, Znakovskaya-12]. The current experimental technique shatters the belief that the localization of the electron cannot be measured using a single wavelength long pulse.

We studied the dissociation dynamics of the O_2^+ molecular ion in IR fields in Chapter 5. Here the method for identifying adiabatic electronic states involved in the dissociation of small molecules was introduced. First, the adiabatic potential curves and electric dipole-coupling matrix elements are calculated with the quantum chemistry code GAMESS. Next, the nuclear

probability-density spectra as a function of time and QB frequency are calculated and compared to the measured data for one molecular potential curve at a time. Finally, after identifying the relevant electronic states, laser-induced dipole-coupling are included in improved wave packet propagation calculations, and the resulting KER spectra are again compared with experimental data. After performing the calculations for different combinations of electronic states of O_2^+, we concluded that the $a^4\Pi_u$ and $f^4\Pi_g$ states are main players in the dissociation dynamics, as the calculated and measured KER are similar with matching oscillation periods and revival times.

In chapter 6, we investigated the dissociation dynamics of noble gas dimers in two-color IR pump-and probe fields. The "delay gap" on the positive side of the KER spectra, observed in the Ar_2^+ dimer, is also present for He_2^+ , Ne_2^+ , Kr_2^+ and Xe_2^+ dimers. This striking feature can be explained by a simple model where the wave packet is coupled by two-color laser pulses on $I(1/2)_u$ (or $^2\Sigma_u^+$) and $II(1/2)_g$ (or $^2\Sigma_g^+$) states of Ng_2^+. Comparing pump-probe-pulse delay-dependent KER spectra for different noble gas dimer cations, we quantitatively discussed quantum mechanical versus classical aspects of the nuclear vibrational motion as a function of the nuclear mass. In addition, based on a study of the variances, as the mass of the system increases, the more it resembles a classical particle, since the wave packet spreads less for the heavier dimers.

Chapter 7 focused on diatomic molecules in XUV laser pulses. We traced the femtosecond nuclear-wave-packet dynamics in ionic states of oxygen and nitrogen molecules by comparing measured KER spectra with classical and quantum mechanical simulations. Experiments were done at the free-electron laser in Hamburg (FLASH) using 38-eV XUV-pump–XUV-probe. The nuclear dynamics were monitored via the detection of coincident ionic fragments using COLTRIMS and a split-mirror setup to generate the pump and probe pulses. Using our classically and quantum mechanically calculated KER spectra, we identified electronic states of the molecular ions that are populated by ionization of the neutral molecule. For specific fragment charge states, this comparison allowed us to assess the relevance of specific dissociation paths.

For the future there are different steps to be taken for improvement of our current quantum model that is used for KER calculations. The model does not include more than two electronic states, nor molecular rotations. A next step would be to implement three and more electronic states in the calculations. Including molecular rotation in the current code without

doing full *ab*-initio calculations [Winter-10] will be more challenging. The study of this project only included diatomic molecules in IR or UV fields. It would be alluring to extend the research to heavier molecules with more than one active degree of freedom that require potential surface calculations.

Bibliography

[**Alnaser-05**] A. S. Alnaser, B. Ulrich, X. M. Tong, I. V. Litvinyuk, C.M. Maharjan, P. Ranitovic, T. Osipov, R. Ali, S. Ghimire, Z. Chang, C. D. Lin, and C. L. Cocke, "*Simultaneous real-time tracking of wave packets evolving on two different potential curves in H_2^+ and D_2^+*", Phys. Rev. A **72**, 030702(R) (2005)

[**Ansari-08**] Z. Ansari, M. Böttcher, B. Manschwetus, H. Rottke, W. Sandner, A. Veroef, M. Lezius, G. G. Paulus, A. Saenz, and D. B. Milošević, "*Interference in strong-field ionization of a two-centreatomic system*", New Journal of Physics **10**, 093027 (2008)

[Aoto-06] T. Aoto, K. Ito, Y. Hikosaka, A. Shibasaki, R. Hirayama, N. Yamamono, and E. Miyoshi, "*Inner-valence states of N_2^+ and the dissociation dynamics studied by threshold photoelectron spectroscopy and configuration interaction calculation*", J. Chem. Phys. **124**, 234306 (2006)

[**Atkins-05**] P. Atkins, and R. Friedman, "*Molecular quantum mechanics*", Oxford university press Inc, New York (2005)

[**Baker-06**] S. Baker, J. S. Robinson, C. A. Haworth, H. Teng, R. A. Smith, C. C. Chirilă, M. Lein, J. W. G. Tisch, J. P. Marangos, "*Probing proton dynamics in molecules on an attosecond time scale* ", Science **312**, 424 (2006)

[**Baltzer-92**] P. Baltzer, M. Larson, L. Karlsson, B. Wannberg, and M. Carlsson Gothe, "*Inner-valence states of N_2^+ studied by UV photoelectron spectroscopy and configuration-interaction calculations*", Phys. Rev. A **46**, 5545 (1992)

[**Bandrauk-81**] A.D. Bandrauk and M.L. Sink. "*Photodissociation in intense laser field: predissociation analogy*", J. Chem. Phys. **74,** 1110 (1981)

[**Bandrauk-99**] A. Bandrauk, D. G. Musaev, and K. Morokuma, "*Electronic states of the triply charged molecular ion N_2^{3+} and laser-induced Coulomb explosion*", Phys. Rev. A **59**, 4309 (1999)

[**Bates-53]** D. R. Bates, K. Ledsham, and A. L. Stewart, "*Wave Functions of the Hydrogen Molecular Ion*", Philos. Trans. R. Soc. London, Ser. A **246**, 215 (1953)

[**Bialynicki-69**] I. Bialynicki-Birula, B. Mielnik, and J. Plebański, "*Explicit Solution of the Continuous Baker-Campbell-Hausdorff Problem and a New Expression for the Phase Operator*", Annals of Physics **51**, 187-200 (1969)

[**Bocharova-08**] I. A. Bocharova, H. Mashiko, M. Magrakvelidze, D. Ray, P. Ranitovic, C. L. Cocke, and I. V. Litvinyuk, "*Direct Coulomb-explosion imaging of coherent nuclear dynamics induced by few-cycle laser pulses in light and heavy hydrogen*", Phys. Rev. A. **77**, 053407 (2008)

[**Bocharova-11**] I. A. Bocharova, A. S. Alnaser, U. Thumm, Th. Niederhausen, D. Ray, C.L. Cocke, and I. V. Litvinyuk, "*Time-resolved coulomb-explosion imaging of nuclear wave-packet dynamics induced in diatomic molecules by intense few-cycle laser pulses*", Phys. Rev. A **83,** 013417 (2011)

[**Boys-50**] S. F. Boys, "*Electronic Wave Functions. I. A General Method of Calculation for the Stationary States of Any Molecular System*", Proc. R. Soc. Lond. A **200,** 542 (1950)

[**Bransden-03**] B. H. Bransden and C. J. Joachain, "*Physics of Atoms and Molecules*", Prentice-Hall, London, 2nd ed. (2003)

[Brichta-06] J. P. Brichta, W-K. Liu, A. A. Zaidi, A. Trottier, and J. H. Sanderson, "*Comparison of ADK ionization rates as a diagnostic for selective vibrational level population measurement*", J. Phys. B **39** 3769 (2006)

[**Brixner-05**] T. Brixner, T. Pfeifer, G. Gerber, M. Wollenhaupt, and T. Baumert, "*Femtosecond Laser Spectroscopy*", edited by P. Hannaford, Springer, New York, Chapter 9 (2005)

[**Bucksbaum-90**] P. H. Bucksbaum, A. Zavriyev, H. G. Muller, and D. W. Schumacher. "*Softening of the H_2^+ molecular bond in intense laser fields*", Phys. Rev. Lett. **64**, 1883 (1990)

[**Budil-93**] K. S. Budil, P. Salieres, M. D. Perry, A. L'Huillier, "*Influence of ellipticity on harmonic generation*", Phys. Rev. A **48**, R3437 (1993)

[**Buenker-83**] R. J. Buenker, and S. D. Peyerimhoff, "*New Horizons of Quantum Chemistry*", edited by P. O. Lowdin and B. Pullman, Reidel: Dordrecht, page 183 (1983)

[**Calvert-10**] C. R. Calvert, W.A. Bryan, W. R. Newell, I. D. Williams, "*Time-resolved studies of ultrafast wavepacket dynamics in hydrogen molecules*", Phys. Rep. **491**, 1 (2010)

[Cao-10] W. Cao, S. De, K.P. Singh, S. Chen, M.S. Schöffler, A.S. Alnaser, I.A. Bocharova, G. Laurent, D. Ray, S. Zherebtsov, M.F. Kling, I. Ben-Itzhak, I.V. Litvinyuk, A. Belkacem, T. Osipov, T. Rescigno, and C.L. Cocke, "*Dynamic modification of the fragmentation of CO^{q+} excited states generated with high-order harmonics*", Phys. Rev. A **82**, 043410 (2010)

[Cao-11] W. Cao, G. Laurent, S. De, M. Schöffler, T. Jahnke, A.S. Alnaser, I.A. Bocharova, C. Stuck, D. Ray, M. F. Kling, I. Ben-Itzhak, Th. Weber, A. L. Landers, A. Belkacem, R. Dörner, A. E. Orel, T. N. Rescigno, and C. L. Cocke, "*Dynamic modification of the fragmentation of autoionizing states of O_2^+*", Phys. Rev. A **84**, 053406 (2011)

[**Cavalieri-07**] A. L. Cavalieri, N. Müller, Th. Uphues, V. S. Yakovlev, A. Baltuška, B. Horvath, B. Schmidt, L. Blümel, R. Holzwarth, S. Hendel, M. Drescher, U. Kleineberg, P. M. Echenique, R. Kienberger, F. Krausz, and U. Heinzmann, "*Attosecond spectroscopy in condensed matter*", Nature **449**, 1029 (2007)

[**Châteauneuf-98**] F. Châteauneuf, T. T. Nguyen-Dang, N. Ouellet, and O. Atabek, "*Dynamical quenching of field-induced dissociation of H_2^+ in intense infrared lasers*", J. Chem. Phys. **108**, 3974 (1998)

[Chelkowski-96] S. Chelkowski, and A. D. Bandrauk. "*Wave-function splitting technique for calculating above-threshold ionization electron spectra*", Int. J. Quantum Chem., **60**, 1685 (1996)

[**Chelkowski-02**] S. Chelkowski and A. D. Bandrauk, "*Measuring moving nuclear wave packets using laser Coulomb-explosion imaging*", Phys. Rev. A **65**, 023403 (2002)

[**Chelkowski-07**] S. Chelkowski, A. D. Bandrauk, A. Staudte, and P. B. Corkum, "*Dynamic nuclear interference structures in the Coulomb explosion spectra of a hydrogen molecule in intense laser fields: Reexamination of molecular enhanced ionization*", Phys. Rev. A **76**, 013405 (2007)

[**Clementi-63**] E. Clementi, and D. L. Raimondi, "*Atomic Screening Constants from SCF Functions*", J. Chem. Phys **38** (11), 2686 (1963)

[**Codling-93**] K. Codling and L. J. Frasinski, "*Dissociative ionization of small molecules in intense laser fields*", J. Phys. B **26**, 783 (1993)

[**Cohen-74**] J. S. Cohen and B. Schneider, "*Ground and excited states of Ne_2 and Ne_2^+. I. Potential curves with and without spin-orbit coupling*", J. Chem. Phys**. 61**, 3230 (1974)

[**Corkum-07**] P. B. Corkum and F. Krausz, "*Attosecond science*", Nat. Phys. **3**, 381 (2007)

[**Cornaggia-91**] C. Cornaggia, J. Lavancier, D. Normand, J. Morellec, P. Agostini, J. P. Chambaret, and A. Antonetti, "*Multielectron dissociative ionization of diatomic molecules in an intense femtosecond laser field*", Phys. Rev. A **44**, 4499 (1991)

[**Cotton-90**] F. A. Cotton, "*Chemical applications of group theory*", a Wiley-Iinterscience Publication, New York, 3rd ed. (1990)

[**Cramer-04**] C. J. Cramer, "*Essentials of computational chemistry: theories and models*", John Wiley & Sons Ltd, England, 2nd ed. (2004)

[**Crespo-Hernández-05**] C. E. Crespo-Hernández, , B. Cohen, & B.Kohler, Base "*Stacking controls excited-state dynamics in A.T DNA*", Nature **436**, 1141 (2005)

[**Dantus-04**] M. Dantus and V. V. Lozovoy, "*Experimental Coherent Laser Control of Physicochemical Processes*", Chem. Rev. (Washington, D.C.) **104**, 1813 (2004)

[**De-09**] S. De, I. Znakovskaya, D. Ray, F. Anis, Nora G. Johnson, I.A. Bocharova, M. Magrakvelidze, B.D. Esry, C.L. Cocke, I.V. Litvinyuk, and M.F. Kling, "*Field-Free Orientation of CO Molecules by femtosecond two-color laser fields*", Phys. Rev. Lett. **103**, 153002 (2009)

[**De-10**] S. De, I. A. Bocharova, M. Magrakvelidze, D. Ray, W. Cao, B. Bergues, U. Thumm, M. F. Kling, I.V. Litvinyuk, and C. L. Cocke, "*Tracking nuclear wave-packet dynamics in molecular oxygen ions with few-cycle infrared laser pulses*", Phys. Rev. A **82**, 013408 (2010)

[**De-11**] S. De, M. Magrakvelidze, I. A. Bocharova, D. Ray, W. Cao, I. Znakovskaya, H. Li, Z. Wang, G. Laurent, U. Thumm, M. F. Kling, I. V. Litvinyuk, I. Ben- Itzhak, and C. L. Cocke, "*Following dynamic nuclear wave packets in N_2,O_2, and CO with few-cycle infrared pulses*", Phys. Rev. A **84,** 043410 (2011)

[**Dietrich-92**] P. Dietrich and P. B. Corkum, "*Ionization and dissociation of diatomic molecules in intense infrared laser fields*", J. Chem. Phys. **97**, 3187 (1992)

[**Diffenderfert-82**] R. N. Diffenderfert and D. R. Yarkony, "*Use of the state-averaged MCSCF procedure: application to radiative transitions in magnesium oxide*", J. Phys. Chem. **86** (26), 5098 (1982)

[**Drescher-02**] M. Drescher, M. Hentschel, R. Kienberger, M. Uiberacker, V. Yakovlev, A. Scrinzi, Th. Westerwalbesloh, U. Kleineberg, U. Heinzmann, and F. Krausz, "*Time-resolved atomic inner-shell spectroscopy*", Nature **419**, 803 (2002)

[Dunning-89] T. H. Dunning, "*Gaussian basis sets for use in correlated molecular calculations. I. The atoms boron through neon and hydrogen*", J. Chem. Phys. **90**, 1007 (1989)

[**Eckle-08-1**] P. Eckle, A. N. Pfeiffer, C. Cirelli, A. Staudte, R. Dörner, H. G. Muller, M. Büttiker, U. Keller, "*Attosecond ionization and tunneling delay time measurements*", Science **322**, 1525 (2008)

[**Eckle-08-2**] P. Eckle, M. Smolarski, P. Schlup, J. Biegert, A. Staudte, M. Schöffler, H. G. Muller, R. Dörner, and U. Keller, "*Attosecond angular streaking*". *Nature Phys.* **4**, 565 (2008)

[**Ellert-98**] Ch. Ellert, H. Stapelfeldt, E. Constant, H. Sakai, J. Wright, D. M. Rayner, and P. B. Corkum. "*Observing molecular dynamics with timed Coulomb explosion imaging*". Phil. Trans. A **356**, 329 (1998)

[**Ergler-05**] Th. Ergler, A. Rudenko, B. Feuerstein, K. Zrost, C. D. Schroöter, R. Moshammer, and J. Ullrich, "*Time-Resolved Imaging and Manipulation of H_2 Fragmentation in Intense Laser Fields*", Phys. Rev. Lett. **95,** 093001 (2005)

[**Ergler-06-1**] Th. Ergler, B. Feuerstein, A. Rudenko, K. Zrost, C. D. Schroter, R. Moshammer, and J. Ullrich. "*Quantum-phase resolved mapping of ground-state vibrational D_2 wave packets via selective depletion in intense laser pulses*", Phys. Rev. Lett. **97**, 103004 (2006)

[**Ergler-06-2**] Th. Ergler, A. Rudenko, B. Feuerstein, K. Zrost, C. D. Schröter, R. Moshammer, and J. Ullrich, "*Spatiotemporal imaging of ultrafast molecular motion: collapse and revival of the D_2^+ nuclear wave packet*", Phys. Rev. Lett. **97**, 193001 (2006)

[**Feuerstein-03-1**] B. Feuerstein, and U. Thumm, "*Mapping of coherent and decohering nuclear wave-packet dynamics in D_2^+ with ultrashort laser pulses*", Phys. Rev. A **67**, 063408 (2003)

[**Feuerstein-03**] B. Feuerstein and U. Thumm, "*On the computation of momentum distributions within wavepacket propagation calculations*", J. Phys. B: At. Mol. Opt. Phys. **36**, 707 (2003)

[**Feuerstein-07**] B. Feuerstein, Th. Ergler, A. Rudenko, K. Zrost, C. D. Schröter, R. Moshammer, J. Ullrich, T. Niederhausen, and U. Thumm, "*Complete characterization of molecular dynamics in ultrashort laser fields*", Phys. Rev. Lett. **99**, 153002 (2007)

[**Frasinski-92**] J. L. Frasinski, M. Stankiewicz, P. A. Hatherly, G. M. Cross, and K. Codling, "*Molecular H_2 in intense laser fields probed by electron-electron, electron-ion, and ion-ion covariance techniques*", Phys. Rev. A **46**, R6789 (1992)

[**Frasinski-99**] L. J. Frasinski, J. H. Posthumus, J. Plumridge, and K. Codling, P. F. Taday and A. J.Langley. "*Manipulation of Bond Hardening in H_2^+ by Chirping of Intense Femtosecond Laser Pulses*", Phys. Rev Lett. **83**, 3625 (1999)

[**Gadea-96**] F. X. Gadea and I. Paidarová, "*Ab-initio calculations for Ar_2^+, He_2^+ and He_3^+, of interest for the modeling of ionic rare-gas clusters*", Chem. Phys. 209, 281 (1996)

[Gagnon-07] E. Gagnon, P. Ranitovic, X. M. Tong, C. L. Cocke, M. M. Murnane, H. C. Kapteyn, and A. S. Sandhu, "*Soft X-ray-driven femtosecond molecular dynamics*", Science **317**, 1374 (2007)

[**Gdanitz-00**] R. J. Gdanitz, "*Accurately solving the electronic Schrödinger equation of atoms and molecules by extrapolating to the basis set limit. I. The helium dimer (He_2)*", J. Chem. Phys. **113**, 5145 (2000)

[**Geißler-12**] D. Geißler, P. Marquetand, J. González-Vázquez, L. González, T. Rozgonyi, and T.Weiacht, "*Control of nuclear dynamics with strong ultrashort laser pulses*", J. Phys. Chem. A **116**, 11434 (2012)

[**Giusti-Suzor-90**] A. Giusti-Suzor, X. He, O. Atabek, and F. H. Mies, "*Above-threshold dissociation of H_2^+ in intense laser fields*", Phys. Rev. Lett. **64**, 515 (1990)

[**Giusti-Suzor-92**] A. Giusti-Suzor and F. H. Mies, "*Vibrational trapping and suppression of dissociation in intense laser fields*", Phys. Rev. Lett. **68**, 3869 (1992)

[**Giusti-Suzor-95**] A. Giusti-Suzor, F. H. Mies, L. F. DiMauro, E. Charron, and B. Yang, "*Dynamics of H_2^+ in intense laser fields*", J. Phys. B **28**, 309 (1995)

[**Gordon-05**] M. S. Gordon and M. W. Schmidt "Advances in electronic structure theory: GAMESS a decade later". In: C. E. Dykstra, G. Frenking. K. S. Lim, and G. E. Scusaria. "*Theory and Applications of Computational Chemistry, the first 40 years*", Amsterdam: Elsevier (2005)

[**Gould-90**] M. D. Gould and J. Paldus, "*Spin-dependent unitary group approach. I. General formalism*", J. Chem. Phys. **92** (12), 7394 (1990)

[**Goulielmakis-04**] E. Goulielmakis, M. Uiberacker, R. Kienberger, A. Baltuska,V. Yakovlev, A. Scrinzi, Th. Westerwalbesloh, U. Kleineberg, U. Heinzmann, M. Drescher, F. Krausz, "*Direct measurement of light waves*", Science **305**, 1267 (2004)

[Goulielmakis-08] E. Goulielmakis, M. Schultze, M. Hofstetter, V. S. Yakovlev, J. Gagnon, M. Uiberacker, A. L. Aquila, E. M. Gullikson, D. T. Attwood, R. Kienberger, F. Krausz, and U. Kleineberg, "*Single-cycle nonlinear optics*", Science **320**, 1614 (2008)

[**Gräfe-08**] S. Gräfe, V. Engel, and M. Yu Ivanov, "*Attosecond photoelectron spectroscopy of electron tunneling in a dissociating hydrogen molecular ion*", Phys. Rev. Lett. **101**, 103001 (2008)

[**Ha-03**] T.-K. Ha, P. Rupper, A. Wüest, and F. Merkt, "*The lowest electronic states of Ne_2^+, Ar_2^+ and Kr_2^+: comparison of theory and experiment*", Mol. Phys. **101**, 827 (2003)

[**Harris-78**] D. C. Harris and M. D. Bertolucci, "*Symmetry and spectroscopy: an introduction to vibrational electronic spectroscopy*", Dover publications, INC., New York (1978)

[**Hartree-28**] D. R. Hartree, "*The Wave Mechanics of an Atom with a Non Coulomb Central Field. Part I. Theory and Methods*", Math. Proc. of the Cambridge Phil. Society **24**, 89 (1928)

[**Havermier-10**] T. Havermeier, T. Jahnke, K. Kreidi, R. Wallauer, S. Voss, M. Schöffler, S. Schössler, L. Foucar, N. Neumann,J. Titze, H. Sann, M. Kühnel, J. Voigtsberger, J. H. Morilla, W. Schöllkopf, H. Schmidt-Böcking,R. E. Grisenti, and R. Dörner, "*Interatomic Coulombic Decay following Photoionization of the Helium Dimer: Observation of Vibrational Structure*", Phys. Rev. Lett. **104**, 133401 (2010)

[**Hay-02**] N. Hay, R. Velotta, M. Lein, R. de Nalda, E. Heesel, M. Castillejo, and J. P. Marangos, "*High-order Harmonic Generation in Laser-aligned Molecules*", Phys. Rev. A **65**, 053805 (2002)

[**He-08-1**] F. He, A. Becker, and U. Thumm, "*Strong-field modulated diffraction effects in the correlated electronic-nuclear motion in dissociating H_2^+*". Phys. Rev. Lett. **101**, 213002 (2008)

[**He-08-2**] F. He, C. Ruiz, and A. Becker, "*Coherent control of electron wave packets in dissociating H_2^+*", J. Phys. B: At. Mol. Opt **41**, 081003 (2008)

[**He-10**] F. He and U. Thumm, "*Dissociative ionization of H_2 in an attosecond pulse train and delayed laser pulse*", Phys. Rev.A **81**, 053413 (2010)

[**He-12**] F. He, "*Control of electron localization in the dissociation of H_2^+ using orthogonally polarized two-color sequential laser pulses*", Phys. Rev. A **86**, 063415 (2012)

[**Hentschel-01**] M. Hentschel, R. Kienberger, Ch. Spielmann, G. A. Reider, N. Milosevic, T. Brabec, P. Corkum, U. Heinzmann, M. Drescher and F. Krausz "*Attosecond metrology*", Nature **414**, 509 (2001)

[**Hertel-06**] I. V. Hertel and W. Radloff, "*Ultrafast dynamics in isolated molecules and molecular clusters*", Rep. Prog. Phys. **69**, 1897 (2006)

[Hinze-67] J. Hinze and C. C. J. Roothaan, "*Multi-Configuration Self-Consistent-Field Theory*", Prog. Theor. Phys. Supplement **40**, 37 (1967)

[Ho-83] Y. K. Ho, "*The method of complex coordinate rotation and its applications to atomic collision processes*", Phys. Rep. **99**, 1, (1983)

[Hoener-10] M. Hoener, L. Fang, O. Kornilov, O. Gessner, S.T. Pratt, M. Gühr, E.P. Kantner, C. Blaga, C. Bostedt, J.D. Bozek, P.H. Bucksbaum, C. Buth, M. Chen, R. Coffee, J. Cryan, L. DiMauro, M. Glownia, E. Hosler, E. Kukk, S.R. Leone, B. McFarland, M. Messerschmidt, B. Murphy, V. Petrovic, D. Rolles, and N. Berrah, "*Ultraintense X-Ray induced ionization, dissociation, and frustrated absorption in molecular nitrogen*", Phys. Rev. Lett. **104**, 253002 (2010)

[**Holmegarrd-10**] L. Holmegarrd, J. L. Hansen, L. Kalhøj, S. L. Kragh, H. Stapelfeldt, F. Filsinger, J. Küpper, G. Meijer, D. Dimitrovski, M. Abu-samha, C. P. J. Martiny, and L. B. Madsen, "*Photoelectron angular distribution from strong-field ionization of orientated molecules*", Nature Phys. **6**, 428-432 (2010)

[Hussain-00] A. N. Hussain, and G. Roberts, "*Procedure for absorbing time-dependent wave functions at low kinetic energies and large bandwidths*", Phys. Rev. A **63**, 012703 (2000)

[**Jagutzki-02**] O. Jagutzki, V. Mergel, K. Ullmann-Pfleger, L. Spielberger, U. Spillmann, R. Dörner, H. Schmidt-Böcking "*A broad-application microchannel-plate detector system for advanced particle or photon*

detection tasks: large area imaging, precise multi-hit timing information and high detection rate", Nucl. Instr. and Meth. in Phys. Res. A **477**, 244 (2002)

[**Jiang-09**] Y. H. Jiang, A. Rudenko, M. Kurka, K.U. Kühnel, Th. Ergler, L. Foucar, M. Schöffler, S. Schössler, T. Havermeier, M. Smolarski, K. Cole, R. Dörner, S. Düsterer, R. Treusch, M. Gensch, C.D. Schröter, R. Moshammer, and J. Ullrich, "*Few-Photon Multiple Ionization of N_2 by Extreme Ultraviolet Free-Electron Laser Radiation*", Phys. Rev. Lett. **102**, 123002 (2009)

[**Jiang-10**] Y. H. Jiang, T. Pfeifer, A. Rudenko, O. Herrwerth, L. Foucar, M. Kurka, K. U. Kühnel, M. Lezius, M. F. Kling, X. Liu, K. Ueda, S. Düsterer, R. Treusch, C. D. Schröter, R. Moshammer, and J. Ullrich, "*Temporal coherence effects in multiple ionization of N_2 via XUV pump-probe autocorrelation*", Phys. Rev. A **82**, 041403(R) (2010)

[**Jiang-10-1**] Y.H. Jiang, A. Rudenko, J.F. Perez-Torres, O. Herrwerth, L. Foucar, M. Kurka, K.U. Kühnel, M. Toppin, E. Plesiat, F. Morales, F. Martin, M. Lezius, M.F. Kling, T. Jahnke, R. Dörner, J.L. Sanz-Vicario, J. van Tilborg, A. Belkacem, M. Schulz, K. Ueda, T.J.M. Zouros, S. Düsterer, R. Treusch, C.D. Schröter, R. Moshammer, and J. Ullrich, "*Investigating two-photon double ionization of D_2 by XUV-pump–XUV-probe experiments*", Phys. Rev. A **81**, 051402(R) (2010)

[**Jiang-10-2**] Y. H. Jiang, A. Rudenko, O. Herrwerth, L. Foucar, M. Kurka, K.U. Kühnel, M. Lezius, M.F. Kling, J. van Tilborg, A. Belkacem, K. Ueda, S. Düsterer, R. Treusch, C.D. Schröter, R. Moshammer, and J. Ullrich, "*Ultrafast extreme ultraviolet induced isomerization of acetylene cations*", Phys. Rev. Lett. **105**, 263002 (2010)

[**Johnsson-07**] P. Johnsson, J. Mauritsson, T. Remetter, A. L'Huillier, and K.J. Schafer, "*Attosecond control of ionization by wave-packet interference*", Phys. Rev. Lett. **99**, 233001 (2007)

[**Kalus-03**] R. Kalus, I. Paidarová, D. Hrivňák, P. Paška, and F. X. Gadéa, "*Modelling of Kr_n^+ clusters (n=2–20). I. Structures and energetics*", Chem. Phys. **294**, 141 (2003)

[Kelkensberg-09] F. Kelkensberg, C. Lefebvre, W. Siu, O. Ghafur, T.T. Nguyen-Dang, O. Atabek, A. Keller, V. Serov, P. Johnsson, M. Swoboda, T. Remetter, A. L'Huillier, S. Zherebtsov, G. Sansone, E. Benedetti, F. Ferrari, M. Nisoli, F. Lepine, M.F. Kling, and M.J.J. Vrakking, "*Molecular dissociative ionization and wave-packet dynamics studied using two-color XUV and IR pump-probe spectroscopy*", Phys. Rev. Lett. **103**, 123005 (2009)

[**Kling-06**] M. F. Kling, Ch. Siedschlag, A. J. Verhoef, J. I. Khan, M. Schultze, Th. Uphues, Y. Ni, M. Uiberacker, M. Drescher, F. Krausz, and M. J. J. Vrakking, "*Control of eectron localization in molecular dissociation*", Science **312**, 246 (2006)

[**Kling-13**] M. Kling, P. von den Hoff, I. Znakovskaya, and R. de Vivie-Riedle, "**(***Sub-) femtosecond control of molecular reactions via tailoring the electric field of light*", Phys. Chem. Chem. Phys. **15**, 9448 (2013)

[Krausz-09] F. Krausz, and M. Ivanov, "*Attosecond physics*", Rev. Mod. Phys. **81**, 163 (2009)

[**Kremer-09**] M. Kremer, B. Fischer, B. Feuerstein, V. L. B. de Jesus, V. Sharma, C. Hofrichter, A. Rudenko, U. Thumm, C. D. Schröter, R. Moshammer, and J. Ullrich, "*Electron localization in molecular fragmentation of H_2 by carrier-envelope phase stabilized laser pulses*", Phys. Rev. Lett. **103**, 213003 (2009)

[**Kulander-96**] K. C. Kulander, F. H. Mies, and K. J. Schafer, "*Model for studies of laser-induced nonlinear processes in molecules*", Phys. Rev. A **53**, 2562 (1996)

[**Kurka-09**] M. Kurka, A. Rudenko, L. Foucar, K.U. Kühnel, Y.H. Jiang, T. Ergler, T. Havermeier, M. Smolarski, S. Schössler, K. Cole, M. Schöffler, R. Dörner, M. Gensch, S. Düsterer, R. Treusch, S. Fritzsche, A.N. Grum-Grzhimailo, E.V. Gryzlova, N.M. Kabachnik, C.D. Schröter, R. Moshammer, and J. Ullrich, "*Two-photon double ionization of Ne by free-electron laser radiation: a kinematically complete experiment*", J. Phys. B. **42**, 141002 (2009)

[**Légaré-05**] F. Légaré, K. F. Lee, I. V. Litvinyuk, P. W. Dooley, A. D. Bandrauk, D. M. Villeneuve, and P. B. Corkum, "*Imaging the time-dependent structure of a molecule as it undergoes dynamics*", Phys. Rev. A **72**, 052717 (2005)

[**Légaré-06**] F. Légaré, K. F. Lee, A. D. Bandrauk, D. M. Villeneuve, and P. B. Corkum, "*Laser Coulomb explosion imaging for probing ultrafast molecular dynamics*", J. Phys. B **39**, S503 (2006)

[**LéPine-07**] F. LéPine, M. F. Kling, Y. F. Ni, J. Khan, O. Ghafur, T. Martchenko, E. Gustafsson, P. Johnsson, K. Varjú, T. Remetter, T. L'huillier, and M. J. J. Vrakking, "*Short XUV pulses to characterize field-free molecular alignment*", J. Mod. Opt. **54**, 953 (2007)

[**L'Huillier-83**] A. L'Huillier, A. L'Lompre, G. Mainfray, and C. Manus, "*Multiply charged ions induced by multiphoton absorption in rare gases at 0.53 μm*", Phys. Rev. A **27**, 2503 (1983)

[**Liang-94**] Y. Liang, S. Augst, S. L. Chin, Y. Beaudoin, and M. Chaker. "*High harmonic generation in atomic and diatomic molecular gases using intense picosecond laser pulses-a comparison*". J. Phys. B **27**, 5119 (1994)

[**Lundqvist-96-1**] M. Lundqvist, D. Edvardsson, P. Baltzer, M. Larsson, and B. Wannberg, "*Observation of predissociation and tunnelling processes in O_2^{2+}: a study using Doppler free kinetic energy release spectroscopy and ab-initio CI calculations*", J. Phys. B **29**, 499 (1996)

[**Lundqvist-96-2**] M. Lundqvist, D. Edvardsson, P. Baltzer, and B. Wannberg, "*Doppler-free kinetic energy release spectrum of N_2^{2+}*", J. Phys. B **29**, 1489 (1996)

[**Magrakvelidze-09**] M. Magrakvelidze, F. He, T. Niederhausen, I. V. Litvinyuk, and U. Thumm, "*Quantum-beat imaging of the nuclear dynamics in D_2^+: Dependence of bond softening and bond hardening on laser intensity, wavelength, and pulse duration*", Phys. Rev. A **79**, 033410 (2009)

[**Magrakvelidze-12-1**] M. Magrakvelidze, C. M. Aikens, and U. Thumm, "*Dissociation dynamics of diatomic molecules in intense laser Fields: a scheme for the selection of relevant adiabatic potential curves*", Phys. Rev. A **86**, 023402 (2012)

[**Magrakvelidze-12-2**] M. Magrakvelidze, O. Herrwerth, Y. H. Jiang, A. Rudenko, M. Kurka, L. Foucar, K. U. Kühnel, M. Kübel, Nora G. Johnson, C. D. Schröter, S. Düsterer, R. Treusch, M. Lezius, I. Ben-Itzhak, R. Moshammer, J. Ullrich, M. F. Kling, and U. Thumm, "*Tracing nuclear-wave-packet dynamics in singly and doubly charged states of N_2 and O_2 with XUV-pump–XUV-probe experiments*", Phys. Rev. A **86**, 013415 (2012)

[**Magrakvelidze-13**] M. Magrakvelidze and U. Thumm, "*Dissociation dynamics of noble gas dimers in intense IR laser fields*" Phys. Rev. A **88**, 013413 (2013)

[**Marian-82**] C. M. Marian, R. Marian, S. D. Peyerimhoff, B. A. Hess, R. J. Buenker, and G. Seger, "*Ab-initio CI calculation of O_2^+ predissociation phenomena induced by a spin-orbit coupling mechanism*", Mol. Phys. **46** (4), 779 (1982)

[**Martín-07**] F. Martín, J. Fernández, T. Havermeier, L. Foucar, Th. Weber, K. Kreidi, M. Schöffler, L. Schmidt, T. Jahnke, O. Jagutzki, A. Czasch, E. P. Benis, T. Osipov, A. L. Landers, A. Belkacem, M. H. Prior, H. Schmidt-Böcking, C. L. Cocke, and R. Dörner, "*Single photon-induced symmetry breaking of H_2 dissociation*", Science **315**, 629 (2007)

[**Mercer-96**] I. Mercer, E. Mevel, R. Zerne, A. L'Huillier, P.Antoine, and C. -G.Wahlström, "*Spatial mode control of high-order harmonics*", Phys. Rev. Lett. **77**, 1731 (1996)

[**Miller-88**] D. R. Miller, "*Atomic and molecular beam methods*", vol. 1, ch. Free Jet Sources, page 14ff, Oxford University Press, Oxford/New York, (1988)

[**Morse-29**] P. M. Morse, Phys. Rev. **34 (1)**, 57 (1929).

[Muga-04] J. G. Muga, J. P. Palao, B. Navarro, and I. L. Egusquiza, "*Complex absorbing potentials*", Phys. Rep. **395**, 357 (2004)

[**Niikura-03**] H. Niikura, P. B. Corkum, and D. M. Villeneuve, "*Controlling vibrational wave packet motion with intense modulated laser fields*", Phys. Rev. Lett. **90**, 203601 (2003)

[**Niederhausen-07**] "*Quantum dynamics in laser-assisted collisions, laser-molecule interactions, and particle-surface scattering*", T. Niederhausen Ph.D. thesis, Kansas State University (2007), can be found online: http://jrm.phys.ksu.edu/theses.html

[Niederhausen-08] T. Niederhausen, and U. Thumm, "*Controlled vibrational quenching of nuclear wave packets in D_2^+*", Phys. Rev. A **77**, 013407 (2008)

[**Niikura-03**] H. Niikura, P. B. Corkum, and D. M. Villeneuve, "*Controlling Vibrational Wave Packet Motion with Intense Modulated Laser Fields*", Phys. Rev. Lett. **90**, 203601 (2003)

[**Niikura-06**] H. Niikura, D. M. Villeneuve, and P. B. Corkum, "*Controlling vibrational wave packets with intense, few-cycle laser pulses*", Phys. Rev. A, **73**, 021402(R) (2006)

[**NIST]** http://webbook.nist.gov/chemistry/

[NR] http://www.nr.com/

[**Paidarová-01**] I. Paidarová and F. X. Gadea, "*Accurate ab-initio calculation of potential energy curves and transition dipole moments of the Xe_2^+ molecular ion*", Chem. Phys. **274**, 1 (2001)

[**Pfeiffer-11**] A. N. Pfeiffer, C. Cirelli, M. Smolarski, R. Dörner, and U. Keller, "*Timing the release in sequential double ionization*", Nature Phys. **7**, 428 (2011)

[**Pfeiffer-12**] A. N. Pfeiffer, C. Cirelli, M. Smolarski, D. Dimitrovski, M. Abu-samha, L. B. Madsen, and U. Keller, "*Attoclock reveals natural coordinates of the laser-induced tunnelling current flow in atoms*", Nature Phys. **8,** 76 (2012)

[Poirier-03] B. Poirier, and T. Carrington, "*Semiclassical optimized complex absorbing potentials of polynomial form: II complex case*", J. Chem. Phys. **119**, 77 (2003)

[**Poisson-07**] L. Poisson, K. D. Raffael, M.. Gaveau, B. Soep, and J. Mestdagh, J. Caillat, R. Taïeb, and A. Maquet, "*Low Field Laser Ionization of Argon Clusters: The Remarkable Fragmentation Dynamics of Doubly Ionized Clusters*", Phys. Rev. Lett. **99,** 103401 (2007)

[**Pople-69**] W. J. Hehre, R. F. Stewart, and J. A. Pople, "*Self-Consistent Molecular-Orbital Methods. Use of Gaussian Expansions of Slater-Type Atomic Orbitals*", J. Chem. Phys. **51**, 2657 (1969)

[**Posthumus-04**] J. H. Posthumus, "*The dynamics of small molecules in intense laser fields*" Rep. Prog. Phys. **67**, 623 (2004)

[**Press-92**] W. H. Press, S. A. Teukolsky, W. T. Vetterling, and B. P. Flannery, "*Numerical Recipes*", Cambridge University Press, Cambridge, England (1992)

[**Quaglia-02**] L. Quaglia, O. Chiappa, G. Granucci, V. Brenner, Ph. Millie, and C. Cornaggia, "*Non-Coulombic states of N_2^{4+} and O_2^{4+} ions probed by laser-induced multi-ionization of N_2 and O_2*", J. Phys. B **35**, L145 (2002)

[**Ray-09**] D. Ray, F. He, S. De, W. Cao, H. Mashiko, P. Ranitovic, K. P. Singh, I. Znakovskaya, U. Thumm, G. G. Paulus, M. F. Kling, I.V. Litvinyuk, and C. L. Cocke, "*Ion-energy dependence of asymmetric dissociation of D_2 by a two-color laser field*". Phys. Rev. Lett. **103**, 223201 (2009)

[**Reinsch-00**] M. W. Reinsch. "*A simple expression for the terms in the Baker-Campbell-Hausdorff series*", J. Math. Phys., **41**, 2434 (2000)

[**Robinett-04**] R. W. Robinett, "*Quantum wave packet revivals*", Phys. Rep. **392**, 1 (2004)

[**Roothaan-51**] C. C. J. Roothaan, "*New Developments in Molecular Orbital Theory*", Rev. Mod. Phys., **23**, 69 (1951)

[**Rudenko-06**] A. Rudenko, T. Ergler, B. Feuerstein, K. Zrost, C. D. Schröter, R. Moshammer, and J. Ullrich, "*Real-time observation of vibrational revival in the fastest molecular system*", Chem. Phys. **329**, 193 (2006)

[**Rudenko-07**] A. Rudenko, Th. Ergler, B. Feuerstein, K. Zrost, C. D. Schröter, R. Moshammer, and J. Ullrich, "*Time-resolved measurements with intense ultrashort laser pulses: a 'molecular movie' in real time*", Journal of Physics: Conference Series **88,** 012050 (2007)

[**Rudenko-10**] A. Rudenko, Y.H. Jiang, M. Kurka, K.U. Kühnel, L. Foucar, O. Herrwerth, M. Lezius, M.F. Kling, C.D. Schröter, R. Moshammer, and J. Ullrich, "*Exploring few-photon, few-electron reactions at FLASH: from ion yield and momentum measurements to time-resolved and kinematically complete experiments*", J. Phys. B **43**, 194004 (2010)

[**Sandhu-08**] A.S. Sandhu, E. Gagnon, R. Santra, V. Sharma, W. Li, P. Ho, P. Ranitovic, C.L. Cocke, M.M. Murnane, and H.C. Kapteyn, "*Observing the creation of electronic Feshbach resonances in soft X-ray–induced O_2 dissociation*", Science **322**, 1081 (2008)

[**Sändig-00**] K. Sändig, H. Figger, and T. W. Hänsch, "*Dissociation Dynamics of H_2^+ in Intense Laser Fields: Investigation of Photofragmentsfrom Single Vibrational Levels*", Phys. Rev. Lett. **85**, 4876 (2000)

[**Sansone-06**] G. Sansone, E. Benedetti, F. Calegari, C. Vozzi, L. Avaldi, R. Flammini, L. Poletto, P. Villoresi, C. Altucci, R. Velotta, S. Stagira, S. De Silvestri, and M. Nisoli, "*Isolated single-cycle attosecond pulses*", Science **314**, 443 (2006)

[**Sansone-10**] G. Sansone, F. Kelkensberg, J. F. Pe´rez-Torres, F. Morales, M. F. Kling, W. Siu, O. Ghafur, P. Johnsson, M. Swoboda, E. Benedetti, F. Ferrari, F. Le´pine, J. L. Sanz-Vicario, S. Zherebtsov, I. Znakovskaya, A. L'Huillier, M.Yu. Ivanov, M. Nisoli, F. Martin, and M. J. J. Vrakking, "*Electron localization following attosecond molecular photoionization*", Nature (London) **465**, 763 (2010)

[**Sayler-07**] A.M. Sayler, P.Q. Wang, K.D. Carnes, B.D. Esry, and I. Ben-Itzhak, "*Determining laser-induced dissociation pathways of multielectron diatomic molecules: Application to the dissociation of O_2^+ by high-intensity ultrashort pulses*", Phys. Rev. A **75**, 063420 (2007)

[**Schmidt-98**] M. W. Schmidt and M. S. Gordon, "*The Construction and Interpretation of MCSCF wavefunctions*", Annu. Rev. Chem. Phys, **49**, 233 (1998)

[**Seideman-95**] T. Seideman, M.Y. Ivanov, and P.B. Corkum. "*Role of Electron Localization in Intense-Field Molecular Ionization*", Phys. Rev. Lett. **75**, 2819 (1995)

[**Singh-10**] K. P. Singh, F. He, P. Ranitovic, W. Cao, S. De, D. Ray, S. Chen, U. Thumm, A. Becker, M.M. Murnane, H. C. Kapteyn, I.V. Litvinyuk, and C. L. Cocke, "*Control of electron localization in deuterium molecular ions using an attosecond pulse train and a many-cycle infrared pulse*", *Phys. Rev. Lett*. **104**, 023001 (2010)

[**Slater-30]** J. C. Slater, "*Atomic Shielding Constants*", Phys. Rev. **36**, 57 (1930)

[**Slavıček-03**] P. Slavček, R. Kaulus, P. Paška, I. Odvárková, P. Hobza, and A. Malijevský, "*State-of-the-art correlated ab-initio potential energy curves for heavy rare gas dimers: Ar_2, Kr_2, and Xe_2*", J. Chem. Phys. **119(4),** 2102 (2003)

[**Strickland-92**] D. T. Strickland, Y. Beaudoin, P. Dietrich, and P. B. Corkum, "*Optical studies of inertially confined molecular iodine ions*", Phys. Rev. Lett. **68**, 2755 (1992)

[**Staudte-07**] A. Staudte, D. Pavičić, S. Chelkowski, D. Zeidler, M. Meckel, H. Niikura, M. Schöffler, S. Schössler, B. Ulrich, P. P. Rajeev, Th. Weber,

T. Jahnke, D. M. Villeneuve, A. D. Bandrauk, C. L. Cocke, P. B. Corkum, and R. Dörner, "*Attosecond Strobing of Two-Surface Population Dynamics in Dissociating H_2^+*", Phys. Rev. Lett. **98**, 073003 (2007)

[**Steinfeld-05**] J. Steinfeld, "*Molecules and radiation*", Dover publications, New York, (2005)

[**Stevens-77**] W. J. Stevens, M. Gardner, A. Karo, and P. Julienne, "*Theoretical determination of bound–free absorption cross sections in Ar_2^+*", J. Chem. Phys. **67**, 2860 (1977)

[**Szabo-82**] A. Szabo, and N. S. Ostlund, "*Modern quantum chemistry: introduction to advanced electronic structure theory*", Macmillan Publishing Co., Inc, New York, (1982)

[**Thumm-08**] U. Thumm, T. Niederhausen, and B. Feuerstein, "*Time-series analysis of vibrational nuclear wave-packet dynamics in D_2^+*", Phys. Rev. A **77**, 063401 (2008)

[**Ullrich-03**] J. Ullrich, R. Moshammer, A. Dorn, R. Dörner, L. Ph. H. Schmidt, and H. Schmidt-Böcking, "*Recoil-ion and electron momentum spectroscopy: reaction-microscopes*". Rep. Prog. Phys. **66**, 1463 (2003)

[**Ullrich-12**] J. Ullrich, A. Rudenko, and R. Moshammer, "*Free-electron lasers: New avenues in molecular Physics and photochemistry*", Annu. Rev. Phys. Chem. **63**, 635 (2012)

[**Voss-04**] S. Voss, A.S. Alnaser, X.M. Tong, C. Maharjan, P. Ranitovic, B. Ulrich, B. Shan, Z. Chang, C.D. Lin, and C.L. Cocke, "*High resolution kinetic energy release spectra and angular distributions from double ionization of nitrogen and oxygen by short laser pulses*", J. Phys. B. **37**, 4239 (2004)

[**Vassen-12**] W. Vassen, C. Cohen-Tannoudji, M. Leduc, D. Boiron, C. I. Westbrook, A. Truscott, K. Baldwin, G. Birkl, P. Cancio, and M. Trippenbach, "*Cold and trapped metastable noble gases*", Rev. Mod. Phys. **84**, 175 (2012)

[**Wadt-80**] W. R. Wadt, "*The electronic states of Ne_2^+, Ar_2^+, Kr_2^+, and Xe_2^+. II. Absorption cross sections for the $1(1/2)_u \rightarrow 1(3/2)_g$, $1(1/2)_g$, $2(1/2)_g$ transitions*", J. Chem. Phys. **73(8),** 3915 (1980); *ibid.* **68(2)**, 402 (1978).

[**Walker-93**] B. Walker, E. Mevel, B. Yang, P. Breger, J. P. Chambaret, A. Antonetti, L. F. DiMauro, and P. Agostini, "*Double ionization in the perturbative and tunneling regimes*", Phys. Rev. A **48**, R894 (1993)

[**Williams-00**] D. Williams, P. McKenna, B. Srigengan, I. M. G. Johnston, W. A. Bryan, J. H. Sanderson, A. El-Zein, T. R. J. Goodworth, W. R. Newell, P. F. Taday, and A. J. Langley, "*Fast-beam study of H_2^+ ions in an intense femtosecond laser field*", J. Phys. B **33**, 2743 (2000)

[**Winter-09**] M. Winter, R. Schmidt, and U. Thumm, "*Multidimensional quantum-beat spectroscopy: Towards the complete temporal and spatial resolution of the nuclear dynamics in small molecules*", Phys. Rev. A **80**, 031401 (2009)

[**Winter-10**] M. Winter, R. Schmidt, and U. Thumm, "*Quantum-beat analysis of the rotational–vibrational dynamics in D_2^+*", New J. Phys. **12**, 023020 (2010)

[**Wu-12**] J. Wu, L. Ph. H. Schmidt, M. Kunitski, M. Meckel, S. Voss, H. Sann, H. Kim, T. Jahnke, A. Czasch, and R. Dörner. "Multiorbital *tunneling ionization of the CO molecule*". Phys. Rev. Lett. **108**, 183001 (2012)

[Wu-13-1] J.Wu, A. Vredenborg, L. Ph. Schmidt, T. Jahnke, A. Czasch, and R. Dörner, "*Comparison of dissociative ionization of H_2, N_2, Ar_2, and CO by elliptically polarized two-color pulses*", Phys. Rev. A **87**, 023406 (2013)

[**Wu-13-2**] J. Wu, M. Magrakvelidze, A. Vredenborg, L. Ph. H. Schmidt, T. Jahnke, A. Czasch, R. Dörner, and U. Thumm, "*Steering the nuclear motion in singly ionized argon dimers with mutually detuned laser pulses*", Phys. Rev. Lett. **110**, 033005 (2013)

[**Wu-13-3**] J. Wu, M. Magrakvelidze, L. Ph. H. Schmidt, M. Kunitski, T. Pfeifer, M. Schöffler, M. Pitzer, M. Richter, S. Voss, H. Sann, H. Kim, T. Jahnke, A. Czasch, U. Thumm, and R. Dörner, "*Attosecond timing of asymmetric chemical bond breaking*", Nature communications **4**, 2177 (2013)

[**Wüest-03**] A. Wüest and F. Merkt, "*Determination of the interaction potential of the ground electronic state of Ne_2 by high-resolution vacuum ultraviolet laser spectroscopy*", J. Chem. Phys. **118**, 8807 (2003)

[Zare-98] R. N. Zare, "*Angular Momentum*", Wiley-Interscience, New York (1998)

[**Zavriyev-90**] A. Zavriyev, P. H. Bucksbaum, H. G. Muller, and D. W. Schumacher, "*Ionization and dissociation of H_2 in intense laser fields at 1.064 μm, 532 nm, and 355 nm*", Phys. Rev. A. **42**, 5500 (1990)

[**Zewail-88**] A. H. Zewail, "*Laser femtochemistry*", *Science* **242**, 1645-1653 (1988)

[**Zewail-00**] A. H. Zewail, "*Femtochemistry: Atomic-Scale Dynamics of the Chemical Bond*", J. Phys. Chem. A **104**, 5660 (2000)

[**Znakovskaya-12**] I. Znakovskaya, P. von den Hoff, G. Marcus, S. Zherebtsov, B. Bergues, X. Gu, Y. Deng, M. J. J. Vrakking, R. Kienberger, F. Krausz, R. de Vivie-Riedle, and M. F. Kling, "*Subcycle controlled charge-directed reactivity with few-cycle mid-infrared pulses*", Phys. Rev. Lett. **108**, 063002 (2012)

[**Zohrabi-11**] M. Zohrabi, J. McKenna, B. Gaire, N. G. Johnson, K. D. Carnes, S. De, I. A. Bocharova, M. Magrakvelidze, D. Ray, I. V. Litvinyuk, C. L. Cocke, and I. Ben-Itzhak, "*Vibrationally resolved structure in O_2^+ dissociation induced by intense ultrashort laser pulses*", Phys. Rev. A **83**, 053405 (2011)

[**Zuo-95**] T. Zuo and A. D. Bandrauk, "*Charge-resonance-enhanced ionization of diatomic molecular ions by intense lasers*", Phys. Rev. A **52**, R2511 (1995)

[Xie-90] J. Xie and R. N. Zare, "*Selection rules for the photoionization of diatomic molecules*", J. Chem. Phys. **93**(1), 3033 (1990)

APPENDICES

Appendix A - Abbreviations

A list of the abbreviations used in this work is given below.

ADK	–	Ammosov-Delone-Krainov
AO	–	Atomic orbital
BH	–	Bond hardening
BO	–	Born-Oppenheimer
BS	–	Bond softening
CI	–	Configuration interaction
CE	–	Coulomb explosion
CEP	–	Carrier envelope phase
CN	–	Crank-Nicolson
COLTRIMS	–	COLd target recoil ion momentum spectroscopy
CREI	–	Charge-resonance enhanced ionization
CSF	–	Configuration state function
CW	–	Continuous wave
FC	–	Frank-Condon
FLASH	–	Free-electron laser in Hamburg
FWHM	–	Full width half maximum
GAMESS	–	General atomic and molecular electronic structure system
GTO	–	Gaussian-type orbitals
HF	–	Hartree-Fock
IR	–	Infra-red
KER	–	Kinetic energy release
MCSCF	–	Multiconfiguration self-consistent field
MO	–	Molecular orbital
NIR	–	Near infra-red
SCF	–	Self-consistent field
STO	–	Slater type orbitals
TDSE	–	Time dependent Schrödinger equation
QB	–	Quantum beat
VD	–	Virtual detector
VMI	–	Velocity map imaging
XUV	–	Extreme ultra-violet

Appendix B - Reduced mass

If the masses of the atoms in a diatomic molecule are m_1 and m_2, the *reduced* mass can be calculated as follows

$$\mu = \frac{m_1 m_2}{m_1 + m_2}$$

If $m_1 = m_2 = m$ (homonuclear diatomic molecules).

$$\mu = \frac{m}{2} = \frac{1}{2} \times \frac{Atomic\ mass\ (\frac{g}{mol})}{Avogadro's\ number\ (mol^{-1})} \times \frac{1}{9.10938\ \text{x}10^{-28}\ g(a.u.)^{-1}}$$

$$\boxed{\mu(a.u.) = Atomic\ mass\ \left(\frac{g}{mol}\right) \times\ 911.44453}$$

Molecule	Atomic mass (g/mol)		Reduced mass (a.u.)
H_2	(H)	1.0079	918.645
D_2	(D)	2.0158	1835.2415
He_2	(He)	4.0026	3648.148
N_2	(N)	14.0067	12766.341
O_2	(O)	15.9994	14582.566
Ne_2	(Ne)	20.1797	18392.677
Ar_2	(Ar)	39.948	36410.386
Kr_2	(Kr)	83.798	76377.229
Xe_2	(Xe)	131.293	119666.287

Appendix C - Single-curve-calculation code

This appendix describes the source code used in single-cation curve calculations. It is written in FORTRAN-90. The code has a main program that uses several subroutines and functions that are divided into different files.

Module	Description
`tdse.f90`	The main program.
`progvars.f90`	Defining program variables and default values.
`wfMath.f90`	Math-related subroutines.
`wfPot.f90`	Reading in potential curves.
`params.f90`	Reads input parameter values.
`CN.f90`	Crank–Nicolson propagation scheme.
`FT.f90`	FT method propagation scheme.
`adk.f90`	ADK depletion of ground state.
`fft.f90`	Fast Fourier transform related subroutines.
`diag.f90`	One dimensional diagonalization soubroutines.
`debug.f90`	Debug related.
`fileswin.f90`	Reading-writing input-output files.
`strings.f90`	String manipulation subroutines.

C.1 Main Program (tdse.f90)

```
program main
    use progvars
    implicit none
    molecule      =  "He2";
    inputFolder   =  "input\";
    curve1        =  "He2_pot_ground.txt"
    outputFolder  =  "output\";
    curve2        = "He2p-Sig-u-Morse.txt"
    call RunOnce();
    print *, 'program completed'
end program main
!-----------------------------------------------------------------------------------------------
subroutine RunOnce()
    use progvars
    use files
    implicit none
    call EnsureFolderExists(outputFolder);
    call init(); print *, 'init completed';
    call find_groundstate_byenergy(); print *, 'find_groundstate completed';
    !here  at this point psi contains ground state
    call calculate_energy(); print *, 'calculate_energy completed';
    ! call Diagonalize();
    useADKpump  =  .false.
    if (useADKpump.eq. .true.) then
       call Apply_ADK();
    endif
    call run(); print *, 'run completed';
    call cleanup();
end subroutine RunOnce
!_____________________________input parameters_____________________________
subroutine init
    use progvars
    use strings;
    use wfMath
    use wfPot
    implicit none
    integer :: nloop
    real*8  :: widthz,pz
    select case (trim(molecule))
        case("D2")
            mass = 1835.241507d0; nz = 1024;  deltaz  = 0.05d0;
        case("He2")
            mass = 3648.148d0; nz =8192;  deltaz  = 0.01d0
    end select
    maxt    = 124024.34d0 ! 3ps                ! maximum time
    deltat  = 1.0d0                            ! delta time
    widthz  = 3.0d0                            ! width of the gaussian
    minz    = 0.0d0                            ! minimum z in a.u.
    maxz    = nz * deltaz                      ! maximum z in a.u.
    centerz = 7.d0                             ! center of the gaussian
    nt      = NINT(maxt/deltat)                ! time steps
    pz      = 0.0d0                            ! not used currently
    !_____________________________FFT section_____________________________
    deltafft    =   20.d0* deltat              ! time step for FFT
    nfft        =   NINT(maxt/deltafft)        ! no of steps for FFT
    !_____________________________absorber parameters_____________________________
    fadewidth    =15.d0                 ! the width of the absorber in a.u.
    fadestrength = 0.1d0  !the maximum heigth of the neg. imaginary potential
    includeAbsorber = .true.                   ! switch for absorber
    !_____________________________E FIELD section_____________________________
    Eo      = 0.1d0                            ! field amplitude
    Eomega  = 0.057d0                          ! laser frequency
    Ephi    = 0.d0                             ! carrier envelope phase
    Ewidth  = 120.d0                           ! width of the envelope
    Eto     = 1000.d0                          ! ecentl.of the Gaus. envelope
    includeField = .false.                     ! switch for efield
    pumpEo         =  0.053 !1E14
```

```
        pumpEwidth     =  3305.8d0 !80fs
70      pumpEomega     =  0.057d0
        pumpEphi       =  0.0d0
        !_____________________________Printing & Plotting Filters_________________
        printFilter = nz
        maxFrequencyFilter = 2000
75      printInterval = 200
        ! print filter upper boundary check
        if(printFilter > nz) then
            printFilter = nz
        end if
80      call allocateArrays();
        do nloop = 1,nz
            Z(nloop) = minz+ (nloop)* deltaz
            P(nloop) = 2*pi*(nloop-(nz/2)-1)/(maxz-minz);
        end do
85      call wfmath_gaussian(widthz,pz)
        !call setabsorber_left(fadewidth, fadestrength) !/deltat
        call setabsorber_right(fadewidth, fadestrength)
        call printpsi(trim(concat(outputFolder,"psi.dat")))
        call potentials_init(nz)              !initialize potential arrays
90      call read_potential();
    end subroutine init
    !-------------------------------------------------------------------------------------------------------
    subroutine read_potential()
        use progvars;
95      use strings;
        use wfPot;
        call potentials_readfromfile_activate(trim(concat(inputFolder,curve1)),1)
        call potentials_readfromfile_activate(trim(concat(inputFolder,curve2)),2);
    end subroutine read_potential
100 !-------------------------------------------------------------------------------------------------------
    subroutine Diagonalize()
        use progvars;
        use strings;
        use wfMath;
105     use wfPot;
        use diag;
        implicit none;
        integer nstate;
        real*8, pointer     :: potarray(:);
110     print *,"-------------------------------------"
        print *,""
        print *,"-> Diagonalizing the potential of gerade curve <-"
        call diag_init(nz,deltaz,mass)      ! needed for diagon. of the potential
        nullify(states%energyarr)           ! ensure proper disas. of the new pointers
115     nullify(states%wavefunctions)
        call potentials_setactive(2);
        call wfPot_FormattedPotentialHC(potarray,curve2);
        open(unit=111,file=trim(concat(outputFolder,"fpot.dat")),status="replace",
             access="sequential",recl=1024)
120     do nstate=1, nz
            write(111,'(E13.3,E12.5)') (nstate*deltaz), potarray(nstate);
        enddo
        close(111)
        call diag_diagonalize(potarray, states)               !find the bound states
125     print *,"Number of bound states: ",states%numbound    !number of bound states
        call diag_plot(states, trim(concat(outputFolder,"test")))
        open(unit=111,file=trim(concat(outputFolder,"fc_factors.dat")),status="replace",
        access="sequential", recl=1024)
        write(111,'(A6,2A12)') "State","Energy","FC-Factor"
130     do nstate=1, states%numbound
          write(111,'(I6,2E12.4)') nstate,states%energyarr(nstate), &
                cdabs(wfmath_overlap(psi(:),states%wavefunctions(nstate,:)))**2
        enddo
        write(111,*)
135     close(111)
        call diag_release(states);
        call diag_done();
    end subroutine Diagonalize
    !_______________________________run_____________________________
```

```
subroutine run
    use progvars
    use strings;
    use wfMath
    use wfPot
    use fft;
    implicit none
    real*8          :: etime, energy1, efield = 0.d0, mom
    complex*16      :: pos,var, mom1, mom2, varP,varMom,  rdeltat
    integer         :: fftloop,tloop, timestep , estep
    logical         :: ufield  = .true.
    call MethodInit()
    !init fft arrays for KER
    call fftInit(nz,deltaz,mass);
    rdeltat         = CMPLX(deltat,0.d0)
    call potentials_setactive(2);
    open(unit=102,file=trim(concat(outputFolder,"wfunc.dat")),status="replace",
         access="sequential",recl=1024)
    open(unit=103,file=trim(concat(outputFolder,"efield.dat")),status="replace",
         access="sequential",recl=1024)
    open(unit=104,file=trim(concat(outputFolder,"position.dat")),status="replace",
         access="sequential",recl=1024)
    open(unit=105,file=trim(concat(outputFolder,"momentum.dat")),status="replace",
         access="sequential",recl=1024)
    open(unit=106,file=trim(concat(outputFolder,"XVariance.dat")),status="replace",
         access="sequential", recl=1024)
    open(unit=108,file=trim(concat(outputFolder,"PXproduct.dat")),status="replace",
         access="sequential", recl=1024)
    open(unit=109,file=trim(concat(outputfolder,"MomVariance.dat")),status="replace",
         access="sequential", recl=1024)
    timestep = NINT(deltafft / deltat)
    do fftloop = 1 , nfft
        !print *,  fftloop*timestep
        do tloop = 1 , timestep
            fftvalues = czero;
            estep =  ((fftloop-1)*timestep + tloop);
            print *,  estep ;
            etime   =  estep * deltat;
            if(includeField .eq. .true.) then
                efield  = wfmath_efield(etime)
            else
                efield  = 0.d0
            end if
            call propagate(rdeltat,efield, ufield, includeAbsorber)
            pos     = wmath_pos(psi)
            write(104,'(E13.4E3, E13.4E3)') etime*0.0242, Real(pos)
            var = wmath_var(psi)
            write(106,'(E13.4E3, E13.4E3)') etime*0.0242, Real(var)
            call fftForward(psi);
            mom = wfmath_momentum3(fftvalues);
            write(105,'(E13.4E3, E13.4E3)') etime, mom
            varMom = wmath_varMom(fftvalues)/((nz *deltaz )**2)
            write(109,'(E13.4E3, E13.4E3)') etime*0.0242, Real(varMom)
            write(108,'(E13.4E3, E13.4E3)') etime*0.0242, sqrt(abs(Real(var*varMom)))
            ufield = includeField
            if(mod(estep,printInterval) .eq. 0) then
                write(102,'(E13.4E3,$)')  cdabs(psi(1:printFilter))**2
                write(102,*)
                write(103,'(E13.4E3 ,E13.4E3)') etime, efield
            end if
        end do
    end do
    close(102)
    close(103)
    close(104)
    close(105)
    close(106)
    close(108)
    close(109)
    call MethodCleanup()
    call fftCleanup();
```

```
    end subroutine run
    !_____________________________find_groundstate_____________________________
    subroutine find_groundstate_byenergy
        use progvars
215     use strings
        use wfMath
        use wfPot
        implicit none
        complex*16                                  :: energy1,energy2
220     real*8                                      :: overlap
        !The preset precision goal
        real*8                                      :: prec = 1.d-11
        !Test convergence by default every 2nd propagation step
        integer                                     :: ctest = 2
225     !The preset maximum iteration to find ground state
        integer                                     :: maxiter = 10000000
        complex*16                                  :: timestep
        integer                                     :: loop
        logical                                     :: ufield  = .true.
230     !wavefunction array to check convergence
        complex*16, pointer, dimension(:)           :: psiwork
        call MethodInit()
        !Create a work array of same shape as psiin
        allocate(psiwork(size(psi)),stat=iAllocStatus)
235     if (iAllocStatus /= 0) then
          print *,"ERROR: can't allocate PSIWORK array"
          stop
        endif
        print *,"TOOLS_GROUNDSTATE: PSIWORK wavefunction array allocated"
240     call potentials_setactive(1);
        psiwork = 0.d0
        timestep = -ii* deltat
        do loop = 1 , maxiter
            call propagate(timestep,0.d0, ufield, .false.)
245         call wfmath_normalize(psi)
            if (mod(loop,ctest).eq.0) then               ! test convergence only every ctest loop
                energy1 = wfmath_energy(psi);
                energy2 = wfmath_energy(psiwork);
                overlap = abs(real(energy1-energy2));
250             print *, loop, real(overlap);
                if (overlap.lt.prec) then
                    ! found ground state .. yeah....
                    print *, "found groundstate"
                    exit
255             end if
                psiwork = psi
            end if
            ufield = .false. !calculate XY only first time for CN Method,not used in any other method
        end do
260     if(loop.gt.maxiter) then
            print *, "groundstate not found"
            stop
        end if
        deallocate(psiwork)
265     call MethodCleanup()
    end subroutine find_groundstate_byenergy
    !-----------------------------------------------------------------------------------------------
    subroutine printpsi(filename)
        use progvars
270     implicit none
        character(len=*), intent(in) :: filename
        integer :: nloop
    open(unit=101,file=filename,status="replace",access="sequential",recl=1024)
        do nloop=1, nz
275         write(101,'(E13.6E3,4x,E13.6E3)') (nloop*deltaz), real(psi(nloop))
        enddo
        close(101)
    end subroutine
    !-----------------------------------------------------------------------------------------------
280 subroutine calculate_energy
        use progvars
```

```
        use strings
        use wfMath
        implicit none
285     complex*16 energy;
        energy = wfmath_energy(psi);
        print *, real(energy);
    open(unit=129,file=trim(concat(outputFolder,"groundstate_energy.dat")),status="replace",access="s
    equential",recl=1024)
290     write(129,'(E13.6)') real(energy);
        close(129)
    end subroutine calculate_energy
    !_____________________________________Absorber_____________________________
    subroutine setabsorber_left(width,strength)
295     use progvars
        implicit none
        ! sets the absorber (optical potential) on the left side of the grid (min z-coordinate)
        real*8, intent(in) :: width, strength
        integer            :: n
300     real*8             :: maskvalue
        do n=1, nint(width / deltaz)
            maskvalue = (((width - (n-1)*deltaz) / width)**2) * strength
            maskvalue = exp(-maskvalue)
            absorber(n) = absorber(n) * maskvalue
305     enddo
    end subroutine setabsorber_left
    !-----------------------------------------------------------------------------------------------
    subroutine setabsorber_right(width,strength)
        use progvars
310     implicit none
        ! sets the absorber (optical potential) on the right side of the grid (max z-coordinate)
        real*8, intent(in) :: width, strength
        integer            :: n
        real*8             :: maskvalue
315     do n=1, nint(width / deltaz)
            maskvalue = (((width - (n-1)*deltaz) / width)**2) * strength
            maskvalue = exp(-maskvalue)
            absorber(nz + 1 - n) = absorber(nz + 1 - n) * maskvalue
        enddo
320 end subroutine setabsorber_right
    !-----------------------------------------------------------------------------------------------
    subroutine setabsorber(width,strength)
        ! sets the absorber (optical potential) on both sides of the potential
        real*8, intent(in) :: width, strength
325     call setabsorber_left(width,strength)
        call setabsorber_right(width,strength)
    end subroutine setabsorber
    !_____________________________________Allocate_____________________________
    subroutine allocateArrays
330     use progvars
        implicit none
        integer i,j
        allocate(Z(nz),P(nz), stat = iAllocStatus)
        if (iAllocStatus /= 0) then
335         print *,"ERROR: can't allocate position vector Z or P"
            stop
        endif
        allocate(psi(nz), psitotal(nz),  stat = iAllocStatus)
        if (iAllocStatus /= 0) then
340         print *,"ERROR: can't allocate wave function psi"
            stop
        endif
        allocate(absorber(nz), stat = iAllocStatus)
        if (iAllocStatus /= 0) then
345         print *,"ERROR: can't allocate Vector absorber"
            stop
        endif
        allocate(fftarray(nz,nfft), stat = iAllocStatus)
        if (iAllocStatus /= 0) then
350         print *,"ERROR: can't allocate Array FFT"
            stop
        endif
```

```
        allocate(fftinput(nfft), stat = iAllocStatus)
        if (iAllocStatus /= 0) then
            print *,"ERROR: can't allocate Array FFT Input"
            stop
        endif
        psi         =   czero
        psitotal    =   czero
        absorber    =   1.d0
        fftarray    =   0.d0
    end subroutine
    !_________________________clean_____________________________
    subroutine cleanup
        use progvars
        use wfPot
        use fft
        implicit none
        deallocate(Z)
        deallocate(P)
        deallocate(psi)
        deallocate(psitotal)
        deallocate(absorber)
        deallocate(fftarray)
        deallocate(fftinput)
        call potentials_done()
    end subroutine
    !-----------------------------------------------------------------------------------------------
    subroutine MethodInit()
        use progvars
        use CN
        use FT
        implicit none
        select case(useMethod)
            case (CNMethod)
                call CNInit()
            case (FTMethod)
                call FTInit()
        end select
    end subroutine
    !-----------------------------------------------------------------------------------------------
    subroutine MethodCleanup()
        use progvars
        use CN
        use FT
        implicit none
        select case(useMethod)
            case (CNMethod)
                call CNCleanup()
            case (FTMethod)
                call FTCleanup()
        end select
    end subroutine
    !-----------------------------------------------------------------------------------------------
    subroutine propagate(timestep,efield, useefield, useabsorber)
        use progvars
        use wfMath
        use CN
        use FT
        implicit none
        complex*16, intent(in)                  :: timestep
        real*8, intent(in)                      :: efield
        logical, intent(in)                     :: useefield
        logical, intent(in)                     :: useabsorber
        select case(useMethod)
            case (CNMethod)
                call CNPropagate(psi, timestep, efield, useabsorber)
            case (FTMethod)
                call FTPropagate(timestep,efield, useefield, useabsorber)
        end select
    end subroutine
    !-----------------------------------------------------------------------------------------------
    subroutine Apply_ADK()
```

```
        use progvars
        use adk
        use wfPot
        use wfMath
        implicit none
        real*8          :: pumpint; ! pump pulse intensity to be calculated from pumpEo.
        pumpint = pumpEo**2;
        if(useADKpump .eq. .true.) then
            print *,"MESSAGE : ADK rate dependent instantaneous ionization "

            !use psitotal temporarly for work
            !first we need a copy of the original ground state wave function
            psitotal = psi

            !ADK deplete this state
            call adk_deplete(psitotal, pot_curve1, pot_curve2, 1.d0, pumpint,
                             pumpEwidth, pumpEomega, pumpEphi)

            !subtract the final ground state from the original - the new excited state
            psi = psi- psitotal

            call wfmath_normalize(psi)
        end if
    end subroutine Apply_ADK
```

C.2 Module defining variables (progvars.f90)

```
    module progvars
        implicit none
        type       :: TEnergies            ! declare a type array for bound state energies
            integer               :: numbound     ! number of bound states
            real*8, pointer       :: energyarr(:) ! the array with the bound energies
        end type
        type       :: TStates              ! declare a type array for bound wave functions
            integer               :: numbound     ! number of bound states, identical to TEnergies
            real*8, pointer       :: energyarr(:) ! the array with the bound energies
            complex*16, pointer   :: wavefunctions(:,:)! the array with the wave functions
        end type
        ! Variable definitions
        real*8      :: mass         ! particle mass
        real*8      :: maxz         ! maximum x
        real*8      :: minz         ! minimum x
        real*8      :: deltaz       ! step size in x direction

        real*8      :: centerz      ! initial position in gaussian
        real*8      :: maxt         ! maximum time
        real*8      :: deltat       ! delta time
        integer     :: nz           ! no of steps in x direction (no of points in the grid)
        integer     :: nt           ! no of time steps
        real*8      :: deltafft     ! time step for FFT
        integer     :: nfft         ! no of time/frequency steps for FFT
        real*8, pointer  :: Z(:), P(:)
        real*8, pointer  :: potential(:)
        complex*16,  pointer :: psi(:)        ! initial wavefunction array
        complex*16, allocatable :: psitotal(:)
        complex*16  :: ii  = (0.d0,1.d0)       ! complex number i
        complex*16  :: czero  = (0.d0,0.d0)
        real*8      :: pi = 3.14159265358979323846264 3d0
        !_____________absorber section_____________________________________________
        real*8  :: fadewidth                    ! the width of the absorber for the electrons
        real*8  :: fadestrength                 ! the strength of the absorbing border potential
        real*8, pointer :: absorber(:)          ! absorber potential
        logical :: includeAbsorber              ! switch for using absorber
        !_____________________E FIELD section_____________________________________
        real*8  :: Eo                           ! field amplitude
        real*8  :: Eomega                       ! laser frequency
        real*8  :: Ephi                         ! carrier envelope phase
        real*8  :: Ewidth                       ! width of the envelope
        real*8  :: Eto                          ! center of the gaussian envelope
```

```
      logical :: includeField                ! switch for using field
!_____________________________Pump Section_____________________________________
      real*8              :: pumpEo     !(pulseint)
      real*8              :: pumpEwidth !(pulselength)
      real*8              :: pumpEomega !(pulseomega)
      real*8              :: pumpEphi   !(pulsephase)

!_____________________________FFT Section_____________________________________
      real*8,  pointer    :: fftarray(:,:)    ! array for FFT
      complex*16, pointer :: fftinput(:)      ! the complex version for one R parameter

!_____________________Diagonalization Section_____________________________
      type(TStates)     :: states
      ! object with wave functions and energies from diagonalization

      !_____________________ Memory allocation_____________________________________
      integer :: iAllocStatus
      !_____________________ Printing & Plotting Filters_____________________________
      integer :: printFilter
      integer :: maxFrequencyFilter
      integer :: printInterval
      real*8  :: frequencyInTHZ = 6579.7d0
      !_____________________Method Selection_____________________________________
      character(len=2),parameter   :: CNMethod  = "CN"        ! Crank-Nicholson method
      character(len=2),parameter   :: FTMethod  = "FT"        ! FFT method
      character(len=2)   :: useMethod  = CNMethod
      !character(len=2)   :: useMethod  = FTMethod
      !_____________________ Output selection _____________________________________
      character(len=120) :: inputFolder;
      character(len=120) :: outputFolder;
      character(len=120) :: curve1, curve2;
      character(len=10)  :: molecule
      !_____________________ ADK Section _____________________________________
      logical             :: useADKpump   ! =  .true.
      logical             :: Powerspectra
end module progvars
```

C.3 Module Wave Function (wfMath.f90)

```
module wfmath
  implicit none
   contains
   !_____________________definind initial wave function_____________________
subroutine wfmath_gaussian(widthz,pz)
    use progvars
    implicit none
    real*8, intent(in)                    :: widthz             ! the width of the wavepacket
    real*8, intent(in)                    :: pz                 ! momentum
    integer                               :: nR
    real*8                                :: rvalue
    complex*16                            :: cvalue
    real*8                                :: z2
    z2 = minz + deltaz
    do nR=1, nz
      rvalue = exp( -((z2-centerz)/widthz)**2 /2 )/ (2*pi*widthz)
      cvalue = cdexp( cmplx(0.0,1.0)*(pz*z2))
      psi(nR) = rvalue * cvalue
      z2 = z2 + deltaz            ! next grid position in x-direction
    enddo
    call wfmath_normalize(psi)
end subroutine wfmath_gaussian
!_____________________________overlap_____________________________________
  function wfmath_overlap(wf1,wf2,centerz1,widthz1) result(overlap)
    use progvars
    implicit none
    ! calculating the overlap of the two given wf's inside the optional given integration areas
    ! algorithm can be improved by a better integration method!
```

```
      complex*16, intent(in), dimension(:) :: wf1, wf2
      real*8, intent(in), optional         :: centerz1  ! the center of the integration window
      real*8, intent(in), optional         :: widthz1   ! the full length of the integration window
      complex*16                           :: overlap
      integer                              :: nzstart, nzend    ! the integration grid boundary

      !initial function result in case of out-of-integration-area
      overlap = cmplx(0.d0,0.d0)
      if (present(centerz1).and.present(widthz1)) then
        ! the integration boundary in x-grid space
        nzstart = int((centerz1 - minz - widthz1/2) / deltaz) + 1
        nzend   = int((centerz1 - minz + widthz1/2) / deltaz) + 1
        if (nzstart.gt.nz) return       ! get out - we run out on the right side
        if (nzend.lt.1) return          ! get out - we run out on the left side
        if (nzstart.lt.1) nzstart = 1   ! correct for left side out of integration area
        if (nzend.gt.nz) nzend = nz     ! correct for right side
      else
        nzstart = 1
        nzend   = nz
      endif
      ! calculate the quantum mechanical overlap of the two wavefunctions
      overlap = sum(conjg(wf1(nzstart:nzend))*wf2(nzstart:nzend))*deltaz
      return
    end function wfmath_overlap
    !_____________________________Energy_____________________________________
    function wfmath_energy(wf) result(energy)
      ! calculates the energy corresponding to the given wavefunction: E=<Psi|H|Psi>
      ! using 5-point formula for H=-1/(2*mass) * (d^2/dx^2 + d^2/dz^2) + V
      ! 5-point formula: f" = 1/(12 Delta^2) * (- f_-2 + 16f_-1 - 30f_0 + 16f_1 - f_2)
      use progvars
      implicit none
      complex*16, intent(in), dimension(:) :: wf  ! the input WF we calculate the energy from
      complex*16                           :: energy! the functional result for the energy
      complex*16                           :: epot, ekinz   ! contributions to the total energy
      ! splitting operator into sum: E=-1/2m <Psi|pz^2|Psi> + <Psi|V|Psi>
      ! First step: Potential energy Epot = <Psi|V|Psi>
      epot = sum(conjg(wf)*wf*potential)*deltaz
      ! Second: kinetic energy
      ekinz = - 1 / (24*mass) / deltaz * &
        sum(conjg(wf(3:nz-2)) * &
        ( -wf(1:nz-4)+16*wf(2:nz-3)-30*wf(3:nz-2)+16*wf(4:nz-1)-wf(5:nz) ) )
      ! Third: return the total (sum) energy
      energy = epot + ekinz
      return
    end function wfmath_energy
    !_____________________________position_____________________________________
    function wmath_pos(wf) result(pos)
      !calculates the expectation value of the position corresponding to the given wavefunction:
      !pos=<Psi|x|Psi>
      use progvars
      implicit none
      !the input wavefunction we calculate the energy from
      complex*16, intent(in), dimension(:) :: wf
      complex*16                           :: pos
      pos=sum(conjg(wf)*wf*Z)*deltaz
      return
    end function wmath_pos

    !_____________________________momentum_____________________________________
     function wfmath_momentum3(wf) result(momentum)
      use progvars
      complex*16, intent(inout), dimension(:) :: wf
      real*8                                  :: momentum, pmax, deltap
      complex*16                              :: mom, norm
      pmax   = 1.d0/(2.d0*deltaz)       ! maximum momentum of the grid (see Nyquist theorem)
      deltap = 2.d0*pmax / nz           ! the momentum resolution
      norm= sum(conjg(wf)*wf*deltap)
      mom = sum(conjg(wf)*wf*P)*deltap/norm
      momentum = Real(mom);
         return
    end function wfmath_momentum3
```

```
    !_____________________________VarianceP_____________________________________________________
105
    function wmath_varMom(wf) result(var)
        use progvars
        implicit none
        !the input wavefunction we calculate the energy from
110     complex*16, intent(in), dimension(:) :: wf
        complex*16                           :: var
        real*8                               :: pmax, deltap
        pmax   = 1.d0/(2.d0*deltaz)          ! maximum momentum of the grid (see Nyquist theorem)
        deltap = 2.d0*pmax / nz              ! the momentum resolution
115     var= sum(conjg(wf)*wf*P**2)*deltap-(sum(conjg(wf)*wf*P)*deltap)**2/(sum(conjg(wf)*wf*deltap))
        return
    end function wmath_varMom
    !_____________________________VarianceX_____________________________________________________
    function wmath_var(wf) result(var)
120     ! calculates the varianceof the position : var = <x^2>-<x>^2
        use progvars
        implicit none
        !the input wavefunction we calculate the energy from
        complex*16, intent(in), dimension(:) :: wf
125     complex*16                           :: var
        var=sum(conjg(wf)*wf*Z**2)*deltaz-(sum(conjg(wf)*wf*Z)*deltaz)**2
        return
    end function wmath_var
    !_____________________________Normalize_____________________________________________________
130 subroutine wfmath_normalize(wf)
        ! nomalizing the given wavefunction
        complex*16, intent(inout), dimension(:) :: wf
        complex*16                              :: wfnorm
        wfnorm = wfmath_overlap(wf,wf)      ! calculate the norm of the whole wavefunction
135     !And divide everything by the square root of the norm -> normalize...
        wf = wf / sqrt(wfnorm) end subroutine wfmath_normalize

    !-----------------------------------------------------------------------------------------------
    function wfmath_efield(lasertime) result(fieldstrength)
140     ! return the field strength of the laser pulse specified in the PROGVAR block
        ! at the given LASERTIME
        ! for an analytical form of the pulse, i.e. a Gaussian pulse.
        use progvars
        implicit none
145     real*8, intent(in) :: lasertime
        real*8             :: fieldstrength
        real*8             :: envelope, phase, ton, toff
        fieldstrength = 0.d0          ! we start with nothing and add whatever we get...
        ! GAUSS SHAPE
150     envelope      = Eo * dexp(- 2.d0 * dlog(2.d0) * ((lasertime-Eto)**2) / (Ewidth**2) )
        phase         = dmod(Eomega*lasertime+Ephi,2*pi)
        fieldstrength = envelope * dcos(phase)
        return
    end function wfmath_efield
155 end module
```

C.4 Module potentials (wfPot.f90)

```
    module wfPot
        implicit none
        real*8, allocatable, target :: pot_curve1(:), pot_curve2(:)
 5      ! these are our 2 potential curves 1 is ground, 2 is gerade/ungerade
        integer     ::  selectedPotentialNumber = 0;
        contains
    !-----------------------------------------------------------------------------------------------
    ! I N I T I A L I Z A T I O N
 10 !-----------------------------------------------------------------------------------------------
        subroutine potentials_init(zdim)
            use debug
            integer, intent(in) :: zdim             ! the dimension of the arrays
            integer             :: iAllocStatus     ! return value
 15         ! allocate potential arrays
            allocate(pot_curve1(zdim),pot_curve2(zdim),stat=iAllocStatus)
```

```
        if (iAllocStatus /= 0) then
            print *,"ERROR: can't allocate POTENTIAL arrays"
            stop
20      endif
        call debugmsg(10,1,"POTENTIALS_INIT: POTENTIAL arrays allocated")
        !And make sure we have an active potential assigned - initialized with the lowest curve.
        call potentials_setactive(1)
        call debugmsg(5,1,"POTENTIALS_INIT: 1D potentials allocated")
25  end subroutine potentials_init
!-----------------------------------------------------------------------------------------------
    subroutine potentials_setactive(potnr)
        use progvars
        implicit none
30      ! chooses which potential curve is the currently active potential curve
        integer, intent(in) :: potnr
        selectedPotentialNumber = potnr;
        select case(potnr)
            case(1)
35              potential => pot_curve1
            case(2)
                potential => pot_curve2
            case default
                print *,"POTENTIALS_SETACTIVE: ERROR - potential number ", potnr,
40                      "is not within [1,2] range"
                stop
        end select
    end subroutine potentials_setactive
!-----------------------------------------------------------------------------------------------
45  subroutine potentials_readfromfile_activate(filename,potnr)
        character(len=*), intent(in) :: filename        ! potential file to read
        integer, intent(in) :: potnr
        call potentials_setactive(potnr)
        call potentials_readfromfile(filename)
50  end subroutine
!-----------------------------------------------------------------------------------------------
    subroutine potentials_readfromfile(filename)
        ! read the potential from a file. In the first column is the position while
        ! the second column gives the potential value.
55      use progvars
        use debug
        implicit none

        character(len=*), intent(in) :: filename        ! potential file to read
60      integer                      :: ios             ! the error for the I/O operation
        real*8                       :: pos, pot        ! position and potential from the file
        integer                      :: nzpos           ! the grid point
        logical                      :: warning         ! the general warning flag
        potential   =   0.d0
65      nzpos       =   1
        warning     =   .false.                         ! no warning condition
        open(unit=501,file=trim(filename),access="sequential",recl=1024,status="old")
        ! open file in binary form to read wavefunction
        do
70          read(501,*,IOSTAT=ios)    pos, pot   ! read one line
            if (ios.ne.0) then
                exit       ! exit the do loop if an error occured, i.e. end of file
            end if
            if(nzpos <= nz) then
75             ! now we have the values from the file and can start assigning them
               ! to our internal array
                potential(nzpos) = pot
                nzpos = nzpos + 1
            else
80              warning     =   .true.                  ! no warning condition
                !exit
            end if
        end do
        if (ios < 0) then
85          if (warning) then
                call debugmsg(5,2,"POTENTIALS_READ: WARNING - potential read,
                                  but file does not match grid")
```

```
            else
                call debugmsg(5,2,"POTENTIALS_READ: data successfully read from file")
            endif
        else
            call debugmsg(5,2,"POTENTIALS_READ: ERROR while reading file")
            print *,"Error number: ",ios
            pause
        endif
        close(501)
    end subroutine potentials_readfromfile
!-----------------------------------------------------------------------------------------
    subroutine potentials_done
        use debug
        integer :: iDeallocStatus     ! return value
        ! deallocate potential arrays
        deallocate(pot_curve1, pot_curve2,stat=iDeallocStatus)
        if (iDeAllocStatus /= 0) then
            print *,"ERROR: can't deallocate POTENTIAL arrays"
            stop
        endif
        call debugmsg(10,1,"POTENTIALS_DONE: POTENTIAL arrays destroyed")
        call debugmsg(5,1,"POTENTIALS_DONE: 1D potentials destroyed")
    end subroutine potentials_done
end module wfPot
```

C.5 Module parameters (params.f90)

```
module params
    implicit none
    contains
     subroutine params_read()
        use progvars
        use debug
        integer                     :: ios            ! the error for the I/O operation
        character(len=50)           :: key
        real*8                      :: value
     end subroutine
end module
```

C.6 Module Crank-Nicolson propagation (CN.f90)

```
module CN
    implicit none
    complex*16, allocatable, private :: psiout(:)     ! local wavefunction for propagation
    complex*16, allocatable, private :: gamma(:)      ! used for CN-propagation algorithm
    complex*16, allocatable, private :: diagarr(:)    ! diagonal elements used for CN-propagation
    contains
    subroutine CNInit()
        use progvars
        use debug
        implicit none;
        ! allocate 1D local wavefunctions
        allocate(psiout(nz),stat=iAllocStatus)
        if (iAllocStatus /= 0) then
            print *,"ERROR: can't allocate 1D local wavefunction array"
            stop
        end if
        call debugmsg (10,1,"PROPAGATOR_INIT: 1D local wavefunction array allocated")
        ! allocate temporary CN-propagator array
        allocate(gamma(nz),stat=iAllocStatus)
        if (iAllocStatus /= 0) then
            print *,"ERROR: can't allocate temporary propagator array GAMMA"
            stop
        end if
        call debugmsg (10,1,"PROPAGATOR_INIT: temporary propagator array GAMMA allocated")
        ! allocate CN diagonal elements array
        allocate(diagarr(nz),stat=iAllocStatus)
```

```
        if (iAllocStatus /= 0) then
            print *,"ERROR: can't allocate DIAGARR array"
            stop
        end if
        call debugmsg (10,1,"PROPAGATOR_INIT: DIAGARR allocated")
        call debugmsg(5,1,"PROPAGATOR_INIT: propagation arrays allocated")
    end subroutine
!-------------------------------------------------------------------------------------------
    subroutine CNCleanup()
        use debug
        integer             :: iDeallocStatus     ! return value
        ! deallocate 1D sub-wavefunctions
        deallocate(psiout,stat=iDeallocStatus)
        if (iDeallocStatus /= 0) then
            print *,"ERROR: can't deallocate 1D local wavefunction array"
            stop
        end if
        call debugmsg (10,1,"PROPAGATOR_DONE: 1D local wavefunction array destroyed")
        deallocate(gamma,stat=iDeallocStatus)
        if (iDeallocStatus /= 0) then
            print *,"ERROR: can't deallocate temporary propagator array GAMMA"
            stop
        end if
        call debugmsg (10,1,"PROPAGATOR_DONE: temporary propagator array GAMMA destroyed")
        deallocate(diagarr,stat=iDeallocStatus)
        if (iDeallocStatus /= 0) then
            print *,"ERROR: can't deallocate DIAGARR"
            stop
        end if
        call debugmsg (10,1,"PROPAGATOR_DONE: DIAGARR destroyed")
        call debugmsg(5,1,"PROPAGATOR_DONE: propagation arrays destroyed")
    end subroutine CNCleanup
!-------------------------------------------------------------------------------------------
    subroutine CNPropagate(wfunc, timestep, efield, useabsorber)
        use progvars
        implicit none
        ! uses Crank-Nicholson propagation scheme to propagate wavefunction for small timestep
        complex*16, intent(inout), dimension(:)    :: wfunc
        complex*16, intent(in)  :: timestep      ! complex for imaginary time propagation
        real*8, intent(in)      :: efield
        logical, intent(in)     :: useabsorber
        complex*16, parameter   :: iu = (0.d0,1.d0)            ! imaginary unit
        !the diagonal elements without potential term
        complex*16              :: diagz
        !the constant off-diagonal elements
        complex*16              :: subdiagz
        ! 1.) Calculate constant tridiagonal elements of propagation matrix (Hamiltonean)
        diagz = 0.5 + iu * timestep / (mass * 4.0 * deltaz**2)
        ! Note: potential is added in propagation loop
        subdiagz = -iu * timestep / (mass * 8.0 * deltaz**2)
        ! 2.) Propagate a full potential and kinetic energy step at once
        diagarr = potential * iu * timestep / 4.d0  + diagz
        ! the diagonal elements including potential
        call tridiag(wfunc,psiout,diagarr,subdiagz)     ! propagate in z-direction
        !! 2.) Propagate half a potential step
        ! wfunc = wfunc * (1.d0 - iu * potential * timestep / 4.d0) /
        ! (1.d0 + iu * potential * timestep / 4.d0)
        !! 3.) Propagate a full timestep T_z in z direction
        ! call tridiag(wfunc,psiout,diagz,subdiagz)              ! propagate in z-direction
        !! write back the result into the wavefunction
        ! wfunc = psiout
        !! 4.) Propagate another half a potential step
        ! wfunc = wfunc * (1.d0 - iu * potential * timestep / 4.d0) /
        ! (1.d0 + iu * potential * timestep / 4.d0)
        ! 5.) Apply the absorber to reduce grid boundary reflections (if absorber array is given)
        if (useabsorber) then
            wfunc = psiout*absorber
        else
            wfunc = psiout
        end if
    end subroutine
```

```
    !-------------------------------------------------------------------------------------------------
100 subroutine tridiag(psiin,psiout,diag,subdiag)
        ! modified NUMERICAL RECIPES TRIDAG routine for constant diagonal
        ! and super/subdiagonal elements
        ! Ref.: Num. Recipes, p.24, sec. 2.4, U. Thumm ITAMP, 6/15/99
        complex*16, intent(in)  :: psiin(:), diag(:)
105     complex*16, intent(out) :: psiout(:)
        complex*16, intent(in)  :: subdiag
        complex*16              :: beta
        integer                 :: j
        beta      = diag(1)
110     psiout(1) = psiin(1) / beta
        do j=2, size(psiin)
            gamma(j) = subdiag / beta
            beta     = diag(j) - subdiag * gamma(j)
            if (beta.eq.0) then
115            pause "ERROR: CNTRIDAG_CONST failed (beta=0)"
               stop
            endif
            psiout(j) = (psiin(j) - subdiag * psiout(j-1)) / beta
        enddo
120     do j=size(psiin)-1,1,-1
            psiout(j) = psiout(j) - gamma(j+1) * psiout(j+1)  ! this loop cries for optimization
        enddo
        psiout = psiout – psiin                                ! subtract initial vector
    end subroutine tridiag
125 end module
```

C.7 Module FFT propagation (FT.f90)

```
    module FT
        implicit none
        complex*16, pointer     ::  K(:)              ! Kinetic Energy part of Hamiltonian
130     contains
        subroutine FTInit()
            use progvars
            use fft
            implicit none
135         integer zloop
            real*8 pn
            allocate(K(nz), stat = iAllocStatus)
            if (iAllocStatus /= 0) then
                print *,"ERROR: can't allocate  vector K"
140             stop
            endif
            !calculate KE part of hamiltonian
            do zloop = 1, nz
                pn      = 2 * pi * (zloop-nz/2-1)/(maxz-minz)
145             K(zloop)= cdexp((-ii * deltat/(4 * mass))*(pn**2))
            enddo
            call fftInit(nz,deltaz,mass)
        end subroutine
    !-------------------------------------------------------------------------------------------------
150     subroutine FTPropagate(timestep, efield, useefield, useabsorber)
            use progvars
            use fft
            use wfMath
            implicit none
155         complex*16, intent(in)  :: timestep
            real*8, intent(in)      :: efield
            logical, intent(in)     :: useefield
            logical, intent(in)     :: useabsorber
            complex*16 K2(nz)
160         integer :: zloop, usee = 0
            if(useefield)  usee = 1
            call FTShift(nz,K,K2)
            call fftForward(psi)
            psi = fftvalues* K2
165         call fftInverse(psi)
            psi = fftvalues
```

```
            psi = psi * cdexp(-ii* timestep*(potential-usee*Z*efield) )
            call fftForward(psi)
            psi = fftvalues* K2
            call fftInverse(psi)
            psi = fftvalues
            if(useabsorber .eq. .true.) then
                psi = psi * absorber
            end if
            call wfmath_normalize(psi)
        end subroutine
    !-------------------------------------------------------------------------------------------
    subroutine FTShift(n,wf, wft)
            implicit none
            integer , intent (in)                    :: n
            complex*16, intent(in), dimension(:)     :: wf       ! the input array to shift
            complex*16, intent(in out), dimension(:) :: wft      ! the target array
            complex*16 wftemp(n)
            integer i
            do i = 1, n/2.
                wftemp(i)= wf(i+n/2)
                wftemp(i+n/2)= wf(i)
            enddo
            wft  = wftemp
        end subroutine
    !-------------------------------------------------------------------------------------------
     subroutine FTCleanup()
            use progvars
            use fft
            implicit none
            call fftCleanup()
        end subroutine
    end module
```

C.8 Module ADK ionization (adk.f90)

```
    module adk
      implicit none
      contains
      subroutine adk_deplete(psiin, potlo, pothi, ioncharge, pulseint, pulselength,
                             pulseomega, pulsephase)
    ! ADK routine for improved Franck-Condon transition but based on atomic ADK rates for molecules,
    ! taken from eq. (5) of J. P. Brichta et al., J. Phys. B 39, 3769 (2006). The initial wave packet
    ! WAVEFUNCTION is originally moving in the lower potential POTLO and exposed to the given
    ! ionizing pulse. Static ADK rates for variing field is used rather than cycle averaged in order
    ! to account for really short pulses and the rapid change in envelope. The given wave funtion
    ! DOES  NOT propagate during the pulse, thus the routine still assumes instantaneous ADK
    ! depletion  and is therefore limited to very short pulses. Output is given in WAVEFUNCTION as
    ! the remaining part of the original wave function and the ionized wave function movin in the
    ! upper potential POTHI can be estimated as (original wave function) - (final wave function).
        use wfmath
        complex*16, dimension(:), intent(inout) :: psiin(:)
        ! the initial wave function for ionization, also return value
        real*8, dimension(:), intent(in)        :: potlo, pothi
        ! both potential curves considered for the ADK transition
        real*8, intent(in)                      :: ioncharge
        ! the total charge of the ION (after the ADK transition)
        real*8, intent(in)                      :: pulseint, pulselength, pulseomega, pulsephase
        ! the laser parameters
        real*8, parameter                       :: pi = 3.14159265358979323846264 3d0
        ! lets start off with something round...
        integer, parameter                      :: ncyclesteps = 128
        ! number of sampling points per laser cycle
        real*8, parameter                       :: sigmawidth = 2.d0
        ! multiplier for the pulselength for total transition time
        real*8                                  :: timestep
        ! the delta t for the ADK calculation
        real*8                                  :: currenttime         ! current time of the pulse
        integer                                 :: nt, ntimesteps      ! for the time step loop
        real*8                                  :: fieldenv
        ! the envelope of the electric field of the laser pulse
```

```
      real*8                                  :: fieldphase
      ! the laser pulse carrier envelope phase
      real*8                                  :: efield
      ! thats the electric field strengh of the laser we need
      real*8                                  :: fieldabs
      ! but only the magnitude of the field matters for ADK
      integer                                 :: iAllocStatus        ! error check
      real*8, dimension(:), allocatable       :: kappa, adkconst
      ! for precomputing ADK constants
      real*8                                  :: e
      ! integrate it and you still have the same function...
      integer                                 :: nR, nRstep
      ! for loop through the R values
      real*8                                  :: rate
      nRstep = size(psiin)        ! size of the wave function array in R
      ! allocate some memory for precomputing some static values
      allocate(kappa(nRstep), adkconst(nRstep), stat=iAllocStatus)
      if (iAllocStatus /= 0) then
        print *,"ERROR: can't allocate temporary ADK work arrays"
        stop
      endif
      ! now procompute the static part of the ADK rates
      e        = dexp(1.d0)                                  ! the Euler constant
      kappa    = dsqrt(2.d0 * (pothi - potlo))/ioncharge
      ! sqrt(2*I_p)/Z with I_p the ionization potential
      adkconst = (3.d0*e/pi)**1.5d0 &
                 *(kappa**4.5d0)/(ioncharge**2.5d0) &
                 *(4.d0*e*(kappa**4)/ioncharge)**(2.d0*ioncharge/kappa-1.5d0)
      timestep   = 2.d0*pi / (pulseomega * ncyclesteps)
      ! calculate an appropriate timestep for each ADK transition
      ntimesteps = nint(sigmawidth*pulselength/timestep)
      ! how many time steps do we have in total?
      do nt=0, ntimesteps-1     ! The ADK time loop
        currenttime = -sigmawidth*pulselength/2.d0 + timestep*nt     ! get ma a clock reading
        ! Calculate the electric field strengh of the laser at the current time
        fieldenv    = dsqrt(pulseint) * dexp(- 2.d0 * dlog(2.d0) * (currenttime**2) /
                         (pulselength**2) )
        fieldphase  = dmod(pulseomega*currenttime+pulsephase,2*pi)
        ! the current laser phase with respect to the maximum of the pulse
        efield      = fieldenv * dcos(fieldphase)
        fieldabs    = dabs(efield)
        ! ADK only depends on the magnitude of the electric field
        if (fieldabs < 1.d-4) cycle
           ! next timestep, if field strength is not large enough
           ! now comes the ADK part - loop through all R value and see how much wave function
           ! we will loose
           !$OMP PARALLEL DO SCHEDULE(STATIC,1) PRIVATE(nR, rate)
           do nR=1, nRstep
              rate = adkconst(nR) * (fieldabs**(1.5d0 - 2.d0*ioncharge/kappa(nR))) &
                 *dexp(-2.d0*kappa(nR)**3/(3.d0*fieldabs))
              ! the current ADK rate at given internuclear distance
              psiin(nR) = psiin(nR)*(1.d0 - dsqrt(dabs(rate*timestep)))
              ! and the depleted ground state wave function
           enddo
           !$OMP END PARALLEL DO
      enddo ! (* time loop *)
      ! and finally remove the precomputed arrays again
      deallocate(kappa, adkconst, stat=iAllocStatus)
      if (iAllocStatus /= 0) then
        print *,"ERROR: can't deallocate temporary ADK work arrays"
        stop
      endif
    end subroutine adk_deplete
  end module adk
```

C.9 Module Fast Fourier transforms (fft.f90)

```
  module fft
    implicit none
    integer, private        :: nzstep         ! the dimenstion of the 1D potentials/wavefunctions
```

```
  integer, private        :: nzstepp2       ! the next larger power of 2
  real*8, private         :: deltaz         ! the grid spacing
  real*8, private         :: mass           ! the mass of particles in a.u.
  real*8, private         :: pmax           ! maximum momentum (from Nyquist theorem)
  real*8, private         :: deltap         ! the momentum resolution
  complex*16, allocatable, target :: fftvalues(:)  ! here goes the FFT stuff
  contains
!-----------------------------------------------------------------------------------------
! I N I T I A L I Z A T I O N
!-----------------------------------------------------------------------------------------
  subroutine fftInit(zdim,dz,particlemass)
    use debug

    integer, intent(in) :: zdim
    real*8, intent(in)  :: dz, particlemass
    integer             :: i, iAllocStatus
    nzstep = zdim
    deltaz = dz
    mass   = particlemass
    nzstepp2 = nzstep                          ! now find next larger power of 2
    if (iand(nzstepp2,nzstepp2-1) /= 0) then    ! dirty trick to check for powers of two.
      i = 1      ! initialize with 1, so we automatically get the NEXT larger power of 2
      do while (nzstepp2 /= 1)
        nzstepp2 = rshift(nzstepp2,1)! shift n to the right until the last bit has been found
        i = i + 1                    ! count how many bits we have to shift
      enddo
      nzstepp2 = 2**i
      ! the next larger power of two - just from counting the number of set bits in zdim
    end if
    ! pmax   = 1.d0/(2.d0*deltaz)    ! maximum momentum of the grid (see Nyquist theorem)
    ! deltap = 2.d0*pmax / nzstepp2  ! the momentum resolution
    ! allocate the FFT array
    allocate(fftvalues(nzstepp2),stat=iAllocStatus)
    if (iAllocStatus /= 0) then
      print *,"ERROR: can't allocate FFT array"
      stop
    endif
    call debugmsg(5,1,"FFT_INIT: FFT array allocated")
    print*,' '
    print*,' FFT_INIT:   input dimension=',zdim,' used dimension=nstepp2=',nzstepp2
    print*,' FFT_INIT:   fftvalues(nzstepp2) allocated'
    print*,' FFT_INIT:   dz=',dz,' particlemass=',sngl(particlemass)   !sngl(dz)
    print*,' '
  end subroutine fftInit
!-----------------------------------------------------------------------------------------
  subroutine fftCleanup
    use debug
    integer :: iDeallocStatus
    ! deallocate the FFT array
    deallocate(fftvalues,stat=iDeallocStatus)
    if (iDeallocStatus /= 0) then
      print *,"ERROR: can't deallocate FFT array"
      stop
    endif
    call debugmsg(5,1,"FFT_DONE: FFT array destroyed")
  end subroutine
!-----------------------------------------------------------------------------------------
  subroutine fftForward(fftinput)
    ! calculates the discrete Fourier transformation of the given function data points
    ! ~ Exp(-2 pi i k n / N)
    ! Source: Numerical Recipes, Chap. 12.2
    complex*16, dimension(:), intent(in) :: fftinput       ! the function values for the FFT
    integer                              :: i, istep, j, m, mmax, n2
    real*8                               :: theta
    complex*16                           :: w, wp, ws
    real*8, parameter                    :: pi = 3.14159265358979323846264338d0
    complex*16                           :: dummy
    ! copy the input data to the FFT array and fill the blanks
    fftvalues(1:nzstep) = fftinput                                  ! copy the input data
    if (nzstep /= nzstepp2) fftvalues(nzstep:nzstepp2) = 0.d0    ! fill the rest with 0
    ! The bit-reversal routine, to rearrange the array
```

```
      n2 = nzstepp2/2
      j  = n2
      do i=1, nzstepp2-2
        if (j > i) then ! swap the values
 80       dummy          = fftvalues(j+1)
          fftvalues(j+1) = fftvalues(i+1)
          fftvalues(i+1) = dummy
        endif
        m = n2
 85     do
          if (m<2 .or. j<m) exit
          j = j-m
          m = m/2
        enddo
 90     j = j+m
      enddo
      ! Danielson-Lanczos algorithm
      mmax = 1
      do                      ! outer loop - executed log_2 N times
 95     if ( nzstepp2 <= mmax ) exit
        istep = 2*mmax
        theta = pi / mmax   ! initialize for trigonometric recurrence
        wp    = cmplx(-2.0d0*sin(0.5d0*theta)**2,sin(theta))
        w     = cmplx(1.0d0,0.0d0)
100     do m=1,mmax           ! here are the two nested inner loops
          ws = w
          do i=m,nzstepp2,istep
            j            = i + mmax
            dummy        = ws*fftvalues(j)    ! this is the Danielson-Lanczos formula
105         fftvalues(j) = fftvalues(i)-dummy
            fftvalues(i) = fftvalues(i)+dummy
          enddo
          w = w*wp+w          ! trigonometric recurrence
        enddo
110     mmax = istep
      enddo
      ! Normalization
      fftvalues = fftvalues / sqrt(dble(nzstepp2))
    end subroutine
115 !-----------------------------------------------------------------------------------------------
    subroutine fftInverse(fftinput)
      ! calculates the inverse discrete Fourier transformation of the given function data points
      ! ~ Exp(2 pi i k n / N)
      ! This is ABSOLUTELY the same routine as FFT_FORWARD,
120   ! except THETA in the D.L. algortihm has a minus.
      complex*16, dimension(:), intent(in) :: fftinput       ! function values for the FFT
      integer                              :: i, istep, j, m, mmax, n2
      real*8                               :: theta
      complex*16                           :: w, wp, ws
125   real*8, parameter                    :: pi = 3.14159265358979323846264 3d0
      complex*16                           :: dummy
      ! copy the input data to the FFT array and fill the blanks
      fftvalues(1:nzstep) = fftinput                                ! copy the input data
      if (nzstep /= nzstepp2) fftvalues(nzstep:nzstepp2) = 0.d0    ! fill the rest with 0
130   ! The bit-reversal routine, to rearrange the array
      n2 = nzstepp2/2
      j  = n2
      do i=1, nzstepp2-2
        if (j > i) then ! swap the values
135       dummy          = fftvalues(j+1)
          fftvalues(j+1) = fftvalues(i+1)
          fftvalues(i+1) = dummy
        endif
        m = n2
140     do
          if (m<2 .or. j<m) exit
          j = j-m
          m = m/2
        enddo
145     j = j+m
      enddo
```

```
      ! Danielson-Lanczos algorithm
        mmax = 1
        do                      ! outer loop - executed log_2 N times
150       if ( nzstepp2 <= mmax ) exit
          istep = 2*mmax
          ! initialize for trigonometric recurrence - minus sign for inverse transformation
          theta = - pi / mmax
          wp    = cmplx(-2.0d0*sin(0.5d0*theta)**2,sin(theta))
155       w     = cmplx(1.0d0,0.0d0)
          do m=1,mmax           ! here are the two nested inner loops
            ws = w
            do i=m,nzstepp2,istep
              j            = i + mmax
160           dummy        = ws*fftvalues(j)    ! this is the Danielson-Lanczos formula
              fftvalues(j) = fftvalues(i)-dummy
              fftvalues(i) = fftvalues(i)+dummy
            enddo
            w = w*wp+w          ! trigonometric recurrence
165       enddo
          mmax = istep
        enddo
        ! Normalization
        fftvalues = fftvalues / sqrt(dble(nzstepp2))
170   end subroutine
     !-------------------------------------------------------------------------------------------------
      subroutine fft_power(fftinput)
        !calculates the power spectrum of the given wave function and stores the magnitude square in
        !the REAL part of FFTVALUES while the phase information (between -Pi and Pi) is stored in the
175     !IMAGINARY part.
        complex*16, dimension(:), intent(in) :: fftinput       ! function values for the FFT
        integer                              :: np
        real*8                               :: magnitude, phase
        complex*16                           :: value
180     call fftForward(fftinput)                              ! first get the DFT of the data
        do np=1, nzstepp2
          value     = fftvalues(np)
          magnitude = value**2
          if (value==0.d0) then
185         phase = dcmplx(0.d0,0.d0)
          else
            phase = datan2(dimag(value),dreal(value))
          endif
          fftvalues(np) = dcmplx(magnitude,phase)
190     enddo
      end subroutine fft_power
     !-------------------------------------------------------------------------------------------------
        subroutine fft_plot(fftinput,filename)
        use debug
195     complex*16, dimension(:), intent(in) :: fftinput       ! function values for the FFT
        character(len=*), intent(in)         :: filename
        integer                              :: np
        real*8                               :: momentum, phase
        complex*16                           :: value
200     call fftInverse(fftinput)
        open(unit=800,file=filename,status="replace",access="sequential")
        write(800,'(5A12)') "Momentum","Psi_Real","Psi_Imag","Psi_Abs","Psi_Phase"
        do np=1,nzstepp2
          value    = fftvalues(np)
205       momentum = -pmax + (np-1)*deltap
          if (value==0.d0) then
            phase = dcmplx(0.d0,0.d0)
          else
            phase = datan2(dimag(value),dreal(value))
210       endif
          write(800,'(5E12.4)') momentum, value, abs(value), phase
        enddo
        close(800)
        call debugmsg(5,2,"FFT_PLOT: momentum spectrum plotted to file")
215   end subroutine fft_plot
     end module fft
```

C.10 Module Diagonalization (diag.f90)

```
   module diag
     use progvars;
     implicit none
 5   integer, private       :: nzstep1   ! the dimenstion of the 1D potentials/wavefunctions
     real*8, private        :: deltaz1   ! the grid spacing
     real*8, private        :: mass1     ! the mass1 of particles in a.u.
     interface diag_release              ! release the objects TEnergies or TStates if allocated
     module procedure diag_release_TEnergies, diag_release_TStates
10 ! define different procedures for the types
     end interface
     interface diag_diagonalize     ! the working horse. diagonalize the potential array.
     module procedure diag_diagonalize_TEnergies, diag_diagonalize_TStates
   ! define different procedures for the types
15   end interface
     interface diag_plot                                        ! Plot the results to file
     module procedure diag_plot_TEnergies, diag_plot_TStates ! define diff. proceds for the types
     end interface
     contains
20   subroutine diag_init(zdim,dz,particlemass1)
       use debug
       integer, intent(in) :: zdim
       real*8, intent(in)  :: dz, particlemass1
       nzstep1 = zdim
25     deltaz1 = dz
       mass1   = particlemass1
       call debugmsg(5,1,"DIAG_INIT: diagonalization routine initialized.")
     end subroutine diag_init
   !-------------------------------------------------------------------------------------------------
30   subroutine diag_done
       use debug
       call debugmsg(5,1,"DIAG_DONE: diagonalization routine closed.")
     end subroutine diag_done
   !-------------------------------------------------------------------------------------------------
35   subroutine diag_release_TEnergies(energies)
       use debug
       type(TEnergies), intent(inout) :: energies           ! we want to release this object
       integer                        :: iDeallocStatus     ! return value
       energies%numbound = 0                                ! we have zero bound states from now on
40     if (associated(energies%energyarr)) then
         deallocate(energies%energyarr,stat=iDeallocStatus)
         if (iDeAllocStatus /= 0) then
           print *,"ERROR: can't deallocate DIAGONALIZATION ENERGY array"
           stop
45       endif
         call debugmsg(10,1,"DIAG_RELEASE: DIAGONALIZATION ENERGY array destroyed")
       endif
       call debugmsg(5,1,"DIAG_RELEASE: object destroyed")
     end subroutine diag_release_TEnergies
50 !-------------------------------------------------------------------------------------------------
     subroutine diag_release_TStates(states)
       use debug
       type(TStates), intent(inout) :: states             ! we want to release this object
       integer                      :: iDeallocStatus     ! return value
55     states%numbound = 0                                ! we have zero bound states from now on
       if (associated(states%energyarr)) then
         deallocate(states%energyarr,stat=iDeallocStatus)
         if (iDeAllocStatus /= 0) then
           print *,"ERROR: can't deallocate DIAGONALIZATION ENERGY array"
60         stop
         endif
         call debugmsg(10,1,"DIAG_RELEASE: DIAGONALIZATION ENERGY array destroyed")
       endif
       if (associated(states%wavefunctions)) then
65       deallocate(states%wavefunctions,stat=iDeallocStatus)
         if (iDeAllocStatus /= 0) then
           print *,"ERROR: can't deallocate DIAGONALIZATION WAVE FUNCTION array"
           stop
```

```
      endif
      call debugmsg(10,1,"DIAG_RELEASE: DIAGONALIZATION WAVE FUNCTION array destroyed")
    endif
    call debugmsg(5,1,"DIAG_RELEASE: object destroyed")
  end subroutine diag_release_TStates
!-----------------------------------------------------------------------------------------------
  subroutine diag_diagonalize_TEnergies(potential, energies)
    ! this routine diagonaalizes the 1d hamiltonean given only by it's potential
    use debug
    real*8, pointer                :: potential(:)           ! the potential array
    type(TEnergies), intent(inout) :: energies               ! type for the returned energies
    integer                        :: iAllocStatus           ! return value
    real*8, allocatable            :: subsuper(:), diagarr(:)
    ! the diagonal, sub- and super-diagonals of the Hamiltonian
    real*8                         :: mine                   ! minimum bound energy
    if (associated(energies%energyarr)) then
      deallocate(energies%energyarr,stat=iAllocStatus)
      if (iAllocStatus /= 0) then
        print *,"ERROR: can't deallocate DIAGONALIZATION ENERGY array"
        stop
      endif
      call debugmsg(10,1,"DIAG_DIAGONALIZE: DIAGONALIZATION ENERGY array destroyed")
    endif
    energies%numbound = 0                              ! first we start with 0 bound states
    allocate(subsuper(nzstep1),diagarr(nzstep1),stat=iAllocStatus)
    if (iAllocStatus /= 0) then
      print *,"ERROR: can't allocate tridiagonal Hamiltonian array"
      stop
    endif
    call debugmsg(10,1,"DIAG_DIAGONALIZE: tridiagonal Hamiltonian array allocated")
    diagarr  = potential + 1.d0/(mass1*deltaz1**2)      ! the diagonal array of the Hamiltonian
    subsuper = -1.d0/(2.d0 * mass1 * deltaz1**2)        ! the sub- and super-diagonals of H

    call debugmsg(5,1,"DIAG_DIAGONALIZE: diagonalizing potential - only energies...")
    call dtqli(diagarr,subsuper)                       ! call the routine from Numerical Recipes

    mine = min(potential(1),potential(nzstep1))        ! find the minimum bound state energy
    energies%numbound = count(diagarr < mine)          ! count the number of bound states
    allocate(energies%energyarr(energies%numbound),stat=iAllocStatus)
    if (iAllocStatus /= 0) then
      print *,"ERROR: can't allocate DIAGONALIZATION ENERGY array"
      stop
    endif
    call debugmsg(10,1,"DIAG_DIAGONALIZE: DIAGONALIZATION ENERGY array allocated")
    energies%energyarr = pack(diagarr, diagarr<mine)
    ! copy only the corresponding energies into the output
    deallocate(subsuper,diagarr,stat=iAllocStatus)
    if (iAllocStatus /= 0) then
      print *,"ERROR: can't deallocate tridiagonal Hamiltonian array"
      stop
    endif
    call debugmsg(10,1,"DIAG_DIAGONALIZE: tridiagonal Hamiltonian array released")
  end subroutine diag_diagonalize_TEnergies
!-----------------------------------------------------------------------------------------------
  subroutine diag_diagonalize_TStates(potential, states)
    ! this routine diagonaalizes the 1d hamiltonean given only by it's potential.
    ! This time WITH wave functions
    use debug
    use wfmath
    implicit none;
    real*8, pointer                :: potential(:)   ! the potential array
    type(TStates), intent(inout)   :: states         ! type for the returned wave functions
    integer                        :: iAllocStatus   ! return value
    ! the diagonal, sub- and super-diagonals of the Hamiltonian
    real*8, allocatable            :: subsuper(:), diagarr(:)
    real*8, allocatable            :: wavefunctions(:,:)  ! temporary wave function array
    real*8                         :: mine                ! minimum bound energy
    integer                        :: n
    if (associated(states%energyarr)) then
      deallocate(states%energyarr,stat=iAllocStatus)
      if (iAllocStatus /= 0) then
```

```
        print *,"ERROR: can't deallocate DIAGONALIZATION ENERGY array",iAllocStatus
        stop
      endif
      call debugmsg(10,1,"DIAG_DIAGONALIZE: DIAGONALIZATION ENERGY array destroyed")
    endif
    if (associated(states%wavefunctions)) then
      deallocate(states%wavefunctions,stat=iAllocStatus)
      if (iAllocStatus /= 0) then
        print *,"ERROR: can't deallocate DIAGONALIZATION WAVE FUNCTION array",iAllocStatus
        stop
      endif
      call debugmsg(10,1,"DIAG_DIAGONALIZE: DIAGONALIZATION WAVE FUNCTION array destroyed")
    endif
    states%numbound = 0                                  ! first we start with 0 bound states
    allocate(subsuper(nzstep1),diagarr(nzstep1),stat=iAllocStatus)
    if (iAllocStatus /= 0) then
      print *,"ERROR: can't allocate tridiagonal Hamiltonian array"
      stop
    endif
    call debugmsg(10,1,"DIAG_DIAGONALIZE: tridiagonal Hamiltonian array allocated")
    allocate(wavefunctions(nzstep1,nzstep1),stat=iAllocStatus)
    if (iAllocStatus /= 0) then
      print *,"ERROR: can't allocate temporary wave function array"
      stop
    endif
    call debugmsg(10,1,"DIAG_DIAGONALIZE: temporary wave function array allocated")
    diagarr  = potential + 1.d0/(mass1*deltaz1**2)    ! the diagonal array of the Hamiltonian
    subsuper = -1.d0/(2.d0 * mass1 * deltaz1**2)      ! the sub- and super-diagonals of H
    wavefunctions = 0.d0
    do n=1, nzstep1
      wavefunctions(n,n) = 1.d0                       ! fill with identity matrix
    enddo
    call debugmsg(5,1,"DIAG_DIAGONALIZE: diagonalizing potential - energies and wave
functions...")
    call dtqli(diagarr,subsuper,wavefunctions)        ! call the routine from Numerical Recipes
    mine = min(potential(1),potential(nzstep1))       ! find the minimum bound state energy
    states%numbound = count(diagarr < mine)           ! count the number of bound states
    allocate(states%energyarr(states%numbound),stat=iAllocStatus)
    if (iAllocStatus /= 0) then
      print *,"ERROR: can't allocate DIAGONALIZATION ENERGY array"
      stop
    endif
    call debugmsg(10,1,"DIAG_DIAGONALIZE: DIAGONALIZATION ENERGY array allocated")
    allocate(states%wavefunctions(states%numbound,nzstep1),stat=iAllocStatus)
    if (iAllocStatus /= 0) then
      print *,"ERROR: can't allocate DIAGONALIZATION WAVE FUNCTION array"
      stop
    endif
    call debugmsg(10,1,"DIAG_DIAGONALIZE: DIAGONALIZATION WAVE FUNCTION array allocated")
    ! copy only the corresponding energies into the output
    states%energyarr = pack(diagarr, diagarr<mine)
    do n=1, nzstep1
       ! and copy the wave functions
       states%wavefunctions(:,n) = pack(wavefunctions(n,:), diagarr<mine)
    enddo
    do n=1, states%numbound
       call wfmath_normalize(states%wavefunctions(n,:)) ! we like normalized wave functions
    enddo
    deallocate(subsuper,diagarr,wavefunctions,stat=iAllocStatus)
    if (iAllocStatus /= 0) then
      print *,"ERROR: can't deallocate diagonalization arrays"
      stop
    endif
    call debugmsg(10,1,"DIAG_DIAGONALIZE: diagonalization arrays released")
  end subroutine diag_diagonalize_TStates
!-------------------------------------------------------------------------------------------------
  subroutine diag_plot_TEnergies(energies,filename)
    use debug
    use strings
    type(TEnergies), intent(in)  :: energies       ! this is what we plot
    character(len=*), intent(in) :: filename
```

```
      integer                       :: n
    open(unit=900,file=trim(concat(filename,"_energies.dat")),status="replace",access="sequential")
      write(900,'(3A12)') "State","Energy_au","Energy_eV"
      do n=1,energies%numbound
215     write(900,'(I12,2E12.4)') n,energies%energyarr(n),energies%energyarr(n)*27.2114d0
      enddo
      close(900)
      call debugmsg(5,2,"DIAG_PLOT: energies plotted to file")
    end subroutine diag_plot_TEnergies
220 !-----------------------------------------------------------------------------------------------
    subroutine diag_plot_TStates(states,filename)
      use debug
      use strings
      type(TStates), intent(in)    :: states       ! this is what we plot
225   character(len=*), intent(in) :: filename
      integer                       :: n
    open(unit=901,file=trim(concat(filename,"_wavefunctions.dat")),status="replace",access="sequentia
    l")
      write(901,'(e12.4,$)') states%energyarr(:)*27.2114d0
230   do n=1,nzstep1
        write(901,'(e12.4,$)') cdabs(states%wavefunctions(:,n))**2
        write(901,*)
      enddo
      close(901)
235   call debugmsg(5,2,"DIAG_PLOT: wave functions plotted to file")
    end subroutine diag_plot_TStates
    !-----------------------------------------------------------------------------------------------
    function dpythag(a, b) result(c)
      ! using Phytagoras a^2 + b^2 = c^2 for a triangle, calculate c in a numerically stable way.
240   real*8, intent(in) :: a, b
      real*8             :: absa, absb
      real*8             :: c
      absa=dabs(a)
      absb=dabs(b)
245   if(absa.gt.absb)then
        c=absa*dsqrt(1.d0+(absb/absa)**2)
      else
        if(absb.eq.0.d0)then
          c=0.d0
250     else
          c=absb*dsqrt(1.d0+(absa/absb)**2)
        endif
      endif
      return
255 end function dpythag
    !-----------------------------------------------------------------------------------------------
    subroutine dtqli(d,e,z)
      ! solver routine from Numerical Recipes for a tridiagonal linear equation
      ! the diagonal and sub- super-diagonals
260   real*8, dimension(:), intent(inout)             :: d, e
      ! returns the wave functions. Must identity matrix at call
      real*8, dimension(:,:), intent(inout), optional :: z
      integer                                         :: n, np, i, iter, k, l , m
      real*8                                          :: b, c, dd, f, g, p, r, s
265   np = size(d)
      n = np
      if (present(z)) then
        write (*,*) 'DTQLI: diagonalization with eigenvectors'
      else
270     write (*,*) 'DTQLI: diagonalization, only eigenvalues'
      endif
      write (*,*) '       matrix is',np,'x',np
      do i=2,n
        e(i-1)=e(i)
275   enddo
      e(n)=0.d0
      do 15 l=1,n
        iter=0
    1   do m=l,n-1
280       dd=dabs(d(m))+dabs(d(m+1))
          if (dabs(e(m))+dd.eq.dd) goto 2
```

```
          enddo
          m=n
      2   if (m.ne.l) then
 285        if (iter.eq.30) pause 'too many iterations in tqli'
            iter=iter+1
            g=(d(l+1)-d(l))/(2.d0*e(l))
            r=dpythag(g,1.d0)
            g=d(m)-d(l)+e(l)/(g+sign(r,g))
 290        s=1.d0
            c=1.d0
            p=0.d0
            do 14 i=m-1,l,-1
              f=s*e(i)
 295          b=c*e(i)
              r=dpythag(f,g)
              e(i+1)=r
              if(r.eq.0.d0)then
                d(i+1)=d(i+1)-p
 300            e(m)=0.d0
                goto 1
              endif
              s=f/r
              c=g/r
 305          g=d(i+1)-p
              r=(d(i)-g)*s+2.d0*c*b
              p=s*r
              d(i+1)=g+p
              g=c*r-b
 310          ! omit lines from here ...
              if (present(z)) then
                do k=1,n
                  f=z(k,i+1)
                  z(k,i+1)=s*z(k,i)+c*f
 315              z(k,i)=c*z(k,i)-s*f
                enddo
              endif
              ! to here when finding only eigenvalues.
     14     continue
 320        d(l)=d(l)-p
            e(l)=g
            e(m)=0.d0
            goto 1
          endif
 325  15  continue
          return
        end subroutine dtqli
      end module diag
```

C.11 Module Debug (debug.f90)

```
      module debug
        implicit none
        integer, private   :: global_debug_level, global_debug_mask
  5     integer, private   :: debugoutput = 0
        contains
        subroutine setdebug(level,mask)
          integer, intent(in)   :: level, mask
          global_debug_level = level
 10       global_debug_mask = mask
        end subroutine setdebug
      !--------------------------------------------------------------------------------
        subroutine debugmsg(level, mask, msg)
          integer             :: level, mask
 15       character (len = *) :: msg
          if
      (((level.le.global_debug_level).or.(iand(mask,global_debug_mask).eq.mask)).and.(debugoutput.eq.0)
      ) then
            print *, msg
 20       endif
        end subroutine debugmsg
```

```
!-------------------------------------------------------------------------------
  subroutine debug_off
    debugoutput = debugoutput + 1
  end subroutine debug_off
!-------------------------------------------------------------------------------
  subroutine debug_on
    if ( debugoutput > 0 ) debugoutput = debugoutput - 1
  end subroutine debug_on
!-------------------------------------------------------------------------------
end module debug
```

C.12 Module Files (filesWin.f90)

```
module files
  implicit none
  contains
    subroutine EnsureFolderExists(folder)
        character(len=*), intent(in)  :: folder
        character(len=120) :: foldername
        logical :: dir_e
        folderName = folder // '.';
        ! a trick to be sure docs is a dir
        inquire( file= trim(folderName), exist=dir_e )
        if ( dir_e ) then
            write(*,*), "dir exists!"
        else
            ! workaround: it calls an extern program...
            call system('mkdir ' // folder);
        end if
    end subroutine EnsureFolderExists
end module files
```

C.13 Module strings (strings.f90)

```
module strings
  implicit none
  contains
  function concat(s1, s2)
    character(len=*), intent(in)             :: s1, s2
    character(len=len_trim(s1)+len_trim(s2)) :: concat  ! function name
    concat = trim(s1) // trim(s2)
  end function concat
!-------------------------------------------------------------------------------------------
  function rmblank(s)
    character(len=*), intent(in) :: s
    character(len=len_trim(s))   :: rmblank             ! function name
    integer                      :: i,j
    j = 0
    rmblank = ''
    do i=1, len(s)
      if (s(i:i).ne.' ') then
        j = j + 1
        rmblank(j:j) = s(i:i)
      endif
    enddo
    rmblank = trim(rmblank)     ! final adjustment
    return
  end function rmblank
!-------------------------------------------------------------------------------------------
function uppercase(s)
    ! returns an uppercase version of a string.
    implicit none
    integer                      :: i,j,n
    character(len=*), intent(in) :: s
    character(len=len(s))        :: uppercase
    uppercase = s
    n = len_trim (uppercase)
```

```
    do i = 1, n
      j = ichar(uppercase(i:i))
      if (97 <= j .and. j <= 122) uppercase(i:i) = char(j - 32)
    end do
    return
  end function uppercase

!-----------------------------------------------------------------------------------------
  function system_checkvariable(var,value) result(exists)
    character(len=*), intent(in)  :: var
    character(len=*), intent(out) :: value
    logical                       :: exists
    character(len=128)            :: argument,variable
    integer                       :: iargc, iargcount, i
    integer                       :: splitpos
    iargcount = iargc()     ! return the number of argument values
    do i=1, iargcount
      call getarg(i,argument)
      splitpos = scan(argument,"=")
      if (splitpos.ne.0) then
        variable = uppercase(trim(argument(1:splitpos-1)))
        if (variable.eq.uppercase(trim(var))) then
          exists = .true.
          value = trim(argument(splitpos+1:len(argument)))
          return
        endif
      endif
    enddo
    exists=.false.
    value = ""
    return
  end function system_checkvariable
!-----------------------------------------------------------------------------------------
  function system_checkcommand(var) result(exists)
    character(len=*), intent(in)  :: var
    logical                       :: exists
    character(len=128)            :: argument,variable
    integer                       :: iargc, iargcount, i
    integer                       :: splitpos
    iargcount = iargc()     ! return the number of argument values
    do i=1, iargcount
      call getarg(i,argument)
      splitpos = scan(argument,"=")
      if (splitpos.eq.0) then
        variable = uppercase(trim(argument))
        if (variable.eq.uppercase(trim(var))) then
          exists = .true.
          return
        endif
      endif
    enddo
    exists=.false.
    return
  end function system_checkcommand
!-----------------------------------------------------------------------------------------
  function system_realvariable(var,default) result(value)
    use debug
    character(len=*), intent(in) :: var
    character(len=80)            :: argvalue
    real*8                       :: value, default
    value = default
    if (system_checkvariable(var,argvalue)) then
      read (argvalue,*) value
      write (argvalue,'(2A,A10,D10.4)') "SYSTEM: used variable ",trim(uppercase(var))," = ",value
      call debugmsg(5,8,trim(argvalue))
    endif
    return
  end function system_realvariable
```

Appendix D - Two-state code

This appendix describes the source code used in the calculations including dipole couplings. It is written in FORTRAN-90. The code has a main programm that uses several subroutines and functions that are divided into different files.

Module	Description
`TDSE.f90`	Main program
`tdsePumpProbe.F90`	Pump and Probe subroutines
`progvars.f90`	Defining program variables and default values.
`wfMath.f90`	Same as C3
`wfPot.f90`	Same as C4 but with two more potentials.
`params.f90`	Same as C5
`CN.f90`	Same as Appendix C6
`FT.f90`	Same as Appendix C7
`adk.f90`	ADK depletion and transition subroutines.
`fft.f90`	Same as C9
`diag.f90`	Same as Appendix C10
`debug.f90`	Same as Appendix C11
`fileswin.f90`	Same as Appendix C12
`strings.f90`	Same as Appendix C13

D.1 Main Program (tdse.f90)

```
program main
    use progvars;
    implicit none

    Tend           = 413.2     !time propagated after probe pulse
    boundStateCutOff=  200     !cut for bound part of WF.

    molecule    = "D2";
    inputFolder = "input/H2curves-0.05-100/";
    curve2  = "H2+pot_gerade.dat";
    curve3  = "H2+pot_ungerade.dat"
    curve4  = "H2+dpcouplings-0.05.dat";
    outputFolder= "Output\D2\CP_False-ADK_False\";


    call RunOnce();

    print *, 'program completed'
```

```
end program main

!-------------------------------------------------------------------------------
subroutine RunOnce()
    use progvars
    use files
    use tdsePumpProbe;
    use tdseMethods;
    use strings;
    use timer;
    use adk;
    implicit none

    call timer_start();

    call timer_printcurrenttime();

    call EnsureFolderExists(outputFolder);

    call init(); print *, 'init completed';

    call timer_printcurrenttime();

    call find_groundstate(psiground,.true.); print *, 'find_groundstate completed';
    call timer_printcurrenttime();

    call Apply_ADK(psiground);
    call printpsi(psiground,trim(concat(outputFolder,"psiground_ADK.dat")))
    call timer_printcurrenttime();

    !here  at this point psi contains ground state
    call calculate_energy(psiground); print *, 'calculate_energy completed';
    call timer_printcurrenttime();

    call adk_init();

    call Run();

    call adk_done();

    print *, 'run completed';

    call cleanup();

    print *, 'cleanup completed';

    call timer_stop();

    print *, 'timer stop completed';

    call timer_writeelapsedtimetofile(trim(concat(outputFolder,"timing.txt")));

    print *, 'completed completed';

end subroutine RunOnce

!_____________________________input parameters_____________________________
subroutine init
    use progvars
    use strings;
    use wfMath;
    use wfPot;
    use tdseMethods;
    implicit none

    integer :: nloop
    real*8  :: widthz,pz

    select case (trim(molecule))
        case("H2")
            mass = 917.66d0; nz = 2048;  deltaz  = 0.05d0;
```

```
        case("D2")
            mass = 1835.241507d0; nz = 1024;  deltaz  = 0.05d0;
        case("N2")
            mass = 12846.69099d0; nz = 512;  deltaz  = 0.01d0;
        case("O2")
            mass = 14681.93206d0; nz =8192 ;  deltaz  = 0.005d0;
        case("Ar2")
            mass = 36447.94123d0; nz = 65536;  deltaz  = 0.002d0;
    end select

    maxt    = 33072.80d0 !800fs                ! maximum time
    deltat  = 1.0d0                            ! delta time
    widthz  = 1.0d0                            ! width of the gaussian
    minz    = 0.05d0                           ! minimum z in a.u.
    maxz    = nz * deltaz                      ! maximum z in a.u.
    centerz = 2.1d0                            ! center of the gaussian
    nt      = NINT(maxt/deltat)                ! time steps
    pz      = 0.d0                             ! not used currently

  !_____________________________FFT Section_____________________________________
    deltafft    =  20.d0* deltat  !1.0d0*deltat ! time step for FFT
    nfft        =   NINT(maxt/deltafft)        ! no of steps for FFT

    !____________________________absorber parameters_____________________________
    fadewidth    = 10.d0                 ! the width of the absorber in a.u.
    fadestrength = 0.01d0                ! the maximum heigth of the negative imaginary potential

    !____________________________E FIELD section_________________________________
    Ewidth  = 1446.2d0        !35fs             ! width of the envelope
    Eo      = 0.053           !E14              ! field amplitude
    Eomega  = 0.057d0         !800nm            ! laser frequency
!   Eomega  = 0.033d0         !1400nm           ! laser frequency
    Ephi    = 0.d0                              ! carrier envelope phase
    Eto     = 1000.d0                           ! ecenter of the Gaussian envelope
    EoPed          = 0.0755 !2E14
    EwidthPed      = 826.638 !20fs
    EomegaPed      = Eomega
    EphiPed        = 0.d0
    EtoPed         = 1000.d0
    EoPump         = 0.053 !1E14  0.00285d0
    EwidthPump     = Ewidth
    EomegaPump     = 0.057d0
    EphiPump       = 0.0d0
    EtoPump        = 0.d0
    includeAbsorber     = .true.                    ! switch for absorber
    includeField        = .true.   ! .false.        ! switch for efield
    includePedestal     = .false.                   ! switch for pedestal

    includeConstantPump = .true.   ! .false.        ! switch for efield
    useADK              = .false.                   ! ADK switch
    calculatePowerSpectra       = .true.
    calculateKERPowerSpectra    = .true. !.false.


    !_____________________________Printing & Plotting Filters_____________________
    printFilter = nz
    maxFrequencyFilter = 500
    printInterval =100 !200
    ! print filter upper boundary check
    if(printFilter > nz) then
        printFilter = nz
    end if
    call allocateArrays();

    do nloop = 1,nz
        Z(nloop) = minz+ (nloop)* deltaz;

        P(nloop) = 2*pi*(nloop-(nz/2)-1)/(maxz-minz);

        E(nloop) = 27.2*(P(nloop)**2)/(4.d0*mass);
```

```
    end do

    call wfmath_gaussian(psiground,widthz,pz)

    call setabsorber_right(fadewidth, fadestrength)
    call printpsi(psiground,trim(concat(outputFolder,"psi_gausssian.dat")))

    call potentials_init(nz)              !initialize potential arrays

    call read_potential();

end subroutine init
!-------------------------------------------------------------------------------
subroutine read_potential()
    use progvars;
    use strings;
    use wfPot;
    call potentials_readfromfile_activate(trim(concat(inputFolder,curve1)),1)
    call potentials_readfromfile_activate(trim(concat(inputFolder,curve2)),2);
    call potentials_readfromfile_activate(trim(concat(inputFolder,curve3)),3)
    call potentials_readfromfile_activate(trim(concat(inputFolder,curve4)),4)
end subroutine read_potential

!_____________________________________Allocate_____________________________
subroutine allocateArrays
    use progvars
    implicit none
    integer i,j

    allocate(Z(nz), stat = iAllocStatus)
    if (iAllocStatus /= 0) then
        print *,"ERROR: can't allocate position vector Z"
        stop
    endif

    allocate(psiground(nz), psigerade(nz), psiungerade(nz), psitotal(nz), stat = iAllocStatus)
    if (iAllocStatus /= 0) then
        print *,"ERROR: can't allocate wave function psi, psitotal, psigerade, psiungerade"
        stop
    endif

    allocate(K(nz), P(nz), E(nz), stat = iAllocStatus)
    if (iAllocStatus /= 0) then
        print *,"ERROR: can't allocate K, P, E"
        stop
    endif

    allocate(absorber(nz), stat = iAllocStatus)
    if (iAllocStatus /= 0) then
        print *,"ERROR: can't allocate Vector absorber"
        stop
    endif

    if(calculatePowerSpectra .eq. .true.) then
        allocate(fftarray(nz,nfft), stat = iAllocStatus)
        if (iAllocStatus /= 0) then
            print *,"ERROR: can't allocate Array FFT"
            stop
        endif
        fftarray    = czero;
    endif

    if(calculateKERPowerSpectra .eq. .true.) then
        allocate(KERfftarray(nz/2,nfft), stat = iAllocStatus)
        if (iAllocStatus /= 0) then
            print *,"ERROR: can't allocate Array KER_FFT"
            stop
        endif
        KERfftarray = czero;
    endif
```

```
    if(calculatePowerSpectra .eq. .true. .OR. calculateKERPowerSpectra .eq. .true.) then
        allocate(fftinput(nfft), stat = iAllocStatus)
        if (iAllocStatus /= 0) then
            print *,"ERROR: can't allocate Array FFT Input"
            stop
        end if
        fftinput = czero;
    end if

    psiground   = czero
    psigerade   = czero
    psiungerade = czero
    psitotal    = czero

    absorber    = 1.d0
    K           = 0.0d0;
    E           = 0.0d0;
    P           = 0.0d0;

end subroutine

!_____________________________clean_____________________________
subroutine cleanup
    use progvars
    use wfPot
    implicit none
    deallocate(Z);
    deallocate(psiground);
    deallocate(psitotal);
    deallocate(psigerade);
    deallocate(psiungerade);
    deallocate(absorber);
    deallocate(K);
    deallocate(P);
    deallocate(E);
    if(calculatePowerSpectra .eq. .true.) then
        deallocate(fftarray);
    end if
    if(calculateKERPowerSpectra .eq. .true.) then
        deallocate(KERfftarray);
    end if
    if(calculatePowerSpectra .eq. .true. .OR. calculateKERPowerSpectra .eq. .true.) then
        deallocate(fftinput);
    end if
    call potentials_done();
end subroutine
```

D.2 Run subroutine (tdsePumpProbe.F90)

```
module tdsePumpProbe
  implicit none
  contains
!--------------------------------------------------------------------------------
    subroutine Run()
        call RunLoopOpt();
    end subroutine Run
!--------------------------------------------------------------------------------
    subroutine RunLoopOpt()
        use progvars;
        use strings;
        use wfMath;
        use wfPot;
        use tdseMethods;
        use fourier;
        use Timer;
        implicit none
        integer     :: fftloop, file_kertotal_endtime=710;
        complex*16  :: psifreeg(nz),psifreeug(nz), dipole;
        real*8      :: probestarttime = 0.0d0, probeendtime=0.0d0, savetime =0.0d0;
```

```
        character(255)  :: filename = ' '
        call MethodInit();
        !init fft arrays for KER
        call fourierInit(nz,deltaz,mass);
        call potentials_setactive(2);
        psifreeg    = psiground;
        psifreeug   = 0.0d0;
        ! print the enery list for KER
        call PrintKEREnergy();
        !open files
        open(unit=104,file=trim(concat(outputFolder,"wf_position.dat")),status="replace",
             access="sequential",recl=1024)
        open(unit=105,file=trim(concat(outputFolder,"wfunc_midpulse.dat")),status="replace",
              access="sequential",recl=1024)
        open(unit=106,file=trim(concat(outputFolder,"wfunc_endtime.dat")),status="replace",
             access="sequential",recl=1024)
        open(unit=107,file=trim(concat(outputFolder,"KER.dat")),status="replace",
              access="sequential", recl=1024)
        open(unit=file_kertotal_endtime,file=trim(concat(outputFolder,
               "KER_fft_total_endtime.dat")),status="replace",access="sequential",recl=1024)

        call timer_printcurrenttime();

        do fftloop = 0 , nfft-1   ! external loop for fft loop

            print *,  fftloop , " of " , nfft
            call timer_printcurrenttime();
            Eto  = deltafft * fftloop;
            probestarttime =  Eto - (Ewidth*2.0d0)
            probeendtime = Eto + (Ewidth*2.0d0)

            if(probestarttime <0.0d0) then
                probestarttime = 0.0d0;
            end if

            psigerade   = psifreeg;
            psiungerade = psifreeug;

            !propagate field free from time zero(or savetime) to start pulse
            !starttime= 0.0d0; endtime = probestarttime;
            call PropagateInTimeEx(savetime, probestarttime,.true., .false.);

            savetime = probestarttime;
            psifreeg = psigerade;          ! save psigerade after free propogation to psifreeg
            psifreeug = psiungerade;       ! save psiungerade after free propogation to psifreeug

            !propagate start pulse to mid pulse - MID PULSE
            !starttime= probestarttime; endtime = Eto;
            call PropagateInTime(probestarttime, Eto, .true.);

            dipole = wfmath_pos(psitotal);
            write(104,'(E13.4E3 ,E13.4E3)') Eto, dreal(dipole);

            write(105,'(E12.4,$)') cdabs(psitotal**2)  !save the wave function at mid probe pulse
            write(105,*)

            if(calculatePowerSpectra .eq. .true.) then
                fftarray(:,fftloop+1) = cdabs(psitotal(:)**2)        !copy psitotal^2 to fftarray
            endif

            !propagate mid pulse to end pulse - END PULSE - no do
            !starttime= Eto; endtime = probeendtime;
            call PropagateInTime(Eto+deltat, probeendtime + Tend, .true.);


            write(106,'(E12.4,$)') cdabs(psitotal**2) ! save the wave function at mid probe pulse
            write(106,*)

            if(calculateKERPowerSpectra .eq. .true.) then
                call CalculateAndPrintKER(file_kertotal_endtime,psitotal,fftloop);
                !call CalculateAndPrintKERNoShift(file_kertotal_endtime,psitotal);
```

```
            endif

 95         end do

            call timer_printcurrenttime();

            close(104);
100         close(105);

            !close KER output file
            close(file_kertotal_endtime);

105         call MethodCleanup()

            call fourierCleanup();

            call PrintEnergyFile();
110
            if(calculatePowerSpectra .eq. .true.) then
                call PowerSpectraFFT();
            end if

115          if(calculateKERPowerSpectra .eq. .true.) then
                call KERPowerSpectraFFT();
            end if
        end subroutine RunLoopOpt

120

    !---------------------------------------------------------------------------
        subroutine PropagateInTime(starttime,endtime,usefield)
            real*8, intent(in) :: starttime         ! start time for propagation
            real*8, intent(in) :: endtime           ! end time for propagation
125         logical,intent(in) :: usefield          ! whether to use efield or not

            call PropagateInTimeEx(starttime,endtime,usefield, .true.);
        end subroutine PropagateInTime
     !---------------------------------------------------------------------------
130
        subroutine PropagateInTimeEx(starttime,endtime,usefield, useadktransition)
            use progvars;
            use wfMath;
            use wfPot;
135         use tdseMethods;
            use adk;
            implicit none;

            real*8, intent(in) :: starttime         ! start time for propagation
140         real*8, intent(in) :: endtime           ! end time for propagation
            logical,intent(in) :: usefield          ! whether to use efield or not

            logical,intent(in) :: useadktransition  ! whether to use useadktransition

145         integer tloop, timestep;
            real*8  etime, efield;
            complex*16 rdeltat;

            rdeltat = CMPLX(deltat,0.d0);
150         timestep= NINT((endtime-starttime) / deltat);

            if(timestep>0) then

                do tloop = 0, timestep                      !internal deltat loop
155
                    etime   =  starttime + (tloop*deltat);  !print *,  etime;

                    if(includeField .AND. usefield) then
                        efield  = wfmath_efield(etime)
160                 else
                        efield  = 0.0d0;
                    end if
```

```
                write(124,'(E12.4,E12.4)') etime, efield;

                if(useADK .eq. .true. .and. useadktransition .eq. .true. ) then
                    ! couple H2+ wave functions to the p+p curve
                    call adk_transition(deltat/2.d0, efield);
                end if

                ! do one coupling between H2+ gerade/ungerade curves for half timestep
                call coupleH2Plus(deltat/2.d0, efield)

                ! propagate in the ungerade potential
                call potentials_setactive(3);

                call propagate(psiungerade, rdeltat,0.0d0, includeAbsorber);

                ! propagate in the gerade potential
                call potentials_setactive(2);

                call propagate(psigerade,rdeltat,0.0d0,includeAbsorber);

                call coupleH2Plus(deltat/2.d0,efield);

                psitotal = psigerade + psiungerade;

             end do

         end if

    end subroutine PropagateInTimeEx

!-------------------------------------------------------------------------------
    subroutine CalculateAndPrintKER(file_kertotal_endtime,wfunc,fftloop)
        use progvars;
        use fourier;
        use tdseMethods;
        implicit none;
        integer , intent(in)                    :: file_kertotal_endtime,fftloop;
        complex*16, allocatable, intent(inout)  :: wfunc(:)

        integer :: zloop;
        real*8  :: Pabs,val;

        K = czero;
        fouriervalues = czero;

        if (boundStateCutOff>0) then
            wfunc(1:boundStateCutOff) = 0.0d0;    !250*0.02=5 a.u.
        endif

        call fourierForward(wfunc);
        call FTShift(nz,fouriervalues,K);
        do zloop= nz/2,1,-1
            Pabs = abs(P(zloop));
            if(Pabs .eq. 0.0d0) then
                Pabs = 1E-18;
            end if

            val = cdabs(K(zloop))**2 /Pabs;

            KERfftarray(zloop,fftloop+1) = val;

            write(file_kertotal_endtime,'(E13.4,$)') val ;
        end do
        write(file_kertotal_endtime,*);

    end subroutine CalculateAndPrintKER;
end module tdsePumpProbe
```

D.3 Module defining variables (progvars.f90)

```
module progvars
   ! use vdetect;
    implicit none

    type :: TEnergies                              ! declare a type array for bound state energies
        integer              :: numbound           ! number of bound states
        real*8, pointer      :: energyarr(:)       ! the array with the bound energies
    end type

    type :: TStates                                ! declare a type array for bound wave functions
        integer              :: numbound           ! number of bound states, identical to TEnergies
        real*8, pointer      :: energyarr(:)             ! the array with the bound energies
        complex*16, pointer  :: wavefunctions(:,:)       ! the array with the wave functions
    end type


    ! Variable definitions
    real*8      :: mass         ! particle mass
    real*8      :: maxz         ! maximum x
    real*8      :: minz         ! minimum x
    real*8      :: deltaz       ! step size in x direction

    real*8      :: centerz      ! initial position in gaussian
    real*8      :: maxt         ! maximum time
    real*8      :: deltat       ! delta time
    integer     :: nz           ! no of steps in x direction (no of points in grid):(maxx/deltax)
    integer     :: nt           ! no of time steps

    real*8      :: deltafft     ! time step for FFT
    integer     :: nfft         ! no of time/frequency steps for FFT

    real*8, pointer  :: Z(:),P(:),E(:)
    real*8, pointer  :: potential(:), coupling(:), potderivative(:);

    ! initial wavefunction array
    complex*16, allocatable :: psiground(:), psigerade(:),psiungerade(:), psitotal(:)

    complex*16, allocatable :: K(:);

    complex*16  :: ii  = (0.d0,1.d0)       ! complex number i
    complex*16  :: czero  = (0.d0,0.d0)
    real*8      :: pi = 3.14159265358979323846264338327950288419716939937510d0
    real*8      :: Tend

    !__________________absorber section_____________________________________________________
    real*8  :: fadewidth                    ! the width of the absorber for the electrons
    real*8  :: fadestrength                 ! the strength of the absorbing border potential
    real*8, pointer :: absorber(:)          ! absorber potential
    logical :: includeAbsorber              ! switch for using absorber

    !_____________________________Probe (E FIELD) section_____________________________________
    real*8  :: Eo                           ! field amplitude
    real*8  :: Eomega                       ! laser frequency
    real*8  :: Ephi                         ! carrier envelope phase
    real*8  :: Ewidth                       ! width of the envelope
    real*8  :: Eto                          ! center of the gaussian envelope
    logical :: includeField                 ! switch for using field


    !____________________pedestal section _____________________________________________

    real*8  :: EoPed                        ! pedestal field amplitude
    real*8  :: EwidthPed                    ! width of the pedestal envelope
    real*8  :: EomegaPed                    ! pedestal laser frequency
    real*8  :: EphiPed                      ! carrier envelope phase
    real*8  :: EtoPed                       ! center of the gaussian envelope
```

```
      logical :: includePedestal             ! switch for pedestal
70
      !_____________________________Pump Section_____________________________________________
      real*8     :: EoPump       !(pulseint)
      real*8     :: EwidthPump   !(pulselength)
      real*8     :: EomegaPump   !(pulseomega)
75    real*8     :: EphiPump     !(pulsephase)
      real*8     :: EtoPump      ! center of the pump envelope

      logical     :: includeConstantPump    ! switch for setting constant pump

80
      !_____________________________ Power Spectra FFT Section_____________________________
      real*8,  pointer    :: fftarray(:,:)    ! array for FFT
      complex*16, pointer :: fftinput(:)      ! the complex version for one R parameter
      logical             :: calculatePowerSpectra  = .true. ! .false.;
85
      !_____________________________ KER Power Spectra FFT Section_________________________
      real*8,  pointer    :: KERfftarray(:,:)    ! array for FFT
      logical             :: calculateKERPowerSpectra  = .true. !.false.;

90    !_____________________________________Diagonalization Section_____________________
      type(TStates)     :: states    ! object with wave functions and energies from diagonalization

      !_____________________________ Memory allocation_____________________________________
      integer :: iAllocStatus
95
      !_______________________________Printing & Plotting Filters_____________________
      integer :: printFilter
      integer :: maxFrequencyFilter
      integer :: printInterval
100
      real*8  :: frequencyInTHZ = 6579.7d0

      !_____________________________________Method Selection_____________________________
      character(len=2),parameter   :: CNMethod  = "CN"        ! Crank-Nicholson method
105   character(len=2),parameter   :: FTMethod  = "FT"        ! FFT method

      character(len=2)   :: useMethod  = CNMethod
      !character(len=2)   :: useMethod  = FTMethod

110   !_____________________________________ Output selection _____________________________
       character(len=120) :: inputFolder  = "input/" ;
       character(len=120) :: outputFolder;
       character(len=120) :: curve1, curve2, curve3, curve4;
       character(len=10)  :: molecule  = "D2";
115
       character(len=255) :: diagFolder  = "input/diag/" ;

       !_____________________________________ KER Bound State _____________________________
       integer             :: boundStateCutOff = 200;
120

       !_____________________________________ ADK Section _____________________________
       logical             :: useADK  = .true. ;

125    real*8              :: e_adk       = dexp(1.d0)    ! the Euler constant
       real*8              :: pi_adk      = dacos(-1.d0)  ! well guess - what could this be...
       ! the total charge of the ION (after the ADK transition)
       real*8              :: ioncharge   = 1.0d0

130    end module progvars
```

D.4 Module ADK ionization (adk.f90)

```
!-------------------------------------------------------------------------------
! DEFINITION OF 1D ADK ROUTINES
!-------------------------------------------------------------------------------
5 ! Author   : Thomas Niederhausen, Maia Magrakvelidze
  ! Sources  : J. P. Brichta et al., J. Phys. B 39, 3769 (2006)
```

```
! Date     : 01 Dec 2006
! Note     : This module is in order to avoid an IFORT compiler bug regarding
!            array passing subroutines
!-------------------------------------------------------------------------------
! usage:
!
! ADK_DEPLETE
! ADK_TRANSITION
!   ...
!

module adk
  implicit none
  !Declare ADK static variables to speed up the calculation of ADK rates
  !lump all the R-dependent factors in here - ground
  real*8, allocatable         :: adk_const(:)
  ! sqrt(2*I_p) - wave vector to ionize from ground
  real*8, allocatable         :: adk_kappa(:)
  contains
!-------------------------------------------------------------------------------
subroutine adk_deplete(psiin, potlo, pothi, ioncharge, pulseint, pulselength, pulseomega,
pulsephase)
    ! ADK routine for improved Franck-Condon transition but based on atomic ADK rates for
    ! molecules, taken from eq. (5) of J. P. Brichta et al., J. Phys. B 39, 3769 (2006).
    ! The initial wave packet WAVEFUNCTION is originally moving in the lower potential POTLO
    ! and exposed to the given ionizing pulse. Static ADK rates for variing field is used rather
    ! than cycle averaged in order to account for really short pulses and the rapid change in
    ! envelope. The given wave funtion DOES NOT propagate during the pulse, thus the routine
    ! still assumes instantaneous ADK depletion and is therefore limited to very short pulses.
    ! Output is given in WAVEFUNCTION as the remaining part of the original wave function and
    ! the ionized wave function moving in the upper potential POTHI can be estimated as
    ! (original wave function) - (final wave function).

    use wfmath
    ! the initial wave function for ionization, also return value
    complex*16, dimension(:), intent(inout) :: psiin(:)
    ! both potential curves considered for the ADK transition
    real*8, dimension(:), intent(in)        :: potlo, pothi
    ! the total charge of the ION (after the ADK transition)
    real*8, intent(in)                      :: ioncharge
    ! the laser parameters
    real*8, intent(in)                      :: pulseint, pulselength, pulseomega, pulsephase

    ! lets start off with something round...
    real*8, parameter                       :: pi = 3.14159265358979323846264 3d0
    ! number of sampling points per laser cycle
    integer, parameter                      :: ncyclesteps = 128
    ! multiplier for the pulselength for total transition time
    real*8, parameter                       :: sigmawidth = 2.d0
    ! the delta t for the ADK calculation
    real*8                                  :: timestep
    ! well - the current time of the pulse
    real*8                                  :: currenttime
    ! for the time step loop
    integer                                 :: nt, ntimesteps
    ! the envelope of the electric field of the laser pulse
    real*8                                  :: fieldenv
    ! the laser pulse carrier envelope phase
    real*8                                  :: fieldphase
    ! thats the electric field strengh of the laser we need
    real*8                                  :: efield
    ! but only the magnitude of the field matters for ADK
    real*8                                  :: fieldabs
    ! error check
    integer                                 :: iAllocStatus
    ! for precomputing ADK constants
    real*8, dimension(:), allocatable       :: kappa, adkconst
    ! integrate it and you still have the same function...
    real*8                                  :: e
    ! for loop through the R values
    integer                                 :: nR, nRstep
```

```
        real*8                                  :: rate

 80     ! size of the wave function array in R
        nRstep = size(psiin)
            ! allocate some memory for precomputing some static values
            allocate(kappa(nRstep), adkconst(nRstep), stat=iAllocStatus)
            if (iAllocStatus /= 0) then
 85           print *,"ERROR: can't allocate temporary ADK work arrays"
              stop
            endif

            ! now procompute the static part of the ADK rates
 90         ! the Euler constant
            e        = dexp(1.d0)
            ! sqrt(2*I_p)/Z with I_p the ionization potential
            kappa    = dsqrt(2.d0 * (pothi - potlo))/ioncharge

 95         adkconst = (3.d0*e/pi)**1.5d0 &
                       *(kappa**4.5d0)/(ioncharge**2.5d0) &
                       *(4.d0*e*(kappa**4)/ioncharge)**(2.d0*ioncharge/kappa-1.5d0)

            ! calculate an appropriate timestep for each ADK transition
100         timestep   = 2.d0*pi / (pulseomega * ncyclesteps)
            ! how many time steps do we have in total?
            ntimesteps = nint(sigmawidth*pulselength/timestep)

            do nt=0, ntimesteps-1     ! The ADK time loop
105           currenttime = -sigmawidth*pulselength/2.d0 + timestep*nt     ! get ma a clock reading

              ! Calculate the electric field strengh of the laser at the current time
              fieldenv    = dsqrt(pulseint) * dexp(- 2.d0 * dlog(2.d0) * (currenttime**2) /
                               (pulselength**2) )
110           ! the current laser phase with respect to the maximum of the pulse
              fieldphase  = dmod(pulseomega*currenttime+pulsephase,2*pi)
              efield      = fieldenv * dcos(fieldphase)
              ! ADK only depends on the magnitude of the electric field
              fieldabs    = dabs(efield)
115
              ! next timestep, if field strength is not large enough
              if (fieldabs < 1.d-4) cycle

              ! now comes the ADK part –
120           ! loop through all R value and see how much wave function we will loose

              !$OMP PARALLEL DO SCHEDULE(STATIC,1) PRIVATE(nR, rate)
              do nR=1, nRstep
                  ! the current ADK rate at given internuclear distance
125               rate = adkconst(nR) * (fieldabs**(1.5d0 - 2.d0*ioncharge/kappa(nR))) &
                       *dexp(-2.d0*kappa(nR)**3/(3.d0*fieldabs))

                  ! and the depleted ground state wave function
                  psiin(nR) = psiin(nR)*(1.d0 - dsqrt(dabs(rate*timestep)))
130           enddo
              !$OMP END PARALLEL DO

            enddo ! (* time loop *)

135         ! and finally remove the precomputed arrays again
            deallocate(kappa, adkconst, stat=iAllocStatus)
            if (iAllocStatus /= 0) then
              print *,"ERROR: can't deallocate temporary ADK work arrays"
              stop
140         endif

        end subroutine adk_deplete
    !---------------------------------------------------------------------------

145     subroutine adk_init
            ! initialize the ADK rate arrays and precompute the static variables
            ! IMPORTANT: it is assumed that the GERADE curve is POTENTIAL(2) and the
            ! UNGERADE curve is POTENTIAL(3)!!!
```

```
        ! The molecular ADK rates are taken from eq. (5) of J. P. Brichta et al.,
        ! J. Phys. B 39, 3769 (2006)

        use progvars
        use wfPot
        use debug

        implicit none

        integer :: adkAllocStatus     ! for I/O operation
        integer :: nR
        real*8  :: rpos, adkground    ! position and ADK rates
        real*8  :: maxfield           ! the maximum electric field strenth of the laser

        allocate(adk_const(nz),adk_kappa(nz), stat=adkAllocStatus)
        if (adkAllocStatus /= 0) then
            print *,"ERROR: can't allocate ADK arrays"
            stop
        endif

        ! now precompute the static part of the ADK rates
        ! sqrt(2*I_p) with I_p the ionization potential
        adk_kappa = dsqrt(2.d0 * (pot_curve2 - pot_curve1))

        adk_const = (3.d0*e_adk/pi_adk)**1.5d0 &
                    *(adk_kappa**4.5d0)/(ioncharge**2.5d0) &
                    *(4.d0*e_adk*(adk_kappa**4)/ioncharge)**(2.d0*ioncharge/adk_kappa-1.5d0)


        call debugmsg (5,1,"adk_init: ADK arrays allocated, precomputed and plotted")

    end subroutine adk_init

!-------------------------------------------------------------------------------

    subroutine adk_transition(timestep, fieldstrength)
        ! this routine does the ADK rate depletion of both H2+ curves to the p+p Coulomb
        ! explosion curve. The ADK rate acts like a optical potential damping the H2+ wave
        ! functions but cannot coherently build up the correct wave function on the 2H+ curve due
        ! to the lost phase information. Instead we poppulate the upper potential curve
        ! constructively and do not propagate this wave function.

        use progvars

        implicit none

        real*8, intent(in) :: timestep;
        real*8, intent(in) :: fieldstrength;
        real*8             :: fieldabs;
        integer            :: nR;
        complex*16         :: tmpground;
        real*8             :: adkground;

        fieldabs = dabs(fieldstrength)
        ! certainly nothing to do here, if there is no field
        if (fieldabs < 1.d-4) return;

        ! The ADK rate transitions are pointwise for every R. We go pointwise through the wave
        ! functions, therefore we can have this loop running in parallel using OpenMP
        ! Since the routine will be called quite often, it has been optimized for speed.

        !$OMP PARALLEL DO SCHEDULE(STATIC,1) PRIVATE(nR, tmpg, tmpu, adkg, adku)
        do nR=1, nz
            ! the current ADK rate from the gerade curve
            adkground = adk_const(nR) * (fieldabs**(1.5d0 - 2.d0*ioncharge/adk_kappa(nR))) &
                        *dexp(-2.d0*adk_kappa(nR)**3/(3.d0*fieldabs))

            ! the ADK transition amplitude subtracted from orginal
            tmpground = psiground(nR) - (dsqrt(dabs(adkground*timestep)) * psiground(nR));
```

```
            ! depletion of the ground state wave function added to gerade
            psigerade(nR)   = psigerade(nR) +  tmpground ;

        enddo
        !$OMP END PARALLEL DO

    end subroutine adk_transition
!-------------------------------------------------------------------------------
    subroutine adk_done

        ! destroy  the ADK arrays
        use progvars
        use debug

        implicit none

        integer :: adkAllocStatus       ! for I/O operation

        deallocate(adk_const, adk_kappa, stat=adkAllocStatus)
        if (adkAllocStatus /= 0) then
        print *,"ERROR: can't deallocate ADK arrays"
        stop
        endif

        call debugmsg (5,1,"adk_done: ADK arrays destroyed")

    end subroutine adk_done

end module adk
```

Appendix E - GAMESS input-output

This appendix summarizes the construction of inputs, compiling, running, and generating outputs in the GAMESS code [*](see remarks at the end of the Appendix). First, the construction of the input files for potential curve and dipole-coupling-element calculations for H_2, H_2^+, O_2 and O_2^+ are given. Second, the compilation procedure is summarized. Below, the Table summarizes the input-output files.

Inputs	Description	Outputs
A.I	*H_2 optimization*	*A.O.*
B.I.	*H_2^+ optimization*	*B.O.*
C.I.	*H_2^+ energy*	*C.O.*
D.I.	*H_2 energy*	*D.O.*
E.I.	*H_2^+ dipole couplings*	-
F.I.	*O_2 optimization*	*F.O.*
G.I.	*O_2^+ optimization*	-
H.I.	*O_2^+ energy*	*H.O.*
J.I.	*O_2^+ dipole coupling*	*J.O.*

Sections A.I through J.I. correspond to the list of inputs, and the sections A.O through J.O correspond to outputs.

The potential-curve (and dipole coupling) calculation procedure is as follows. First, we optimize the geometry of a given molecule. As an example, for the H_2 molecule the input file for geometry optimization is given below:

– – – – – – – – –– –

A.I. *Input for H_2 optimization calculations:*

```
$CONTRL RUNTYP=optimize SCFTYP=RHF ISPHER=1 $END
$SYSTEM TIMLIM=90000 mwords=100 $END
$BASIS GBASIS=CCT $END
$STATPT OPTTOL=0.00001 NSTEP=20 $END
$DATA
 H2 optimization - cartesian coordinates
Dnh 4

H         1.0   0.0000000000   0.0000000000   0.4407446852
$END
```

– – – – – – – – –– –

Here we explain each term in the input file. More details can be found below [*].

The “control” group identifies the type of wavefunctions and the type of calculation to be done; it also specifies the charge and spin of the molecule, the coordinate system, the use of core potentials, spherical harmonics, and similar types of parameters.

RUNTYP=optimize --- computation type, in this case geometry optimization

SCFTYP=RHF ---- Restricted Hartree-Fock calculation

ISPHER=1 --- spherical harmonics option (Cartesian basis functions). Used for basis set.

The "system" group governs computer-related options.

Basis types and related parameters are given in "Basis" group.

GBASIS=CCT --- Dunning-type correlation consistent basis sets (cc-pVnZ). For the general case, CCn - n=T means triplet.

"Data" covers the characteristics of the molecule, such as the number of atoms and the geometry. In our case, we have two H atoms located at coordinates (0, 0, 0.44…) and (0, 0, -0.44…) due to the D_{4h} symmetry. For diatomic molecules symmetry should be $D_{\infty h}$, but calculations cannot be done with an infinite number of basis sets so GAMESS sets the symmetry for diatomic molecules as D_{4h}.

As an example, geometry optimization is given for the H_2^+ molecular ion below:

B.I. *Input for H_2^+ optimization calculations:*

```
 $CONTRL RUNTYP=optimize SCFTYP=UHF ICHARG=1 MULT=2 ISPHER=1 $END
 $SYSTEM TIMLIM=90000 mwords=100 $END
 $BASIS GBASIS=CCT $END
 $STATPT OPTTOL=0.00001 NSTEP=20 $END
 $DATA
H2+ optimization
Dnh  4

H 1.0   0.0000000000   0.0000000000   0.3561149584
 $END
```

The next step is to use the optimized geometry in the actual calculations for the energy. GAMESS calculates the energy (in a.u.) for a given internuclear distance R (in Angstroms), so one needs to repeat the calculations for different R (that means constructing different input files for different internuclear distances and running them). As an example, the energy calculations for one R=1.057 Å for the H_2^+ molecular ion is given below:

C.I. *Input for H_2^+ energy curve calculations:*

```
$CONTRL RUNTYP=energy SCFTYP=MCSCF ICHARG=1 MULT=2 ISPHER=1 $END
$SYSTEM TIMLIM=90000 mwords=100 $END
$BASIS GBASIS=CCT  $END
$STATPT OPTTOL=0.00001 NSTEP=20 $END
$DET NCORE=0 NACT=2 NELS=1 NSTATE=2 WSTATE(1)=0.1,0.9 $END
$GUESS GUESS=MOREAD norb=28 $END
$DATA
H2+ energies
```

```
Dnh  4

 H 1.0   0.0000000000   0.0000000000   0.5285771035
 $END
 $VEC
 1  1 2.43921181E-01 3.14632011E-01 2.61389538E-02 0.00000000E+00 0.00000000E+00
 1  2 2.44757728E-02 0.00000000E+00 0.00000000E+00 4.01315821E-02-2.46399747E-03
 1  3-2.46399747E-03 4.92799493E-03 0.00000000E+00 0.00000000E+00 0.00000000E+00
 1  4 2.43921181E-01 3.14632011E-01 2.61389538E-02 0.00000000E+00 0.00000000E+00
 1  5-2.44757728E-02 0.00000000E+00 0.00000000E+00-4.01315821E-02-2.46399747E-03
.....
$END
```

The "VEC" group was taken from the "file name".dat file of the optimization run of H_2^+. For the energy calculations at different internuclear distances, one needs to add 0.1 Å (or any step size interval preferred) to the internuclear distance(in this case Z=0.52857...) of H^+ (molecule is aligned along Z axis, thus Z coordinate corresponds to the internuclear distance) .

An example of H_2 ground state calculations is given below. Please note that here RUNTYP = surface is used (not energy). In this case GAMESS calculates energies for different internuclear distances automatically. There is no need to manually add 0.1 Å and generate another input file for different internuclear distance. Note that for some reason the RUNTYP=surface does not give correct values for heavier molecules.

D.I. *Input for H_2 energy curve calculations:*

```
 $CONTRL RUNTYP=surface SCFTYP=RHF CCTYP=EOM-CCSD ICHARG=0 MULT=1 $END
 $SYSTEM TIMLIM=90000 mwords=100 $END
 $BASIS GBASIS=STO NGAUSS=3 $END
 $STATPT OPTTOL=0.00001 NSTEP=20 $END
 $CCINP MAXCC=1000 $END
 $SURF ivec1(1)=1,2 igrp1=2
       disp1=0.1 ndisp1=50 orig1=-0.5 $END
 $DATA
H2 energies
Dnh  4

 H 1.0   0.0000000000   0.0000000000   0.3561149584
 $END
```

An example for the calculation of the dipole matrix elements for H_2^+ states is given below:

E.I. *Input for H_2^+ dipole coupling element calculations:*

```
$CONTRL RUNTYP=TRANSITN SCFTYP=NONE CITYP=GUGA ICHARG=1 MULT=2 ISPHER=1 $END
$SYSTEM TIMLIM=90000 mwords=100 $END
$BASIS GBASIS=CCT $END
$STATPT OPTTOL=0.00001 NSTEP=20 $END
$TRANST OPERAT=DM NFZC=0 IROOTS(1)=2  NOCC=3 $END
$DRT1 GROUP=c1 IEXCIT=2 NFZC=0 NDOC=0 NALP=1 NEXT=-1 NVAL=2 $END
$DATA
H2+ energies
Dnh  4
```

```
H    1.0   0.0000000000   0.0000000000   0.5285771035
 $END
 $VEC1
 1  1 2.43921181E-01 3.14632011E-01 2.61389538E-02 0.00000000E+00 0.00000000E+00
 1  2 2.44757728E-02 0.00000000E+00 0.00000000E+00 4.01315821E-02-2.46399747E-03
 1  3-2.46399747E-03 4.92799493E-03 0.00000000E+00 0.00000000E+00 0.00000000E+00
1   4 2.43921181E-01 3.14632011E-01 2.61389538E-02 0.00000000E+00 0.00000000E+00
….
$END
```

H_2 (H_2^+) molecule outputs

A.O. *Output for H_2 optimization calculations:*

```
...
 ECHO OF THE FIRST FEW INPUT CARDS -
 INPUT CARD>! Example 1 optimization
 INPUT CARD> $CONTRL RUNTYP=optimize SCFTYP=RHF $END
 INPUT CARD> $SYSTEM TIMLIM=90000 mwords=100 $END
 INPUT CARD> $BASIS GBASIS=STO NGAUSS=3 $END
 INPUT CARD> $STATPT OPTTOL=0.00001 NSTEP=20 $END
 INPUT CARD> $DATA
 INPUT CARD>H2 optimization - cartesian coordinates
 INPUT CARD>Dnh 4
 INPUT CARD>
 INPUT CARD>H         1.0   0.0000000000   0.0000000000   0.4407446852
 INPUT CARD> $END
  100000000 WORDS OF MEMORY AVAILABLE

     BASIS OPTIONS
     -------------
     GBASIS=STO          IGAUSS=       3      POLAR=NONE
     NDFUNC=       0     NFFUNC=       0     DIFFSP=       F
     NPFUNC=       0      DIFFS=       F     BASNAM=


     RUN TITLE
     ---------
 H2 optimization - cartesian coordinates

 THE POINT GROUP OF THE MOLECULE IS DNH
 THE ORDER OF THE PRINCIPAL AXIS IS     4

 ATOM      ATOMIC                      COORDINATES (BOHR)
           CHARGE         X                   Y                   Z
 H           1.0     0.0000000000        0.0000000000       -0.8328866856
 H           1.0     0.0000000000        0.0000000000        0.8328866856

          INTERNUCLEAR DISTANCES (ANGS.)
          ------------------------------

                1 H          2 H

   1 H       0.0000000    0.8814894 *
   2 H       0.8814894 *  0.0000000

  * ... LESS THAN  3.000


     ATOMIC BASIS SET
     ----------------
 THE CONTRACTED PRIMITIVE FUNCTIONS HAVE BEEN UNNORMALIZED
 THE CONTRACTED BASIS FUNCTIONS ARE NOW NORMALIZED TO UNITY

  SHELL TYPE  PRIMITIVE        EXPONENT          CONTRACTION COEFFICIENT(S)
```

```
H

     2   S       1            3.4252509    0.154328967295
     2   S       2            0.6239137    0.535328142282
     2   S       3            0.1688554    0.444634542185

TOTAL NUMBER OF BASIS SET SHELLS             =    2
NUMBER OF CARTESIAN GAUSSIAN BASIS FUNCTIONS =    2
NUMBER OF ELECTRONS                          =    2
CHARGE OF MOLECULE                           =    0
SPIN MULTIPLICITY                            =    1
NUMBER OF OCCUPIED ORBITALS (ALPHA)          =    1
NUMBER OF OCCUPIED ORBITALS (BETA )          =    1
TOTAL NUMBER OF ATOMS                        =    2
THE NUCLEAR REPULSION ENERGY IS        0.6003217588

THIS MOLECULE IS RECOGNIZED AS BEING LINEAR,
ORBITAL LZ DEGENERACY TOLERANCE ETOLLZ= 1.00E-06

    $NEO OPTIONS
    ------------
    NUNIQN=       0     BASNUC=DZSNB        NEOSCF=NONE
    NEOCI =NONE         NUMULT=       2     NUCST =       1
    NAUXNB=       0     VNUCEX=       F     NUCOPT=       F
    NTAUXB=       0     NEOHSS=       F     HSSINI=READH
    HSSUPD=POWELLUP     DIRNUC=       F     SYMNUC=       F
    QMTOLN= 0.0E+00     USRDEX=       F
    POSNEO=       F     POSPRP=       F
    NEONCI=       F     LOCORB=       0

    $CONTRL OPTIONS
    ---------------
SCFTYP=RHF          RUNTYP=OPTIMIZE     EXETYP=RUN
MPLEVL=       0     CITYP =NONE         CCTYP =NONE         VBTYP =NONE
DFTTYP=NONE         TDDFT =NONE
MULT  =       1     ICHARG=       0     NZVAR =       0     COORD =UNIQUE
PP    =NONE         RELWFN=NONE         LOCAL =NONE         NUMGRD=       F
ISPHER=      -1     NOSYM =       0     MAXIT =      30     UNITS =ANGS
PLTORB=       F     MOLPLT=       F     AIMPAC=       F     FRIEND=
NPRINT=       7     IREST =       0     GEOM  =INPUT
NORMF =       0     NORMP =       0     ITOL  =      20     ICUT  =       9
INTTYP=BEST         GRDTYP=BEST         QMTTOL= 1.0E-06

    $SYSTEM OPTIONS
    ---------------
 REPLICATED MEMORY=   100000000 WORDS (ON EVERY NODE).
DISTRIBUTED MEMDDI=           0 MILLION WORDS IN AGGREGATE,
MEMDDI DISTRIBUTED OVER   1 PROCESSORS IS           0 WORDS/PROCESSOR.
TOTAL MEMORY REQUESTED ON EACH PROCESSOR=   100000000 WORDS.
TIMLIM=       90000.00 MINUTES, OR      62.5 DAYS.
PARALL= F  BALTYP=  DLB     KDIAG=    0  COREFL= F
MXSEQ2=     300 MXSEQ3=     150

         ---------------
         PROPERTIES INPUT
         ---------------

MOMENTS            FIELD           POTENTIAL          DENSITY
IEMOM =       1    IEFLD =       0   IEPOT =       0   IEDEN =       0
WHERE =COMASS      WHERE =NUCLEI     WHERE =NUCLEI     WHERE =NUCLEI
OUTPUT=BOTH        OUTPUT=BOTH       OUTPUT=BOTH       OUTPUT=BOTH
IEMINT=       0    IEFINT=       0                     IEDINT=       0
                                                       MORB  =       0
         EXTRAPOLATION IN EFFECT
ORBITAL PRINTING OPTION: NPREO=     1     2     2     1

    ------------------------------
    INTEGRAL TRANSFORMATION OPTIONS
    ------------------------------
    NWORD  =         0     CUTOFF = 1.0E-09
```

```
    MPTRAN =         0     DIRTRF =       F
    AOINTS =DUP

         ---------------------
         INTEGRAL INPUT OPTIONS
         ---------------------
 NOPK  =       1 NORDER=       0 SCHWRZ=       F

    ----------------------------------------
    THE POINT GROUP IS DNH, NAXIS= 4, ORDER=16
    ----------------------------------------

    DIMENSIONS OF THE SYMMETRY SUBSPACES ARE
 A1G =    1     A1U =    0     B1G =    0     B1U =    0     A2G =    0
 A2U =    1     B2G =    0     B2U =    0     EG  =    0     EU  =    0

 ..... DONE SETTING UP THE RUN .....
 STEP CPU TIME =     0.02 TOTAL CPU TIME =        0.0 (    0.0 MIN)
 TOTAL WALL CLOCK TIME=        0.0 SECONDS, CPU UTILIZATION IS 106.67%


         ----------------------------
         STATIONARY POINT LOCATION RUN
         ----------------------------

 OBTAINING INITIAL HESSIAN, HESS=GUESS
 CARTESIAN COORDINATE OPTIMIZATION USING BADGER'S RULE FORCE CONSTANT GUESS

         PARAMETERS CONTROLLING GEOMETRY SEARCH ARE
         METHOD =QA                UPHESS =BFGS
         NNEG   =         0        NFRZ   =         0
         NSTEP  =        20        IFOLOW =         1
         HESS   =GUESS             RESTAR =         F
         IHREP  =         0        HSSEND =         F
         NPRT   =         0        NPUN   =         0
         OPTTOL = 1.000E-05        RMIN   = 1.500E-03
         RMAX   = 1.000E-01        RLIM   = 7.000E-02
         DXMAX  = 3.000E-01        PURIFY =         F
         MOVIE  =         F        TRUPD  =         T
         TRMAX  = 5.000E-01        TRMIN  = 5.000E-02
         ITBMAT =         5        STPT   =         F
         STSTEP = 1.000E-02        PROJCT=          T

 BEGINNING GEOMETRY SEARCH POINT NSERCH=   0 ...
...
    ***** EQUILIBRIUM GEOMETRY LOCATED *****
 COORDINATES OF SYMMETRY UNIQUE ATOMS (ANGS)
   ATOM   CHARGE       X              Y              Z
 ------------------------------------------------------------
 H          1.0   0.0000000000   0.0000000000   0.3561149584
 COORDINATES OF ALL ATOMS ARE (ANGS)
   ATOM   CHARGE       X              Y              Z
 ------------------------------------------------------------
 H          1.0  -0.0000000000  -0.0000000000  -0.3561149584
 H          1.0   0.0000000000   0.0000000000   0.3561149584

         INTERNUCLEAR DISTANCES (ANGS.)
         ------------------------------

              1 H          2 H

   1 H       0.0000000    0.7122299 *
   2 H       0.7122299 *  0.0000000

   * ... LESS THAN  3.000
...
```

The equilibrium geometry (in red) is given in Angstroms. One of the H atoms is located at Z = 0.356 Å and the other is at Z = - 0.356 Å. The internuclear distance in atomic units R = 2*0.35611 Å / 0.529 = 1.35 a.u.

***B.O**. Output for H_2^+ optimization calculations:*

```
 ...
 ECHO OF THE FIRST FEW INPUT CARDS -
 INPUT CARD> $CONTRL RUNTYP=optimize SCFTYP=UHF ICHARG=1 MULT=2 ISPHER=1 $END
 INPUT CARD> $SYSTEM TIMLIM=90000 mwords=100 $END
 INPUT CARD> $BASIS GBASIS=CCT $END
 INPUT CARD> $STATPT OPTTOL=0.00001 NSTEP=20 $END
 INPUT CARD> $DATA
 INPUT CARD>H2+ optimization
 INPUT CARD>Dnh  4
 INPUT CARD>
 INPUT CARD>H 1.0   0.0000000000   0.0000000000   0.3561149584
 INPUT CARD> $END
 INPUT CARD>
  100000000 WORDS OF MEMORY AVAILABLE

     BASIS OPTIONS
     -------------
     GBASIS=CCT          IGAUSS=       0      POLAR=NONE
     NDFUNC=       0     NFFUNC=       0     DIFFSP=       F
     NPFUNC=       0      DIFFS=       F     BASNAM=


     RUN TITLE
     ---------
 H2+ optimization

 THE POINT GROUP OF THE MOLECULE IS DNH
 THE ORDER OF THE PRINCIPAL AXIS IS     4

 ATOM      ATOMIC                      COORDINATES (BOHR)
           CHARGE         X                   Y                   Z
 H           1.0     0.0000000000        0.0000000000       -0.6729596915
 H           1.0     0.0000000000        0.0000000000        0.6729596915

          INTERNUCLEAR DISTANCES (ANGS.)
          ------------------------------

                1 H          2 H

   1 H       0.0000000    0.7122299 *
   2 H       0.7122299 *  0.0000000

  * ... LESS THAN  3.000
...

      ***** EQUILIBRIUM GEOMETRY LOCATED *****
 COORDINATES OF SYMMETRY UNIQUE ATOMS (ANGS)
   ATOM   CHARGE       X              Y              Z
 ------------------------------------------------------------
 H           1.0  -0.0000000000   0.0000000000   0.5285771035
 COORDINATES OF ALL ATOMS ARE (ANGS)
   ATOM   CHARGE       X              Y              Z
 ------------------------------------------------------------
 H           1.0  -0.0000000000   0.0000000000  -0.5285771035
 H           1.0  -0.0000000000   0.0000000000   0.5285771035

          INTERNUCLEAR DISTANCES (ANGS.)
          ------------------------------

                1 H          2 H

   1 H       0.0000000    1.0571542 *
```

```
   2 H       1.0571542 *  0.0000000

  * ... LESS THAN  3.000
...
```

_ _ _ _ _ _ _ _ __ _

The equilibrium geometry (in red) is given in Angstroms. One of the H atoms is located at Z = 0.5286Å and the other is at Z = - 0.5286Å. The internuclear distance in atomic units R = 2*0.35611Å/0.529 = 1.998 a.u.

_ _ _ _ _ _ _ _ __ __

D.O. *Output for* H_2^+ *energy calculations:*

```
 ECHO OF THE FIRST FEW INPUT CARDS -
 INPUT CARD> $CONTRL RUNTYP=energy SCFTYP=MCSCF ICHARG=1 MULT=2 ISPHER=1 $END
 INPUT CARD> $SYSTEM TIMLIM=90000 mwords=100 $END
 INPUT CARD> $BASIS GBASIS=CCT  $END
 INPUT CARD> $STATPT OPTTOL=0.00001 NSTEP=20 $END
 INPUT CARD> $DET NCORE=0 NACT=2 NELS=1 NSTATE=2 WSTATE(1)=0.1,0.9 $END
 INPUT CARD> $GUESS GUESS=MOREAD norb=28 $END
 INPUT CARD> $DATA
 INPUT CARD>H2+ energies
 INPUT CARD>Dnh  4
 INPUT CARD>
 INPUT CARD> H 1.0   0.0000000000   0.0000000000   0.5285771035
 INPUT CARD> $END
 INPUT CARD> $VEC
 INPUT CARD> 1  1 2.43921181E-01 3.14632011E-01 2.61389538E-02 0.00000000E+00 0.00000000E+00
 INPUT CARD> 1  2 2.44757728E-02 0.00000000E+00 0.00000000E+00 4.01315821E-02-2.46399747E-03
...
CI EIGENVECTORS WILL BE LABELED IN GROUP=C1
 PRINTING ALL NON-ZERO CI COEFFICIENTS

 STATE   1  ENERGY=       -0.6022446912  S=  0.50  SZ=  0.50  SPACE SYM=A

ALPH|BETA| COEFFICIENT
----|----|------------
 10 | 00 |   1.0000000

 STATE   2  ENERGY=       -0.1664191926  S=  0.50  SZ=  0.50  SPACE SYM=A

ALPH|BETA| COEFFICIENT
----|----|------------
 01 | 00 |   1.0000000
```

_ _ _ _ _ _ _ _ __ __

State 1 is $1s\sigma_g$ and state 2 is $2p\sigma_u$.

_ _ _ _ _ _ _ _ __ __

C.O. *Output for* H_2 *energy calculations:*

```
...
 ECHO OF THE FIRST FEW INPUT CARDS -
 INPUT CARD>! Example 2 energy
 INPUT CARD> $CONTRL RUNTYP=surface SCFTYP=RHF CCTYP=EOM-CCSD ICHARG=0 MULT=1 $END
 INPUT CARD> $SYSTEM TIMLIM=90000 mwords=100 $END
 INPUT CARD> $BASIS GBASIS=STO NGAUSS=3 $END
 INPUT CARD> $STATPT OPTTOL=0.00001 NSTEP=20 $END
 INPUT CARD> $CCINP MAXCC=1000 $END
 INPUT CARD> $SURF ivec1(1)=1,2 igrp1=2
 INPUT CARD>       disp1=0.1 ndisp1=50 orig1=-0.5 $END
 INPUT CARD> $DATA
 INPUT CARD>H2 energies
 INPUT CARD>Dnh  4
 INPUT CARD>
 INPUT CARD>H 1.0   0.0000000000   0.0000000000   0.3561149584
 INPUT CARD> $END
```

```
 INPUT CARD>
  100000000 WORDS OF MEMORY AVAILABLE

     BASIS OPTIONS
     -------------
     GBASIS=STO          IGAUSS=       3      POLAR=NONE
     NDFUNC=       0     NFFUNC=       0     DIFFSP=       F
     NPFUNC=       0      DIFFS=       F     BASNAM=


     RUN TITLE
     ---------
 H2 energies
...
               ---- SUMMARY OF EOM-CCSD CALCULATIONS ----

                 EXCITATION      EXCITATION      TOTAL
    SYMMETRY     ENERGY (H)      ENERGY (EV)     ENERGY (H)          ITERATIONS
       A         1.97041385        53.618         1.98943600          CONVERGED

 ..... DONE WITH EOM-CCSD .....
 STEP CPU TIME =     0.06 TOTAL CPU TIME =        0.2 (    0.0 MIN)
 TOTAL WALL CLOCK TIME=        1.3 SECONDS, CPU UTILIZATION IS  14.73%
 ---- SURFACE MAPPING GEOMETRY ----
 COORD 1=-0.500 COORD 2= 0.000
 HAS ENERGY VALUE       0.019022
 H      0.00000   0.00000  -0.35611
 H      0.00000   0.00000  -0.14389
 --------------------------------
...
               ---- SUMMARY OF EOM-CCSD CALCULATIONS ----

                 EXCITATION      EXCITATION      TOTAL
    SYMMETRY     ENERGY (H)      ENERGY (EV)     ENERGY (H)          ITERATIONS
       A         1.72993576        47.074         1.07478324          CONVERGED

 ..... DONE WITH EOM-CCSD .....
 STEP CPU TIME =     0.00 TOTAL CPU TIME =        0.2 (    0.0 MIN)
 TOTAL WALL CLOCK TIME=        1.3 SECONDS, CPU UTILIZATION IS  15.50%
 ---- SURFACE MAPPING GEOMETRY ----
 COORD 1=-0.400 COORD 2= 0.000
 HAS ENERGY VALUE      -0.655153
 H      0.00000   0.00000  -0.35611
 H      0.00000   0.00000  -0.04389
 --------------------------------
...
```

As mentioned above, GAMESS calculates energies for different internuclear distances (in red) with steps of 0.1 Å that can be changed by changing disp1=0.1.

Inputs for O_2 (O_2^+) molecule

F.I. *Input for O_2 optimization calculations:*

```
 $CONTRL RUNTYP=optimize SCFTYP=ROHF MULT=3 ISPHER=1 $END
 $SYSTEM TIMLIM=90000 mwords=100 $END
 $BASIS GBASIS=CCT $END
 $STATPT OPTTOL=0.00001 NSTEP=20 $END
 $DATA
O2 optimization - cartesian coordinates
Dnh 4
```

```
 O         8.0   0.0000000000   0.0000000000   0.72
 $END
```

— —

G.I*. Input for* O_2^+ *optimization calculations:*

```
 $CONTRL RUNTYP=optimize SCFTYP=ROHF ICHARG=1 MULT=2 ISPHER=1 $END
 $SYSTEM TIMLIM=90000 mwords=100 $END
 $BASIS GBASIS=CCT $END
 $STATPT OPTTOL=0.00001 NSTEP=20 $END
 $DATA
O2 optimization - cartesian coordinates
Dnh 4

 O         8.0   0.0000000000   0.0000000000   0.72
 $END
```

— —

H.I. *Input for* O_2^+ *energy curve calculations:*

```
 $CONTRL RUNTYP=energy SCFTYP=MCSCF ICHARG=1 MULT=2 ISPHER=1 $END
 $SYSTEM TIMLIM=90000 mwords=100 $END
 $BASIS GBASIS=CCT $END
 $SURF ivec1(1)=1,2 igrp1=2
       disp1=0.1 ndisp1=80 orig1=0 $END
 $DET NCORE=4 NACT=6 NELS=7 NSTATE=22 $END
 $DET  WSTATE(1)=1,1,1,1,1,1,1,1,1,1,1,1,1,1 $END
 $DET IROOT=14 $END
 $GUESS GUESS=MOREAD norb=60 $END
 $DATA
O2p MCSCF energy- cartesian coordinates
Dnh 4

 O         8.0   0.0000000000  0.0000000000     0.5435216138
 $END
 $VEC
 1  1 6.90462181E-01 5.90682505E-04 3.08141581E-02 1.25056362E-03-0.00000000E+00
 1  2-0.00000000E+00 2.05835947E-03-0.00000000E+00-0.00000000E+00-4.74935703E-04
 1  3-0.00000000E+00-0.00000000E+00 1.89563601E-04-7.68704919E-05-7.68704919E-05
 1  4 1.53740984E-04-0.00000000E+00-0.00000000E+00-0.00000000E+00 1.30415410E-04
 ….
 $END
```

— —

The "VEC" group was taken from the ***.dat file of the optimization run of O_2^+.

— —

J.I. *Input for* O_2^+ *dipole coupling element calculations:*

```
 $CONTRL RUNTYP=TRANSITN SCFTYP=NONE CITYP=GUGA ISPHER=1 ICHARG=1 MULT=2 $END
 $SYSTEM TIMLIM=90000 mwords=100 $END
 $BASIS GBASIS=CCT $END
 $STATPT OPTTOL=0.00001 NSTEP=20 $END
 !$DET NCORE=4 NACT=6 NELS=5 $END
 !$GUESS GUESS=MOREAD norb=60 $END
 $GUGDIA ITERMX=300 $END
 $TRANST OPERAT=DM NFZC=2 IROOTS(1)=16 NOCC=11 $END
 $DRT1 GROUP=c1 IEXCIT=2 NFZC=2 NDOC=4 NALP=3 NEXT=-1 NVAL=2 $END
 $DATA
O2p MCSCF energy- cartesian coordinates
Dnh 4

 O         8.0   0.0000000000  0.0000000000     0.5435216138
 $END
 $VEC1
 1  1 6.90602729E-01 8.53547880E-04 3.05852604E-02 8.28470661E-04-0.00000000E+00
 1  2-0.00000000E+00 3.05629834E-03-0.00000000E+00-0.00000000E+00 7.59436047E-04
```

```
 1  3-0.00000000E+00-0.00000000E+00 4.99154416E-04-2.15514717E-04-2.15514717E-04
 1  4 4.31029435E-04-0.00000000E+00-0.00000000E+00-0.00000000E+00 9.31725941E-05
….
$END
```

outputs for O_2 (O_2^+) molecule

F.O. Output for O_2 optimization calculations

```
  ...
ECHO OF THE FIRST FEW INPUT CARDS -
INPUT CARD> $CONTRL RUNTYP=optimize SCFTYP=ROHF MULT=3 ISPHER=1 $END
INPUT CARD> $SYSTEM TIMLIM=90000 mwords=100 $END
INPUT CARD> $BASIS GBASIS=CCT $END
INPUT CARD> $STATPT OPTTOL=0.00001 NSTEP=20 $END
INPUT CARD> $DATA
INPUT CARD>O2 optimization - cartesian coordinates
INPUT CARD>Dnh 4
INPUT CARD>
INPUT CARD> O         8.0   0.0000000000   0.0000000000   0.72
INPUT CARD> $END
 100000000 WORDS OF MEMORY AVAILABLE

    BASIS OPTIONS
    -------------
    GBASIS=CCT          IGAUSS=       0      POLAR=NONE
    NDFUNC=       0     NFFUNC=       0     DIFFSP=       F
    NPFUNC=       0      DIFFS=       F     BASNAM=


    RUN TITLE
    ---------
O2 optimization - cartesian coordinates

THE POINT GROUP OF THE MOLECULE IS DNH
THE ORDER OF THE PRINCIPAL AXIS IS     4

ATOM      ATOMIC                      COORDINATES (BOHR)
          CHARGE         X                 Y                 Z
O           8.0     0.0000000000        0.0000000000       -1.3606027112
O           8.0     0.0000000000        0.0000000000        1.3606027112

         INTERNUCLEAR DISTANCES (ANGS.)
         ------------------------------

               1 O          2 O

  1 O       0.0000000    1.4400000 *
  2 O       1.4400000 *  0.0000000

 * ... LESS THAN  3.000


    ATOMIC BASIS SET
    ----------------
THE CONTRACTED PRIMITIVE FUNCTIONS HAVE BEEN UNNORMALIZED
THE CONTRACTED BASIS FUNCTIONS ARE NOW NORMALIZED TO UNITY

 SHELL TYPE  PRIMITIVE        EXPONENT          CONTRACTION COEFFICIENT(S)

O

    11   S       1         15330.0000000    0.000520198307
    11   S       2          2299.0000000    0.004023344781
    11   S       3           522.4000000    0.020729083329
    11   S       4           147.3000000    0.081082327080
    11   S       5            47.5500000    0.236226352118
    11   S       6            16.7600000    0.443518209420
```

```
    11   S       7            6.2070000    0.358670588689
    11   S       8            0.6882000   -0.008349797237

    12   S       9        15330.0000000   -0.000197236012
    12   S      10         2299.0000000   -0.001535010700
    12   S      11          522.4000000   -0.007951183914
    12   S      12          147.3000000   -0.032113452892
    12   S      13           47.5500000   -0.100269643049
    12   S      14           16.7600000   -0.234047111838
    12   S      15            6.2070000   -0.301410927756
    12   S      16            0.6882000    1.034919649508

    13   S      17            1.7520000    1.000000000000

    14   S      18            0.2384000    1.000000000000

    15   P      19           34.4600000    0.041163489568
    15   P      20            7.7490000    0.257762835858
    15   P      21            2.2800000    0.802419274427

    16   P      22            0.7156000    1.000000000000

    17   P      23            0.2140000    1.000000000000

    18   D      24            2.3140000    1.000000000000

    19   D      25            0.6450000    1.000000000000

    20   F      26            1.4280000    1.000000000000

 TOTAL NUMBER OF BASIS SET SHELLS             =   20
 NUMBER OF CARTESIAN GAUSSIAN BASIS FUNCTIONS =   70
 NOTE: THIS RUN WILL RESTRICT THE MO VARIATION SPACE TO SPHERICAL HARMONICS.
 THE NUMBER OF ORBITALS KEPT IN THE VARIATIONAL SPACE WILL BE PRINTED LATER.
 NUMBER OF ELECTRONS                          =   16
 CHARGE OF MOLECULE                           =    0
 SPIN MULTIPLICITY                            =    3
 NUMBER OF OCCUPIED ORBITALS (ALPHA)          =    9
 NUMBER OF OCCUPIED ORBITALS (BETA )          =    7
 TOTAL NUMBER OF ATOMS                        =    2
 THE NUCLEAR REPULSION ENERGY IS       23.5189888551

 THIS MOLECULE IS RECOGNIZED AS BEING LINEAR,
 ORBITAL LZ DEGENERACY TOLERANCE ETOLLZ= 1.00E-06

     $NEO OPTIONS
     ------------
     NUNIQN=       0     BASNUC=DZSNB        NEOSCF=NONE
     NEOCI =NONE         NUMULT=       2     NUCST =       1
     NAUXNB=       0     VNUCEX=       F     NUCOPT=       F
     NTAUXB=       0     NEOHSS=       F     HSSINI=READH
     HSSUPD=POWELLUP     DIRNUC=       F     SYMNUC=       F
     QMTOLN= 0.0E+00     USRDEX=       F
     POSNEO=       F     POSPRP=       F
     NEONCI=       F     LOCORB=       0

     $CONTRL OPTIONS
     ---------------
 SCFTYP=ROHF         RUNTYP=OPTIMIZE     EXETYP=RUN
 MPLEVL=       0     CITYP =NONE         CCTYP =NONE         VBTYP =NONE
 DFTTYP=NONE         TDDFT =NONE
 MULT  =       3     ICHARG=       0     NZVAR =       0     COORD =UNIQUE
 PP    =NONE         RELWFN=NONE         LOCAL =NONE         NUMGRD=       F
 ISPHER=       1     NOSYM =       0     MAXIT =      30     UNITS =ANGS
 PLTORB=       F     MOLPLT=       F     AIMPAC=       F     FRIEND=
 NPRINT=       7     IREST =       0     GEOM  =INPUT
 NORMF =       0     NORMP =       0     ITOL  =      20     ICUT  =       9
 INTTYP=BEST         GRDTYP=BEST         QMTTOL= 1.0E-06
...
      ***** EQUILIBRIUM GEOMETRY LOCATED *****
 COORDINATES OF SYMMETRY UNIQUE ATOMS (ANGS)
```

```
  ATOM   CHARGE       X              Y              Z
------------------------------------------------------------
O           8.0  -0.0000000000   0.0000000000   0.5761650783
COORDINATES OF ALL ATOMS ARE (ANGS)
  ATOM   CHARGE       X              Y              Z
------------------------------------------------------------
O           8.0  -0.0000000000   0.0000000000  -0.5761650783
O           8.0  -0.0000000000   0.0000000000   0.5761650783

         INTERNUCLEAR DISTANCES (ANGS.)
         ------------------------------

              1 O          2 O

  1 O       0.0000000    1.1523302 *
  2 O       1.1523302 *  0.0000000

 * ... LESS THAN  3.000


         NUCLEAR ENERGY    =       29.3903129730
         ELECTRONIC ENERGY =     -179.0487339259
         TOTAL ENERGY      =     -149.6584209529
...
```

The equilibrium geometry (in red) is given in Angstroms. One O atom is at Z = 0.576 Å and the other is at Z = - 0.576 Å. The internuclear distance in atomic units R = (2 * 0.576165 / 0.529) Å = 2.178318 a.u.

H.O. *Output for* O_2^+ *energy calculations*

```
...
 ECHO OF THE FIRST FEW INPUT CARDS -
 INPUT CARD> $CONTRL RUNTYP=energy SCFTYP=MCSCF ICHARG=1 MULT=2 ISPHER=1 $END
 INPUT CARD> $SYSTEM TIMLIM=90000 mwords=100 $END
 INPUT CARD> $BASIS GBASIS=CCT $END
 INPUT CARD> $SURF ivec1(1)=1,2 igrp1=2
 INPUT CARD>       disp1=0.1 ndisp1=80 orig1=0 $END
 INPUT CARD> $DET NCORE=4 NACT=6 NELS=7 NSTATE=22 $END
 INPUT CARD> $DET  WSTATE(1)=1,1,1,1,1,1,1,1,1,1,1,1 $END
 INPUT CARD> $DET IROOT=14 $END
 INPUT CARD> $GUESS GUESS=MOREAD norb=60 $END
 INPUT CARD> $DATA
 INPUT CARD>O2p MCSCF energy- cartesian coordinates
 INPUT CARD>Dnh 4
 INPUT CARD>
 INPUT CARD> O         8.0   0.0000000000  0.0000000000     0.5435216138
 INPUT CARD> $END
 INPUT CARD> $VEC
 INPUT CARD> 1  1 6.90462181E-01 5.90682505E-04 3.08141581E-02 1.25056362E-03-0.00000000E+00
...
         -------------------
          LAGRANGIAN CONVERGED
          -------------------

 FINAL MCSCF ENERGY IS     -148.7396712377 AFTER  11 ITERATIONS

 -MCCI- BASED ON OPTIMIZED ORBITALS
 ----------------------------------

 PLEASE NOTE: IF THE ACTIVE ORBITALS ARE CANONICALIZED BELOW,
 THE FOLLOWING CI EXPANSION COEFFICIENTS AND THE DENSITY DO NOT
 CORRESPOND TO THE PRINTED ORBITALS.  THE PRINTED EXPANSIONS MATCH
 THE ORBITALS USED DURING THE LAST ITERATION.  IF YOU WISH TO SEE
 CI EXPANSIONS BASED ON THE CANONICAL (OR NATURAL) ORBITALS, YOU
 MUST RUN A CI CALCULATION WITH THAT ORBITAL CHOICE READ IN $VEC.
```

```
 CI EIGENVECTORS WILL BE LABELED IN GROUP=C1
 PRINTING CI COEFFICIENTS LARGER THAN  0.050000

 STATE   1  ENERGY=      -149.3507802341  S=  0.50  SZ=  0.50  SPACE SYM=A

 ALPHA   | BETA    | COEFFICIENT
---------|---------|------------
 111010 | 111000 |    0.9624018
 101110 | 101100 |   -0.1701232
 101110 | 011010 |    0.1164666
 111010 | 001110 |    0.0849530
 110011 | 011010 |    0.0582635
 111010 | 010011 |    0.0543940
 110011 | 110001 |    0.0524254
 110011 | 101100 |   -0.0522195

 STATE   2  ENERGY=      -149.3506810746  S=  0.50  SZ=  0.50  SPACE SYM=A

 ALPHA   | BETA    | COEFFICIENT
---------|---------|------------
 111100 | 111000 |    0.9623072
 011110 | 011010 |    0.1708770
 011110 | 101100 |   -0.1163062
 111100 | 001110 |    0.0847515
 110101 | 101100 |   -0.0580896
 111100 | 100101 |   -0.0542410
 110101 | 110001 |    0.0524191
 110101 | 011010 |    0.0523061

 STATE   3  ENERGY=      -149.0967759996  S=  1.50  SZ=  0.50  SPACE SYM=A

 ALPHA   | BETA    | COEFFICIENT
---------|---------|------------
 011110 | 111000 |    0.5720578
 111100 | 011010 |    0.5720578
 111010 | 011100 |   -0.5720578

 STATE   4  ENERGY=      -149.0964642230  S=  1.50  SZ=  0.50  SPACE SYM=A

 ALPHA   | BETA    | COEFFICIENT
---------|---------|------------
 111100 | 101010 |    0.5720447
 111010 | 101100 |   -0.5720447
 101110 | 111000 |    0.5720447

 STATE   5  ENERGY=      -149.0520698627  S=  0.50  SZ=  0.50  SPACE SYM=A

 ALPHA   | BETA    | COEFFICIENT
---------|---------|------------
 111010 | 011100 |    0.6158673
 111100 | 101100 |   -0.5472204
 011110 | 111000 |    0.5046989
 111010 | 101010 |    0.1743647
 111100 | 011010 |    0.1111683
 011110 | 001110 |   -0.0637585
 101110 | 010101 |   -0.0518447
 100111 | 011100 |    0.0505619

 STATE   6  ENERGY=      -149.0520086510  S=  0.50  SZ=  0.50  SPACE SYM=A

 ALPHA   | BETA    | COEFFICIENT
---------|---------|------------
 111100 | 101010 |    0.6129513
 111010 | 011010 |   -0.5502528
 101110 | 111000 |   -0.5052103
 111100 | 011100 |    0.1758562
 111010 | 101100 |    0.1077410
 101110 | 001110 |    0.0633246
 011110 | 100011 |   -0.0517026
 010111 | 101010 |    0.0504117
```

```
 STATE   7  ENERGY=      -149.0183209308  S=  1.50  SZ=  0.50  SPACE SYM=A

 ALPHA   | BETA    | COEFFICIENT
---------|---------|------------
 111010 | 110100 |    0.5664673
 111100 | 110010 |   -0.5664673
 110110 | 111000 |   -0.5664673
 101110 | 010110 |    0.0902954
 011110 | 100110 |   -0.0902954
 110110 | 001110 |   -0.0902954

 STATE   8  ENERGY=      -149.0046104820  S=  0.50  SZ=  0.50  SPACE SYM=A

 ALPHA   | BETA    | COEFFICIENT
---------|---------|------------
 111100 | 101010 |    0.4973532
 111010 | 101100 |    0.4963582
 111010 | 011010 |    0.4943406
 111100 | 011100 |   -0.4939782

 STATE   9  ENERGY=      -149.0046104753  S=  0.50  SZ=  0.50  SPACE SYM=A

 ALPHA   | BETA    | COEFFICIENT
---------|---------|------------
 111010 | 101010 |    0.4970304
 111100 | 101100 |   -0.4966890
 111100 | 011010 |   -0.4946560
 111010 | 011100 |   -0.4936548

 STATE  10  ENERGY=      -148.9463646876  S=  0.50  SZ=  0.50  SPACE SYM=A

 ALPHA   | BETA    | COEFFICIENT
---------|---------|------------
 111010 | 110100 |    0.6889153
 111100 | 110010 |    0.6886060
 101110 | 010110 |    0.1428209
 011110 | 100110 |    0.1427614

...

 STATE  22  ENERGY=      -148.6986348926  S=  1.50  SZ=  0.50  SPACE SYM=A

 ALPHA   | BETA    | COEFFICIENT
---------|---------|------------
 011110 | 101100 |    0.5618101
 111100 | 001110 |    0.5618101
 101110 | 011100 |   -0.5618101
 010111 | 111000 |    0.0974533
 111010 | 010101 |    0.0953235
 110101 | 011010 |   -0.0947354
 111100 | 010011 |   -0.0840480
 110011 | 011100 |    0.0834599
 011110 | 110001 |    0.0813301
...
_ _ _ _ _ _ _ _ _ _ _ _ _ _ _ _ _ _ _ _ _ _ _ _ _ _ _ _ _ _ _ _ _ _ _ _ _ _ _ _ _ _
```

Because in the input for a fixed internuclear distance *R* we had NSTATE=22, the output will have 22 energy states (in red). Alpha and beta are the spin up and spin down electronic states, and depending on the configuration we have different states. For example, the ground state of O_2^+ has the configuration $(1\sigma_g)^2(1\sigma_u)^2(2\sigma_g)^2(2\sigma_u)^2(3\sigma_g)^2(1\pi_u)^4(1\pi_g)^1(3\sigma_u)^0$, thus missing an electron from $1\pi_g$ (See appendix G). In the input, the $1\sigma_g$,$1\sigma_u$,$2\sigma_g$,$2\sigma_u$ orbitals are assumed to be fixed, and electrons are allowed to move around only on the $3\sigma_g$,$1\pi_u$,$1\pi_g$,$3\sigma_u$ orbitals. There

are 6 orbitals with 2 spaces for electrons (spin up and spin down) on each. For STATE 1 in the output under ALPHA and BETA, we have **111010 | 111000,** meaning that we have a KK$(3\sigma_g)^2(1\pi_u)^4(1\pi_g)^1(3\sigma_u)^0$ configuration (KK=$(1\sigma_g)^2(1\sigma_u)^2(2\sigma_g)^2(2\sigma_u)^2$).

S= 0.5 or S=1.5 is indicative of doublet or quartet states. One needs to repeat this calculation for different R.

_ _

J.O. *Output for O_2^+ dipole coupling element calculations:*

```
...
 ECHO OF THE FIRST FEW INPUT CARDS -
 INPUT CARD> $CONTRL RUNTYP=TRANSITN SCFTYP=NONE CITYP=GUGA ISPHER=1 ICHARG=1 MULT=2 $END
 INPUT CARD> $SYSTEM TIMLIM=90000 mwords=100 $END
 INPUT CARD> $BASIS GBASIS=CCT $END
 INPUT CARD> $STATPT OPTTOL=0.00001 NSTEP=20 $END
 INPUT CARD> !$DET NCORE=4 NACT=6 NELS=5 $END
 INPUT CARD> !$GUESS GUESS=MOREAD norb=60 $END
 INPUT CARD> $GUGDIA ITERMX=300 $END
 INPUT CARD> $TRANST OPERAT=DM NFZC=2 IROOTS(1)=16 NOCC=11 $END
 INPUT CARD> $DRT1 GROUP=c1 IEXCIT=2 NFZC=2 NDOC=4 NALP=3 NEXT=-1 NVAL=2 $END
 INPUT CARD> $DATA
 INPUT CARD>O2p MCSCF energy- cartesian coordinates
 INPUT CARD>Dnh 4
 INPUT CARD>
 INPUT CARD> O         8.0   0.0000000000  0.0000000000     0.5435216138
 INPUT CARD> $END
 INPUT CARD> $VEC1
 INPUT CARD> 1  1 6.90602729E-01 8.53547880E-04 3.05852604E-02 8.28470661E-04-0.00000000E+00
...
-------------------------------------------------
 NON-ABELIAN CI WAVEFUNCTION STATE SYMMETRY DRIVER
          WRITTEN BY DMITRI FEDOROV.
     MEMORY USED IS   124381 WORDS
 -------------------------------------------------

 ORBITAL  3(A1G ) HAS ROW FRACTIONS 100.%
 ORBITAL  4(A2U ) HAS ROW FRACTIONS 100.%
 ORBITAL  5(A1G ) HAS ROW FRACTIONS 100.%
 ORBITAL  6(EU  ) HAS ROW FRACTIONS 100.%   0.%
 ORBITAL  7(EU  ) HAS ROW FRACTIONS   0.% 100.%
 ORBITAL  8(EG  ) HAS ROW FRACTIONS 100.%   0.%
 ORBITAL  9(EG  ) HAS ROW FRACTIONS   0.% 100.%
 ORBITAL 10(A2U ) HAS ROW FRACTIONS 100.%
 ORBITAL 11(A2U ) HAS ROW FRACTIONS 100.%

 STATE #    1  ENERGY =    -149.118516486

      CSF      COEF    OCCUPANCY (IGNORING CORE)
      ---      ----    --------- --------- -----
       35    0.987229  222211100
      559    0.103933  221111210
     1858   -0.070783  220211120
 THE PROJECTION OF THIS CI STATE ONTO SPACE SYMMETRY EU   WEIGHS 1.0000E+00


 STATE #    2  ENERGY =    -149.118516486

      CSF      COEF    OCCUPANCY (IGNORING CORE)
      ---      ----    --------- --------- -----
       13    0.987229  222121100
      558   -0.098412  221112110
      618    0.050133  221112110
     1736    0.070783  220121120
 THE PROJECTION OF THIS CI STATE ONTO SPACE SYMMETRY EU   WEIGHS 1.0000E+00
```

```
 STATE #    3  ENERGY =    -149.081770996

      CSF      COEF    OCCUPANCY (IGNORING CORE)
      ---      ----    --------- --------- -----
        5   -0.104469  221112200
        8   -0.106718  212121200
       12   -0.059513  122112200
       23    0.809561  221221100
       30   -0.106718  212212100
       32    0.534715  122221100
      523   -0.057262  220121210
      638   -0.057262  220212110
      693   -0.061688  211221110
 THE PROJECTION OF THIS CI STATE ONTO SPACE SYMMETRY A2G  WEIGHS 9.6721E-01

 THE PROJECTION OF THIS CI STATE ONTO SPACE SYMMETRY B2G  WEIGHS 3.2794E-02
...
          ---- LENGTH FORM ----

 THE NEXT PAIR ARE THE SAME STATE, SO THIS IS AN EXPECTATION VALUE,
 RATHER THAN A TRANSITION MOMENT.

 CI STATE NUMBER=  1  1 STATE MULTIPLICITY=  4  4
 NUMBER OF CSF-S=      1932      1932
 STATE ENERGIES          -149.1185164863     -149.1185164863
 TRANSITION ENERGY=  0.0000E+00 [1/SEC] =        0.00 [1/CM] =        0.00 [EV]
                        X [Z]       Y [Z]       Z [Z]       NORM
 CENTER OF MASS    =    0.000000    0.000000    0.000000             BOHR
 TRANSITION DIPOLE =   -0.000000   -0.000000    0.000000    0.000000 E*BOHR
 TRANSITION DIPOLE =   -0.000000   -0.000000    0.000000    0.000000 DEBYE
 STEP CPU TIME =     0.02 TOTAL CPU TIME =       44.3 (    0.7 MIN)
 TOTAL WALL CLOCK TIME=       44.8 SECONDS, CPU UTILIZATION IS  98.90%

 CI STATE NUMBER=  1  2 STATE MULTIPLICITY=  4  4
 NUMBER OF CSF-S=      1932      1932
 STATE ENERGIES          -149.1185164863     -149.1185164863
 TRANSITION ENERGY=  1.8701E+02 [1/SEC] =        0.00 [1/CM] =        0.00 [EV]
                        X [Z]       Y [Z]       Z [Z]       NORM
 CENTER OF MASS    =    0.000000    0.000000    0.000000             BOHR
 TRANSITION DIPOLE =   -0.000000   -0.000000   -0.000000    0.000000 E*BOHR
 TRANSITION DIPOLE =   -0.000000   -0.000000   -0.000000    0.000000 DEBYE
 OSCILLATOR STRENGTH =    0.000000
 EINSTEIN COEFFICIENTS: A=  0.0000E+00 1/SEC; B=  0.0000E+00 SEC/G
 STEP CPU TIME =     0.00 TOTAL CPU TIME =       44.3 (    0.7 MIN)
 TOTAL WALL CLOCK TIME=       44.8 SECONDS, CPU UTILIZATION IS  98.90%

 CI STATE NUMBER=  1  3 STATE MULTIPLICITY=  4  4
 NUMBER OF CSF-S=      1932      1932
 STATE ENERGIES          -149.1185164863     -149.0817709959
 TRANSITION ENERGY=  2.4177E+14 [1/SEC] =     8064.52 [1/CM] =        1.00 [EV]
                        X [C]       Y [C]       Z [Z]       NORM
 CENTER OF MASS    =    0.000000    0.000000    0.000000             BOHR
 TRANSITION DIPOLE =   -0.000091   -0.332025   -0.000000    0.332025 E*BOHR
 TRANSITION DIPOLE =   -0.000231   -0.843930   -0.000000    0.843930 DEBYE
 OSCILLATOR STRENGTH =    0.002701
 EINSTEIN COEFFICIENTS: A=  1.1715E+05 1/SEC; B=  4.4738E+07 SEC/G
 STEP CPU TIME =     0.00 TOTAL CPU TIME =       44.3 (    0.7 MIN)
 TOTAL WALL CLOCK TIME=       44.8 SECONDS, CPU UTILIZATION IS  98.90%

 ...
```

Reading out the dipole coupling elements from the output is not straight forward. The input has IROOTS(1)=16, indicating that the output file will have 16 states. For identifying

which states are there, one needs to look at OCCUPANCY. There are nine numbers given under the occupancy out of which the first 8 are: $2\sigma_g$, $2\sigma_u$, $3\sigma_g$, two $1\pi_u$, two $1\pi_g$, and $3\sigma_u$ orbitals, and one extra virtual orbital. The **222211100** combination means we have 2 electrons in each of the $2\sigma_g$, $2\sigma_u$, and $3\sigma_g$ orbitals, 2 electrons on $1\pi_u^x$, one on $1\pi_u^y$, one electron in each of the $1\pi_g^x$ and $1\pi_g^y$ orbitals, and nothing in $3\sigma_u$ (see Appendix G). This combination corresponds to a $a^4\Pi_u$ state (see Chapter 5). If one needs to find the dipole coupling matrix elements between $a^4\Pi_u$ and some other state, for example $f^4\Pi_g$ (222111200), a state with corresponding electron combination needs to be found.

E.1 Compiling and running WIN-GAMESS

In the WinGAMESS version of GAMESS, compiling of the input file is possible with "batmaker.exe".

Step1: Double-click on "batmaker.exe" (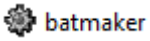). The window shown in Fig.E1 will pop up.

Step2: One can add an input file by clicking on the "Add file to list" button (Fig.E1, E2). After collecting the input file, the executable ***.bat file needs to be named and saved in the preferred output folder (Fig.E3).

Step3: Double-click on the generated ***.bat file in the output folder (where it has been saved) and GAMESS will run. Generated output files will be located in the preferred output folder where the input and .bat files were saved (note that ***.dat files required for $VEC are generated in the "C\WinGAMESS\temp" folder).

For further information, please consult the GAMESS website [*]

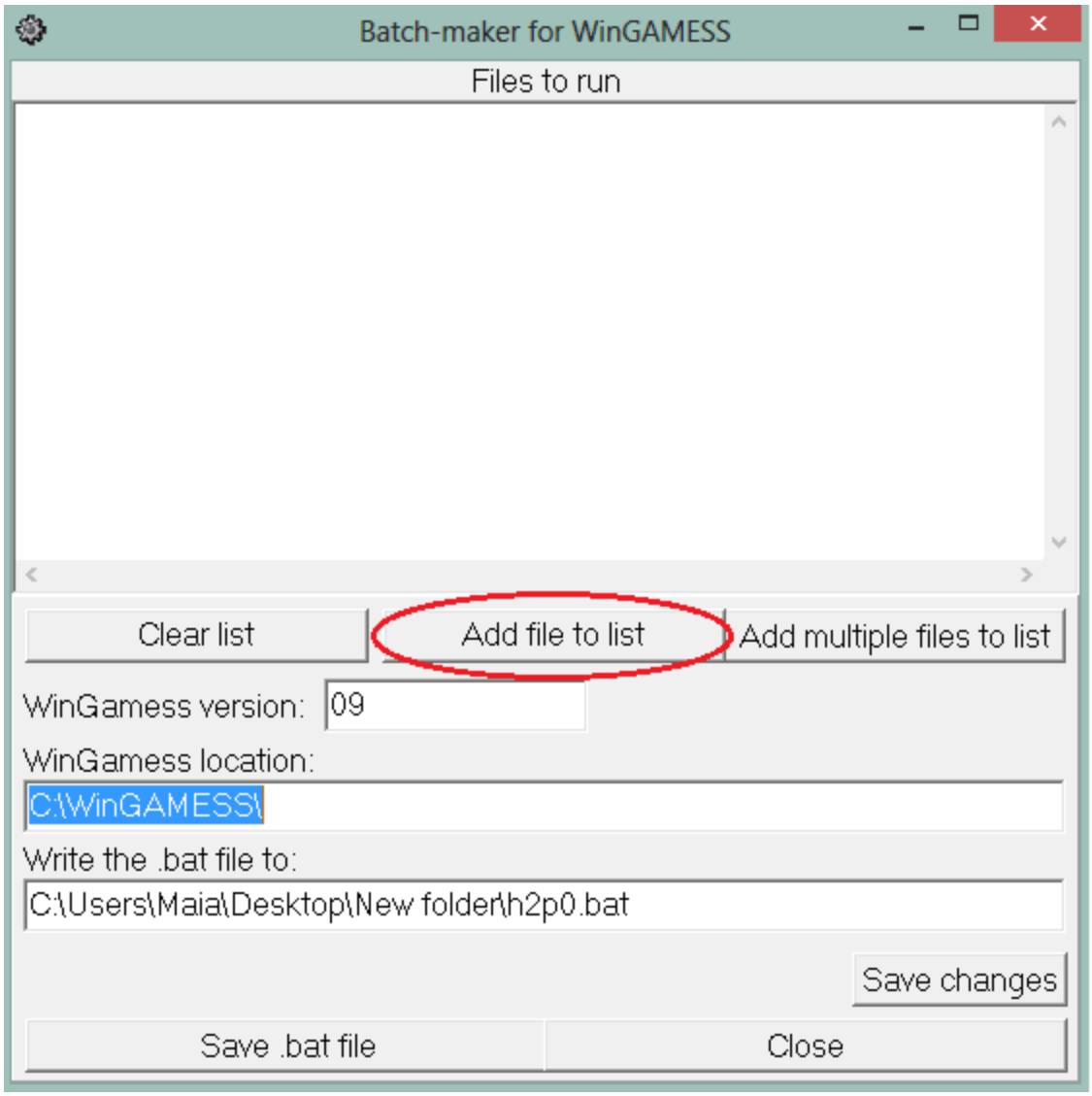

Figure 7 "*Batmaker*" *compiler display.*

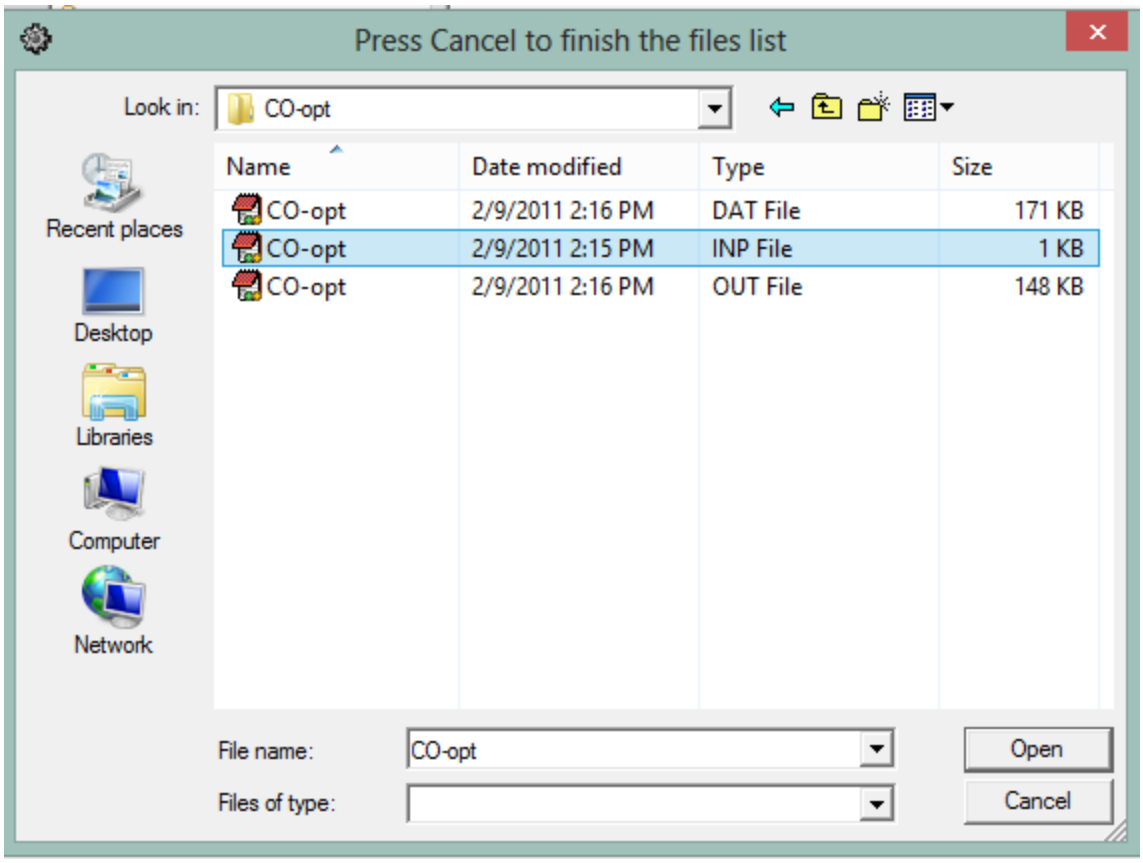

Figure 8 ***Choosing input files already generated.***

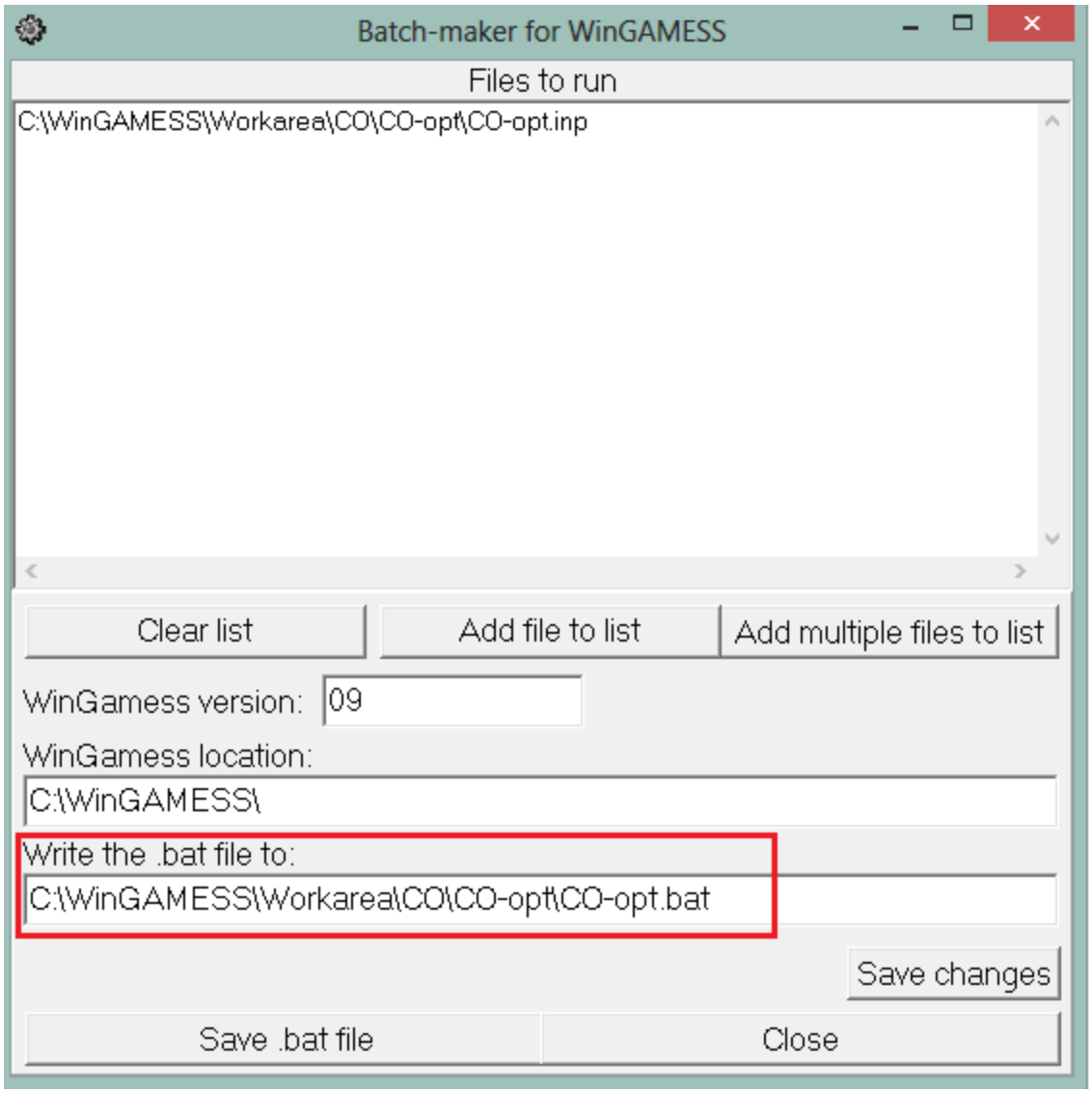

Figure 9 ***Choosing the name and place for outputs and .bat file .***

[*] Website for GAMESS: http://www.msg.ameslab.gov/gamess/documentation.html

Appendix F - Atomic units and useful formulas

The SI unit system is based on four constants of nature: length - meter, time - second, mass - kilogram, and current - ampere. In atomic physics, it is more convenient to use atomic units, where,

Atomic unit of action:	$\hbar$	=	1
Atomic unit of mass:	m_e	=	1
Atomic unit of charge:	e	=	1
Atomic unit of the Coulomb force constant:	$1/4\pi\varepsilon_0$	=	1

The unit of length in atomic units is the Bohr radius of the hydrogen atom. The Bohr radius is the radius of the orbit of the electron in the ground state of hydrogen:

$$a_0 = \frac{(4\pi\varepsilon_0)\hbar^2}{me^2} = 5.29177 \times 10^{-11} m \qquad \text{(A.1)}$$

The unit of mass is taken to be the mass of the electron, the unit of charge is the electron's charge, and the unit of angular momentum is $\hbar$. The unit of velocity is taken to be the velocity of the electron in the first Bohr orbit of hydrogen:

$$v_0 = \frac{e^2}{(4\pi\varepsilon_0)\hbar} = \alpha c \ , \qquad \text{(A.2)}$$

where α is the fine structure constant and equal to 1/137 and c is the speed of the light, so in atomic units the speed of light is 137.

In atomic units, the energy level for the principal quantum number n is:

$$E_n = -\frac{Z^2}{2n^2} \qquad \text{(A.3)}$$

For hydrogen, the energy in atomic units is -0.5, such that the atomic unit of energy (which is called hartree) is 27.2 eV. The table below summarizes conversion from atomic units to SI units.

dimension	formula	a.u.	SI units
length	a_0	1	5.29177×10^{-11} m
time	a_0/v_0	1	2.41888×10^{-17} s
mass	m_e	1	9.10938×10^{-31} kg
charge	q_e	1	1.60218×10^{-19} C
velocity	v_0	1	2.18769×10^{6} m/ s
intensity	$1/2\ c\varepsilon_0(e/(4\ \pi\varepsilon_0 a_0^2))^2$	1	3.50953×10^{16} W/cm^2
energy	$e^2/(4\ \pi\varepsilon_0 a_0)$	1	27.2116 eV = 1 hartree
momentum	$m_e v_0$	1	1.99285×10^{-24} kg m /s
angular momentum	$\hbar = a_0 m_e v_0$	1	$1.05457 \times 10-34$ kg m^2/ s
frequency	$v_0/(2\pi a_0)$	1	6.57969×10^{15} Hz
angular frequency	v_0/a_0	1	4.13414×10^{16} Hz
action	$\hbar = e^2/(4\ \pi\varepsilon_0 v_0)$	1	1.05457×10^{-34} J s
electric field	$e/(4\ \pi\varepsilon_0 a^2_0)$	1	5.14221×10^{11} V/m
magnetic field	$\hbar/(e a_0^2)$	1	2.35052×10^{5} T

Table F.1 ***Conversion from atomic units to SI units***

Appendix G - Molecular orbital diagrams for diatomic molecules

For diatomic molecules, the electronic configurations look like those shown in Fig. G1 for the example of the electronic configurations of N_2 and O_2 [Harris-78]. A molecular orbital scheme similar to N_2 is used for Li_2-N_2 diatomic molecules and a scheme similar to O_2 is used for F_2.

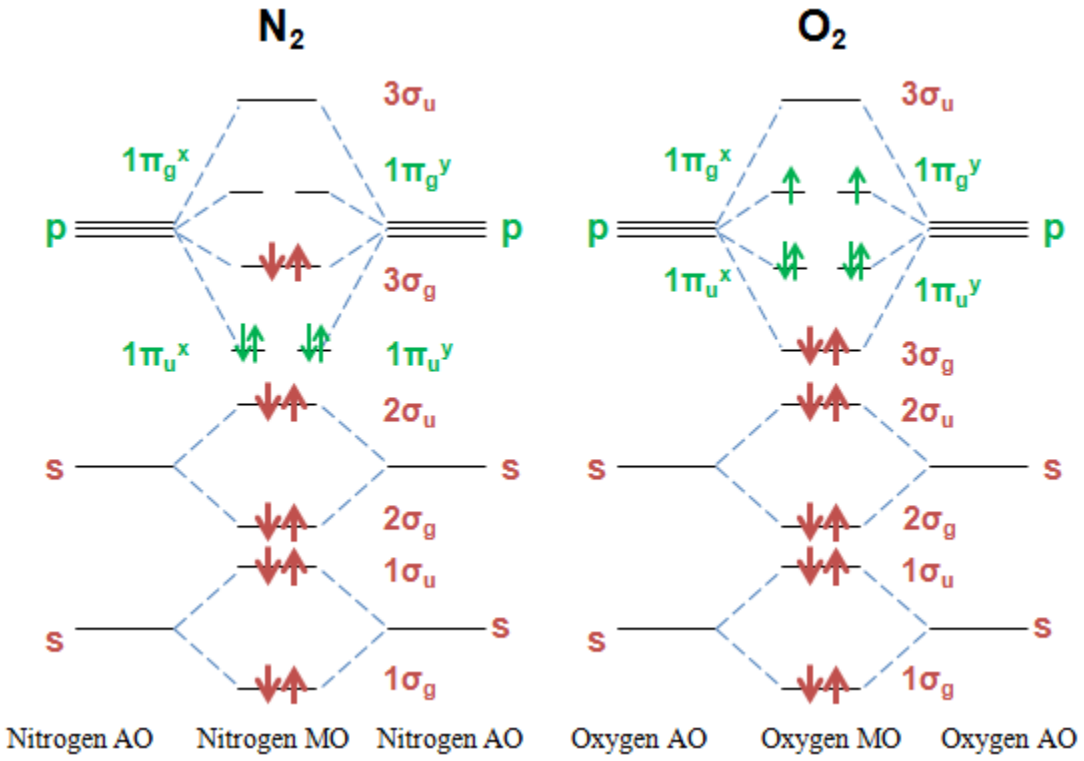

Figure 10 ***Molecular orbital diagram for N_2 and O_2 molecules.***

My publications related to the thesis work

1. "**Dissociation dynamics of noble gas dimers in intense IR laser fields**" - M. Magrakvelidze and U. Thumm, *Physical Review A.* **88**, 013413 (2013)
2. "**Attosecond timing of asymmetric chemical bond breaking**" - J. Wu, M. Magrakvelidze, L. Ph. H. Schmidt, M. Kunitski, T. Pfeifer, M. Schöffler, M. Pitzer, M. Richter, S. Voss, H. Sann, H. Kim, T. Jahnke, A. Czasch, U. Thumm, and R. Dörner, *Nature communications* **4**, 2177 (2013)
3. "**Steering the nuclear motion in singly ionized argon dimers with mutually detuned laser pulses**" - J. Wu, M. Magrakvelidze, A. Vredenborg, L. Ph. H. Schmidt, T. Jahnke, A. Czasch, R. Dörner, and U. Thumm, *Physical Review Letters* **110**, 033005 (2013)
4. "**Dissociation dynamics of diatomic molecules in intense laser Fields: a scheme for the selection of relevant adiabatic potential curves**"- M. Magrakvelidze, C. M. Aikens, and U. Thumm, *Physical Review A* **86**, 023402 (2012)
5. "**Tracing nuclear wave-packet dynamics in singly and doubly charged states of N_2 and O_2 with XUV pump – XUV probe experiments**" - M. Magrakvelidze, O. Herrwerth, Y.H. Jiang, A. Rudenko, M. Kurka, L. Foucar, K.U. Kühnel, M. Kübel, Nora G. Johnson, C.D. Schröter, S. Düsterer, R. Treusch, M. Lezius, I. Ben-Itzhak, R. Moshammer, J. Ullrich, M.F. Kling, and U. Thumm, *Physical Review A* **86,** 013415 (2012)
6. "**Following dynamic nuclear wave packets in N_2, O_2, and CO with few-cycle infrared pulses**" - S. De, M. Magrakvelidze, I. A. Bocharova, D. Ray, W. Cao, I. Znakovskaya, H. Li, Z. Wang, G. Laurent, U. Thumm, M. F. Kling, I. V. Litvinyuk, I. Ben- Itzhak, and C. L. Cocke *Physical Review A* **84,** 043410 (2011)
7. "**Tracking nuclear wave-packet dynamics in molecular oxygen ions with few-cycle infrared laser pulses**" - S. De, I. A. Bocharova, M. Magrakvelidze, D. Ray, W. Cao, B. Bergues, U. Thumm, M. F. Kling, I.V. Litvinyuk, and C. L. Cocke, , *Phys. Rev. A* **82**, 013408 (2010)
8. "**Angular dependence of the strong-field ionization measured in randomly oriented hydrogen molecules**" - Maia Magrakvelidze, Feng He, Sankar De, Irina Bocharova, Dipanwita Ray, Uwe Thumm, and I. V. Litvinyuk, *Physical Review A* **79,** 033408 (2009)
9. "**Quantum-beat imaging of the nuclear dynamics in D_2^+: Dependence of bond softening and bond hardening on laser intensity, wavelength, and pulse duration**" – Maia Magrakvelidze, Feng He, Thomas Niederhausen, Igor V. Litvinyuk, and Uwe Thumm, *Physical Review A* **79,** 033410 (2009)

Work to be published

"Complementary Imaging of the Nuclear Dynamics in Laser-Excited Diatomic Molecular Ions in the Time and Frequency Domains" - M. Magrakvelidze, A. Kramer, K. Bartschat, and U. Thumm *J. Phys. B*